

**SYNTHESIS AND REACTIVITY OF
CHROMIUM α -DIIMINE COMPLEXES AND
1,4-DIMETHYL-OXA-NORBORNENE**

by

Lan Wang

A dissertation submitted to the Faculty of the University of Delaware in partial fulfillment of the requirements for the degree of Doctor of Philosophy in Chemistry and Biochemistry

Winter 2018

© 2018 Lan Wang
All Rights Reserved

**SYNTHESIS AND REACTIVITY OF
CHROMIUM α -DIIMINE COMPLEXES AND
1,4-DIMETHYL-OXA-NORBORNENE**

by

Lan Wang

Approved: _____
Brian J. Bahnson, Ph.D.
Chair of the Department of Chemistry and Biochemistry

Approved: _____
George H. Watson, Ph.D.
Dean of the College of Arts and Sciences

Approved: _____
Ann L. Ardis, Ph.D.
Senior Vice Provost for Graduate and Professional Education

I certify that I have read this dissertation and that in my opinion it meets the academic and professional standard required by the University as a dissertation for the degree of Doctor of Philosophy.

Signed:

Klaus H. Theopold, Ph.D.
Professor in charge of dissertation

I certify that I have read this dissertation and that in my opinion it meets the academic and professional standard required by the University as a dissertation for the degree of Doctor of Philosophy.

Signed:

Mary P. Watson, Ph.D.
Member of dissertation committee

I certify that I have read this dissertation and that in my opinion it meets the academic and professional standard required by the University as a dissertation for the degree of Doctor of Philosophy.

Signed:

Svilen S. Bobev, Ph.D.
Member of dissertation committee

I certify that I have read this dissertation and that in my opinion it meets the academic and professional standard required by the University as a dissertation for the degree of Doctor of Philosophy.

Signed:

Raul F. Lobo, Ph.D
Member of dissertation committee

ACKNOWLEDGMENTS

First I would like to thank my advisor, Dr. Klaus H. Theopold, for his academic guidance, support and offering me the opportunity to conduct my research in his laboratory. I'm also grateful to my research group members both in Dr. Theopold's group and in Catalysis Center for Energy Innovation, past and present, for their time and help to me professionally and personally. I'm also greatly indebted to Dr. Glenn P. A. Yap for helping me to pick up crystals and to solve structures. I would like to thank my dissertation committee members for taking the time out of their schedules to advise me in the preparation and presentation of this research. Furthermore, I want to thank the Chemistry and Biochemistry departmental staff for their help and support. I am grateful to the University of Delaware for providing me with excellent academic and research services as well as the opportunity to earn this degree. Lastly, I would like to thank the National Science Foundation and Department of Energy for their continued financial support of my research career at the University of Delaware.

TABLE OF CONTENTS

LIST OF TABLES	vii
LIST OF SCHEMES	ix
LIST OF FIGURES	xii
ABSTRACT	xv
 Chapter	
1 INTRODUCTION	1
2 THE REACTIVITY OF A QUINTUPLE-BONDED CHROMIUM DIMER SUPPORTED BY α -DIIMINE LIGANDS	13
2.1 Introduction	13
2.2 Results and Discussion	19
2.3 Experimental.....	41
2.3.1 General Considerations	41
2.3.2 Preparation of $[\text{H}^{\text{L}^{\text{iPr}}}\text{Cr}]_2(\mu\text{-CO})$ (1)	42
2.3.3 Preparation of $(\text{L-CO}_2)_2\text{Cr}_2$ (2).....	42
2.3.4 Preparation of $[\text{H}^{\text{L}^{\text{iPr}}}\text{Cr}]_2(\mu\text{-}\eta^2\text{:}\eta^2\text{-CS})(\mu\text{-S})$ (3)	43
2.3.5 General considerations for X-ray diffraction	43
2.3.6 Single crystal X-ray diffraction studies.....	44
3 THE SYNTHESIS OF THE DINUCLEAR CHROMIUM ALKYL/ARYL HYDRIDE COMPLEXES SUPPORTED BY α -DIIMINE LIGANDS	50
3.1 Introduction	50
3.2 Results and Discussion	56
3.3 Experimental.....	126
3.3.1 General Considerations	126
3.3.2 Preparation of $(\text{H}^{\text{L}^{\text{iPr}}}\text{Cr})_2(\mu\text{-H})_2$ (4)	127
3.3.3 Preparation of $[(\text{H}^{\text{L}^{\text{iPr}}}\text{Cr})_2(\mu\text{-Me})(\mu\text{-H})_2]^-[\text{Li}(\text{THF})_4]^+$ (5)	128
3.3.4 Preparation of $[(\text{H}^{\text{L}^{\text{iPr}}}\text{Cr})_2(\mu\text{-Ph})(\mu\text{-H})_2]^-[\text{Li}(\text{THF})_4]^+$ (6)	129
3.3.5 Preparation of $[(\text{H}^{\text{L}^{\text{iPr}}}\text{Cr})_2(\mu\text{-CH}_2\text{TMS})(\mu\text{-H})_2]^-$ $[\text{Li}(\text{THF})_3(\text{Et}_2\text{O})]^+$ (7).....	129

3.3.6	Preparation of $[(^H L^{iPr}Cr)_2(\mu-CH_2^tBu)(\mu-H)_2]^- [Li(THF)_3(Et_2O)]^+$ (8).....	130
3.3.7	Preparation of $[(^H L^{iPr}Cr)_2(\mu-CH_2Ph)(\mu-H)_2]^- [Li(THF)_4]^+$ (9) ...	130
3.3.8	Preparation of $[(^H L^{iPr}Cr)_2(\mu-Me)_2(\mu-H)]^- [Li(THF)_3(Et_2O)]^+$ (10)	131
3.3.9	Preparation of $[(^H L^{iPr}Cr)_2(\mu-Ph)_2(\mu-H)]^- [Li(THF)]^+$ (11).....	132
3.3.10	Preparation of $(^H L^{iPr}Cr) (^{Me,H_2} L^{iPr}Cr)(\mu-CH_2TMS)(\mu-H)_2$ (12). 132	
3.3.11	General considerations for X-ray diffraction	133
3.3.12	Single crystal X-ray diffraction studies.....	133
4	SYNTHESIS, ISOLATION AND CHARACTERIZATION OF DIMETHYL-OXA-NORBORNENE AND CATALYSTS SEARCH FOR AROMATIZATION AND DIELAS-ALDER REACTIONS.....	139
4.1	Introduction	139
4.2	Results and Discussion	142
4.3	Experimental.....	175
4.3.1	General Considerations	175
4.3.2	Preparation of 1,4-dimethyl-7-oxa-bicyclo[2,1]hept-2-ene-5-endo-carboxyl-acid (13)	175
4.3.3	Preparation of 1,4-dimethyl-7-oxa-bicyclo[2,1]heptane-5-endo-carboxyl-acid (14)	176
4.3.4	Preparation of 1,4-dimethyl-7-oxa-bicyclo[2,1]hept-2-ene (15)	176
4.3.5	Typical Aromatization Procedure for reactions	177
4.3.6	Typical retro-Diels-Alder procedure for reactions	178
Appendix		
	ABBREVIATION	183

LIST OF TABLES

Table 2.1	Bond distances (Å) of the α -diimine backbone for the α -diimine ligand in various oxidation states.	18
Table 2.2	Interatomic distances (Å) and angles (°) for $[\text{H}^{\text{iPr}}\text{Cr}](\mu\text{-CO})$ (1).....	21
Table 2.3	Interatomic distances (Å) and angles (°) for $(\mu\text{-}\eta^1\text{:}\eta^1\text{-L})_2\text{Cr}_2$ (2).	27
Table 2.4	Interatomic distances (Å) and angles (°) for $[\text{H}^{\text{iPr}}\text{Cr}]_2(\mu\text{-}\eta^2\text{:}\eta^2\text{-CS})(\mu\text{-S})$ (3).....	33
Table 2.5	Crystallographic data for complexes 1-3.....	45
Table 3.1	Interatomic distances (Å) and angles (°) for $(\text{H}^{\text{iPr}}\text{Cr})_2(\mu\text{-H})_2$ (4).....	58
Table 3.2	Interatomic distances (Å) and angles (°) for $[(\text{H}^{\text{iPr}}\text{Cr})_2(\mu\text{-Me})(\mu\text{-H})_2]^- [\text{Li}(\text{THF})_4]^+$ (5).....	69
Table 3.3	Interatomic distances (Å) and angles (°) for $[(\text{H}^{\text{iPr}}\text{Cr})_2(\mu\text{-Ph})(\mu\text{-H})_2]^- [\text{Li}(\text{THF})_4]^+$ (6).....	75
Table 3.4	Interatomic distances (Å) and angles (°) for $[(\text{H}^{\text{iPr}}\text{Cr})_2(\mu\text{-CH}_2\text{TMS})(\mu\text{-H})_2]^- [\text{Li}(\text{THF})_3(\text{Et}_2\text{O})]^+$ (7).....	81
Table 3.5	Interatomic distances (Å) and angles (°) for $[(\text{H}^{\text{iPr}}\text{Cr})_2(\mu\text{-CH}_2\text{tBu})(\mu\text{-H})_2]^- [\text{Li}(\text{THF})_3(\text{Et}_2\text{O})]^+$ (8).....	85
Table 3.6	Interatomic distances (Å) and angles (°) for $[(\text{H}^{\text{iPr}}\text{Cr})_2(\mu\text{-CH}_2\text{Ph})(\mu\text{-H})_2]^- [\text{Li}(\text{THF})_4]^+$ (9).....	91
Table 3.7	Interatomic distances (Å) and angles (°) for $[(\text{H}^{\text{iPr}}\text{Cr})_2(\mu\text{-Me})_2(\mu\text{-H})]^- [\text{Li}(\text{THF})_3(\text{Et}_2\text{O})]^+$ (10).....	98
Table 3.8	Interatomic distances (Å) and angles (°) for $[(\text{H}^{\text{iPr}}\text{Cr})_2(\mu\text{-Ph})_2(\mu\text{-H})]^- [\text{Li}(\text{THF})]^+$ (11).....	102
Table 3.9	Selected bond distances (Å) of the diimine backbone, Cr-Cr distances, intramolecular bond distances, τ_5 values and room temperature magnetic moment per Cr (μ_{B}) for complexes 5-11.....	108

Table 3.10	Interatomic distances (Å) and angles (°) for $(^{\text{H}}\text{L}^{\text{iPr}}\text{Cr})(^{\text{Me,H}^2}\text{L}^{\text{iPr}}\text{Cr})(\mu\text{-CH}_2\text{TMS})(\mu\text{-H})_2$ (12)	117
Table 3.11	Crystallographic data for complexes 4-12.....	134
Table 4.1	Rate constants of thermal retro-Diels-Alder reaction of 13	153
Table 4.2	Rate constants and activation parameters of thermal retro-Diels-Alder reaction of 13.....	154
Table 4.3	Rate constants of thermal retro-Diels-Alder reaction of 15	163
Table 4.4	Rate constants and activation parameters of thermal retro-Diels-Alder reaction of 15.....	164
Table 4.5	Stability of three 1,4-dimethy-oxa-norbornene derivatives	165
Table 4.6	Summery of retro-Diels-Alder tests with dimethyl-oxa-norbornene	170
Table 4.7	Activation parameters of the retro-Diels-Alder reactions	172

LIST OF SCHEMES

Scheme 1.1	Early examples of C-H activation	3
Scheme 1.2	Current examples of first row transition metal alkyl hydride complexes from literature.....	5
Scheme 1.3	Upgrade cellulose to para-xylene	7
Scheme 2.1	Small molecule activation with $(\text{Tp}^{\text{t-Bu,Me}}\text{Cr})_2\text{N}_2$	14
Scheme 2.2	Small molecule activation with $(\text{NacNacCr})_2\text{N}_2$	14
Scheme 2.3	Small molecule activation with Cr-Cr quintuply bonded complexes.....	16
Scheme 2.4	Small molecule activation with $(\mu\text{-}\eta^1\text{:}\eta^1\text{-HL}^{\text{iPr}})_2\text{Cr}_2$	17
Scheme 2.5	The metal-ligand redox interaction in α -diimine complexes.....	18
Scheme 2.6	CO addition of $(\mu\text{-}\eta^1\text{:}\eta^1\text{-HL}^{\text{iPr}})_2\text{Cr}_2$	19
Scheme 2.7	Reaction of $(\mu\text{-}\eta^1\text{:}\eta^1\text{-HL}^{\text{iPr}})_2\text{Cr}_2$ and CO_2	25
Scheme 2.8	The reaction of $(\mu\text{-}\eta^1\text{:}\eta^1\text{-HL}^{\text{iPr}})_2\text{Cr}_2$ with hexafluoro-2-butyne and plausible mechanism of formation of 2.....	31
Scheme 2.9	Reaction of $(\mu\text{-}\eta^1\text{:}\eta^1\text{-HL}^{\text{iPr}})_2\text{Cr}_2$ and CS_2	32
Scheme 2.10	Plausible mechanism of formation of 3.....	38
Scheme 2.11	Synthesis of $(\text{PipisoFe})_2(\mu\text{-S})(\mu\text{-CS})$	39
Scheme 2.12	Comparison of bond distances in complexes featuring $\text{M}_2(\mu\text{-}\eta^2\text{:}\eta^1\text{-CS})$ core	40
Scheme 3.1	Synthesis of first row transition metal alkyl hydride complexes via hydrogenation	54
Scheme 3.2	DFT calculations of oxidative addition of CH_4 to NacNacCr(I) fragment (relative stability in terms of enthalpy)	55

Scheme 3.3	Synthesis of first row transition metal alkyl hydride complexes via β -elimination and ethylene insertion	55
Scheme 3.4	Preparation of $(^{\text{H}}\text{L}^{\text{iPr}}\text{Cr})_2(\mu\text{-H})_2$	57
Scheme 3.5	Reaction of 4 with ethylene	66
Scheme 3.6	Reaction of $(^{\text{H}}\text{L}^{\text{iPr}}\text{Cr})_2(\mu\text{-H})_2$ with lithium alkyls	67
Scheme 3.7	Reaction of $(^{\text{H}}\text{L}^{\text{iPr}}\text{Cr})_2(\mu\text{-H})_2$ with lithium reagent in THF	96
Scheme 3.8	Plausible mechanism of formation of chromium di-phenyl hydride complex	107
Scheme 3.9	Selected bond distances and angles in $\text{Cr}_2(\mu\text{-Me})_2(\mu\text{-H})$ and $\text{Ti}_2(\mu\text{-Me})(\mu\text{-H})$ core	112
Scheme 3.10	Selected bond distances and angles in $\text{Cr}_2(\mu\text{-Ph})(\mu\text{-H})_2$, $\text{Cr}_2(\mu\text{-Ph})_2(\mu\text{-H})$ and $\text{Cr}_2(\mu\text{-Ph})(\mu\text{-H})$ core	113
Scheme 3.11	Selected bond distances and angles in $\text{Cr}_2(\mu\text{-CH}_2\text{TMS})(\mu\text{-H})_2$ and $\text{Cr}_2(\mu\text{-CH}_2\text{TMS})(\mu\text{-H})$ core	114
Scheme 3.12	Reaction of $[(^{\text{H}}\text{L}^{\text{iPr}}\text{Cr})_2(\mu\text{-CH}_2\text{TMS})(\mu\text{-H})_2]^-$ with Me_3OBF_4	115
Scheme 3.13	Plausible mechanisms of decomposition reaction of 5-9	123
Scheme 4.1	Process steps for dimethylfuran production from cellulose and synthesis of PX from dimethylfuran and ethylene with zeolite	140
Scheme 4.2	Initial attempts of synthesizing dimethyl-oxa-norbornene	144
Scheme 4.3	[3+2] Diels-Alder reaction promoted by TpW complex	146
Scheme 4.4	Examples of cation-radical catalyzed Diels-Alder reactions	148
Scheme 4.5	Synthesis plans of 2,5-dimethyl-oxa-norbornene via nitroethylene and epoxidation	149
Scheme 4.6	Preparation of 1,4-dimethyl-oxa-norbornene-5-carboxylic acid	150
Scheme 4.7	Synthetic strategy from dimethylfuran to oxa-norbornene	151
Scheme 4.8	Barton decarboxylation of 13 initiated by UV-light	155

Scheme 4.9 Alternative synthetic strategy from dimethylfuran to oxa-norbornene .	156
Scheme 4.10 Oxidative decarboxylation of 14	157
Scheme 4.11 retro-Diels-Alder of dimethyl-oxa-norbornene	161
Scheme 4.12 Dehydration of dimethyl-oxa-norbornene and accessibility toward different catalyst.	166
Scheme 4.13 Possible mechanisms of Diels-Alder reaction.....	171
Scheme 4.14 Kinetic studies of Diels-Alder and retro-Diels-Alder reactions of furans and maleic anhydride by Dewar et al.	172
Scheme 4.15 Proposed future works.....	174

LIST OF FIGURES

Figure 2.1	Molecular structure of $[\text{H}^{\text{iPr}}\text{L}^{\text{Cr}}](\mu\text{-CO})$ (1) with thermal ellipsoids at the 30% probability level. Isopropyl groups and hydrogen atoms have been omitted for clarity.	20
Figure 2.2	Molecular structure of $(\text{L-CO}_2)_2\text{Cr}_2$ (2) with thermal ellipsoids at the 30% probability level. Isopropyl groups and hydrogen atoms have been omitted for clarity.	26
Figure 2.3	Molecular structure of $[\text{H}^{\text{iPr}}\text{L}^{\text{Cr}}]_2(\mu\text{-}\eta^2\text{:}\eta^1\text{-CS})(\mu\text{-S})$ (3) with thermal ellipsoids at the 30% probability level. Isopropyl groups and hydrogen atoms have been omitted for clarity.	33
Figure 3.1	Molecular structure of $(\text{H}^{\text{iPr}}\text{L}^{\text{Cr}})_2(\mu\text{-H})_2$ (4) with thermal ellipsoids at the 30% probability level. H1 has been located on a difference map. Isopropyl groups and hydrogen atoms have been omitted for clarity.	58
Figure 3.2	Tracking $^1\text{H-NMR}$ spectra of $(\text{H}^{\text{iPr}}\text{L}^{\text{Cr}})(\text{CH}_2\text{TMS})(\text{THF})$ reacting with 1 atm of H_2 in C_6D_6 at room temperature. (a) The full NMR spectra range from -120 to 130 ppm to exhibit the reaction progress of hydrogenation. (b) The NMR spectra range from -25 to 20 ppm to exhibit the growth and disappearance of two peaks potentially associated with intermediates at -21 and 16 ppm. (c) The NMR spectra range from -1 to 10 ppm to exhibit the increasing of two peaks at 3.8 and 5.4 ppm. The (*) denotes the characteristic peak belong to $(\text{H}^{\text{iPr}}\text{L}^{\text{Cr}})(\text{CH}_2\text{TMS})(\text{THF})$ and the (#) denotes the characteristic peak belong to 4.	63
Figure 3.3	$^1\text{H-NMR}$ of ethylene insertion and oligomerization with 4 in C_6D_6 . The (*) denotes the characteristic peak belong to 4 and the (#) denotes the characteristic peak belong to 1-hexene. The (a) denotes the unknow complex a and the (b) denotes the unknow complex b.	65
Figure 3.4	Molecular structure of $[(\text{H}^{\text{iPr}}\text{L}^{\text{Cr}})_2(\mu\text{-Me})(\mu\text{-H})_2][\text{Li}(\text{THF})_4]^+$ (5) with thermal ellipsoids at the 30% probability level. H1 H2 have been located on a difference map. Isopropyl groups and hydrogen atoms have been omitted for clarity.	68

Figure 3.5	Molecular structure of $[(^{\text{H}}\text{L}^{\text{iPr}}\text{Cr})_2(\mu\text{-Ph})(\mu\text{-H})_2]^{-}[\text{Li}(\text{THF})_4]^{+}$ (6) with thermal ellipsoids at the 30% probability level. H1 has been located on a difference map. Isopropyl groups and hydrogen atoms have been omitted for clarity.	74
Figure 3.6	Molecular structure of $[(^{\text{H}}\text{L}^{\text{iPr}}\text{Cr})_2(\mu\text{-CH}_2\text{TMS})(\mu\text{-H})_2]^{-}[\text{Li}(\text{THF})_3(\text{Et}_2\text{O})]^{+}$ (7) with thermal ellipsoids at the 30% probability level. Lithium atoms, isopropyl groups, most of the hydrogen atoms and solvent molecules have been omitted for clarity. H1, H2, H53A and H53B have been located on a difference map.	80
Figure 3.7	Molecular structure of $[(^{\text{H}}\text{L}^{\text{iPr}}\text{Cr})_2(\mu\text{-CH}_2^{\text{tBu}})(\mu\text{-H})_2]^{-}[\text{Li}(\text{THF})_3(\text{Et}_2\text{O})]^{+}$ (8) with thermal ellipsoids at the 30% probability level. Lithium atoms, isopropyl groups, most of the hydrogen atoms and solvent molecules have been omitted for clarity. H1, H2, H53A and H53B have been located on a difference map.	85
Figure 3.8	Molecular structure of $[(^{\text{H}}\text{L}^{\text{iPr}}\text{Cr})_2(\mu\text{-CH}_2\text{Ph})(\mu\text{-H})_2]^{-}[\text{Li}(\text{THF})_4]^{+}$ (9) with thermal ellipsoids at the 30% probability level. Lithium atoms, isopropyl groups, most of the hydrogen atoms and solvent molecules have been omitted for clarity. H1, H2, H53A and H53B have been located on a difference map.	90
Figure 3.9	Molecular structure of $[(^{\text{H}}\text{L}^{\text{iPr}}\text{Cr})_2(\mu\text{-Me})_2(\mu\text{-H})]^{-}[\text{Li}(\text{THF})_3(\text{Et}_2\text{O})]^{+}$ (10) with thermal ellipsoids at the 30% probability level. Lithium atoms, isopropyl groups, most of the hydrogen atoms and solvent molecules have been omitted for clarity. H1, H27A, H27B and H27C have been located on a difference map.	97
Figure 3.10	Molecular structure of $[(^{\text{H}}\text{L}^{\text{iPr}}\text{Cr})_2(\mu\text{-Ph})_2(\mu\text{-H})]^{-}[\text{Li}(\text{THF})]^{+}$ (11) with thermal ellipsoids at the 30% probability level. H1 has been located on a difference map. Isopropyl groups and hydrogen atoms have been omitted for clarity.	101
Figure 3.11	^1H -NMR spectra of 5,7,8,9 in C_6D_6 and 6 in THF- d_8 due to poor solubility in C_6D_6	110
Figure 3.12	Molecular structure of $(^{\text{H}}\text{L}^{\text{iPr}}\text{Cr})(^{\text{Me,H}^2}\text{L}^{\text{iPr}}\text{Cr})(\mu\text{-CH}_2\text{TMS})(\mu\text{-H})_2$ (12) with thermal ellipsoids at the 30% probability level. H1, H2, H27A, H27B, H53A, H53B, H57A, H57B and H57C have been located on a difference map. Isopropyl groups and hydrogen atoms have been omitted for clarity.	116

Figure 3.13	$^1\text{H-NMR}$ spectra of reductive elimination of 7. The (#) denotes the characteristic peak belong to 7, the (*) denotes the chemical shift of tetramethylsilane and (x) denotes the coordinated solvent of 7	121
Figure 3.14	First order decay of 7 and 8 in THF	125
Figure 4.1	Computed free energy barriers of dimethylfuran converted to p-xylene with ethylene and to 2,5-hexanedione with water at 300 °C in H-BEA framework. All computed data are carried out calculations at the M062X/6-311+G(d,p) theory level.	142
Figure 4.2	Electron demand for Diels-Alder reactions.	143
Figure 4.3	First order decay of 13 monitored by $^1\text{H-NMR}$ at 19 °C over 172 h. The time between two spectra is not fixed. (a) denotes the chemical shifts of 13; (b) denotes the chemical shifts of 2,5-dimethylfuran; (c) denotes the chemical shifts of acrylic acid.	152
Figure 4.4	The rate measurements of thermal retro-Diels-Alder reaction of 13 at different temperature	153
Figure 4.5	Linear fitting for Eyring equation of the first order decay of 13.....	154
Figure 4.6	NMR spectra of 15: (a) $^1\text{H-NMR}$ spectrum of 15 in CDCl_3 ; (b) $^{13}\text{C-NMR}$ spectrum of 15; (c) HSQC spectrum of 15.....	160
Figure 4.7	First order decay of 15 monitored by $^1\text{H-NMR}$ at 125 °C over 192 h. (a) denotes the chemical shifts of 15; (b) denotes the chemical shifts of 2,5-dimethylfuran; (c) denotes the chemical shifts of ethylene; (d) denotes the chemical shifts of 1,4-dimethyl-oxa-norbornane; (e) denotes the chemical shifts of pentanes	162
Figure 4.8	The rate measurements of thermal retro-Diels-Alder reaction of 15 at different temperature	163
Figure 4.9	Linear fitting for Eyring equation of the first order decay of 15.....	164
Figure 4.10	First order dehydration of 15 (0.024 M) with $\text{B}(\text{C}_6\text{F}_5)_3$ (0.008 M) acid catalyst monitored by $^1\text{H-NMR}$ at 45 °C over 40 min. (a) denotes the chemical shifts of 15; (b) denotes the chemical shifts of pX.	167
Figure 4.11	First order dehydration of 15 catalyzed by TFA and $\text{B}(\text{C}_6\text{F}_5)_3$	168

ABSTRACT

This dissertation describes research on α -diimine chromium complexes and 1,4-dimethyl-7-oxabicyclo[2,2,1]hept-2-ene (aka: 1,4-dimethyl-oxa-norbornene). Specifically, the first part focused on synthesis of chromium complexes in low formal oxidation state (+I/+II) and investigation of their reactivity and electronic structures. In the second part, 1,4-dimethyl-7-oxabicyclo[2,2,1]hept-2-ene was synthesized and its kinetic and thermodynamic data were measured.

Chapter 1 continues the exploration of the reactivity of quintuply bonded compound $(\mu\text{-}\eta^1\text{:}\eta^1\text{-HL}^{\text{iPr}})_2\text{Cr}_2$ by describing the results of its exposure to several small molecules. Careful treatment of $(\mu\text{-}\eta^1\text{:}\eta^1\text{-HL}^{\text{iPr}})_2\text{Cr}_2$ with 1 equivalent of CO forms quadruply bonded dinuclear chromium CO adduct $[\text{HL}^{\text{iPr}}\text{Cr}]_2(\mu\text{-CO})$ (**1**), which is the precursor for previously reported compound $[\text{HL}^{\text{iPr}}\text{Cr}](\text{CO})_4$. When exposed to CO_2 , $(\mu\text{-}\eta^1\text{:}\eta^1\text{-HL}^{\text{iPr}})_2\text{Cr}_2$ activates the carbon on CO_2 gas, leads to electrophilic attack of CO_2 on the backbone carbons of the α -diimine ligands and forms a symmetric dinuclear chromium complex $(\mu\text{-}\eta^1\text{:}\eta^1\text{-L}^{\text{iPr}})_2\text{Cr}_2$ (**2**). Upon exposure to CS_2 , $(\mu\text{-}\eta^1\text{:}\eta^1\text{-HL}^{\text{iPr}})_2\text{Cr}_2$ was found to break one of the CS double bonds and to form an asymmetric dinuclear chromium complex $[\text{HL}^{\text{iPr}}\text{Cr}]_2(\mu\text{-}\eta^2\text{:}\eta^2\text{-CS})(\mu\text{-S})$ (**3**).

Chapter 2 describes the synthesis of a series of alkyl(aryl)/hydride bridged chromium dinuclear complexes. $(\text{HL}^{\text{iPr}})_2\text{Cr}_2(\mu\text{-H})_2$ (**4**), the precursor of alkyl(aryl)/hydride complexes, was synthesized by treating $[\text{HL}^{\text{iPr}}\text{Cr}](\text{CH}_2\text{TMS})(\text{THF})$ with hydrogen gas. Alkylations(arylations) of **4** with various lithium alkyls (LiMe, LiPh, LiCH_2TMS , LiCH_2^tBu , LiCH_2Ph) produce the corresponding

alkyl(aryl)/dihydride complexes: $[(^{\text{H}}\text{L}^{\text{iPr}}\text{Cr})_2(\mu\text{-Me})(\mu\text{-H})_2][\text{Li}(\text{THF})_4]^+$ (**5**), $[(^{\text{H}}\text{L}^{\text{iPr}}\text{Cr})_2(\mu\text{-Ph})(\mu\text{-H})_2][\text{Li}(\text{THF})_4]^+$ (**6**), $[(^{\text{H}}\text{L}^{\text{iPr}}\text{Cr})_2(\mu\text{-CH}_2\text{TMS})(\mu\text{-H})_2][\text{Li}(\text{THF})_3(\text{Et}_2\text{O})]^+$ (**7**), $[(^{\text{H}}\text{L}^{\text{iPr}}\text{Cr})_2(\mu\text{-CH}_2^t\text{Bu})(\mu\text{-H})_2][\text{Li}(\text{THF})_3(\text{Et}_2\text{O})]^+$ (**8**) and $[(^{\text{H}}\text{L}^{\text{iPr}}\text{Cr})_2(\mu\text{-CH}_2\text{Ph})(\mu\text{-H})_2][\text{Li}(\text{THF})_4]^+$ (**9**) in a solvent mixture of pentane with a few drops of THF. In contrast, the reactions of **4** with LiMe and LiPh in THF leads to dialkyl(diaryl)/hydrido complexes $[(^{\text{H}}\text{L}^{\text{iPr}}\text{Cr})_2(\mu\text{-Me})_2(\mu\text{-H})][\text{Li}(\text{THF})_3(\text{Et}_2\text{O})]^+$ (**10**) and $[(^{\text{H}}\text{L}^{\text{iPr}}\text{Cr})_2(\mu\text{-Ph})_2(\mu\text{-H})][\text{Li}(\text{THF})]^+$ (**11**). Alkyl(aryl)/hydrido complexes bearing different alkyl(aryl) ligands show significant differences in the stability of reductive elimination which was monitored by $^1\text{H-NMR}$. Treating compound **7** with $\text{Me}_3\text{O}^+\text{BF}_4^-$ gave an unusual ligand activated complex $(^{\text{H}}\text{L}^{\text{iPr}}\text{Cr})(^{\text{Me,H}^2}\text{L}^{\text{iPr}}\text{Cr})(\mu\text{-CH}_2\text{TMS})(\mu\text{-H})_2$ (**12**).

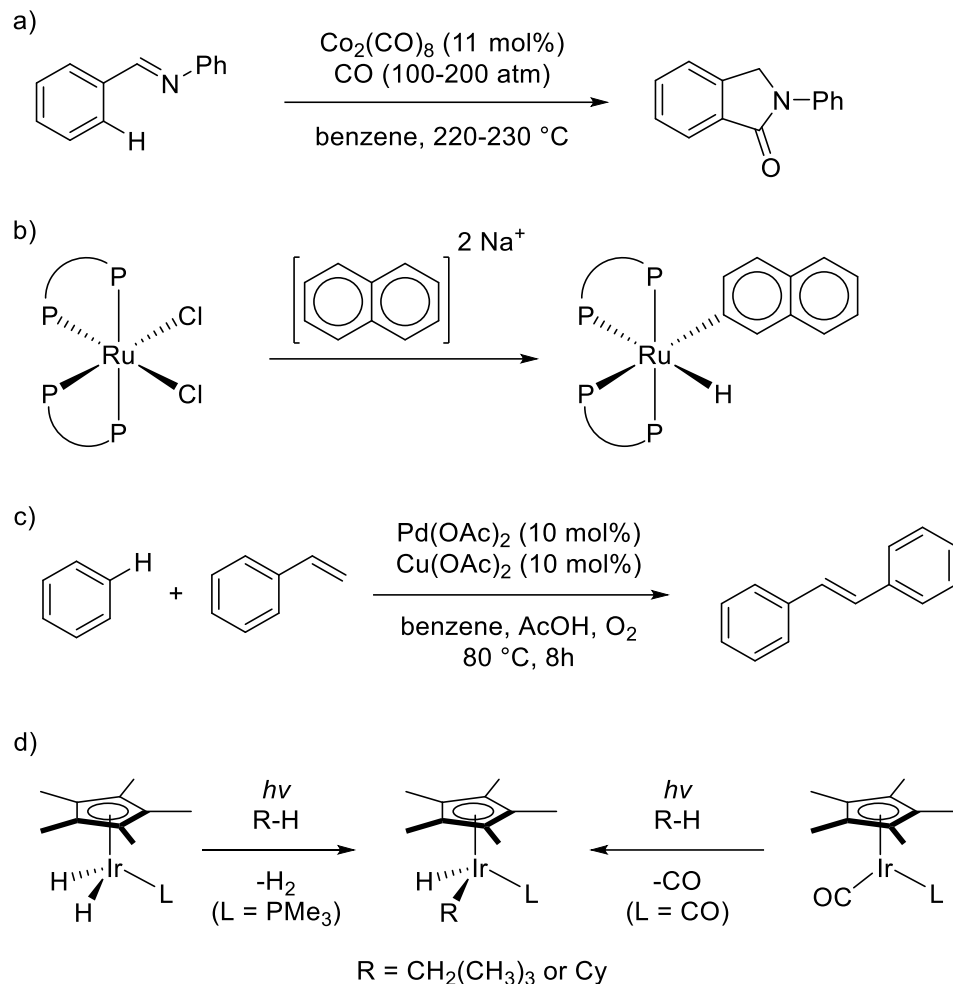
Chapter 3 presents the synthesis, purification and characterization of 1,4-dimethyl-7-oxabicyclo[2,2,1]hept-2-ene (**15**), which is the presumed intermediate of the Diels-Alder reaction of 2,5-dimethylfuran and ethylene to *para*-xylene. The activation parameters of retro-Diels-Alder reaction of dimethyl-oxa-norbornene in d_6 -benzene were measured and compared to computational studies. The rate of dehydration with Bronsted acid and Lewis acid was also investigated by $^1\text{H-NMR}$ spectroscopy. Several inorganic salts (AgOTf , $\text{Sc}(\text{OTf})_3$, $\text{Cu}(\text{OTf})_2$, PdCl_2 , AgNO_3 , Pd/C , $\text{Rh}_4(\text{CO})_{12}$, $\text{W}(\text{CO})_6$, $\text{RhCl}(\text{PPh}_3)_3$, $\text{Pt}(\text{PPh}_3)_3$, $\text{Mo}(\text{CO})_6$ and $\text{Ar}_3\text{N}^+\text{SbCl}_6^-$) were tested as catalysts for retro-Diels-Alder reaction. By the principle of microscopic reversibility, such catalysts should also facilitate the forward-Diels-Alder reaction.

Chapter 1

INTRODUCTION

Utilization of transition metals to activate thermodynamically stable substances and/or to promote kinetically inert reactions is an extensive and ever growing field both in inorganic and organic chemistry. Ever since the discovery of a platinum-ethylene complex by William Christopher Zeise in 1830¹, organometallic chemistry has experienced an explosive development. Many organometallic compounds such as dimethyl zinc discovered by Edward Frankland², Ni(CO)₄ discovered by Ludwig Mond³, and organomagnesium compound discovered by Victor Grignard⁴ have been synthesized and applied soon after. Nowadays the transition-metal chemistry has entered a brandnew era. Admirable examples of transition-metal-catalyzed reactions include cross coupling reaction between nucleophiles and electrophiles by Pd catalysts;⁵ olefin metathesis enabled by Ru and Mo catalysts;^{6,7} and asymmetric hydrogenation reactions catalyzed by Rh, Ru and Ir catalysts.⁸ Even through the discovery of those catalysts has greatly expanded synthetic chemistry, most of the known transition-metal catalysts do not meet the requirement of modern industrial manufacturing for cleaner and higher efficiency process due to the need for tedious functional-group transformation. One of the most promising processes in transition-metal chemistry is highly efficient catalytic C-H bond functionalization. By directly activating the C-H bond, those reactions proved new routes for synthesizing useful compounds in high atom- and step- economy.

The first reported C-H functionalization reaction via transition metal catalyst was the $\text{Co}_2(\text{CO})_8$ catalyzed carbonylative ring closure of (E)-N,1-diphenylmethanimine toward 2-phenylisoindolin-1-one (Scheme **1-1a**), published by Shunsuke Murahashi in 1955.⁹ By heating a benzene solution of benzaldehyde anil (5g) with dicobalt octacarbonyl catalyst (1g) under 100-200 atmospheres pressure of CO at 220-230 °C for 5-6 hours, the 2-phenylphthalimidine was obtained in 80% yield. Later in 1965, Joseph Chatt reported a more straightforward example of C-H activation in the formation of $\text{Ru}(\text{dmpe})_2(\text{H})(2\text{-naphthyl})$ complex by treating $\text{RuCl}_2(\text{dmpe})_2$ with sodium reduced naphthalene (dmpe = 1,2-bis(dimethylphosphino)ethane) (Scheme **1-1b**).¹⁰ The oxidative addition of C-H bond onto Ru center and the formation of hydrido-aryl complex clearly showed the cleavage of C-H bond, which was traditionally considered unreactive. In 1969, Yuzo Fujiwara reported the $\text{Pd}(\text{OAc})_2$ and $\text{Cu}(\text{OAc})_2$ catalyzed Heck-reaction-like cross coupling of benzene and styrene into trans-stilbene (Scheme **1-1c**).¹¹ The activation of benzene molecule was believed to be the σ -metathesis of PdX_2 and benzene C-H bond, as another general category of C-H activation. Arene has played a very big role in C-H activation/functionalization until the publication of two independent reports of iridium-mediated intermolecular C-H activation of unactivated and fully saturated hydrocarbons by R.G. Bergman¹² and W.A.G. Graham¹³ in 1982 (Scheme **1-1d**). The irradiation of $\text{Cp}^*\text{Ir}(\text{PMe}_3)(\text{H})_2$ (Bergman) or $\text{Cp}^*\text{Ir}(\text{CO})_2$ (Graham) in the presence of cyclohexane and neopentane by high pressure Hg lamp generated the hydrido-alkyl Ir complexes (Cp* = pentamethylcyclopentadienyl ligand).

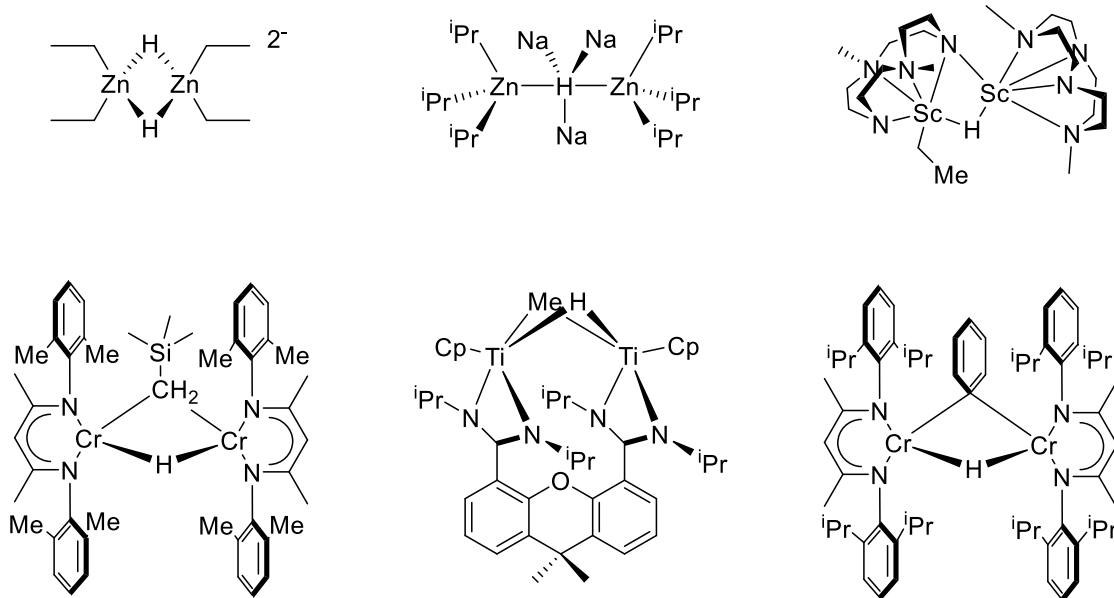


Scheme 1.1 Early examples of C-H activation

However, the current development of C-H activation reactions has encountered challenges like the need for high catalyst loading¹⁴, harsh conditions¹⁵, and lack of control for selectivity.^{16,17} The fundamental understanding of the C-H activation process is certainly the key to the discovery of new transition-metal catalyst for this promising transformation. In order to address this issue, one strategy is to synthesize the key intermediate of metal alkyl hydrides and to study their reactivity. Furthermore,

the replacement of rare and expensive transition metals like Pd, Ru and Ir with abundant and non-precious first row transition metals has become a rising trend.¹⁸ Many Ni catalysts, as the replacement of expensive Pd metal, have been invented and applied for transition-metal catalyzed cross coupling reactions such as Heck reaction¹⁹, Suzuki reaction²⁰, Kumada coupling²¹, and Negishi coupling²². It is unquestionable that this trend will impact the chemistry of transition-metal catalyzed C-H functionalization even through it is still at an early stage.

To date, only a few examples of first row transition metal alkyl hydride exist in the literature and even less for Cr complexes. Since 1980's our group has been activate in the field of organochromium chemistry and has shown interests in Cr mediated C-H activation. As early as 2003, MacAdams from our group reported the first chromium alkyl hydride, [(2,6-Me₂Ph)₂nacnacCr]₂(μ-H)(μ-CH₂SiMe₃).²³ In the same year, Hagadorn and McNevin synthesized and isolated a titanium dimer featuring a Ti^{III}(μ-Me)(μ-H)Ti^{III} core.²⁴ Both cases were achieved by hydrogenation of their metal alkyl precursor. Later in 2007, Jagner *et al* reported the synthesis of hydridoalkylzincates involving β-H elimination of trialkylzincate.²⁵ Monillas from our group also reported a pair of isomers including a phenyl-hydrido chromium dimer, namely [(2,6-*i*PrPh)₂nacnacCr]₂(μ-H)(μ-Ph) and [(2,6-*i*PrPh)₂nacnacCr]₂(μ-η⁶:η⁶-Ph) in 2007.²⁶ Recently, Okuda reported the synthesis of a scandium alkyl hydride complex featuring a Sc₂(μ-H)(Et) core by ethylene insertion of its hydrido precursor.²⁷ The structures are presented in Scheme 1.2. Due to the limited scope of first row transition metal alkyl hydrides, the detailed study of this chemistry is rare. Thus, one of our major effort is to expand the scope of organochromium alkyl hydride chemistry.



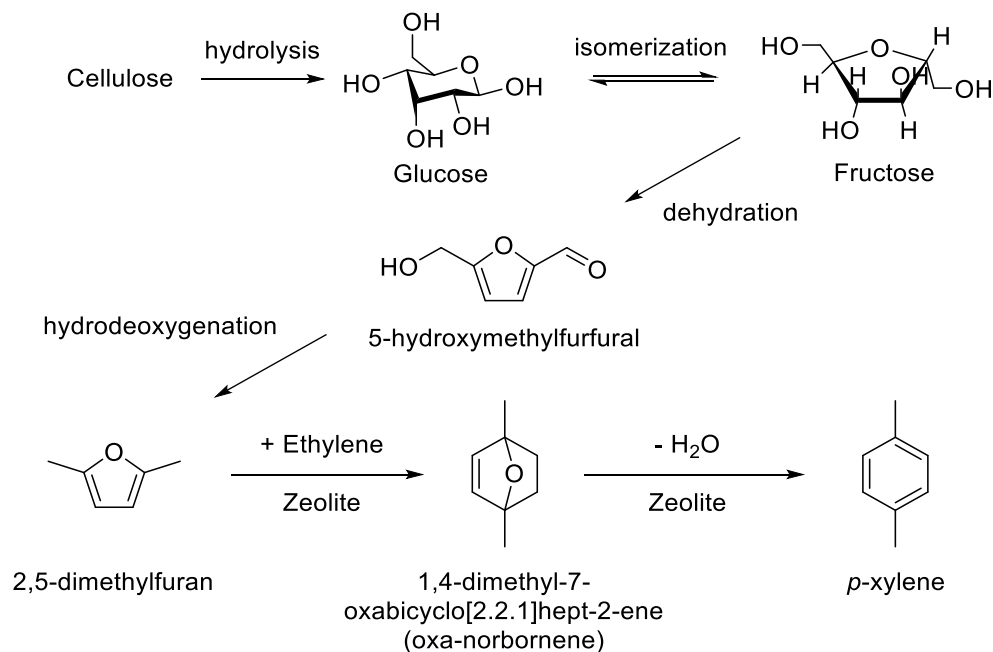
Scheme 1.2 Current examples of first row transition metal alkyl hydride complexes from literature.

Another two growing trends are the development of catalytic processes for fundamental transformations including activation of CO and CO₂ into one-carbon (C1) building block²⁸, and the conversion of biomass into renewable fuels and chemicals.²⁹ The polyester industry is one of the enterprises that will benefit from those trends. In the polyester family, polyethylene terephthalate (PET) is the most common thermoplastic and has been widely used as material for fiber, film, containers and household consumables. As a consequence of the increasing rate of urbanization worldwide and the growth of global economy, the worldwide consumption of polyethylene terephthalate (PET) has been increasing steadily and rapidly, while *para*-xylene (pX), as the precursor of PET, is still mainly produced from fossil fuel.³⁰ Approximately 97% of pX is used to manufacture PET. The annual demand of pX has reached 36 million tons in 2014 and is estimated to exceed 62 million tons by 2020.³¹

Conventionally, xylenes are produced from petroleum refining or naphtha/gas oil cracking.³² High purity pX for PET synthesis can be obtained from the xylene rich mixture by either crystallization or adsorptive separation. Both process are energetically costly. Due to the urgent call for sustainable production of *p*-xylene, government organizations such as Department of Energy (DOE) and major consumers of PET bottles including Coca-Cola and Pepsi have been supporting research and development efforts for the production of renewable PET. Conversion of biomass-derived 2,5-dimethylfuran and ethylene into high purity *p*-xylene has attracted much attentions as one of the most promising methods.³³ The 2,5-dimethylfuran can be obtained from lignocellulose by several steps: 1) hydrolysis of lignocellulose to glucose, 2) catalytic isomerization and dehydration of glucose to 5-hydroxymethylfurfural (HMF) and 3) catalytic hydrodeoxygenation of HMF.^{34,35} Then the biomass-derived dimethylfuran can be upgraded to pX via Diels-Alder reaction with ethylene and dehydration/aromatization (Scheme **1.3**).

The Catalysis Center for Energy Innovation (CCEI) at the University of Delaware is an Energy Frontier Research Center established in 2009 and has been active in the innovation of heterogeneous catalysts technologies to transform lignocellulosic biomass materials into fuels and chemicals. One of the major research focuses is the upgrading of cellulose and hemicellulose to furans, and then to aromatics in a green and sustainable route. The discovery and optimization of beta-zeolite catalyst to convert 2,5-dimethylfuran and ethylene into *p*-xylene has reached impressive yield and selectivity.³⁶ The computational studies revealed that acidic zeolite catalyst only promoted the dehydration of 1,4-dimethyl-oxa-norbornene toward pX, while the Diel-Alder reaction of 2,5-dimethylfruan and ethylene to generate 1,4-

dimethyl-oxa-norbornene was uncatalyzed.³⁷ The big barrier between 2,5-dimethylfuran/ethylene and 1,4-dimethyl-oxa-norbornene not only limited the reaction rate but also increased energy (300 °C) and material (500 psi ethylene pressure) demands. Although 1,4-dimethyl-oxa-norbornene is widely accepted as the intermediate between 2,5-dimethylfuran/ethylene and pX, there is no literature report of the synthesis, isolation or characterization of this compound.^{38,39,40} As more and more parallel investigations of producing pX in a clean and sustainable way are in progress⁴¹, an efficient catalyst for Diels-Alder reaction of 2,5-dimethylfuran and ethylene would be the key to solving this difficult and important problem. And the synthesis and isolation of 1,4-dimethyl-oxa-norbornene could enable a search of the catalyst for the Diels-Alder reaction and provide us an insight of its properties and reactivity.



Scheme 1.3 Upgrade cellulose to para-xylene

In conclusion, the synthesis of Cr alkyl hydrides would expand the scope of this chemistry and should provide us new insights of C-H activation via first row transition metals. In the same fashion, the synthetic and kinetic study of 1,4-dimethyl-oxa-norbornene should be the key to enable a search of an efficient catalyst for Diels-Alder reaction. This thesis describes unique research in synthetic and reactivity studies of dinuclear chromium complexes supported by non-innocent α -diimine ligands and 1,4-dimethyl-oxa-norbornene, the intermediate from 2,5-dimethylfuran/ethylene toward *p*-xylene. Chapter 1 discusses the reactivity of quintuply bonded chromium dimer toward several unsaturated small molecules. Chapter 2 details the synthetic and activities investigations of a series of dinuclear chromium alkyl hydride complexes. Finally, Chapter 3 discusses the synthesis, stability and reactivity of 1,4-dimethyl-oxa-norbornene.

REFERENCES

1. L. B. Hunt, *Platinum Met. Rev.* **1984**, 28, 76W. C. Zeise, *Ann. Phys. (Berl.)* **1831**, 97, 497-541.
2. E. Frankland, *Q. J. Chem. Soc.* **1850**, 2, 263-296D. Seyferth, *Organomet.* **2001**, 20, 2940-2955.
3. L. Mond, C. Langer, F. Quincke, *J. Chem. Soc., Trans.* **1890**, 57, 749-753.
4. G. Bram, E. Peralez, J.-C. NÉgrel, M. Chanon, *Comptes Rendus Acad. Sci.* **1997**, 325, 235-240.
5. C. C. Johansson Seechurn, M. O. Kitching, T. J. Colacot, V. Snieckus, *Angew. Chem. Int. Ed. Engl.* **2012**, 51, 5062-5085.
6. G. C. Vougioukalakis, R. H. Grubbs, *Chem. Rev.* **2010**, 110, 1746-1787.
7. R. R. Schrock, A. H. Hoveyda, *Angew. Chem. Int. Ed. Engl.* **2003**, 42, 4592-4633.
8. Z. Zhang, N. A. Butt, W. Zhang, *Chem. Rev.* **2016**, 116, 14769-14827.
9. S. Murahashi, *J. Am. Chem. Soc.* **1955**, 77, 6403-6404.
10. J. Chatt, J. M. Davidson, *J. Chem. Soc.* **1965**.
11. Y. Fujiwara, I. Moritani, S. Danno, R. Asano, S. Teranishi, *J. Am. Chem. Soc.* **1969**, 91, 7166-7169.
12. J. K. Hoyano, W. A. G. Graham, *J. Am. Chem. Soc.* **1982**, 104, 3723-3725.
13. A. H. Janowicz, R. G. Bergman, *J. Am. Chem. Soc.* **1982**, 104, 352-354.
14. H. M. Davies, D. Morton, *J. Org. Chem.* **2016**, 81, 343-350.
15. T. Gensch, M. N. Hopkinson, F. Glorius, J. Wencel-Delord, *Chem. Soc. Rev.* **2016**, 45, 2900-2936.
16. D. S. Kim, W. J. Park, C. H. Jun, *Chem. Rev.* **2017**, 117, 8977-9015.
17. X. S. Xue, P. Ji, B. Zhou, J. P. Cheng, *Chem. Rev.* **2017**, 117, 8622-8648.

-
18. (a) X. X. Guo, D. W. Gu, Z. Wu, W. Zhang, *Chem. Rev.* **2015**, *115*, 1622-1651; (b) I. Bauer, H. J. Knolker, *Chem. Rev.* **2015**, *115*, 3170-3387; (c) S. Z. Tasker, E. A. Standley, T. F. Jamison, *Nature* **2014**, *509*, 299-309; (d) G. Cahiez, A. Moyeux, *Chem. Rev.* **2010**, *110*, 1435-1462.
 19. T. M. Gogsig, J. Kleimark, S. O. Lill, S. Korsager, A. T. Lindhardt, P. O. Norrby, T. Skrydstrup, *J. Am. Chem. Soc.* **2012**, *134*, 443-452.
 20. F. S. Han, *Chem. Soc. Rev.* **2013**, *42*, 5270-5298.
 21. W. Dai, J. Xiao, G. Jin, J. Wu, S. Cao, *J. Org. Chem.* **2014**, *79*, 10537-10546.
 22. D. Haas, J. M. Hammann, R. Greiner, P. Knochel, *ACS Catal.* **2016**, *6*, 1540-1552.
 23. L. A. MacAdams, G. P. Buffone, C. D. Incarvito, J. A. Golen, A. L. Rheingold, K. H. Theopold, *Chem. Commun. (Camb.)* **2003**, 1164-1165.
 24. J. R. Hagadorn, M. J. McNevin, *Organomet.* **2003**, *22*, 609-611.
 25. A. Lennartson, M. Hakansson, S. Jagner, *Angew. Chem. Int. Ed. Engl.* **2007**, *46*, 6678-6680.
 26. W. H. Monillas, G. P. Yap, K. H. Theopold, *Angew. Chem. Int. Ed. Engl.* **2007**, *46*, 6692-6694.
 27. P. Cui, T. P. Spaniol, L. Maron, J. Okuda, *Chem. Commun. (Camb.)* **2014**, *50*, 424-426.
 28. Q. Liu, L. Wu, R. Jackstell, M. Beller, *Nat. Commun.* **2015**, *6*, 5933.
 29. D. Carpenter, T. L. Westover, S. Czernik, W. Jablonski, *Green Chem.* **2014**, *16*, 384-406.
 30. M. J. Bidy, C. Scarlata, C. Kinchin, *Chemicals from Biomass: A Market Assessment of Bioproducts with Near-Term Potential*, NREL/TP-5100-65509, **2016**

-
31. Paraxylene Market Analysis By Application (Dimethyl Terephthalate (DMT), Purified Terephthalic Acid (PTA)) And Segment Forecasts To 2022
32. H. O'Neil, P. Wantanachaisaeng, *Capturing Opportunities for para-Xylene Production: A Report from the Aromatics (Thailand) Public Co., Ltd. And UOP LLC*, **2007**.
33. (a) J. Y. Yu, S. Y. Zhu, P. J. Dauenhauer, H. J. Cho, W. Fan, R. J. Gorte, *Catal Sci Technol* **2016**, *6*, 5729-5736; (b) J. J. Pacheco, J. A. Labinger, A. L. Sessions, M. E. Davis, *ACS Catal.* **2015**, *5*, 5904-5913; (c) X. Feng, C. Shen, C. Tian, T. Tan, *Ind. Eng. Chem. Res.* **2017**, *56*, 5852-5859; (d) J. C. Kim, T. W. Kim, Y. Kim, R. Ryoo, S. Y. Jeong, C. U. Kim, *Appl. Catal., B* **2017**, *206*, 490-500; (e) Y. P. Wijaya, H. P. Winoto, Y. K. Park, D. J. Suh, H. Lee, J. M. Ha, J. Jae, *Catal. Today* **2017**, *293*, 167-175.
34. J. B. Binder, R. T. Raines, *J. Am. Chem. Soc.* **2009**, *131*, 1979-1985.
35. T. Thananathanachon, T. B. Rauchfuss, *Angew. Chem. Int. Ed. Engl.* **2010**, *49*, 6616-6618.
36. (a) C. C. Chang, S. K. Green, C. L. Williams, P. J. Dauenhauer, W. Fan, *Green Chem.* **2014**, *16*, 585-588; (b) E. Mahmoud, J. Yu, R. J. Gorte, R. F. Lobo, *ACS Catal.* **2015**, *5*, 6946-6955; (c) N. Nikbin, S. Caratzoulas, D. G. Vlachos, *ChemSusChem* **2013**, *6*, 2066-2068; (d) C. L. Williams, C. C. Chang, P. Do, N. Nikbin, S. Caratzoulas, D. G. Vlachos, R. F. Lobo, W. Fan, P. J. Dauenhauer, *ACS Catal.* **2012**, *2*, 935-939.
37. (a) C. L. Williams, C. C. Chang, P. Do, N. Nikbin, S. Caratzoulas, D. G. Vlachos, R. F. Lobo, W. Fan, P. J. Dauenhauer, *ACS Catal.* **2012**, *2*, 935-939; (b) R. E. Patet, W. Fan, D. G. Vlachos, S. Caratzoulas, *Chemcatchem* **2017**, *9*, 2523-2535; (c) R. E. Patet, M. Koehle, R. F. Lobo, S. Caratzoulas, D. G. Vlachos, *J. Phys. Chem. C* **2017**, *121*, 13666-13679; (d) Y.-P. Li, M. Head-Gordon, A. T. Bell, *J. Phys. Chem. C* **2014**, *118*, 22090-22095.
38. P. T. Do, J. R. McAtee, D. A. Watson, R. F. Lobo, *ACS Catal.* **2013**, *3*, 41-46.
39. M. Ines, A. J. Mendonca, A. P. Esteves, D. I. Mendonca, M. J. Medeiros, *C R Chim* **2009**, *12*, 841-849.

-
40. G. O. Schenck, K. Gollnick, G. Buchwald, S. Schroeter, G. Ohloff, *Liebigs Ann.* **1964**, 674, 93-117.
41. (a) J. J. Pacheco, J. A. Labinger, A. L. Sessions, M. E. Davis, *ACS Catal.* **2015**, 5, 5904-5913; (b) X. Feng, C. Shen, C. Tian, T. Tan, *Ind. Eng. Chem. Res.* **2017**, 56, 5852-5859; (c) J. C. Kim, T. W. Kim, Y. Kim, R. Ryoo, S. Y. Jeong, C. U. Kim, *Appl. Catal., B* **2017**, 206, 490-500; (d) Y. P. Wijaya, H. P. Winoto, Y. K. Park, D. J. Suh, H. Lee, J. M. Ha, J. Jae, *Catal. Today* **2017**, 293, 167-175; (e) B. Saha, M. M. Abu-Omar, *ChemSusChem* **2015**, 8, 1133-1142; (f) M. Shiramizu, F. D. Toste, *Chem. Eur. J.* **2011**, 17, 12452-12457; (g) S. Song, G. J. Wu, W. L. Dai, N. J. Guan, L. D. Li, *J. Mol. Catal. A: Chem.* **2016**, 420, 134-141; (h) I. F. Teixeira, B. T. Lo, P. Kostetsky, M. Stamatakis, L. Ye, C. C. Tang, G. Mpourmpakis, S. C. Tsang, *Angew. Chem. Int. Ed. Engl.* **2016**, 55, 13061-13066; (i) D. Wang, C. M. Osmundsen, E. Taarning, J. A. Dumesic, *Chemcatchem* **2013**, 5, 2044-2050.

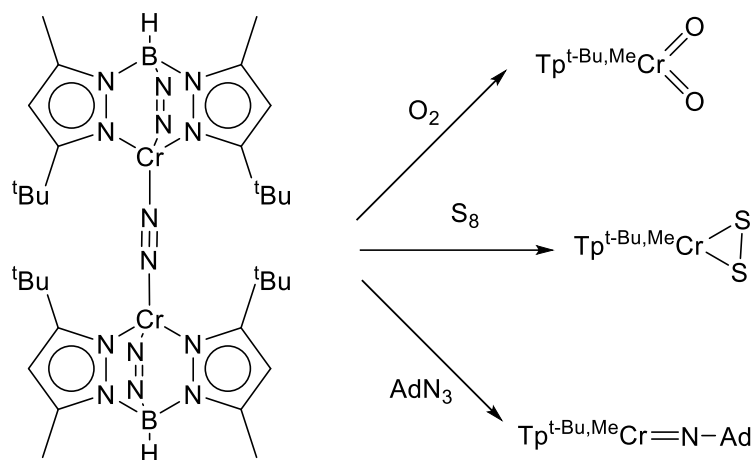
Chapter 2

THE REACTIVITY OF A QUINTUPLE-BONDED CHROMIUM DIMER SUPPORTED BY α -DIIMINE LIGANDS

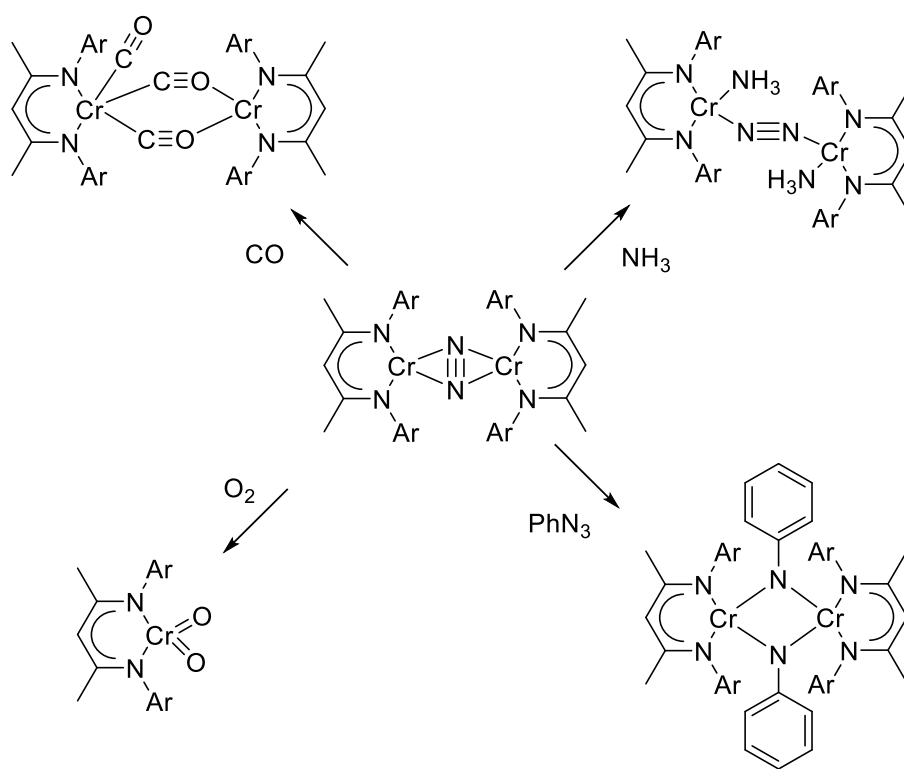
2.1 Introduction

Small molecule activation has always been a hot topic in inorganic and organometallic chemistry due to abundance of the former and the potential applications. Numerous transition metal complexes have been designed and synthesized to activate small molecules.¹ Activation of small molecules implies change of molecule's structure and electronic configuration; this can result in the small molecule simply binding to the metal center or in its use as a building block to synthesize other molecules.

Our group has been interested in small molecule activation with chromium complexes using different ligand systems, such as tris(pyrazolyl)borate (Tp), β -diketiminato (NacNac) and α -diimine (L). Recently, Akturk *et al.* have reported that chromium dinitrogen complex ($\text{Tp}^{\text{-Bu,Me}}\text{Cr}$)₂N₂ can activate different kinds of small molecules (Scheme 2.1).² In the nacnac ligand system, Monillas *et al.* reported that nacnac chromium(I) complex can simply replace the dinitrogen ligand or the acetylene ligand with other small molecules to generate new complexes (Scheme 2.2).³

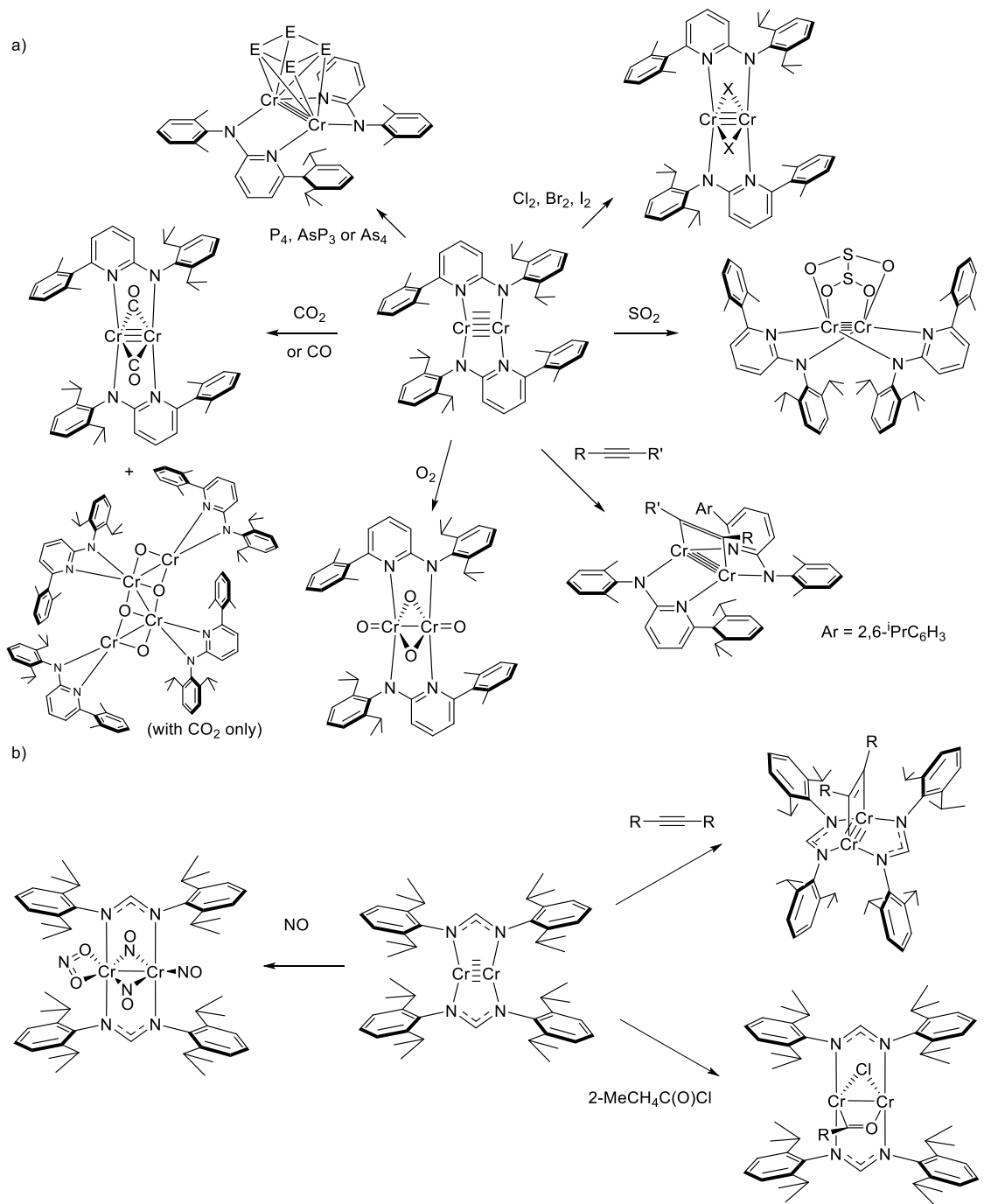


Scheme 2.1 Small molecule activation with $(\text{Tp}^{t\text{-Bu,Me}}\text{Cr})_2\text{N}_2$

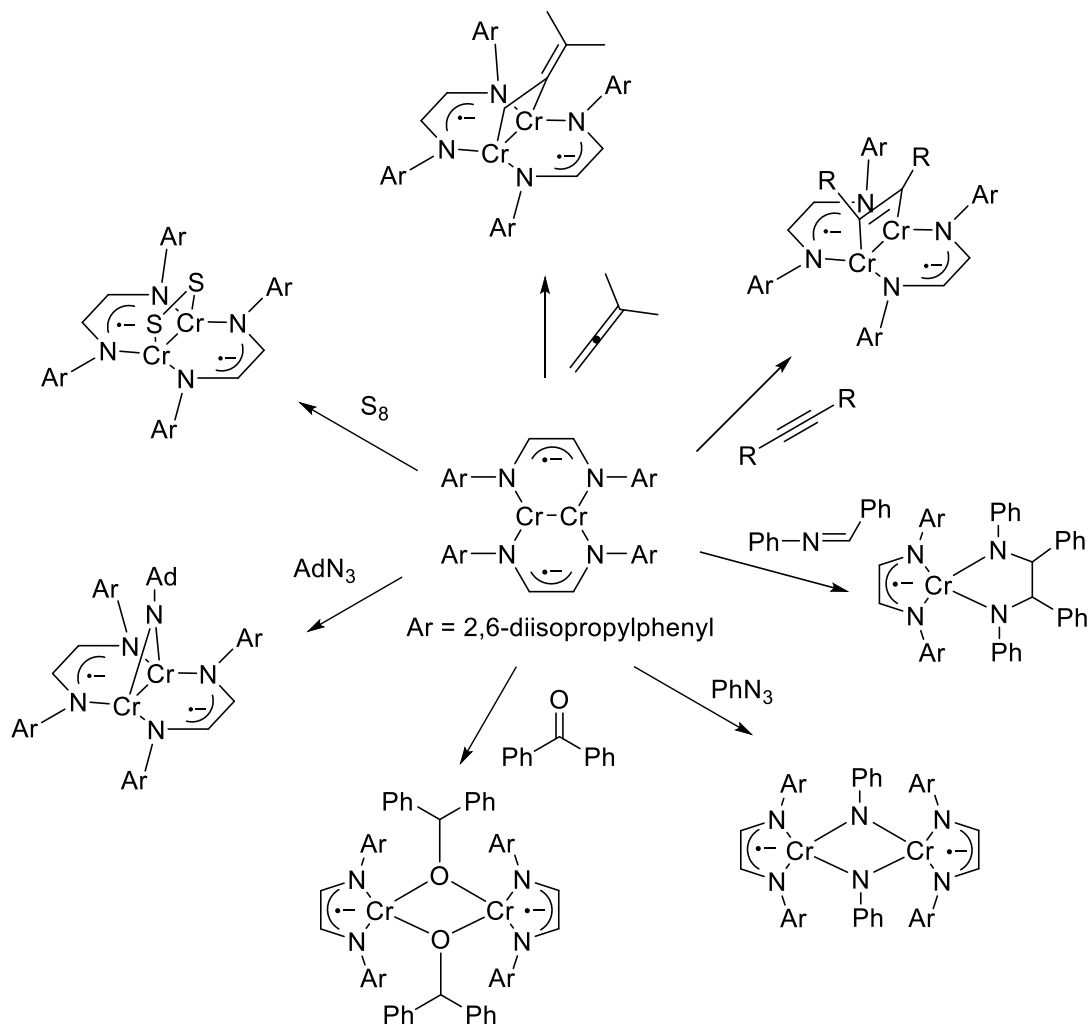


Scheme 2.2 Small molecule activation with $(\text{NacNacCr})_2\text{N}_2$

Due to the rarity of quintuply bonded transition metal complexes, their reactivity remains largely unexplored. Early examples include the carboalumination of the quintuply bonded aminopyridinate Cr dimer and NO and adamantanyl azide activation of $\text{Ar}'\text{CrCrAr}'$ ($\text{Ar}'=\text{C}_6\text{H}_3\text{-2,6-(C}_6\text{H}_3\text{-2,6-}^i\text{Pr}_2)_2$).^{4, 5} In 2011, Kempe *et al.* reported the synthesis and characterization of several Cr-Cr quadruple bond adducts with unsaturated small molecules (P_4 , As_4 , AsP_3).⁶ Later in 2014 they reported that the amino-pyridinato dichromium quintuple bond complex could also activate CO_2 and SO_2 to give new complexes (Scheme **2.3 a**).⁷ The Cr-Cr quintuple bond complex supported by amidinate ligand also shows reactivity with small molecules as reported by Tsai *et al* (Scheme **2.3 b**).⁸ Recently, Shen *et al.* have shown that Cr-Cr quintuple bonds complex bearing α -diimine ligands can bind and activate a series of small molecules featuring C-C, C-O, C-S or N-N multiple bonds, and give mono- or dinuclear complexes: $[\text{HL}^{\text{iPr}}\text{Cr}]_2(\mu\text{-}\eta^1\text{:}\eta^1\text{-H}_2\text{CCMe}_2)$, $[\text{HL}^{\text{iPr}}\text{Cr}]_2(\text{S}_2)$, $[\text{HL}^{\text{iPr}}\text{Cr}(\mu\text{-NPh})]_2$, $[\text{HL}^{\text{iPr}}\text{Cr}]_2(\text{NAd})$, $[\text{HL}^{\text{iPr}}\text{Cr}(\mu\text{-OCPh}_2)]_2$ and $[\text{HL}^{\text{iPr}}\text{Cr}(\kappa_2\text{-N}_2\text{C}_{28}\text{H}_{22})]$ (Scheme **2.4**).⁹

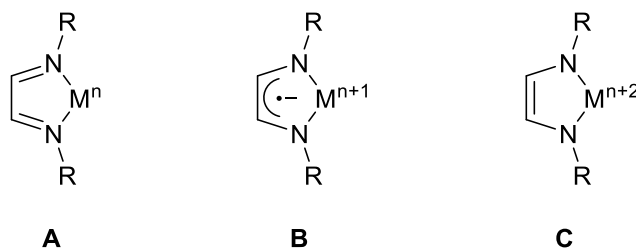


Scheme 2.3 Small molecule activation with Cr-Cr quintuply bonded complexes.



Scheme 2.4 Small molecule activation with $(\mu\text{-}\eta^1\text{:}\eta^1\text{-HLiPr})_2\text{Cr}_2$

α -Diimine ligands are well known as a growing group of redox non-innocent ligands.¹⁰ Their electronic structure reflects the three oxidation levels of the ligands: the neutral α -diimine A, the monoanionic π radical B and the two-electron reduced enediamide form C (Scheme 2.5). With the help of X-ray crystallography, the oxidation state of the diimine can be assigned by comparing the C-N and C-C bond lengths in ligand backbone (Table 2.1).^{11, 12}



Scheme 2.5 The metal-ligand redox interaction in α -diimine complexes

Table 2.1 Bond distances (\AA) of the α -diimine backbone for the α -diimine ligand in various oxidation states.

Compound	C-N Distances (\AA)	C-C Distances (\AA)
$[\text{HL}^{\text{iPr}}]$	1.263(2)	1.468(2)
$[\text{HL}^{\text{tBu}}]^-$ ^a	1.32(1), 1.33(1)	1.41(1), 1.40(1)
$[\text{HL}^{\text{iPr}}]^{2-}$	1.423(4), 1.409(4), 1.403(4), 1.431(4)	1.352(4), 1.355(4)

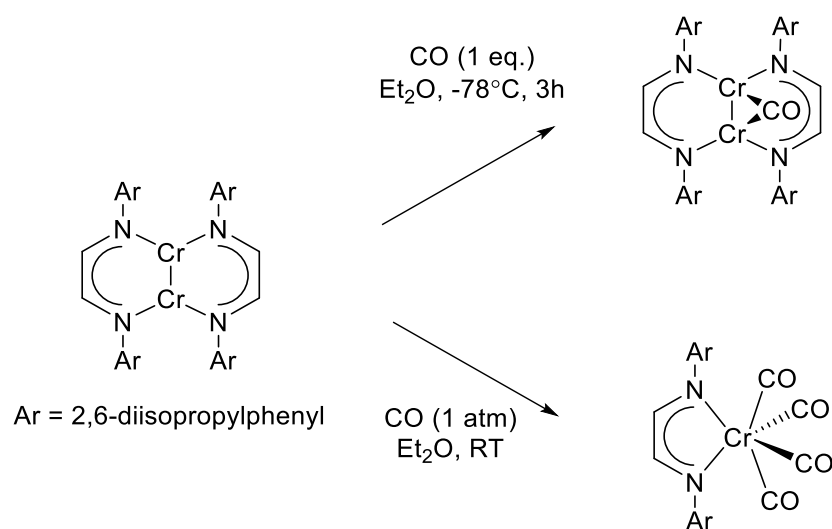
(a) t-butyl groups are bound directly to the diimine nitrogen atoms.

As shown in Table 2.1, the neutral α -diimine ligand has a pair of C-N double bond with bond length around 1.26 \AA and a C-C single bond with bond length around 1.46 \AA . For dianionic α -diimine ligand, the C-N bond length around 1.42 \AA is clearly single bonded and the C-C bond length around 1.35 \AA shows double bonded features. If the C-N and C-C bond lengths fall in between single bonded and double bonded range (C-N \sim 1.32 \AA and C-C \sim 1.40 \AA), the α -diimine ligand would be considered as monoanionic.

This chapter presents the different reactivity of the dinuclear quintuply bonded Cr complex $(\mu-\eta^1:\eta^1\text{-HL}^{\text{iPr}})_2\text{Cr}_2$ with several gaseous small molecules with carbon-chalcogen multiple bonds. CO, CO₂ and CS₂, were reacted with $(\mu-\eta^1:\eta^1\text{-HL}^{\text{iPr}})_2\text{Cr}_2$ in stoichiometric amount and gave three unique structures namely: $[\text{HL}^{\text{iPr}}\text{Cr}](\mu\text{-CO})$, $(\mu-\eta^1:\eta^1\text{-L})_2\text{Cr}_2$ and $[\text{HL}^{\text{iPr}}\text{Cr}]_2(\mu-\eta^2:\eta^2\text{-CS})(\mu\text{-S})$.

2.2 Results and Discussion

With the help of transition metal catalysts carbon monoxide has been utilized in organic synthesis as C1 building block, such as Pauson-Khand reaction¹³, aminocarbonylation¹⁴ and carbonylative cross coupling¹⁵. Previously, Shen *et al.* have reported that the reaction of $(\mu-\eta^1:\eta^1\text{-HL}^{\text{iPr}})_2\text{Cr}_2$ with excess of carbon monoxide produces diamagnetic monomeric $\text{HL}^{\text{iPr}}\text{Cr}(\text{CO})_4$, as confirmed by $^1\text{H-NMR}$ spectroscopy and X-ray crystallography. An intermediate was observed by $^1\text{H-NMR}$ with chemical shifts at 5.62 and 1.03 ppm. It is of some interest to synthesize and isolate the intermediate and to explore its properties. By treating an Et_2O solution of $(\mu-\eta^1:\eta^1\text{-HL}^{\text{iPr}})_2\text{Cr}_2$ with 1 eq. of carbon monoxide at -78°C , a diamagnetic dinuclear monocarbonyl chromium complex, namely $[\text{HL}^{\text{iPr}}\text{Cr}](\mu\text{-CO})$, **1**, was synthesized and captured (Scheme 2.6).



Scheme 2.6 CO addition of $(\mu-\eta^1:\eta^1\text{-HL}^{\text{iPr}})_2\text{Cr}_2$

1 is both air- and heat-sensitive. Any excess of CO would lead to further reaction to $\text{H}^{\text{iPr}}\text{Cr}(\text{CO})_4$, and gentle heat would remove CO ligand from the complex to give the isomer of quintuple bond Cr dimer, i.e. $(\mu\text{-}\eta^2\text{:}\eta^6\text{-H}^{\text{iPr}})_2\text{Cr}_2$. For comparison, the quintuply bonded Cr-Cr complex supported by aminopyridinato ligand, the reactions with CO or CO_2 gave a similar CO bridging complex as reported by Kempe *et al.* (Scheme **2.3 a**).⁷ **1** has been characterized by X-ray diffraction; the solid state structure, interatomic distances, and angles for **1** are displayed in Figure **2.1** and Table **2.2** respectively.

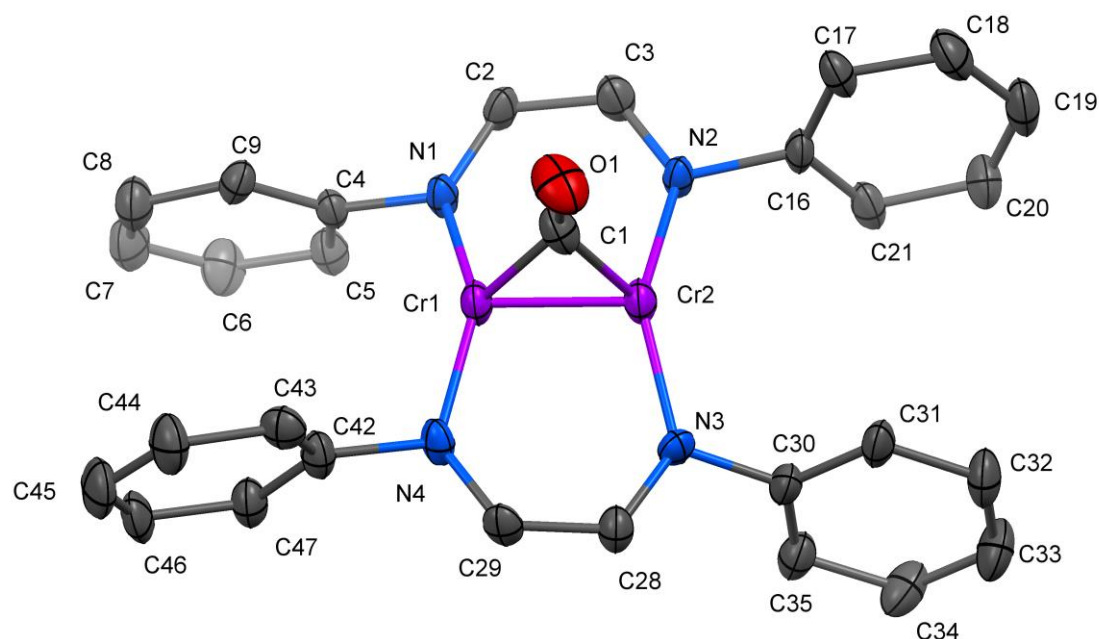


Figure 2.1 Molecular structure of $[\text{H}^{\text{iPr}}\text{Cr}](\mu\text{-CO})$ (**1**) with thermal ellipsoids at the 30% probability level. Isopropyl groups and hydrogen atoms have been omitted for clarity.

Table 2.2 Interatomic distances (Å) and angles (°) for [HLⁱPrCr](μ-CO) (1).

Distances (Å)			
Cr1-N1	1.879(5)	Cr1-N4	1.912(5)
Cr1-Cr2	1.964(2)	Cr1-C1	2.021(8)
Cr2-N3	1.873(5)	Cr2-N2	1.887(5)
Cr2-C1	2.016(8)	O1-C1	1.150(8)
N1-C2	1.368(8)	N1-C4	1.463(8)
N2-C3	1.357(8)	N2-C16	1.484(8)
N3-C28	1.380(8)	N3-C30	1.436(8)
N4-C29	1.364(7)	N4-C42	1.479(8)
C2-C3	1.389(8)	C4-C9	1.375(9)
C4-C5	1.407(9)	C5-C6	1.427(9)
C5-C11	1.514(9)	C6-C7	1.357(9)
C7-C8	1.36(1)	C8-C9	1.414(9)
C9-C14	1.494(9)	C10-C11	1.524(9)
C11-C12	1.544(9)	C13-C14	1.527(9)
C14-C15	1.541(8)	C16-C21	1.394(9)
C16-C17	1.399(9)	C17-C18	1.384(9)
C17-C23	1.513(9)	C18-C19	1.37(1)
C19-C20	1.36(1)	C20-C21	1.420(9)
C21-C26	1.48(1)	C22-C23	1.512(9)
C23-C24	1.546(9)	C25-C26	1.526(9)
C26-C27	1.569(9)	C28-C29	1.364(8)
C30-C35	1.388(9)	C30-C31	1.408(9)
C31-C32	1.417(9)	C31-C37	1.49(1)
C32-C33	1.356(9)	C33-C34	1.363(9)
C34-C35	1.399(9)	C35-C40	1.55(1)
C36-C37	1.540(9)	C37-C38	1.54(1)
C39-C40	1.526(9)	C40-C41	1.514(9)
C42-C43	1.361(9)	C42-C47	1.423(9)
C43-C44	1.414(9)	C43-C49	1.503(9)
C44-C45	1.37(1)	C45-C46	1.373(9)
C46-C47	1.404(9)	C47-C52	1.504(9)

C48-C49	1.499(9)	C49-C50	1.543(9)
C51-C52	1.520(8)	C52-C53	1.510(9)
C54-C55	1.5045	C55-C60	1.3993
C55-C56	1.3994	C56-C57	1.3939
C57-C58	1.3936	C58-C59	1.3937
C59-C60	1.3939		

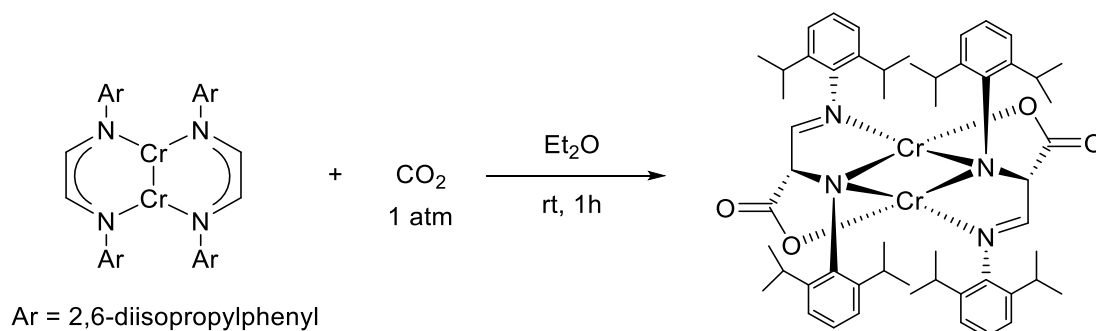
Angles (°)

N1-Cr1-N4	146.9(2)	N1-Cr1-Cr2	101.8(2)
N4-Cr1-Cr2	104.8(2)	N1-Cr1-C1	109.9(3)
N4-Cr1-C1	100.2(3)	Cr2-Cr1-C1	60.7(2)
N3-Cr2-N2	146.8(3)	N3-Cr2-Cr1	102.7(2)
N2-Cr2-Cr1	104.8(2)	N3-Cr2-C1	107.1(3)
N2-Cr2-C1	102.4(3)	Cr1-Cr2-C1	61.0(2)
C2-N1-C4	112.9(5)	C2-N1-Cr1	132.9(5)
C4-N1-Cr1	114.2(4)	C3-N2-C16	113.9(6)
C3-N2-Cr2	132.2(5)	C16-N2-Cr2	113.1(4)
C28-N3-C30	112.6(6)	C28-N3-Cr2	132.3(5)
C30-N3-Cr2	115.1(5)	C29-N4-C42	113.5(6)
C29-N4-Cr1	130.8(5)	C42-N4-Cr1	114.9(5)
O1-C1-Cr2	151.0(7)	O1-C1-Cr1	150.7(7)
Cr2-C1-Cr1	58.2(2)	N1-C2-C3	122.5(7)
N2-C3-C2	122.3(7)	C9-C4-C5	123.2(7)
C9-C4-N1	120.9(7)	C5-C4-N1	115.8(6)
C4-C5-C6	117.2(7)	C4-C5-C11	123.4(7)
C6-C5-C11	119.4(7)	C7-C6-C5	119.6(8)
C6-C7-C8	121.9(8)	C7-C8-C9	121.4(8)
C4-C9-C8	116.6(7)	C4-C9-C14	121.6(7)
C8-C9-C14	121.6(7)	C5-C11-C10	110.9(7)
C5-C11-C12	111.6(6)	C10-C11-C12	110.4(7)
C9-C14-C13	109.6(6)	C9-C14-C15	114.3(6)
C13-C14-C15	110.2(6)	C21-C16-C17	123.9(7)
C21-C16-N2	117.9(7)	C17-C16-N2	118.3(7)

C18-C17-C16	116.9(8)	C18-C17-C23	120.1(8)
C16-C17-C23	123.0(7)	C19-C18-C17	121.4(8)
C20-C19-C18	121.1(8)	C19-C20-C21	121.1(8)
C16-C21-C20	115.6(8)	C16-C21-C26	124.9(7)
C20-C21-C26	119.5(8)	C17-C23-C22	112.1(7)
C17-C23-C24	110.1(7)	C22-C23-C24	110.7(7)
C21-C26-C25	116.9(7)	C21-C26-C27	109.2(7)
C25-C26-C27	107.4(7)	C29-C28-N3	123.7(7)
N4-C29-C28	123.2(7)	C35-C30-C31	122.0(7)
C35-C30-N3	119.3(7)	C31-C30-N3	118.7(7)
C30-C31-C32	115.9(8)	C30-C31-C37	122.2(7)
C32-C31-C37	121.8(7)	C33-C32-C31	122.0(8)
C32-C33-C34	120.9(8)	C33-C34-C35	120.3(8)
C30-C35-C34	118.8(7)	C30-C35-C40	121.4(7)
C34-C35-C40	119.8(8)	C31-C37-C38	108.7(7)
C31-C37-C36	115.2(7)	C38-C37-C36	110.7(7)
C41-C40-C39	110.1(7)	C41-C40-C35	111.3(7)
C39-C40-C35	111.0(6)	C43-C42-C47	124.6(7)
C43-C42-N4	118.7(7)	C47-C42-N4	116.5(7)
C42-C43-C44	117.6(8)	C42-C43-C49	124.8(7)
C44-C43-C49	117.6(8)	C45-C44-C43	120.2(8)
C44-C45-C46	120.7(8)	C45-C46-C47	122.4(8)
C46-C47-C42	114.4(7)	C46-C47-C52	122.6(7)
C42-C47-C52	122.8(7)	C48-C49-C43	114.2(7)
C48-C49-C50	112.8(7)	C43-C49-C50	108.9(6)
C47-C52-C53	111.6(7)	C47-C52-C51	113.5(6)
C53-C52-C51	108.6(7)	C60-C55-C56	118.1
C60-C55-C54	121.0	C56-C55-C54	121.0
C57-C56-C55	121.1	C58-C57-C56	120.1
C57-C58-C59	119.4	C58-C59-C60	120.1
C59-C60-C55	121.1		

1 crystallizes in the monoclinic space group $P2_1/n$. The carbon monoxide interacts with quintuple bond via a [2+1] cycloaddition and gives a coplanar μ_2 -CO triangle geometry. This structure is similar to the selenide, telluride and 1-azidoadamantane adducts of $(\mu\text{-}\eta^1\text{:}\eta^1\text{-HL}^{\text{iPr}})_2\text{Cr}_2$ and is comparable to Kempe's $\text{Cr}_2(\mu\text{-CO})_2$ adduct (Scheme **2.3a**).⁷ The C-O bond length of 1.150(8) Å in **1** is slightly longer than neutral CO bond distance of 1.128 Å, and is similar to CO bond length of 1.154(8) in Kempe's $\text{Cr}_2(\mu\text{-CO})_2$. And the newly formed Cr-C single bonds with bond length of 2.021(8) Å and 2.016(8) Å are significantly longer than Cr-C bond length in $(\text{HL}^{\text{iPr}})\text{Cr}(\text{CO})_4$ (average Cr-C = 1.882 (2) Å), but are slightly shorter than those in Kempe's $\text{Cr}_2(\mu\text{-CO})_2$ (Cr-C = 2.092(8) and 2.066(8) Å). The CO stretching frequency of 1758 cm^{-1} is on the edge of μ_2 -bridging carbonyl infrared stretching frequencies (1850 – 1750 cm^{-1}). Kempe's $\text{Cr}_2(\mu\text{-CO})_2$ adduct has higher wave number absorption bands at 1924 and 1806 cm^{-1} . The C-N bond length of ligand backbone range from 1.357(8) to 1.380(8) Å and the C-C bond length are 1.389(8) and 1.364(8) Å. There is no appreciable change in the backbone bond lengths of the diimine ligands between **1** and $(\mu\text{-}\eta^1\text{:}\eta^1\text{-HL}^{\text{iPr}})_2\text{Cr}_2$, thus **1** is best described as Cr(I)-Cr(I) complex. The Cr-Cr bond of 1.964(2) Å falls into the range of 'super-short' chromium-chromium quadruple bonds (Cr-Cr < 2.0 Å).¹⁶ The Cr-Cr distances in selenide, telluride and 1-azidoadamantane adducts of $(\mu\text{-}\eta^1\text{:}\eta^1\text{-HL}^{\text{iPr}})_2\text{Cr}_2$ are 1.919(1), 1.918(2) and 1.9557(9) Å respectively. Considering that both chromium ions are Cr(I) d^5 , **2** still has a Cr-Cr quintuple bond. The elongation of the Cr-Cr multiple bonds is presumably due to the formation of two new Cr-C covalent bonds. In Kempe's aminopyridinato ligand system, the Cr-Cr distance in $\text{Cr}_2(\mu\text{-CO})_2$ is 1.89(2) Å. This complex is diamagnetic due to extensive metal-metal bonds. The broaden ¹H-NMR resonances and chemical

shifts at 6.99-6.75, 5.62, 3.31, 1.41, 1.03 and 0.75 ppm are almost identical to those of $(\mu\text{-}\eta^1\text{:}\eta^1\text{-H}^{\text{iPr}})_2\text{Cr}_2$. **1** is relatively unstable and slowly decomposes into $(\mu\text{-}\eta^1\text{:}\eta^1\text{-H}^{\text{iPr}})_2\text{Cr}_2$ and $\text{H}^{\text{iPr}}\text{Cr}(\text{CO})_4$ over time, even at $-30\text{ }^\circ\text{C}$. Treatment of **1** with other small molecules like ethylene or THF resulted in ligand replacement and formation of $\text{H}^{\text{iPr}}\text{Cr}(\text{CO})_4$.



Scheme 2.7 Reaction of $(\mu\text{-}\eta^1\text{:}\eta^1\text{-H}^{\text{iPr}})_2\text{Cr}_2$ and CO_2

Valorization of carbon dioxide as chemical feedstock has been intensely studied for decades.^{17,18,19} Some reactions have even been industrialized, such as synthesis of ethene carbonate from ethylene and CO_2 , conversion of CO_2 and ammonia into urea, and production of salicylic acid by pressuring sodium phenol salt with CO_2 .²⁰ Due to the fact that CO_2 is the most oxidized form of carbon and is thermodynamically stable, activation and utilization of carbon dioxide has been challenging. It was interesting to see if the Cr quintuple bond complex is able to activate CO_2 . The ten electrons held in between two low valent Cr centers might be the key to reduce CO_2 . Exposure of a diethyl ether solution of $(\mu\text{-}\eta^1\text{:}\eta^1\text{-H}^{\text{iPr}})_2\text{Cr}_2$ to 1 atmosphere of carbon dioxide at room temperature caused an instant color change

from green to blue and then to red. The $^1\text{H-NMR}$ of the red species in C_6D_6 showed a series of broad resonance with chemical shifts at 7.34-6.57, 1.95, 1.73, 1.41 and 1.00 ppm. After standard work up, diimine ligand activated complex $(\text{L-CO}_2)_2\text{Cr}_2$ (**2**) was synthesized, isolated and characterized by X-ray crystallography (Scheme 2.7) The solid state structure, bond distances, and angle for **2** are displayed in Figure 2.2 and Table 2.3 respectively.

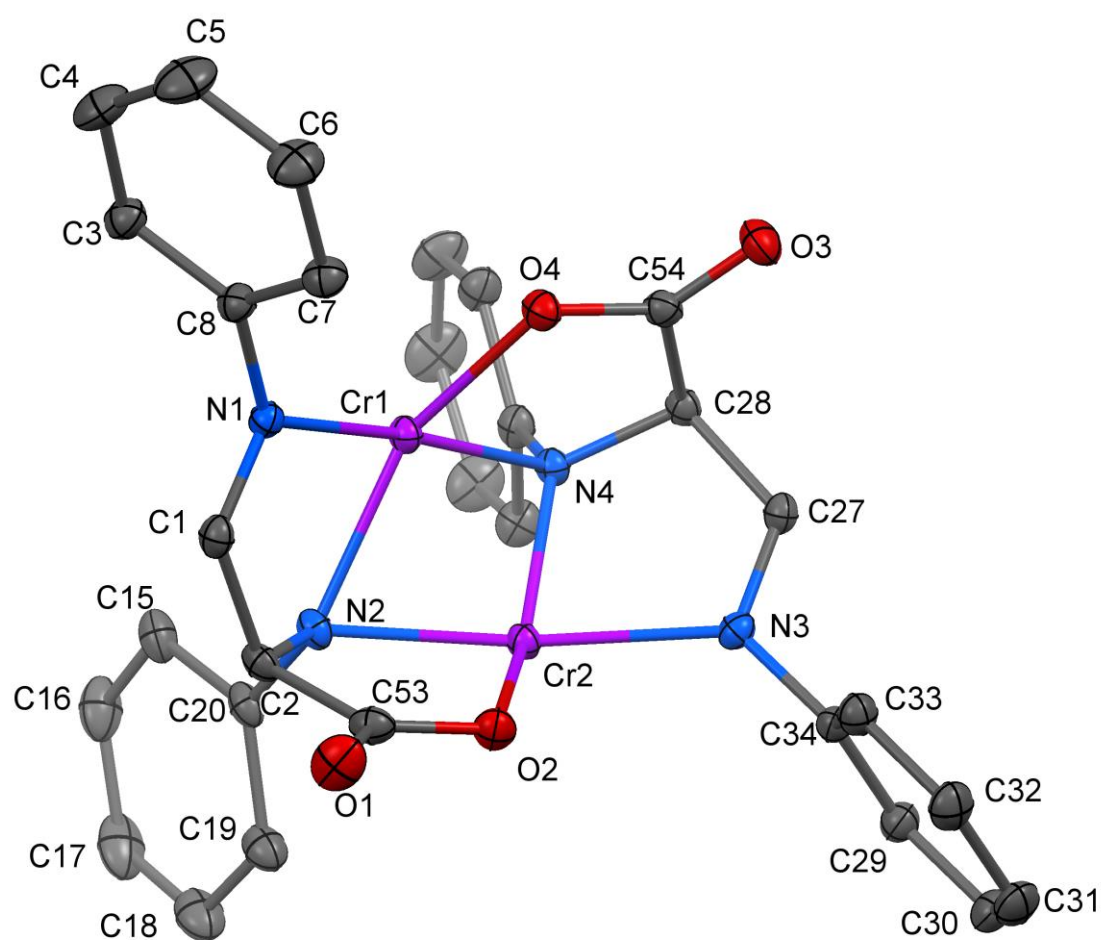


Figure 2.2 Molecular structure of $(\text{L-CO}_2)_2\text{Cr}_2$ (**2**) with thermal ellipsoids at the 30% probability level. Isopropyl groups and hydrogen atoms have been omitted for clarity.

Table 2.3 Interatomic distances (Å) and angles (°) for $(\mu\text{-}\eta^1\text{:}\eta^1\text{-L})_2\text{Cr}_2$ (2).

Distances (Å)			
Cr1-O4	1.967(2)	C15-C22	1.507(4)
Cr1-N4	2.044(2)	C16-C17	1.367(4)
Cr1-N1	2.081(2)	C17-C18	1.365(4)
Cr1-N2	2.109(2)	C18-C19	1.396(3)
Cr1-Cr2	2.3343(4)	C19-C20	1.418(3)
Cr2-O2	1.978(2)	C19-C25	1.518(4)
Cr2-N2	2.047(2)	C21-C22	1.521(4)
Cr2-N3	2.087(2)	C22-C23	1.537(3)
Cr2-N4	2.116(2)	C24-C25	1.511(4)
N1-C1	1.277(3)	C25-C26	1.517(4)
N1-C8	1.456(3)	C27-C28	1.505(3)
N2-C20	1.459(3)	C28-C54	1.573(3)
N2-C2	1.484(2)	C29-C34	1.399(3)
N3-C27	1.279(3)	C29-C30	1.394(3)
N3-C34	1.460(2)	C29-C36	1.512(3)
N4-C46	1.462(2)	C30-C31	1.377(3)
N4-C28	1.479(2)	C31-C32	1.377(3)
O1-C53	1.216(2)	C32-C33	1.396(3)
O2-C53	1.295(2)	C33-C34	1.399(3)
O3-C54	1.220(2)	C33-C39	1.514(3)
O4-C54	1.292(2)	C35-C36	1.534(4)
C1-C2	1.506(3)	C36-C37	1.526(4)
C2-C53	1.561(3)	C38-C39	1.539(3)
C3-C8	1.395(3)	C39-C40	1.526(3)
C3-C4	1.393(3)	C41-C42	1.398(3)
C3-C10	1.512(3)	C41-C46	1.407(3)
C4-C5	1.378(4)	C41-C48	1.512(3)
C5-C6	1.377(4)	C42-C43	1.369(4)
C6-C7	1.393(3)	C43-C44	1.372(4)
C7-C8	1.403(3)	C44-C45	1.398(3)
C7-C13	1.511(3)	C45-C46	1.422(3)
C9-C10	1.533(3)	C45-C51	1.525(3)
C10-C11	1.522(3)	C47-C48	1.525(4)
C12-C13	1.533(3)	C48-C49	1.531(3)
C13-C14	1.530(3)	C50-C51	1.534(3)
C15-C16	1.397(3)	C51-C52	1.526(3)
C15-C20	1.414(3)		

Angles (°)

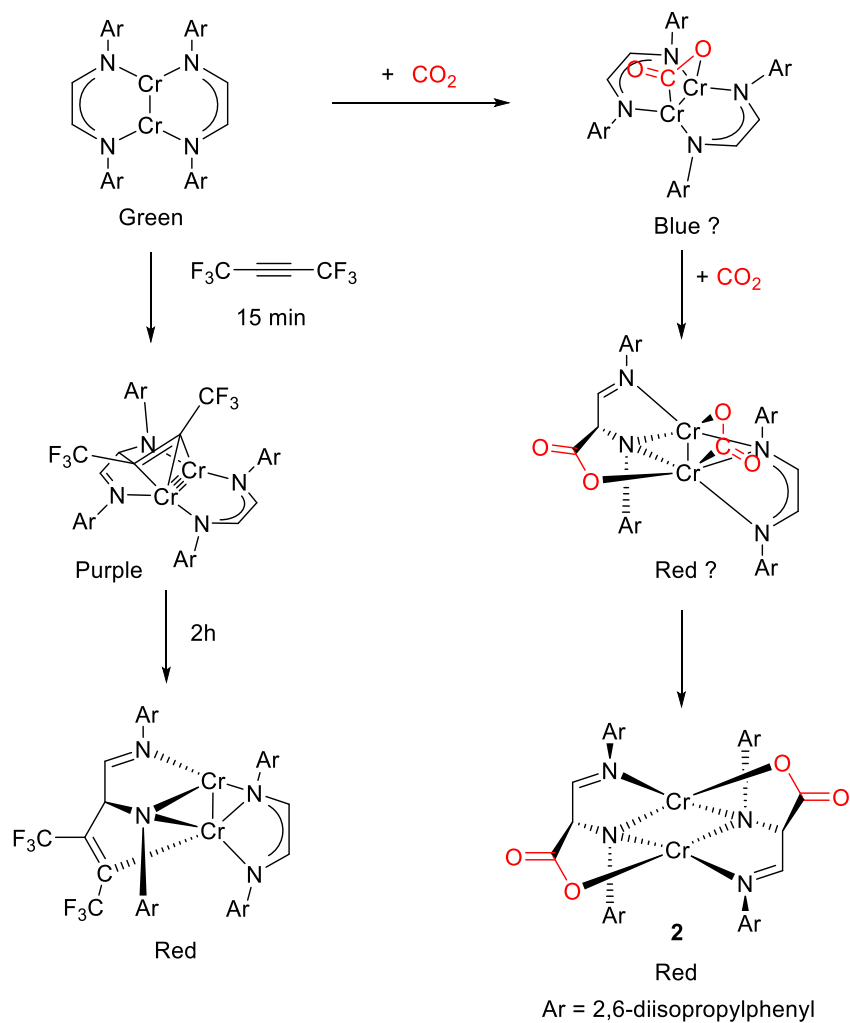
O4-Cr1-N4	84.16(6)	C16-C15-C22	116.8(2)
O4-Cr1-N1	95.42(6)	C20-C15-C22	123.8(2)
N4-Cr1-N1	173.27(6)	C17-C16-C15	121.8(3)
O4-Cr1-N2	152.03(7)	C18-C17-C16	119.3(2)
N4-Cr1-N2	94.78(6)	C17-C18-C19	122.2(3)
N1-Cr1-N2	82.43(6)	C18-C19-C20	118.7(2)
O4-Cr1-Cr2	103.43(4)	C18-C19-C25	116.9(2)
N4-Cr1-Cr2	57.35(5)	C20-C19-C25	124.3(2)
N1-Cr1-Cr2	116.43(5)	C19-C20-C15	118.7(2)
N2-Cr1-Cr2	54.57(5)	C19-C20-N2	121.0(2)
O2-Cr2-N2	84.04(6)	C15-C20-N2	120.3(2)
O2-Cr2-N3	95.89(6)	C15-C22-C23	108.5(2)
N2-Cr2-N3	173.02(7)	C15-C22-C21	113.5(2)
O2-Cr2-N4	151.92(7)	C23-C22-C21	110.4(2)
N2-Cr2-N4	94.48(6)	C24-C25-C19	112.8(2)
N3-Cr2-N4	82.28(6)	C24-C25-C26	109.9(3)
O2-Cr2-Cr1	103.31(5)	C19-C25-C26	112.3(3)
N2-Cr2-Cr1	57.10(5)	N3-C27-C28	120.4(2)
N3-Cr2-Cr1	116.33(5)	N4-C28-C27	112.5(2)
N4-Cr2-Cr1	54.42(4)	N4-C28-C54	112.4(2)
C1-N1-C8	118.7(2)	C27-C28-C54	103.2(2)
C1-N1-Cr1	111.9(2)	C34-C29-C30	117.7(2)
C8-N1-Cr1	128.8(2)	C34-C29-C36	122.3(2)
C20-N2-C2	113.2(2)	C30-C29-C36	119.9(2)
C20-N2-Cr2	116.1(2)	C31-C30-C29	121.3(2)
C2-N2-Cr2	109.0(2)	C30-C31-C32	119.8(2)
C20-N2-Cr1	136.5(2)	C31-C32-C33	121.7(2)
C2-N2-Cr1	104.3(1)	C32-C33-C34	117.3(2)
Cr2-N2-Cr1	68.34(5)	C32-C33-C39	119.7(2)
C27-N3-C34	117.7(2)	C34-C33-C39	122.9(2)
C27-N3-Cr2	111.2(2)	C29-C34-C33	122.2(2)
C34-N3-Cr2	130.4(2)	C29-C34-N3	119.0(2)
C46-N4-C28	113.4(2)	C33-C34-N3	118.8(2)
C46-N4-Cr1	115.6(2)	C29-C36-C35	109.6(2)
C28-N4-Cr1	109.0(2)	C29-C36-C37	112.5(2)
C46-N4-Cr2	136.4(2)	C35-C36-C37	111.2(2)
C28-N4-Cr2	104.5(1)	C33-C39-C38	109.2(2)
Cr1-N4-Cr2	68.23(5)	C33-C39-C40	112.5(2)
C53-O2-Cr2	117.4(2)	C38-C39-C40	111.3(2)

C54-O4-Cr1	118.0(2)	C42-C41-C46	119.1(2)
N1-C1-C2	119.5(2)	C42-C41-C48	116.5(2)
N2-C2-C1	112.5(2)	C46-C41-C48	124.0(2)
N2-C2-C53	112.7(2)	C43-C42-C41	122.2(2)
C1-C2-C53	102.8(2)	C42-C43-C44	118.9(2)
C8-C3-C4	117.5(2)	C43-C44-C45	121.9(2)
C8-C3-C10	123.3(2)	C44-C45-C46	119.0(2)
C4-C3-C10	119.2(2)	C44-C45-C51	117.3(2)
C5-C4-C3	121.4(2)	C46-C45-C51	123.6(2)
C6-C5-C4	119.9(2)	C41-C46-C45	118.8(2)
C5-C6-C7	121.6(2)	C41-C46-N4	120.5(2)
C8-C7-C6	117.1(2)	C45-C46-N4	120.8(2)
C8-C7-C13	123.6(2)	C41-C48-C47	113.9(2)
C6-C7-C13	119.2(2)	C41-C48-C49	108.1(2)
C3-C8-C7	122.6(2)	C47-C48-C49	110.4(2)
C3-C8-N1	119.4(2)	C45-C51-C50	114.4(2)
C7-C8-N1	118.0(2)	C45-C51-C52	111.8(2)
C11-C10-C3	113.1(2)	C50-C51-C52	109.2(2)
C11-C10-C9	110.2(2)	O1-C53-O2	126.1(2)
C3-C10-C9	109.6(2)	O1-C53-C2	118.7(2)
C7-C13-C12	109.7(2)	O2-C53-C2	115.2(2)
C7-C13-C14	112.4(2)	O3-C54-O4	126.5(2)
C12-C13-C14	111.3(2)	O3-C54-C28	118.9(2)
C16-C15-C20	119.1(2)	O4-C54-C28	114.6(2)

2 crystallized in the triclinic space group *P*-1. To our surprise, **2** doesn't follow the typical [2+2] or [2+1] cycloaddition reaction between an unsaturated molecule and $(\mu\text{-}\eta^1\text{:}\eta^1\text{-HL}^{\text{iPr}})_2\text{Cr}_2$. Rather, each diimine ligand has added one carboxylate group on its backbone and generated a C2 symmetric Cr-Cr dimer supported by two amino acid ligands. Each newly formed ligand has one neutral imine nitrogen (N1, N3) coordinating to one Cr, one anionic carboxylate O (O2, O4) coordinating to another Cr and the anionic amide nitrogen (N2, N4) bridging in between both Cr centers. Thus, the quintuply bonded dimer was oxidized to a Cr(II)-Cr(II) dimer. The Cr-Cr distance of 2.3343(4) Å indicates the reduction of Cr-Cr quintuple bond order. The

coordination geometry around each chromium is best described as square planer with sum of angles of 356.78° for Cr1 and 356.68° for Cr2. The bond distances of Cr to imine N are 2.081(2) Å for Cr1-N1 and 2.087(2) Å for Cr2-N3. The bridging amide N is closer to one Cr than the other one, presumably due to the trans influence of carboxylate coordinating site. The average Cr-N bond length trans to carboxylate site is 2.113(2) Å and the average cis Cr-N bond length is 2.045(2) Å.

The quick color change via blue suggested the formation of an intermediate. Unfortunately, the CO₂ activation process happens too fast either to capture the short-lived intermediate or to monitor it by ¹H NMR spectroscopy. Attempts of synthesizing and isolating the blue intermediate by adding 1 equivalent of CO₂ to a Et₂O solution of (μ-η¹:η¹-HⁱLⁱPr)₂Cr₂ were unsuccessful. The blue species could be observed when 1 eq. of CO₂ was slowly introduced into a Et₂O solution of (μ-η¹:η¹-HⁱLⁱPr)₂Cr₂ at -78°C. But this blue intermediate disappeared and reformed the starting material upon warm up and/or when vacuum was applied. A similar color change was observed in the reaction of (μ-η¹:η¹-HⁱLⁱPr)₂Cr₂ with hexafluoro-2-butyne.⁹ A purple intermediate was isolated after 15 min reaction of (μ-η¹:η¹-HⁱLⁱPr)₂Cr₂ with hexafluoro-2-butyne and the prolonged reaction resulted in a red ligand functionalized product as shown in Scheme 2.8. Presumably, **2** could be generated via a [2+2] cycloadduct intermediate of CO₂ and the Cr-Cr multi-bond center (Scheme 2.8), similar to the reaction of (μ-η¹:η¹-HⁱLⁱPr)₂Cr₂ with allene (Scheme 2.4). A closer look of **2** revealed that the newly formed L-CO₂ ligands have chiral centers on C2 and C28. The *P*-1 space group of solid structure indicated that the CO₂ addition product is racemic.

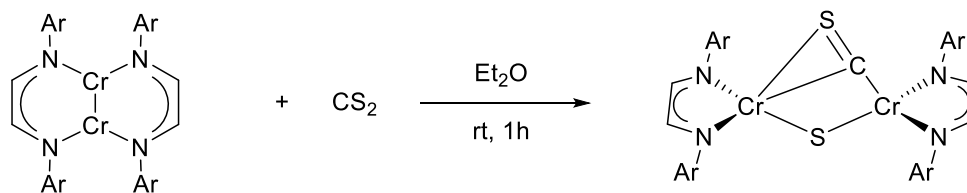


Scheme 2.8 The reaction of $(\mu\text{-}\eta^1:\eta^1\text{-H}^i\text{Pr})_2\text{Cr}_2$ with hexafluoro-2-butyne and plausible mechanism of formation of **2**

Diimine ligand functionalization is not unusual in the literature and many examples have been reported by reacting neutral diimine ligands with metal alkyls.^{21,22,23,24} Alkyl migration via 1,2-insertion to form a new C-C bond on the ligand backbone has been presented in the literature.^{25,26} Addition of a neutral compound to the ligand backbone is relatively rare for diimine complexes. The only

other examples are the reaction of $(\mu\text{-}\eta^1\text{:}\eta^1\text{-HL}^{\text{iPr}})_2\text{Cr}_2$ with hexafluoro-2-butyne⁹, reaction of $(\alpha\text{-diimine})\text{TaCl}_3$ with CCl_4 ²⁷ and reaction of $(\alpha\text{-diimine})\text{W}(\text{NAr})(\text{CH}_2\text{Ph})_2$ with CCl_4 ²⁸. In the cases of Ta and W, the diimine ligand has added a CCl_3 radical on the ligand backbone and the complex was transformed to a metal halide with a localized iminoamide ligand. Comparing the addition of CO_2 and CF_3CCCF_3 to $(\mu\text{-}\eta^1\text{:}\eta^1\text{-HL}^{\text{iPr}})_2\text{Cr}_2$, they both have an electron deficient carbon on the small molecule. Presumably, the small molecule addition onto the diimine ligand is driven by the interaction of ligand based HOMO of $(\mu\text{-}\eta^1\text{:}\eta^1\text{-HL}^{\text{iPr}})_2\text{Cr}_2$ and electrophilic carbon on CO_2 or CF_3CCCF_3 .²⁹ It is noticeable that the reaction of Kempe's quintuply bonded Cr dimer with CO_2 gave a $\text{Cr}_2(\mu_2\text{-CO})_2$ adduct as the major product and, plausibly, a $(\text{CrO})_4$ complex as the byproduct (Scheme 2.3 a).

It was of some interest to explore whether the reaction between $(\mu\text{-}\eta^1\text{:}\eta^1\text{-HL}^{\text{iPr}})_2\text{Cr}_2$ and CS_2 might proceed differently, as CS_2 has a less electrophilic carbon. Upon slowly adding 1 eq. of CS_2 into a Et_2O solution of $(\mu\text{-}\eta^1\text{:}\eta^1\text{-HL}^{\text{iPr}})_2\text{Cr}_2$ at -78°C , the green solution of quintuply bonded Cr dimer turned yellow rapidly. After removing unreacted CS_2 and solvent under vacuum, $[\text{HL}^{\text{iPr}}\text{Cr}]_2(\mu\text{-}\eta^2\text{:}\eta^1\text{-CS})(\mu\text{-S})$ (**3**) was crystallized from Et_2O solution at -30°C (Scheme 2.9). The solid state structure, bond distances, and angle for **3** are displayed in Figure 2.3 and Table 2.4 respectively.



Ar = 2,6-diisopropylphenyl

Scheme 2.9 Reaction of $(\mu\text{-}\eta^1\text{:}\eta^1\text{-HL}^{\text{iPr}})_2\text{Cr}_2$ and CS_2

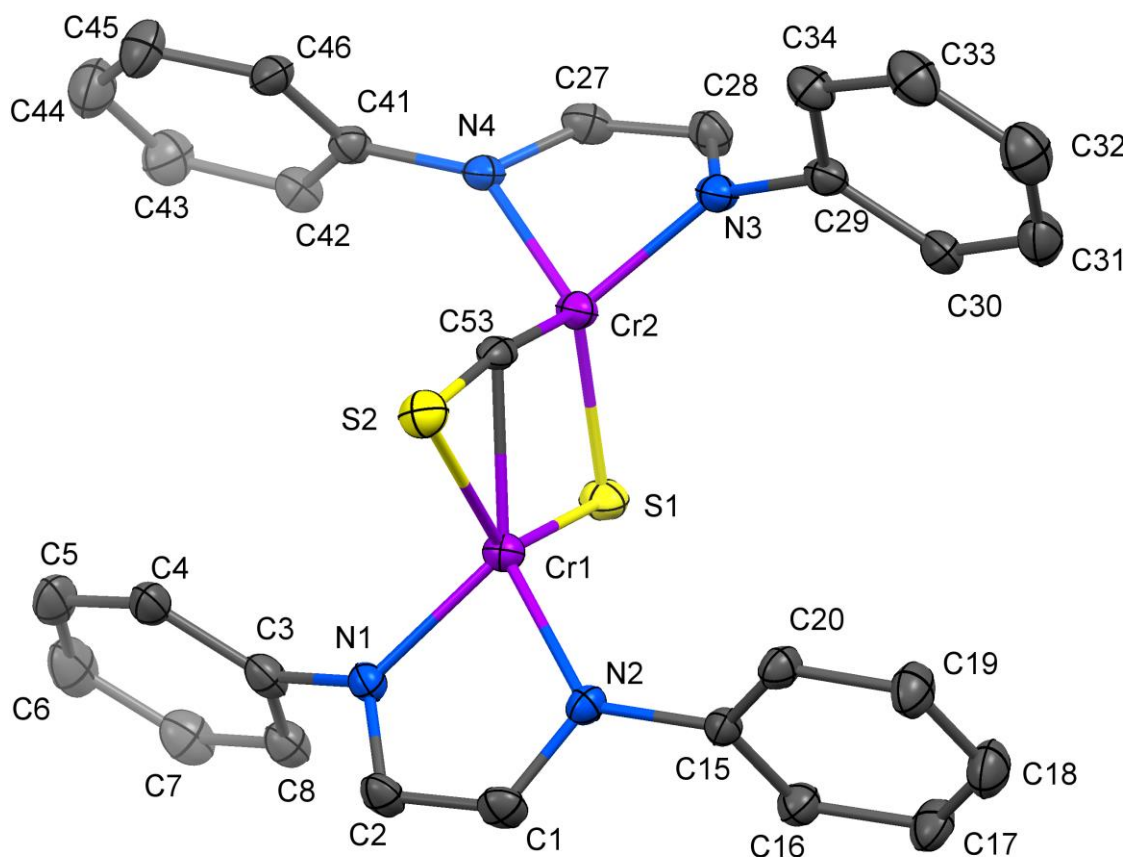


Figure 2.3 Molecular structure of $[\text{HL}^{\text{iPr}}\text{Cr}]_2(\mu\text{-}\eta^2:\eta^1\text{-CS})(\mu\text{-S})$ (**3**) with thermal ellipsoids at the 30% probability level. Isopropyl groups and hydrogen atoms have been omitted for clarity.

Table 2.4 Interatomic distances (Å) and angles (°) for $[\text{HL}^{\text{iPr}}\text{Cr}]_2(\mu\text{-}\eta^2:\eta^2\text{-CS})(\mu\text{-S})$ (**3**).

Distances (Å)			
Cr1-N2	1.943(3)	Cr1-N1	1.943(3)
Cr1-C53	2.090(4)	Cr1-S1	2.250(2)
Cr1-S2	2.422(2)	Cr1-Cr2	2.742(1)
Cr2-C53	1.781(4)	Cr2-N3	1.871(3)
Cr2-N4	1.881(3)	Cr2-S1	2.155(2)

S2-C53	1.594(4)	N2-C1	1.345(5)
N2-C15	1.446(5)	N1-C2	1.333(5)
N1-C3	1.444(5)	N3-C28	1.343(5)
N3-C29	1.437(5)	N4-C27	1.353(5)
N4-C41	1.431(5)	C1-C2	1.388(6)
C3-C8	1.394(6)	C3-C4	1.404(6)
C4-C5	1.396(6)	C4-C12	1.518(7)
C5-C6	1.378(7)	C6-C7	1.378(7)
C7-C8	1.409(6)	C8-C9	1.516(6)
C9-C10	1.521(7)	C9-C11	1.524(6)
C12-C13	1.518(7)	C12-C14	1.525(7)
C15-C16	1.402(6)	C15-C20	1.409(6)
C16-C17	1.400(6)	C16-C24	1.522(6)
C17-C18	1.376(6)	C18-C19	1.389(6)
C19-C20	1.388(6)	C20-C21	1.515(6)
C21-C23	1.527(6)	C21-C22	1.529(7)
C24-C25	1.529(7)	C24-C26	1.533(6)
C28-C27	1.392(6)	C29-C34	1.392(6)
C29-C30	1.409(6)	C30-C31	1.395(6)
C30-C38	1.515(6)	C38-C40	1.529(7)
C38-C39	1.543(7)	C31-C32	1.368(7)
C32-C33	1.379(7)	C34-C33	1.394(6)
C34-C35	1.516(6)	C35-C37	1.522(6)
C35-C36	1.546(7)	C41-C42	1.405(6)
C41-C46	1.406(6)	C42-C43	1.400(6)
C42-C47	1.520(6)	C47-C48	1.521(6)
C47-C49	1.522(6)	C43-C44	1.357(7)
C44-C45	1.382(7)	C45-C46	1.386(6)
C50-C46	1.513(6)	C50-C52	1.520(6)
C50-C51	1.529(6)	C54-C55	1.37(2)
C55-O1	1.38(2)	O1-C56	1.40(2)
C56-C57	1.37(2)		

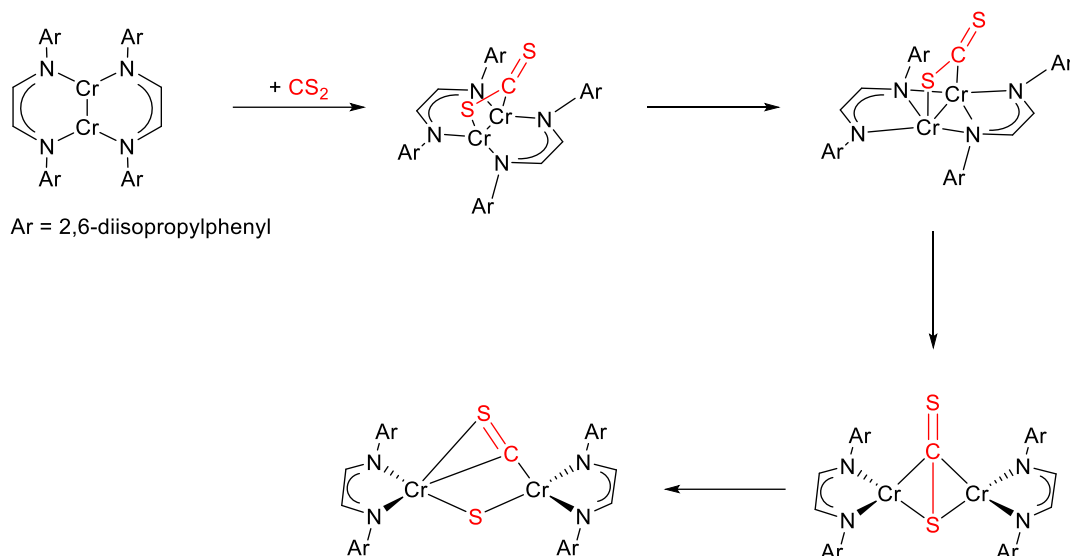
Angles (°)

N2-Cr1-N1	81.2(2)	N2-Cr1-C53	132.3(2)
N1-Cr1-C53	132.8(2)	N2-Cr1-S1	111.2(1)
N1-Cr1-S1	108.5(1)	C53-Cr1-S1	90.5(2)
N2-Cr1-S2	106.6(1)	N1-Cr1-S2	107.1(1)
C53-Cr1-S2	40.5(1)	S1-Cr1-S2	130.98(5)
N2-Cr1-Cr2	138.5(1)	N1-Cr1-Cr2	136.6(1)
C53-Cr1-Cr2	40.5(1)	S1-Cr1-Cr2	49.96(4)
S2-Cr1-Cr2	81.03(4)	C53-Cr2-N3	111.7(2)
C53-Cr2-N4	109.5(2)	N3-Cr2-N4	88.8(2)
C53-Cr2-S1	102.8(2)	N3-Cr2-S1	122.1(1)
N4-Cr2-S1	121.7(1)	C53-Cr2-Cr1	49.6(1)
N3-Cr2-Cr1	135.7(1)	N4-Cr2-Cr1	133.4(1)
S1-Cr2-Cr1	53.08(4)	Cr2-S1-Cr1	76.96(5)
C53-S2-Cr1	58.4(2)	C1-N2-C15	117.8(4)
C1-N2-Cr1	112.7(3)	C15-N2-Cr1	129.0(3)
C2-N1-C3	118.1(4)	C2-N1-Cr1	113.7(3)
C3-N1-Cr1	127.7(3)	C28-N3-C29	123.0(4)
C28-N3-Cr2	96.6(3)	C29-N3-Cr2	138.8(3)
C27-N4-C41	122.4(4)	C27-N4-Cr2	96.2(3)
C41-N4-Cr2	137.3(3)	N2-C1-C2	115.6(4)
N1-C2-C1	114.8(4)	C8-C3-C4	122.2(5)
C8-C3-N1	117.9(4)	C4-C3-N1	119.9(4)
C5-C4-C3	118.0(5)	C5-C4-C12	119.7(5)
C3-C4-C12	122.3(4)	C6-C5-C4	120.9(5)
C7-C6-C5	120.4(5)	C6-C7-C8	121.1(5)
C3-C8-C7	117.4(5)	C3-C8-C9	123.8(4)
C7-C8-C9	118.8(5)	C8-C9-C10	112.1(4)
C8-C9-C11	112.9(4)	C10-C9-C11	110.1(4)
C4-C12-C13	110.8(4)	C4-C12-C14	113.6(5)
C13-C12-C14	110.6(5)	C16-C15-C20	121.1(4)
C16-C15-N2	118.1(4)	C20-C15-N2	120.7(4)
C17-C16-C15	118.2(4)	C17-C16-C24	118.2(4)

C15-C16-C24	123.6(4)	C18-C17-C16	121.2(5)
C17-C18-C19	119.9(5)	C20-C19-C18	121.2(5)
C19-C20-C15	118.3(4)	C19-C20-C21	119.0(4)
C15-C20-C21	122.7(4)	C20-C21-C23	110.1(4)
C20-C21-C22	111.5(4)	C23-C21-C22	111.4(4)
C16-C24-C25	111.6(4)	C16-C24-C26	111.4(4)
C25-C24-C26	109.9(4)	S2-C53-Cr2	170.7(3)
S2-C53-Cr1	81.0(2)	Cr2-C53-Cr1	89.8(2)
N3-C28-C27	117.9(4)	C34-C29-C30	121.8(4)
C34-C29-N3	118.0(4)	C30-C29-N3	120.1(4)
C31-C30-C29	117.5(5)	C31-C30-C38	120.6(5)
C29-C30-C38	121.9(4)	C30-C38-C40	111.3(5)
C30-C38-C39	110.2(4)	C40-C38-C39	110.8(5)
C32-C31-C30	121.3(5)	C31-C32-C33	120.5(5)
C29-C34-C33	118.1(5)	C29-C34-C35	121.0(4)
C33-C34-C35	120.9(4)	C34-C35-C37	110.7(4)
C34-C35-C36	111.7(4)	C37-C35-C36	110.2(4)
N4-C27-C28	116.5(4)	C42-C41-C46	121.7(4)
C42-C41-N4	120.4(4)	C46-C41-N4	117.9(4)
C43-C42-C41	117.5(5)	C43-C42-C47	119.7(4)
C41-C42-C47	122.8(4)	C48-C47-C49	111.3(5)
C48-C47-C42	112.0(4)	C49-C47-C42	110.5(4)
C44-C43-C42	121.3(5)	C43-C44-C45	120.6(5)
C44-C45-C46	121.2(5)	C46-C50-C52	110.9(4)
C46-C50-C51	113.0(4)	C52-C50-C51	110.9(4)
C45-C46-C41	117.6(5)	C45-C46-C50	120.8(4)
C41-C46-C50	121.6(4)	C32-C33-C34	120.8(5)
C54-C55-O1	117(2)	C55-O1-C56	116(2)
C57-C56-O1	116(2)		

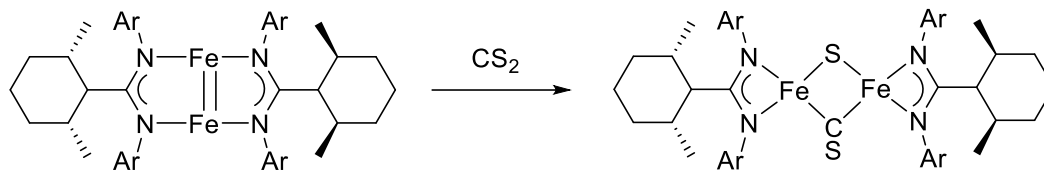
3 crystallized in the monoclinic space group $P2_1/c$. Unlike for CO₂, in **3** one of the C-S double bond is completely split by Cr-Cr center and gives a (μ - η^2 : η^1 -CS) and (μ -S) bridging chromium binuclear complex. The coordination geometry of both Cr

centers is tetrahedral. One of the Cr-S bonds is significantly shorter than the other side (Cr1-S1 = 2.251(2) Å vs. Cr2-S1 = 2.423(2) Å). The bridging CS ligand adopted the four-electron donor η^2 - μ -CS bridging structure with Cr2-C53 bond length of 1.781(4) Å and Cr1-C53 bond length of 2.090(4) Å.³⁰ The C-S bond length of 1.594(4) Å is longer than the free carbon monosulfide triple bond of 1.5349 Å and closer to a C=S double bond of 1.611 Å in thioformaldehyde³¹, suggesting that the CS ligand is formally dianionic. The backbone length of the diimine ligands are in the monoanionic range (average C-C = 1.390 Å and average C-N = 1.343 Å), thus the formal charge of Cr centers is Cr(III)-Cr(III). The two electrons used to split the C-S double bond are from two chromium atoms. The long Cr-Cr distance of 2.742(1) Å indicates the absence of strong bonding interaction between two Cr ions. The differences of reactivity between CO₂ and CS₂ toward $(\mu$ - η^1 : η^1 -HⁱLⁱPr)₂Cr₂ could be due to the less electron deficient carbon center of CS₂ and weaker C=S bond. Presumably, both molecules would form a [2+2] adduct with Cr-Cr quintuple bond center, but the stronger electrophilic carbon center of CO₂ would undergo electrophilic attack onto the electron rich backbone of diimine ligands while the CS₂ was split by Cr-Cr quintuple bond center (Scheme **2.10**).



Scheme 2.10 Plausible mechanism of formation of 3

Due to the instability of carbon monosulfide (unstable at temperature above - 100 °C)³²⁻³³, metal thiocarbonyls are usually prepared by using carbon disulfide or thiophosgene as CS sources. In 1966 Baird and Wilkinson reported the first metal thiocarbonyl complex, $(\text{Ph}_3\text{P})_2\text{Rh}(\text{CS})\text{Cl}$, from reaction of $(\text{Ph}_3\text{P})_3\text{RhCl}$ and CS_2 followed by elimination of Ph_3PS . There are many examples of CS_2 double bond cleavage by transition metal clusters, like $(\text{C}_5\text{H}_5\text{Co})_3(\mu_3\text{-S})(\mu_3\text{-CS})$ ³⁴⁻³⁵, $\text{Fe}_4(\text{CO})_{12}(\text{S})(\text{CS})$ ³⁶, $(\text{C}_5\text{H}_5\text{Co})_2\{\text{Fe}(\text{CO})_2(\text{PPh}_3)\}(\mu_3\text{-S})(\mu_3\text{-CS})$ ³⁷, $\text{H}_2\text{Os}_3(\text{CO})_7(\text{CS})(\text{S})_2$ ³⁸, $\text{Os}_4(\text{CO})_{12}(\text{CS})(\text{S})$ ³⁹ and $\text{Ru}_3(\text{CO})_5(\text{CS})(\mu\text{-H})(\mu\text{-P}^t\text{Bu}_2)(\mu\text{-PCy}_2)_2(\mu_3\text{-S})$ ⁴⁰. This kind of reactions typically requires higher temperature to proceed. For dinuclear systems, $\text{W}_2\text{Cp}_2(\text{CO})_5(\mu\text{-}\eta^1\text{:}\eta^2\text{-CH}_2\text{CO})$ ⁴¹, $\text{Re}_2\text{Br}_4(\mu\text{-dpam})_2$ ⁴² and $[\text{Fe}(\mu\text{-Pipiso})]_2$ ⁴³ react with CS_2 and split one of the $\text{C}=\text{S}$ double bond under mild condition (room temperature to -40 °C). Based on the search in Cambridge Structural Database (CSD)⁴⁴⁻⁴⁵⁻⁴⁶, **3** is the first example of CS_2 cleavage by chromium complex.



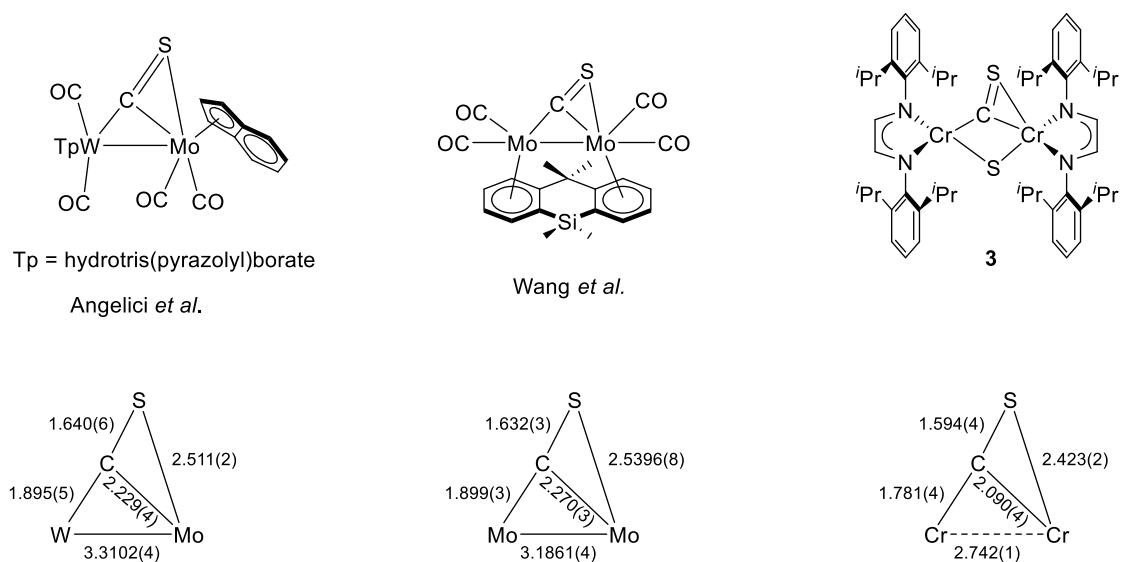
Ar = 2,6-diisopropylphenyl

Scheme 2.11 Synthesis of $(\text{PipisoFe})_2(\mu\text{-S})(\mu\text{-CS})$

The comparison of $(\text{PipisoFe})_2(\mu\text{-S})(\mu\text{-CS})$ and **3** is some of interest. They are both dinuclear sulfide/thiocarbonyl bridged complex generated by exposing low valent metal-metal multiple bond complexes to CS_2 . The Cr-Cr distance of 2.742(1) Å is longer than the Fe-Fe distance of 2.5800(6) Å, presumably because of $(\eta^1:\eta^2)$ coordination of the thiocarbonyl ligand in **3** and the bigger covalent radii of Cr(III) than Fe(II). The average Cr-S bond length (average Cr-S = 2.203(2) Å) is slightly longer than the average Fe-S bond length (average Fe-S = 2.1330(9) Å). Despite the fact that the bridging carbon in **3** is closer to Cr2 than Cr1, the average Cr-C bond length of 1.935(4) Å is close to the average Fe-C bond length of 1.938(3) Å in $(\text{PipisoFe})_2(\mu\text{-S})(\mu\text{-CS})$.

It's also worth noting that the side-on bridging structure of thiocarbonyl is very rare. The only two other complexes featuring $\text{M}_2(\mu\text{-}\eta^2:\eta^1\text{-CS})$ core were reported by Angelici *et al.* in 1989 and Wang *et al.* in 2008 (Scheme 2.12). The comparison of bond distances in the $\text{M}_2(\mu\text{-}\eta^2:\eta^1\text{-CS})$ cores of those complexes was shown in Scheme 2.12 as well. The metal to S distances in all three complexes were shorter than 2.54 Å and indicated M-S bonding. The C-S distances ranged from 1.594(4) to 1.640(6) Å and were clearly longer than CS triple bond length of 1.535 Å. The metal-C σ bonds (1.781(4) – 1.899(3) Å) were significantly shorter than metal-C π bonds (2.090(4) –

2.270(3) Å). Thus, all three complexes have a side-on bridging thiocarbonyl ligand, and **3** is the first example of first row transition metal complex featuring a $M_2(\mu-\eta^2:\eta^1-CS)$ core. Interestingly, all transition metals in the three complexes were from group 6.



Scheme 2.12 Comparison of bond distances in complexes featuring $M_2(\mu-\eta^2:\eta^1-CS)$ core

In conclusion, the quintuply bonded complex $(\mu-\eta^1:\eta^1-H^iPr)_2Cr_2$ showed different reactivity toward CO, CO₂ and CS₂. It was found that reaction with 1 eq. of CO gave simple mono-carbonyl adduct **1**. The reaction with CO₂ would activate the carbon of CO₂ and gave a symmetric ligand-functionalized binuclear complex **2**, i.e. $(L-CO_2)_2Cr_2$. The reaction with CS₂ would not trigger the nucleophilic addition on the ligands, but split one C=S double bond to generate complex **3** featuring a $Cr_2(\mu-\eta^2:\eta^1-CS)(\mu-S)$ core.

2.3 Experimental

2.3.1 General Considerations

All manipulations were carried out with standard Schlenk, high vacuum line, and glovebox techniques. Pentane, diethyl ether, tetrahydrofuran, and toluene were dried by passing the solvent through activated aluminum columns followed by a nitrogen purge to remove dissolved oxygen. THF-d₈ was predried over potassium metal and stored under vacuum over Na/K. CD₂Cl₂ was predried with P₂O₅ and stored under vacuum over 4 Å molecular sieves. C₆D₆ was predried with sodium metal and stored under vacuum over Na/K. CrCl₃ (anhydrous) and sodium metal were purchased from Strem Chemical Co.. CrCl₃(THF)₃, and the diimine ligand was prepared by literature procedures.⁴⁷⁴⁸ All other reagents were purchased from Aldrich or Acros and dried using standard procedures when necessary.

NMR spectra were recorded on a Bruker DRX-400 spectrometer and were referenced to the residual protons of the solvent (THF-d₈, 1.73 and 3.58 ppm; CD₂Cl₂, 5.32 ppm; CDCl₃, 7.27 ppm; C₆D₆, 7.15 ppm). FTIR spectra were taken on a Nicolet Magna- IR E. S. P. 560 spectrometer. UV/vis spectra were taken on a Thermo UV-1 spectrophotometer. Mass spectral data were collected at the University of Delaware Mass Spectrometry Facility in electron ionization mode (+15eV). Room-temperature magnetic susceptibility (χ_m) measurements were carried out using a Johnson Matthey magnetic susceptibility balance unless otherwise stated. Molar magnetic susceptibilities were corrected for diamagnetism using Pascal constants and converted into effective magnetic moments (μ_{eff}).

2.3.2 Preparation of $[\text{HL}^{\text{iPr}}\text{Cr}]_2(\mu\text{-CO})$ (**1**)

To a 50 ml Et_2O solution of $(\mu\text{-}\eta^1\text{:}\eta^1\text{-HL}^{\text{iPr}})_2\text{Cr}_2$ (250 mg, 0.291 mmol), 1 eq. of CO was added at -78°C . After stirring for 3h, the solution slowly turn from green into teal color. The remaining CO and Et_2O was removed via vacuum at -78°C and crude product was extracted with pentane. The solution was filtered, concentrated and cooled to -30°C to yield teal crystals of **1** (141 mg, 55 % yield). ^1H NMR (C_6D_6): 6.99-6.75 (12H, Ar), 5.62, 3.31 (8H, iPr), 1.41 (24H, iPr), 1.03, 0.75 (24H, iPr) ppm. IR (KBr; cm^{-1}): 3058 (w), 3016(w), 2956 (s), 2923 (m), 2865 (m), 1758 (m), 1525 (s), 1460 (m), 1432 (m), 1359 (m), 1321 (m), 1245 (s), 1230 (s), 1186 (s), 1099 (m), 1058 (w), 935 (w), 869 (w), 796 (m), 752 (s). UV/Vis (pentane; λ_{max} , nm (ϵ , $\text{M}^{-1}\text{cm}^{-1}$): 620 (5310), 704 (4867). M.p.: 91°C decomp.

2.3.3 Preparation of $(\text{L-CO}_2)_2\text{Cr}_2$ (**2**)

At room temperature, a 50 ml E_2O solution of $(\mu\text{-}\eta^1\text{:}\eta^1\text{-HL}^{\text{iPr}})_2\text{Cr}_2$ (250 mg, 0.291 mmol) was exposed to 1 atm of CO_2 . An immediate color change from green to blue to red can be observed. After stirring for 1h, the CO_2 and Et_2O were removed under vacuum. The residue was extracted by pentane. The solution was filtered, concentrated and cooled to -30°C to yield red crystals of **2** (240 mg, 87 % yield). ^1H NMR (C_6D_6): 7.34-6.57 (12H, Ar), 1.95 (12H, iPr), 1.73 (12H, iPr), 1.41 (12H, iPr), 1.00 (12H, iPr) ppm. IR (KBr; cm^{-1}): 3062 (w), 2960 (s), 2927 (m), 2867 (m), 1758 (m), 1525 (m), 1465 (m), 1440 (m), 1384 (m), 1361 (m), 1324 (m), 1257 (m), 1240 (m), 1186 (m), 1110 (m), 1058 (m), 939 (m), 798 (m), 754 (m). UV/Vis (ϵ , $\text{M}^{-1}\text{cm}^{-1}$) 624 (989), 907 (643). μ_{eff} (294K) = 1.2(1) μ_{B} . M.p.: 186°C .

2.3.4 Preparation of $[\text{HL}^{\text{iPr}}\text{Cr}]_2(\mu\text{-}\eta^2\text{:}\eta^2\text{-CS})(\mu\text{-S})$ (**3**)

To a 50 ml Et_2O solution of $(\mu\text{-}\eta^1\text{:}\eta^1\text{-HL}^{\text{iPr}})_2\text{Cr}_2$ (250 mg, 0.291 mmol), 1 eq. of CS_2 (17.6 μL , 0.291 mmol) was added at -78°C . After stirring for 1h, the solution slowly turned from green to brown. Then the solution was allowed to warm up to room temperature. The remaining CS_2 and Et_2O was removed under vacuum and crude product was extracted by pentane. The solution was filtered, concentrated and cooled to -30°C to yield yellow to brown crystals of **3** (195 mg, 72 % yield). ^1H NMR (C_6D_6): 16.49 (4H, Ar), 10.74 (4H, Ar), 1.17 (48H, iPr), -3.32 (4H, Ar), -13.10 (4H, Ar), ppm. IR (KBr; cm^{-1}): 3062 (w), 2964 (s), 2927 (m), 2867 (m), 1737 (w), 1652 (w), 1627 (w), 1461 (m), 1443 (m), 1384 (m), 1363 (m), 1326 (w), 1257 (m), 1220 (w), 1180 (w), 1110 (m), 1058 (w), 1022 (w), 1014 (w), 937 (w), 800 (m), 755 (m). UV/Vis (ϵ , $\text{M}^{-1}\text{cm}^{-1}$). $\mu_{\text{eff}}(294\text{K}) = 2.0(1) \mu_{\text{B}}$. M.p.: 213°C .

2.3.5 General considerations for X-ray diffraction

Single crystal X-ray diffraction studies were performed under the following conditions. Crystals were selected, sectioned as required, and mounted on MiTeGenTM plastic mesh with viscous oil and flash-cooled to the data collection temperature. Diffraction data were collected on a Bruker-AXS APEX CCD diffractometer with graphite-monochromated Mo- $\text{K}\alpha$ radiation ($\lambda=0.71073 \text{ \AA}$). The data-sets were treated with SADABS absorption corrections based on redundant multiscan data⁴⁹.

The structures were solved using direct methods and refined with full-matrix, least squares procedures on F^2 . Unit cell parameters were determined by sampling three different sections of the Ewald sphere. Nonhydrogen atoms were refined with anisotropic displacement parameters. Hydrogen atoms were treated as idealized

contributions. Structure factors and anomalous dispersion coefficients are contained in the SHELXTL 6.12 program library⁴⁹.

2.3.6 Single crystal X-ray diffraction studies

The unit cell parameters and systematic absences in the diffraction data were consistent for space groups $P2_1/n$ for **1**; $P-1$ for **3**; $P2_1/c$ for **3**. No symmetry higher than triclinic was observed in the diffraction data for **3**. Structural solution in the centrosymmetric space group options yielded chemically reasonable and computationally stable results of refinement. The toluene solvent molecule in **1** and the diethyl ether solvent molecule in **2** and **3** had slight yet unresolvable disorder and was treated with idealized geometry.

Table 2.5 Crystallographic data for complexes 1-3

	1 (kla0597)	2 (kla0946)	3 (kla0613)
Formula	C ₆₀ H ₈₀ Cr ₂ N ₄ O	C ₁₁₂ H ₁₅₄ Cr ₄ N ₈ O ₉	C ₅₅ H ₇₇ Cr ₂ N ₄ O _{0.50} S ₂
Formula Wt.	977.28	1964.42	970.32
Space group	<i>P2₁/n</i>	<i>P</i> -1	<i>P2₁/c</i>
Color	Teal	Red	Brown
a, Å	13.551(5)	12.6918(5)	21.025(3)
b, Å	19.991(8)	14.4241(6)	13.169(2)
c, Å	20.998(8)	15.9069(7)	20.782(3)
α, deg	90	71.960(1)	90
β, deg	104.226(18)	82.160(2)	108.010(4)
γ, deg	90	75.896(1)	90
V, Å ³	5514.(4)	2679.55(19)	5472.1(14)
Z	4	1	2
D(calcd), g•cm ⁻³	1.177	1.217	1.178
μ(Mo Kα), mm ⁻¹	0.436	0.454	0.512
Temp., K	200	200	200
T _{max} /T _{min}	0.952/0.905	0.746/0.697	0.977/0.927
no. data/params	12677/606	15965/614	12605/613
GOF on F ₂	0.713	1.007	1.014
R(F), % ^a	6.97	5.43	6.81
Rw(F ₂), % ^a	19.25	14.60	16.63

a Quantity minimized: $R_w(F^2) = \sum[w(F_o^2 - F_c^2)^2] / \sum[(wF_o^2)^2]^{1/2}$; $R = \sum \Delta / \sum(F_o)$,
 $\Delta = |(F_o - F_c)|$

REFERENCES

1. (a) F. H. Stephens, J. S. Figueroa, C. C. Cummins, O. P. Kryatova, S. V. Kryatov, E. V. Rybak-Akimova, J. E. McDonough, C. D. Hoff, *Organomet.* **2004**, *23*, 3126-3138; (b) S. Yao, M. Driess, *Acc. Chem. Res.* **2012**, *45*, 276-287; (c) T. G. Ostapowicz, M. D. Fryzuk, *Inorg. Chem.* **2015**, *54*, 2357-2366; (d) U. Jayarathne, S. R. Parmelee, N. P. Mankad, *Inorg. Chem.* **2014**, *53*, 7730-7737; (e) D. M. Ermert, L. J. Murray, *J. Chem. Soc., Dalton Trans.* **2016**, *45*, 14499-14507; (f) W. S. Farrell, B. L. Yonke, J. P. Reeds, P. Y. Zavalij, L. R. Sita, *Organomet.* **2016**, *35*, 1132-1140; (g) P. Zimmermann, C. Limberg, *J. Am. Chem. Soc.* **2017**, *139*, 4233-4242; (h) O. J. Metters, S. J. Forrest, H. A. Sparkes, I. Manners, D. F. Wass, *J. Am. Chem. Soc.* **2016**, *138*, 1994-2003.
2. (a) E. S. Akturk, G. P. Yap, K. H. Theopold, *Angew. Chem. Int. Ed. Engl.* **2015**, *54*, 14974-14977; (b) E. S. Akturk, G. P. Yap, K. H. Theopold, *Chem. Commun. (Camb.)* **2015**, *51*, 15402-15405.
3. W. H. Monillas, G. P. Yap, L. A. MacAdams, K. H. Theopold, *J. Am. Chem. Soc.* **2007**, *129*, 8090-8091.
4. C. Ni, B. D. Ellis, G. J. Long, P. P. Power, *Chem. Commun. (Camb.)* **2009**, 2332-2334.
5. A. Noor, G. Glatz, R. Müller, M. Kaupp, S. Demeshko, R. Kempe, *Nat. Chem.* **2009**, *1*, 322-325.
6. C. Schwarzmaier, A. Noor, G. Glatz, M. Zabel, A. Y. Timoshkin, B. M. Cossairt, C. C. Cummins, R. Kempe, M. Scheer, *Angew. Chem. Int. Ed. Engl.* **2011**, *50*, 7283-7286.
7. A. Noor, S. Qayyum, T. Bauer, S. Schwarz, B. Weber, R. Kempe, *Chem. Commun. (Camb.)* **2014**, *50*, 13127-13130.
8. P. F. Wu, S. C. Liu, Y. J. Shieh, T. S. Kuo, G. H. Lee, Y. Wang, Y. C. Tsai, *Chem. Commun. (Camb.)* **2013**, *49*, 4391-4393.
9. (a) J. Shen, G. P. Yap, K. H. Theopold, *J. Am. Chem. Soc.* **2014**, *136*, 3382-3384; (b) J. Shen, G. P. Yap, K. H. Theopold, *Chem. Commun. (Camb.)* **2014**, *50*, 2579-2581; (c) J. Shen, G. P. Yap, J. P. Werner, K. H. Theopold, *Chem. Commun. (Camb.)* **2011**, *47*, 12191-12193.

-
10. (a) J. Liu, D. R. Chen, H. Wu, Z. F. Xiao, H. Y. Gao, F. M. Zhu, Q. Wu, *Macromolecules* **2014**, *47*, 3325-3331; (b) D. F. Zhang, E. T. Nadres, M. Brookhart, O. Daugulis, *Organomet.* **2013**, *32*, 5136-5143; (c) V. C. Gibson, R. K. O'Reilly, W. Reed, D. F. Wass, A. J. P. White, D. J. Williams, *Chem. Commun.* **2002**, 1850-1851; (d) T. L. Lohr, W. E. Piers, M. Parvez, *Inorg. Chem.* **2012**, *51*, 4900-4902; (e) P. P. M. de Lange, E. Alberts, M. v. Wijnkoop, H.-W. Frühauf, K. Vrieze, H. Kooijman, A. L. Spek, *J. Organomet. Chem.* **1994**, *465*, 241-249; (f) N. Muresan, K. Chlopek, T. Weyhermuller, F. Neese, K. Wieghardt, *Inorg. Chem.* **2007**, *46*, 5327-5337; (g) H. tom Dieck, A. Kinzel, *Angew. Chem. Int. Ed. Engl.* **1979**, *18*, 324-325.
 11. K. A. Kreisel, G. P. Yap, K. H. Theopold, *Inorg. Chem.* **2008**, *47*, 5293-5303.
 12. R. F. Chen, K. Tatsumi, *J. Coord. Chem.* **2002**, *55*, 1219-1222.
 13. J. Blanco-Urgoiti, L. Anorbe, L. Perez-Serrano, G. Dominguez, J. Perez-Castells, *Chem. Soc. Rev.* **2004**, *33*, 32-42.
 14. R. S. Mane, B. M. Bhanage, *J. Org. Chem.* **2016**, *81*, 1223-1228.
 15. K. T. Neumann, S. R. Laursen, A. T. Lindhardt, B. Bang-Andersen, T. Skrydstrup, *Org. Lett.* **2014**, *16*, 2216-2219.
 16. Cotton, F. A.; Murillo, L. A.; Walton, R. A. *Multiple Bonds Between Metal Atoms*, 3rd ed.; Springer: Berlin, 2005.
 17. M. Mikkelsen, M. Jorgensen, F. C. Krebs, *Energ Environ Sci* **2010**, *3*, 43-81.
 18. T. Sakakura, J. C. Choi, H. Yasuda, *Chem. Rev.* **2007**, *107*, 2365-2387.
 19. C. Maeda, Y. Miyazaki, T. Ema, *Catal Sci Technol* **2014**, *4*, 1482-1497.
 20. M. Aresta, A. Dibenedetto, A. Angelini, *Chem. Rev.* **2014**, *114*, 1709-1742.
 21. K. Mashima, R. Ohnishi, T. Yamagata, H. Tsurugi, *Chem. Lett.* **2007**, *36*, 1420-1421.

-
22. P. J. Bailey, R. A. Coxall, C. M. Dick, S. Fabre, S. Parsons, L. J. Yellowlees, *Chem. Commun. (Camb.)* **2005**, 4563-4565.
 23. G. X. Du, Y. L. Wei, L. Ai, Y. Y. Chen, Q. Xu, X. A. Liu, S. W. Zhang, Z. M. Hou, X. F. Li, *Organomet.* **2011**, *30*, 160-170.
 24. P. De Waele, B. A. Jazdzewski, J. Klosin, R. E. Murray, C. N. Theriault, P. C. Vosejka, J. L. Petersen, *Organomet.* **2007**, *26*, 3896-3899.
 25. V. Riollet, C. Copret, J.-M. Basset, L. Rousset, D. Bouchu, L. Grosvalet, M. Perrin, *Angew. Chem. Int. Ed.* **2002**, *41*.
 26. K. A. Kreisel, G. P. A. Yap, K. H. Theopold, *Eur. J. Inorg. Chem.* **2012**, *2012*, 520-529.
 27. H. Tsurugi, T. Saito, H. Tanahashi, J. Arnold, K. Mashima, *J. Am. Chem. Soc.* **2011**, *133*, 18673-18683.
 28. H. Tanahashi, H. Tsurugi, K. Mashima, *Organomet.* **2015**, *34*, 731-741.
 29. K. A. Kreisel, G. P. Yap, O. Dmitrenko, C. R. Landis, K. H. Theopold, *J. Am. Chem. Soc.* **2007**, *129*, 14162-14163.
 30. R. B. King, Z. Zhang, Q. S. Li, H. F. Schaefer, 3rd, *PCCP* **2012**, *14*, 14743-14755.
 31. G. P. Raine, H. F. Schaefer, R. C. Haddon, *J. Am. Chem. Soc.* **1983**, *105*, 194-198.
 32. R. Steudel, *Z. Anorg. Allg. Chem.* **1968**, *361*, 180-194.
 33. M. A. P. Hogg and J. E. Spice, *J. Chem. Soc.* **1958**, 4196.
 34. C. P. Casey, R. A. Widenhoefer, R. K. Hayashi, *Inorg. Chem.* **1995**, *34*, 1138-1144.
 35. H. Werner, K. Leonhard, O. Kolb, E. Röttinger, H. Vahrenkamp, *Ber.* **1980**, *113*, 1654-1662.
 36. P. V. Broadhurst, B. F. G. Johnson, J. Lewis, P. R. Raithby, *J. Chem. Soc., Chem. Commun.* **1980**.

-
37. A. R. Manning, L. O'Dwyer, P. A. McArdle, D. Cunningham, *J. Organomet. Chem.* **1998**, *551*, 139-149.
38. P. V. Broadhurst, B. F. G. Johnson, J. Lewis, A. G. Orpen, P. R. Raithby, J. R. Thornback, *J. Organomet. Chem.* **1980**, *187*, 141-145.
39. P. V. Broadhurst, B. F. G. Johnson, J. Lewis, P. R. Raithby, *J. Chem. Soc., Dalton Trans.* **1982**, 1641-1644.
40. H.-C. Böttcher, M. Graf, K. Merzweiler, C. Wagner, *Z. Anorg. Allg. Chem.* **2001**, *627*, 2657-2662.
41. L. J. J. Wang, S. J. You, S. L. Huang, Y. L. Yang, Y. C. Lin, G. H. Lee, S. M. Peng, *J. Chem. Soc., Dalton Trans.* **1999**, 2243-2248.
42. J. S. Qi, P. W. Schrier, P. E. Fanwick, R. A. Walton, *Inorg. Chem.* **1992**, *31*, 258-262.
43. L. Fohlmeister, C. Jones, *Aust. J. Chem.* **2014**, *67*, 1011-1016.
44. Y. N. Huang, H. W. L. Uhm, D. F. R. Gilson, I. S. Butler, *Inorg. Chem.* **1994**, *33*, 804-807.
45. S. Lotz, R. R. Pille, P. H. Van Rooyen, *Inorg. Chem.* **1986**, *25*, 3053-3057.
46. M. J. McGlinchey, J. L. Fletcher, B. G. Sayer, P. Bougeard, R. Faggiani, C. J. L. Lock, A. D. Bain, C. Rodger, E. P. Kündig, D. Astruc, J.-R. Hamon, P. Le Maux, S. Top, G. Jaouen, *J. Chem. Soc., Chem. Commun.* **1983**, 634-636.
47. W. Herwig, H. H. Zeiss, *J. Org. Chem.* **1958**, *23*, 1404-1404.
48. A. J. Arduengo, R. Krafczyk, R. Schmutzler, H. A. Craig, J. R. Goerlich, W. J. Marshall, M. Unverzagt, *Tetrahedron* **1999**, *55*, 14523-14534.
49. G. M. Sheldrick, *Acta Crystallogr. A* **2008**, *64*, 112-122.

Chapter 3

THE SYNTHESIS OF THE DINUCLEAR CHROMIUM ALKYL/ARYL HYDRIDE COMPLEXES SUPPORTED BY α -DIIMINE LIGANDS

3.1 Introduction

Direct functionalization of C-H bonds is one of the most attractive fields of synthetic and organometallic chemistry, which could free chemists from tedious functional group transformation in classical cross coupling catalysis and maximize atom- and step- economy. Due to the high strength of C-H bonds (~100 kcal/mol typically), harsh conditions such as high temperature, strong base or acid and strong oxidants or reductants are unavoidable in most reactions involving C-H activations. The application of those processes in organic synthesis was also directly limited due to poor functional group tolerance and selectivity. In the early stage of C-H activation, the efforts were mainly directed to discovery of catalytic systems involving direct insertion of metal catalyst into the C-H bond and functionalization of the resulting hydridoalkyl metal intermediate. In 1955 Shunsuke Murahashi reported the first C-H functionalization reaction of carbonylative ring closure of (E)-N,1-diphenylmethanimine toward 2-phenylisoindolin-1-one catalyzed by $\text{Co}_2(\text{CO})_8$.¹ Joseph Chatt reported the formation of formation of $\text{Ru}(\text{dmpe})_2(\text{H})(2\text{-naphthyl})$ complex by treating $\text{RuCl}_2(\text{dmpe})_2$ with sodium reduced naphthalene (dmpe = 1,2-bis(dimethylphosphino)ethane).² The direct insertion of Ru center into C-H bond clearly showed the cleavage of C-H bond and could not be done without strong reductant. Irradiation could also promote the C-H activation. In 1982, R.G. Bergman³

and W.A.G. Graham⁴ independently reported the synthesis of hydrido alkyl Ir complexes from Cp*Ir(PMe₃)(H)₂ (Bergman) or Cp*Ir(CO)₂ (Graham) in presence of cyclohexane and neopentane by high pressure Hg lamp irradiation. C-H functionalization has gained incredible progress in the past 15 years.⁵ Nowadays, more and more attention has been focused on design and develop new protocols of efficient catalytic C-H activation under mild conditions.^{6,7}

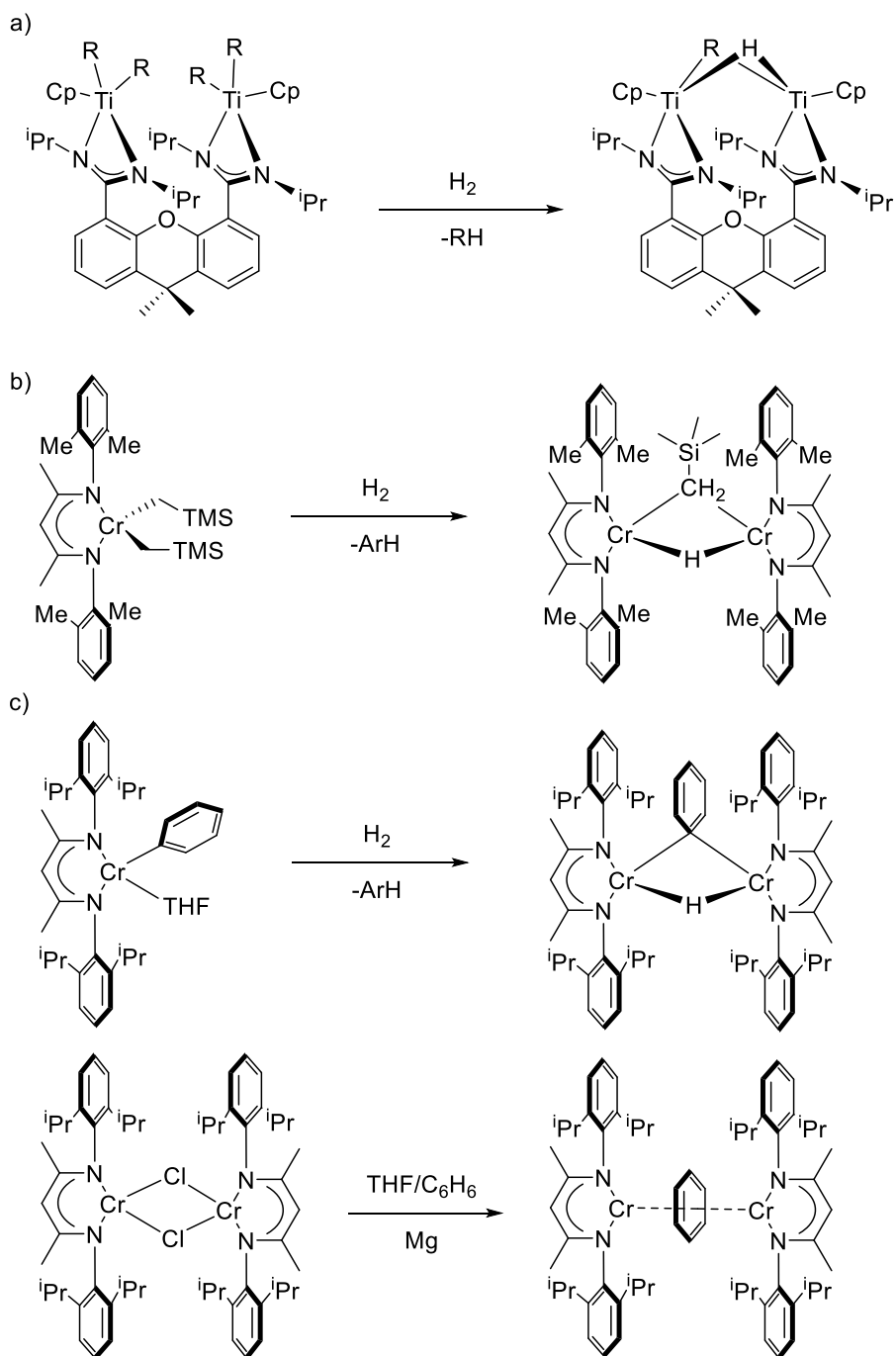
However, without a clear guideline, those discoveries were quite unpredictable sometimes. To date, no widespread application of C-H activation has been found under mild conditions with high selectivity and efficiency. Thus, the fundamental understanding of the C-H activation process is certainly the key to the discovery of new transition-metal catalysts for this promising transformation. In order to address this issue, one strategy is to synthesize the key intermediate of metal alkyl hydrides and to study their reactivities. The field of C-H activation is still dominated by second-row transition metals such as Pd, Ru and Rh. The use of cost-effective and abundant first row transition metals such as Cr, Mn, Fe, Co, Ni and Cu is largely unexplored, especially for Cr.

As the reductive elimination of alkane (or arene) is both thermodynamically favorable and kinetically facile, there are few examples of stable and isolable alkyl- or aryl-hydrido complexes of first-row transition metal.^{8,9,10,11,12} Conversely, these can be considered the product of transition metal C-H activation. By synthesizing and studying the stable alkyl- or aryl-hydride, we could have a clearer understanding of C-H activation via abundant and inexpensive first row transition metals. Until recently, there were only a few stable first row transition metal alkyl-(aryl-) hydrides reported. In 2003, Hagadorn and McNevin synthesized and isolated a titanium dinuclear

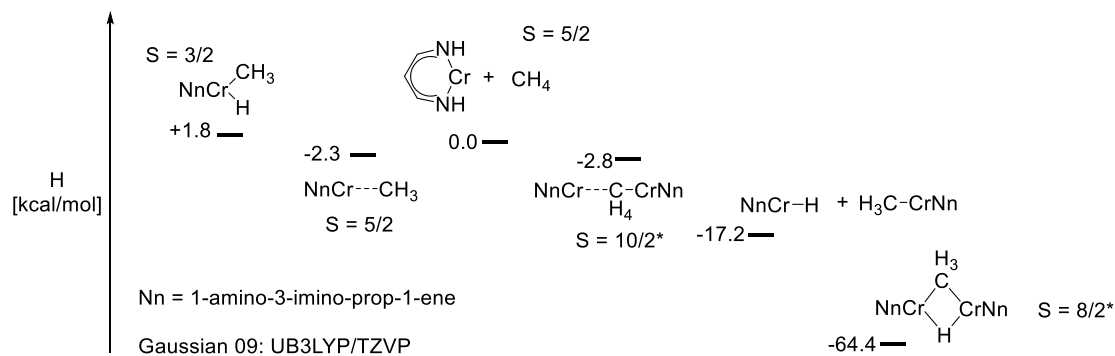
complex featuring a $\text{Ti}^{\text{III}}(\mu\text{-Me})(\mu\text{-H})\text{Ti}^{\text{III}}$ core (Scheme **3.1 a**).⁸ In the same year, MacAdams from our group reported the first chromium alkyl hydride, $[(2,6\text{-Me}_2\text{Ph})_2\text{nacnacCr}]_2(\mu\text{-H})(\mu\text{-CH}_2\text{SiMe}_3)$ (Scheme **3.1 b**).⁹ Previously, in our group, Monillas *et al.* reported a pair of isomers which included a phenyl-hydride chromium complex, namely $[(2,6\text{-}i\text{PrPh})_2\text{nacnacCr}]_2(\mu\text{-H})(\mu\text{-Ph})$ and $[(2,6\text{-}i\text{PrPh})_2\text{nacnacCr}]_2(\mu\text{-}\eta^6\text{:}\eta^6\text{-Ph})$ (Scheme **3.1 c**).¹⁰ All these alkyl hydrides were synthesized by hydrogenation of the their alkyl precursor. To our surprise, the Cr alkyl hydrides supported by NacNac ligands showed extraordinary thermal stability. No reductive elimination was observed on the NacNac Cr alkyl hydrides. For example, the pair of isomers, $[(2,6\text{-}i\text{PrPh})_2\text{nacnacCr}]_2(\mu\text{-H})(\mu\text{-Ph})$ and $[(2,6\text{-}i\text{PrPh})_2\text{nacnacCr}]_2(\mu\text{-}\eta^6\text{:}\eta^6\text{-Ph})$ (Scheme **3.1 c**), could not be converted one into the other under conditions before their total decomposition. The DFT calculations carried out by Theopold *et al.* regarding the relative stabilities (in terms of enthalpy) of various NacNac Cr alkyl hydrides suggested that the binuclear alkyl hydrides, at least for NacNac systems, might be perfectly stable against reductive elimination of R-H (Scheme **3.2**). However, differences in molecular and electronic structure might provide informative differences in reactivity. α -Diimine ligands, as bidentate nitrogen donors, are structurally closely related to the NacNac ligands, but their well-established redox non-innocent characters show significant different electronic structures. Thus, the synthesis of α -diimine Cr alkyl hydrides is not only synthetic interesting but also provide an excellent comparison to its closely related NacNac Cr systems.

First row transition metal alkyl hydrides could also be synthesized by other methods. In 2007, Jagner *et al.* reported the synthesis of hydridoalkylzincates involving β -H elimination of trialkylzincate (Scheme **3.3 a**).¹¹ Recently, Okuda *et al.*

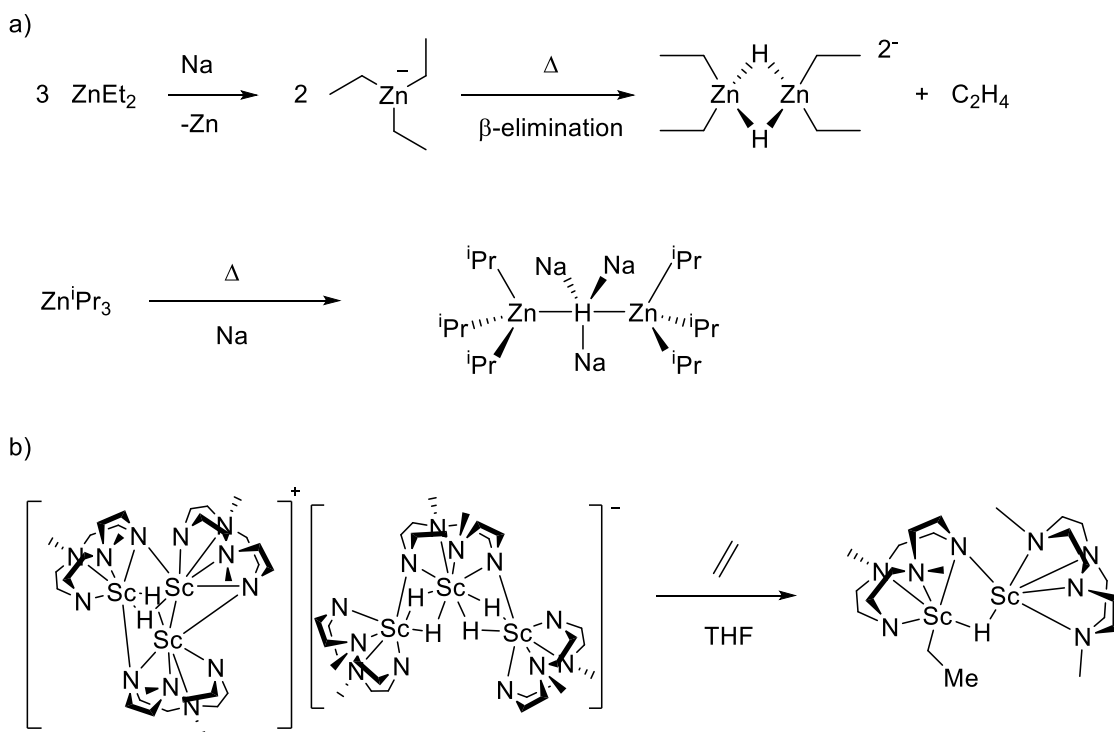
also reported the synthesis of a Sc complex featuring a $\text{Sc}_2(\mu\text{-H})(\text{Et})$ core by ethylene insertion of its hydrido precursor (Scheme **3.3 b**).¹² Due to the limited numbers of alkyl(aryl)-hydride complexes, one of our main purpose is to expand the scope of this chemistry. And inspired by the successful synthesis of various alkyl hydride featured diverse ligand/metal systems via different synthetic routs described above, the synthesis of α -diimine Cr alkyl hydrides may well be feasible.



Scheme 3.1 Synthesis of first row transition metal alkyl hydride complexes via hydrogenation



Scheme 3.2 DFT calculations of oxidative addition of CH_4 to NacnacCr(I) fragment (relative stability in terms of enthalpy)

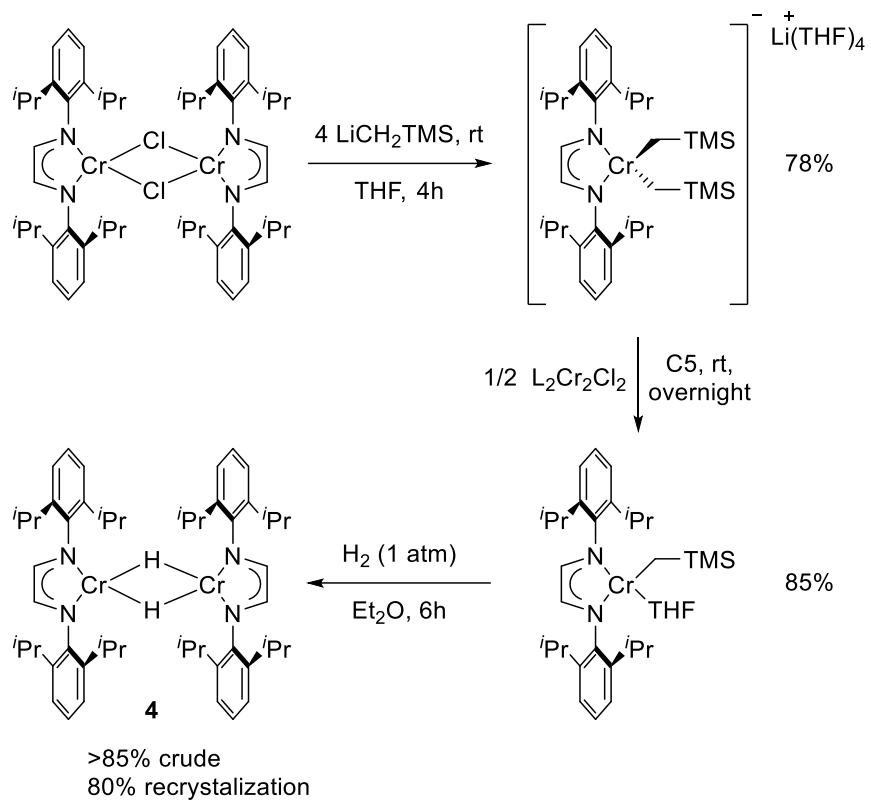


Scheme 3.3 Synthesis of first row transition metal alkyl hydride complexes via β -elimination and ethylene insertion

This chapter is organized into two parts, addressing the synthesis, isolation and characterization of chromium alkyl(aryl)-hydrides bearing α -diimine ligands and their properties. The first part focus on the synthesis of a series of chromium alkyl(aryl)-hydrides containing different bridging alkyl(aryl)- ligands. The second part discusses their kinetic properties of reductive elimination and attempted hydride abstraction with Me_3OBF_4 .

3.2 Results and Discussion

As shown in Scheme 3.1, hydrogenation of metal alkyls may generate binuclear bridging alkyl hydrides in both chromium and titanium chemistry. Inspired by those results, neutral chromium mono-alkyl complexes supported by α -diimine ligands were prepared and the hydrogenation of Cr alkyl toward alkyl hydride was tested. The initial attempts to synthesize an alkyl-hydride complex by exposure of a diethyl ether solution of $(^{\text{H}}\text{L}^{\text{iPr}}\text{Cr})(\text{CH}_2\text{TMS})(\text{THF})$ to 1 atm of hydrogen did not work as we planned. Instead, the dinuclear hydride complex $(^{\text{H}}\text{L}^{\text{iPr}}\text{Cr})_2(\mu\text{-H})_2$ (**4**) was synthesized and isolated (Scheme 3.4). After standard work up, **4** was recrystallized out of pentane solution at -30°C in 80% yield and characterized by X-ray diffraction crystallography. The solid state structure, bond distances, and angles of **4** are displayed in Figure 3.1 and Table 3.1 respectively.



Scheme 3.4 Preparation of $(\text{HL}^{\text{iPr}}\text{Cr})_2(\mu\text{-H})_2$

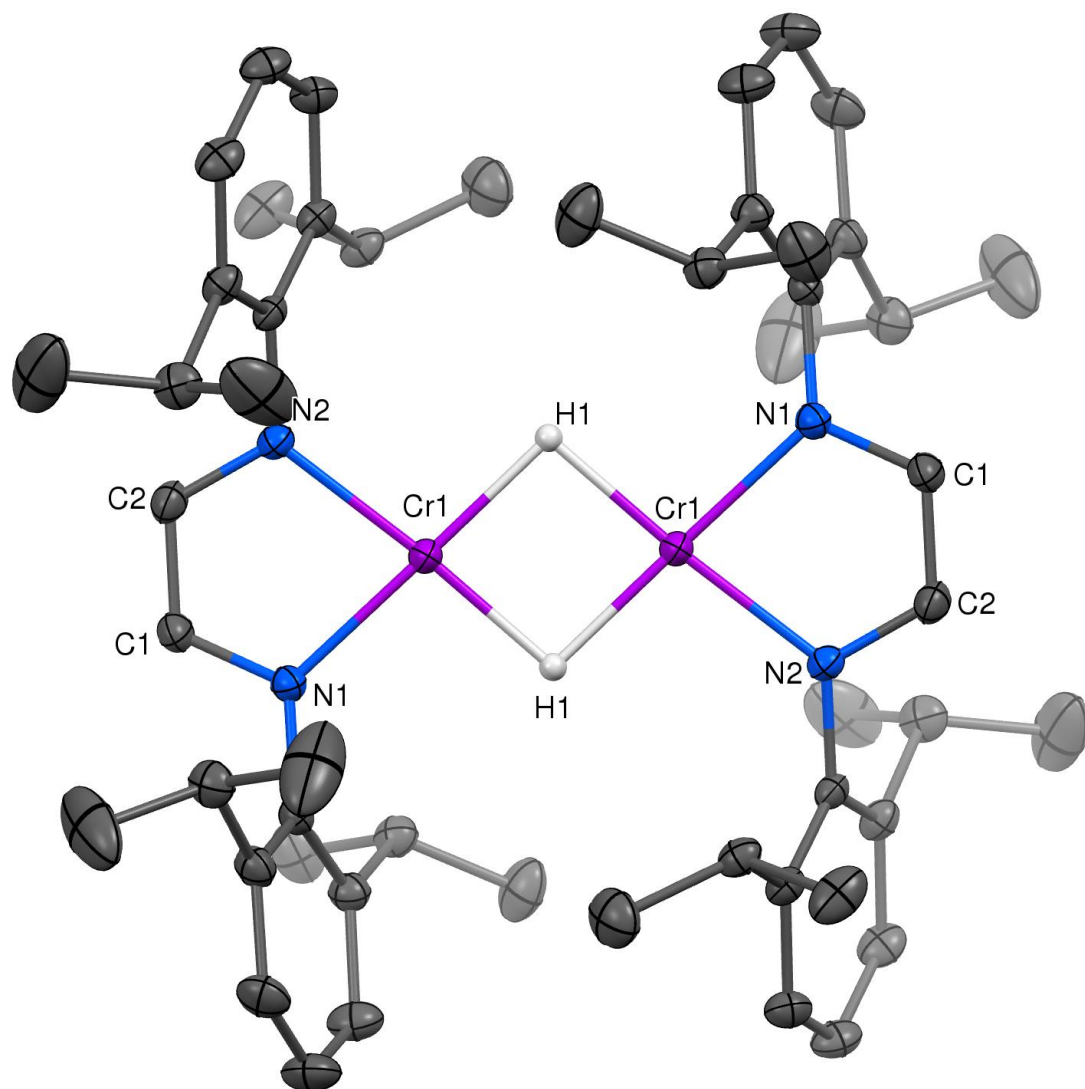


Figure 3.1 Molecular structure of $(^{\text{H}}\text{LiPrCr})_2(\mu\text{-H})_2$ (**4**) with thermal ellipsoids at the 30% probability level. H1 has been located on a difference map. Isopropyl groups and hydrogen atoms have been omitted for clarity.

Table 3.1 Interatomic distances (Å) and angles (°) for $(^{\text{H}}\text{LiPrCr})_2(\mu\text{-H})_2$ (**4**)

Distance (Å)			
Cr1-N1	2.000(2)	Cr1-N2	2.010(2)
Cr1-Cr1	2.6831(5)	Cr1-H1	1.80(2)
N1-C8	1.433(2)	N1-C1	1.336(2)

N2-C20	1.432(2)	N2-C2	1.336(2)
C3-C4	1.396(3)	C1-C2	1.394(3)
C3-C10'	1.520(7)	C3-C8	1.407(3)
C4-C5	1.378(3)	C3-C10	1.53(2)
C6-C7	1.397(3)	C5-C6	1.380(3)
C7-C13	1.516(3)	C7-C8	1.405(2)
C13-C14	1.522(3)	C12-C13	1.516(3)
C15-C20	1.409(2)	C15-C16	1.397(3)
C16-C17	1.380(3)	C15-C22	1.522(3)
C18-C19	1.391(2)	C17-C18	1.384(3)
C19-C25	1.522(2)	C19-C20	1.405(2)
C22-C23	1.509(4)	C21-C22	1.509(4)
C25-C26	1.522(3)	C24-C25	1.522(3)
C27-C32	1.402	C27-C28	1.397
C29-C30	1.396	C28-C29	1.397
C31-C32	1.402	C30-C31	1.396
C9-C10	1.53(1)	C32-C33	1.507
C9'-C10'	1.523(8)	C10-C11	1.54(1)
C10'-C11'	1.532(8)		

Angles (°)

N1-Cr1-N2	80.32(6)	N1-Cr1-Cr1	138.52(4)
N1-Cr1-H1	174.8(7)	N2-Cr1-H1	98.6(7)
N2-Cr1-Cr1	140.89(4)	H1-Cr1-H1	84.6(7)
C1-N1-C8	118.9(2)	C8-N1-Cr1	128.4(1)
C1-N1-Cr1	112.6(1)	C2-N2-Cr1	112.3(1)
C2-N2-C20	119.0(2)	N1-C1-C2	116.5(2)
C20-N2-Cr1	128.2(1)	C4-C3-C8	117.7(2)
N2-C2-C1	116.5(2)	C8-C3-C10'	122.0(4)
C4-C3-C10'	120.2(4)	C8-C3-C10	121.2(7)
C4-C3-C10	120.8(6)	C4-C5-C6	120.0(2)
C5-C4-C3	121.4(2)	C6-C7-C8	117.9(2)
C5-C6-C7	121.2(2)	C8-C7-C13	121.5(2)
C6-C7-C13	120.5(2)	C7-C8-N1	119.4(2)
C7-C8-C3	121.6(2)	C12-C13-C7	110.4(2)
C3-C8-N1	118.9(2)	C7-C13-C14	112.9(2)
C12-C13-C14	111.3(2)	C16-C15-C22	119.6(2)
C16-C15-C20	118.2(2)	C17-C16-C15	121.1(2)
C20-C15-C22	122.1(2)	C17-C18-C19	120.9(2)
C16-C17-C18	120.1(2)	C18-C19-C25	119.9(2)
C18-C19-C20	118.7(2)	C19-C20-C15	120.9(2)
C20-C19-C25	121.3(2)	C15-C20-N2	119.1(2)

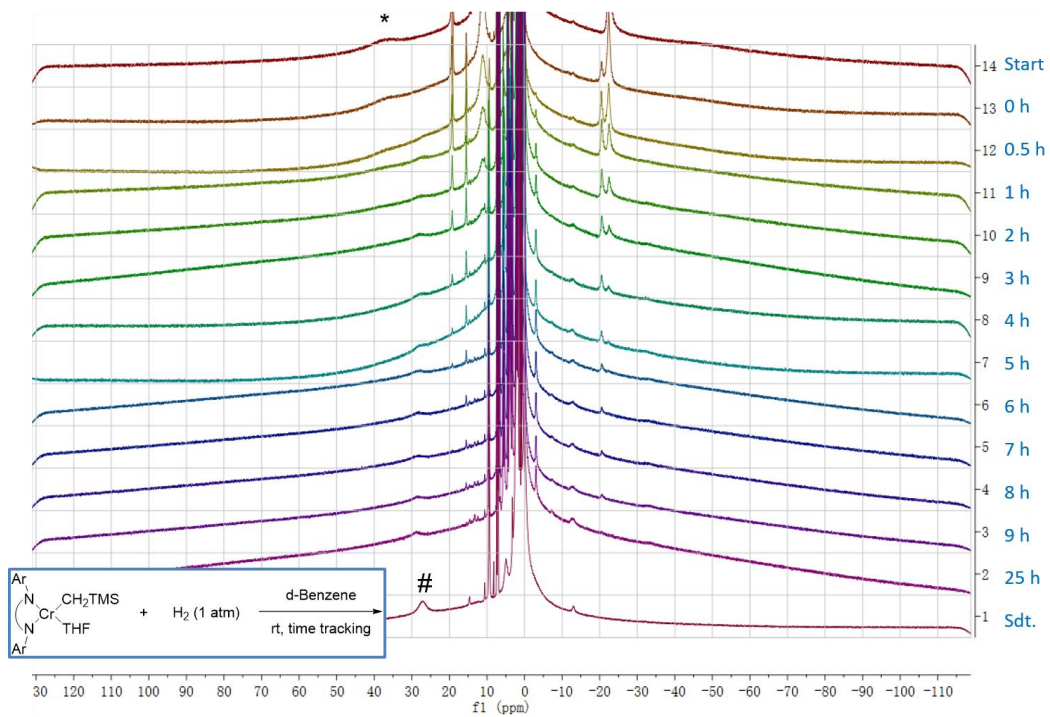
C19-C20-N2	112.0(2)	C23-C22-C15	112.9(2)
C23-C22-C21	110.3(3)	C19-C25-C26	112.7(2)
C21-C22-C15	111.6(2)	C26-C25-C24	110.7(2)
C19-C25-C24	109.9(2)	C27-C28-C29	120.1
C28-C27-C32	121.1	C31-C30-C29	120.1
C30-C29-C28	119.5	C31-C32-C27	118.1
C30-C31-C32	121.1	C27-C32-C33	120.9
C31-C32-C33	121	C3-C10-C11	113(1)
C3-C10-C9	110(1)	C3-C10'-C9'	113.4(7)
C9-C10-C11	109.9(9)	C9'-C10'-C11'	112.6(5)
C3-C10'-C11'	108.9(5)		

Complex **4** crystallized in the monoclinic space group $P2_1/c$ and contains a crystallographically imposed C2 axis bisecting the C1-C1 and C2-C2 vectors and perpendicular to Cr1-H1-Cr1-H1 plane. The bridging hydride H1 was located on a difference map. Despite the unavoidable systematic error associated with bond distances and angles of H atoms determined by X-ray crystallography, the Cr1-H1 bond length of 1.80(2) is comparable to other reported bridging hydride chromium complexes.¹³ The Cr-N bond length of 2.000(2) and 2.010(1) Å are in the range of α -diimine Cr complexes. The two Cr centers are 2.6831(5) Å away from each other. The average C-N bond length of 1.336(2) Å and C-C bond length of 1.394(3) Å of the ligand's backbone indicated that the ligand is monoanionic. Thus, **4** should be considered a Cr(II)-Cr(II) complex. The square planar coordination geometry of the Cr center, with ligand angles range from 98.6(7)° to 80.32(6)°, is consistent with the Cr(II) oxidation state assignment.

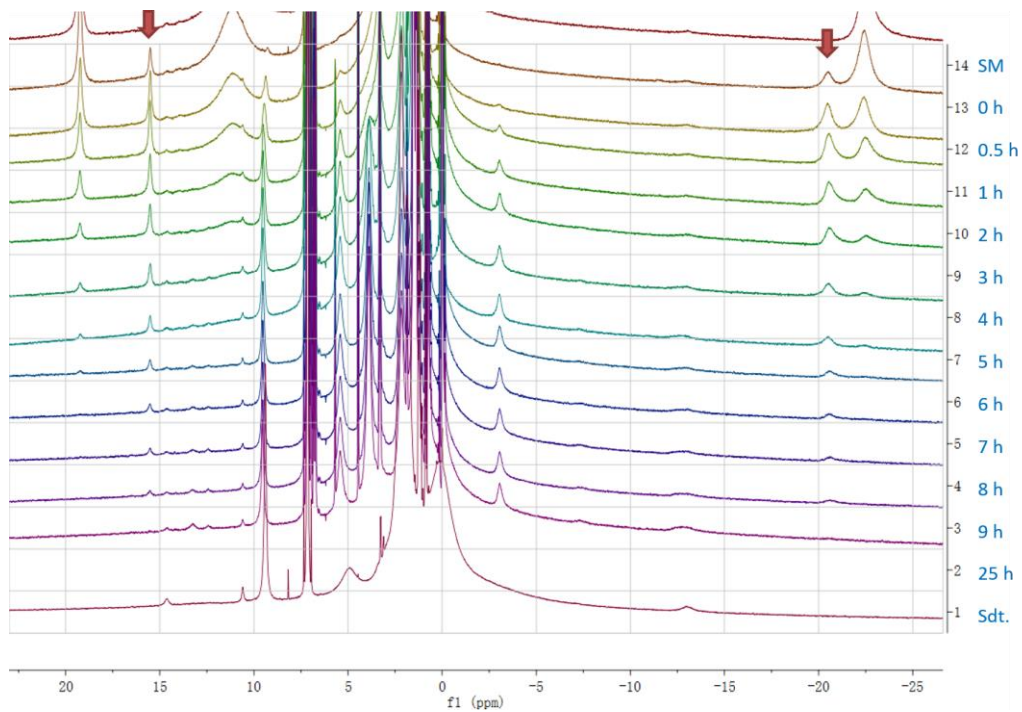
A green C₆D₆ solution of **4** showed broadened ¹H-NMR chemical shifts at 27.90, 4.47, 2.17, 2.16 and 0.20 ppm. The magnetic moment of dinuclear **4** in the solid state at room temperature was measured to be $\mu_{\text{eff}}(298 \text{ K}) = 2.3(1) \mu_{\text{B}}$ (1.6(1) μ_{B} for each Cr), which is much lower than the spin only moment for a Cr(II), d⁴ ion (4.8 μ_{B} ,

S = 1). This is presumably due to the strongly antiferromagnetic coupling between Cr atoms.

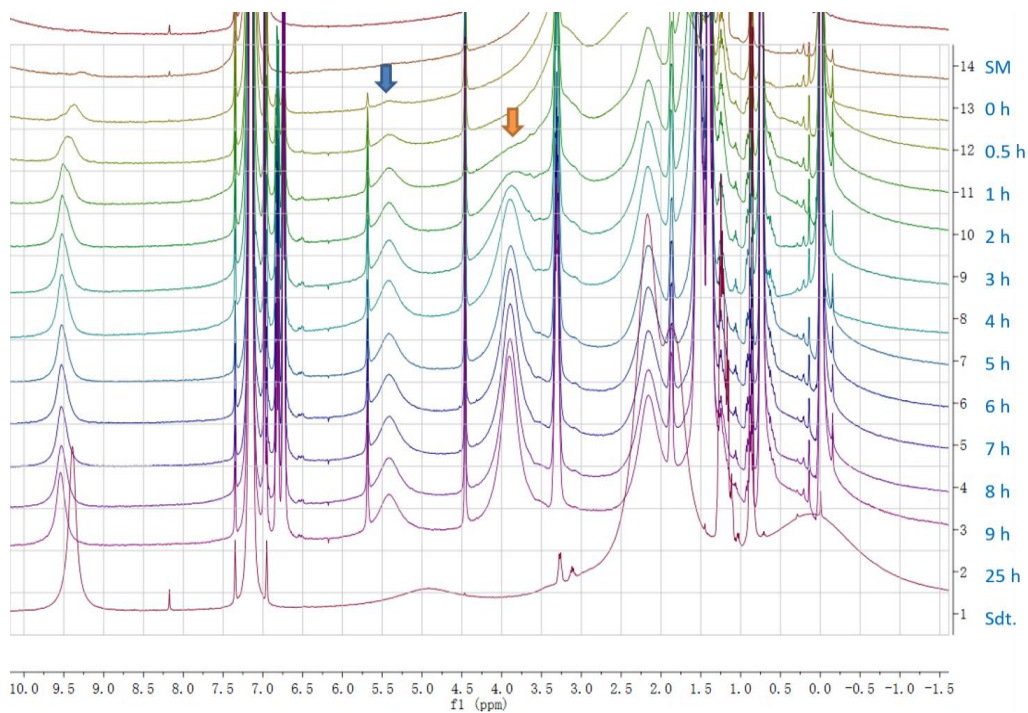
Close monitoring of the hydrogenation reaction of $(^{\text{H}}\text{L}^{\text{iPr}}\text{Cr})(\text{CH}_2\text{TMS})(\text{THF})$ by ^1H -NMR revealed that several intermediates were generated as the reaction proceeded (see Figure **3.2**). Presumably, there might be a chromium alkyl hydride intermediate formed before complete hydrogenation (Scheme **3.4**). Although the efforts to isolate the intermediates failed, it implied that the existence of a diimine ligand supported chromium alkyl hydride is possible.



(a)



(b)



(c)

Figure 3.2 Tracking ^1H -NMR spectra of $(^{\text{H}}\text{L}^{\text{iPr}}\text{Cr})(\text{CH}_2\text{TMS})(\text{THF})$ reacting with 1 atm of H_2 in C_6D_6 at room temperature. (a) The full NMR spectra range from -120 to 130 ppm to exhibit the reaction progress of hydrogenation. (b) The NMR spectra range from -25 to 20 ppm to exhibit the growth and disappearance of two peaks potentially associated with intermediates at -21 and 16 ppm. (c) The NMR spectra range from -1 to 10 ppm to exhibit the increasing of two peaks at 3.8 and 5.4 ppm. The (*) denotes the characteristic peak belong to $(^{\text{H}}\text{L}^{\text{iPr}}\text{Cr})(\text{CH}_2\text{TMS})(\text{THF})$ and the (#) denotes the characteristic peak belong to **4**.

With **4** in hand, the alkene insertion method, as shown in Scheme 3.3 b, was tested. A green Et_2O solution of **4** was exposed to 1 atm of ethylene at room temperature. The ^1H -NMR monitoring experiment was performed in a J-Young tube with C_6D_6 as solvent. No obvious color change was observed, but the ^1H -NMR spectra showed that an oligomerization of ethylene was promoted by **4** and a new complex

was generated (Figure 3.3). All attempts to isolate the new complex by crystallization only resulted in recovery of **4** as identified product. Presumably, the excess ethylene drove the reaction toward dimerization or trimerization of ethylene and **4** was recovered at the end via β -hydrogen elimination (Scheme 3.5). Thus, a stoichiometric amount of ethylene was introduced into a Et₂O solution of **4** in order to prevent oligomerization. The ¹H-NMR monitoring experiment in a J-Young tube showed that with limited amount of ethylene the oligomerization was suppressed and that a new complex was generated (Figure 3.2). Unfortunately, only **4** could be crystallized out and identified by X-ray diffraction. The reactions of **4** with ethylene implied the existence of a hydridoethyl chromium complex. Thus, 1 eq. of styrene and cyclohexene were separately reacted with **4** at room temperature and low temperature (-78 °C). The reaction with styrene led to rapid polymerization of styrene and the reaction with cyclohexene still yielded **4** as the only crystallized product. Considering the rapid β -elimination has been a problem to isolate the potential hydridoalkyl Cr complex, the strategy of olefin insertion (as shown in Scheme 3.3 b) was ruled out and only alkyls without β -H were applied in later syntheses.

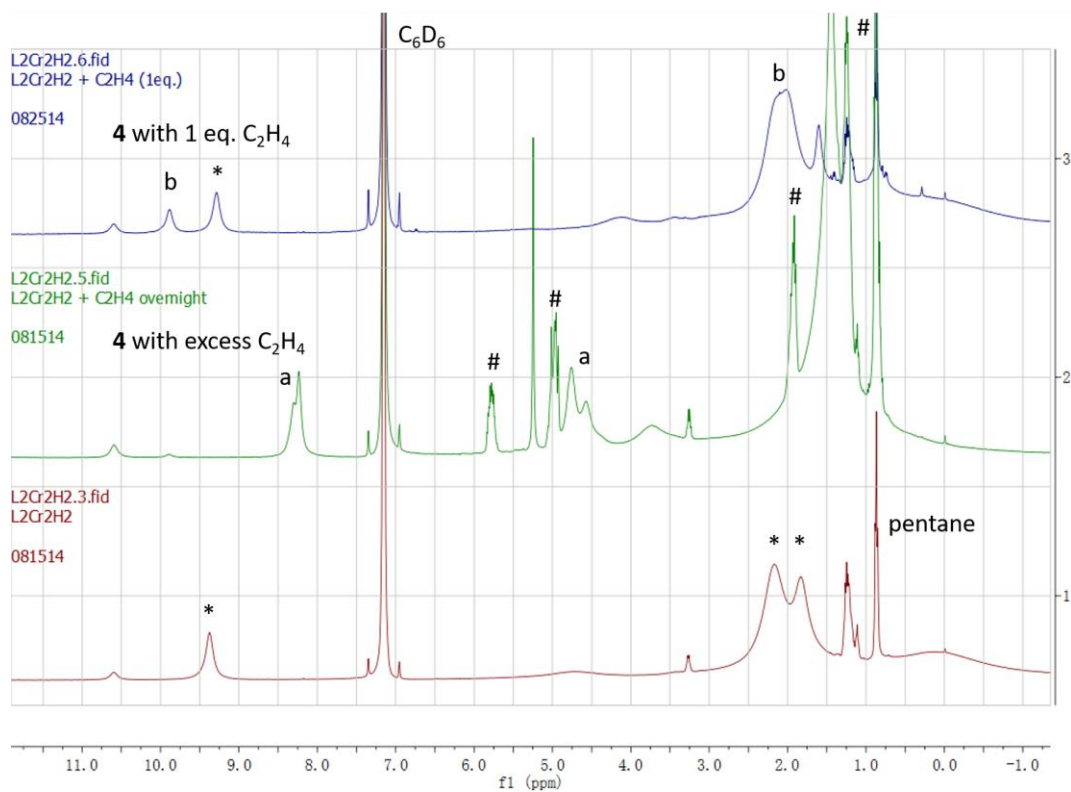
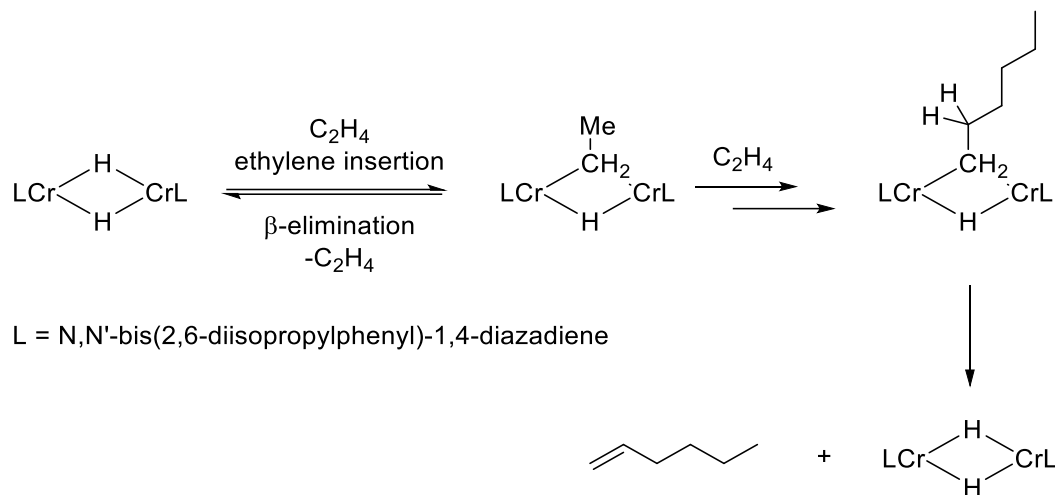


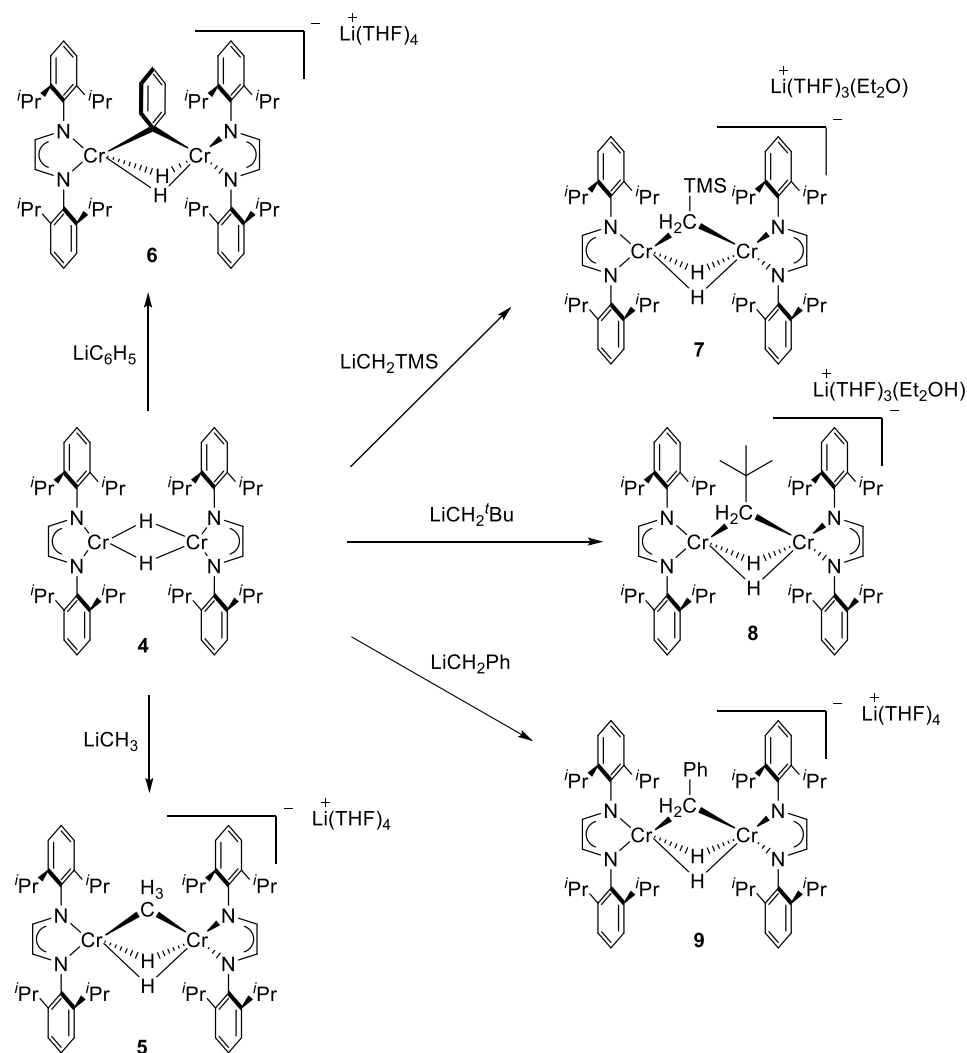
Figure 3.3 $^1\text{H-NMR}$ of ethylene insertion and oligomerization with 4 in C_6D_6 . The (*) denotes the characteristic peak belong to 4 and the (#) denotes the characteristic peak belong to 1-hexene. The (a) denotes the unknown complex a and the (b) denotes the unknown complex b.



Scheme 3.5 Reaction of **4** with ethylene.

Since the methods reported in the literature (as shown in Scheme 3.1 and 3.3) did not work for the α -diimine Cr system, a new strategy of synthesizing chromium alkyl hydrides via alkylation was explored. As reported by Kreisel *et al.*, the reactions of $L_2Cr_2(\mu-Cl)_2$ with 3 eq. of MeLi or $LiBEt_3H$ resulted in $L_2Cr_2(\mu-R)_3[Li(THF)_4]$ ($R = Me$ or H).¹⁶ Presumably, the formation of $L_2Cr_2(\mu-Me)_3^-$ resulted from the methylation of $L_2Cr_2(\mu-Me)_2$ intermediate with MeLi. Thus, the methylation of $L_2Cr_2(\mu-H)_2$ should give a $L_2Cr_2(\mu-Me)(\mu-H)_2^-$ complex. Reaction of **4** with 1 eq. of MeLi at $-30^\circ C$ in a mixed solvent of pentane and 5 drops of THF gave a violet slurry after stirring for 15 min. The solvent needed to be removed immediately after the reaction was done in order to prevent side-reactions. Thereafter, the dark violet solid was washed with pentane, extracted with THF and recrystallized by layering with pentane to give a diimine ligand supported binuclear chromium bis(hydrido)methyl complex $[(^H L^{iPr}Cr)_2(\mu-Me)(\mu-H)_2][Li(THF)_4]^+$ (**5**) in 63% crystalline yield. In a similar fashion, **4** could react with wide scope of lithium alkyls and thereby gave

$[(^H\text{L}^{\text{iPr}}\text{Cr})_2(\mu\text{-Ph})(\mu\text{-H})_2]^- [\text{Li}(\text{THF})_4]^+$ (**6**), $[(^H\text{L}^{\text{iPr}}\text{Cr})_2(\mu\text{-CH}_2\text{TMS})(\mu\text{-H})_2]^-$
 $[\text{Li}(\text{THF})_3(\text{Et}_2\text{O})]^+$ (**7**), $[(^H\text{L}^{\text{iPr}}\text{Cr})_2(\mu\text{-CH}_2^t\text{Bu})(\mu\text{-H})_2]^- [\text{Li}(\text{THF})_3(\text{Et}_2\text{O})]^+$ (**8**) and
 $[(^H\text{L}^{\text{iPr}}\text{Cr})_2(\mu\text{-CH}_2\text{Ph})(\mu\text{-H})_2]^- [\text{Li}(\text{THF})_4]^+$ (**9**) in moderate to good yield (65% - 72%,
 crystalline yield) (Scheme 3.6). The solid state structures, bond distances, and angles
 of **5-9** are displayed in Figure 3.4 - 3.8 and Tables 3.2 - 3.6 respectively.



Scheme 3.6 Reaction of $(^H\text{L}^{\text{iPr}}\text{Cr})_2(\mu\text{-H})_2$ with lithium alkyls

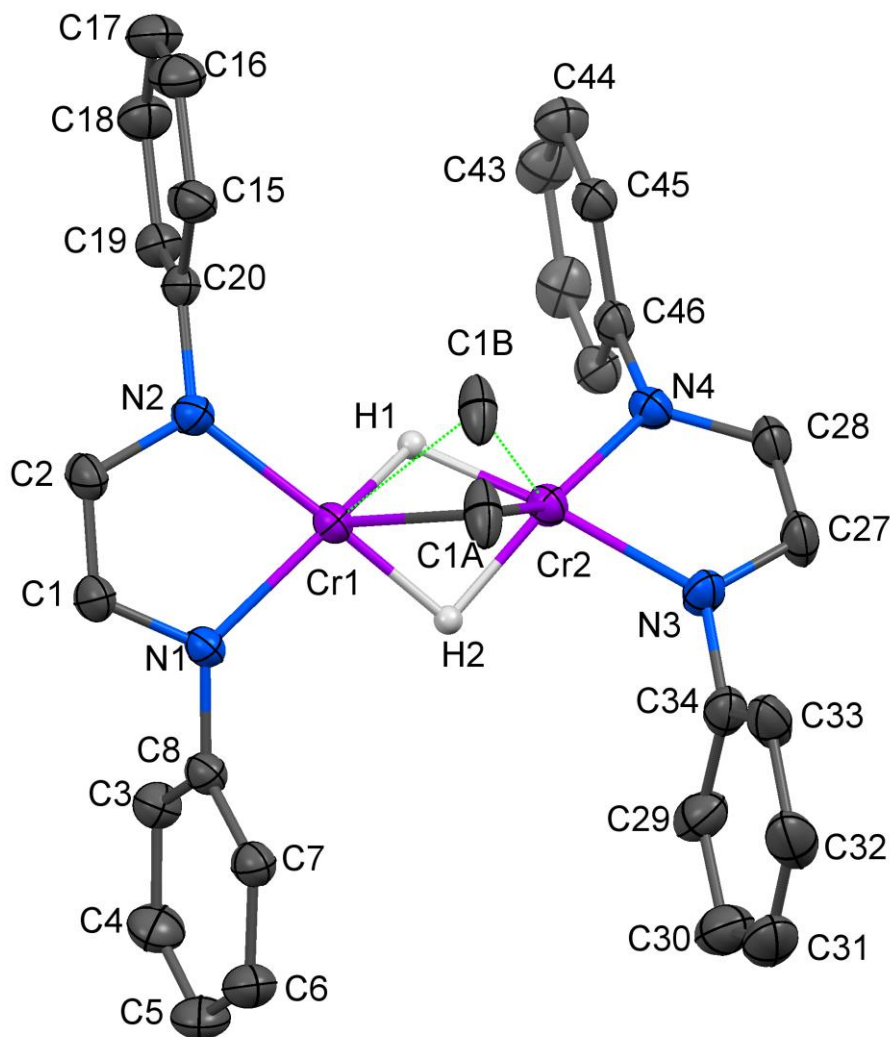


Figure 3.4 Molecular structure of $[(\text{H}^{\text{iPr}}\text{Cr})_2(\mu\text{-Me})(\mu\text{-H})_2][\text{Li}(\text{THF})_4]^+$ (**5**) with thermal ellipsoids at the 30% probability level. H1 H2 have been located on a difference map. Isopropyl groups and hydrogen atoms have been omitted for clarity.

Table 3.2 Interatomic distances (Å) and angles (°) for [(^HL^{iPr}Cr)₂(μ-Me)(μ-H)₂]⁻ [Li(THF)₄]⁺ (5)

		Distance (Å)	
Cr1-N1	1.956(3)	Cr1-N2	1.959(4)
Cr1-C1A	2.236(9)	Cr1-C1B	2.303(9)
Cr1-Cr2	2.442(1)	Cr2-N4	1.960(4)
Cr2-N3	1.966(4)	Cr2-C1B	2.224(9)
Cr2-C1A	2.31(1)	N1-C1	1.364(6)
N1-C8	1.433(6)	N2-C2	1.373(6)
N2-C20	1.432(5)	N3-C27	1.367(6)
N3-C34	1.431(6)	N4-C28	1.369(6)
N4-C46	1.435(6)	C1-C2	1.330(7)
C3-C4	1.391(7)	C3-C8	1.411(7)
C3-C10	1.520(7)	C4-C5	1.374(8)
C5-C6	1.374(9)	C6-C7	1.392(7)
C7-C8	1.397(7)	C7-C13	1.524(7)
C9-C10	1.535(9)	C10-C11	1.504(8)
C12-C13	1.540(8)	C13-C14	1.502(8)
C15-C16	1.406(7)	C15-C20	1.407(7)
C15-C22	1.519(8)	C16-C17	1.376(8)
C17-C18	1.359(8)	C18-C19	1.408(7)
C19-C20	1.406(7)	C19-C25	1.511(7)
C21-C22	1.50(1)	C22-C23	1.52(1)
C24-C25	1.518(8)	C25-C26	1.503(8)
C27-C28	1.331(7)	C29-C30	1.386(8)
C29-C34	1.400(8)	C29-C36	1.521(9)
C30-C31	1.38(1)	C31-C32	1.36(1)
C32-C33	1.416(8)	C33-C34	1.407(8)
C33-C39	1.513(9)	C35-C36	1.49(1)
C36-C37	1.54(1)	C39-C40	1.47(1)
C39-C38	1.53(1)	C41-C42	1.392(7)
C41-C46	1.413(7)	C41-C48	1.524(7)
C42-C43	1.368(8)	C43-C44	1.373(8)
C44-C45	1.404(7)	C45-C46	1.394(7)
C45-C51	1.518(7)	C47-C48	1.511(8)
C48-C49	1.511(9)	C50-C51	1.522(8)
C51-C52	1.525(8)	Li1-O1_3	1.91(2)
Li1-O1_2	1.93(2)	Li1-O1_4	1.94(2)
Li1-C11_1	2.27(2)	Li2-O1_5	1.91(2)
Li2-O1_7	1.91(2)	Li2-O1_6	1.97(2)
Li2-C11_1	2.26(2)	O1_2-C4_2	1.408(9)

O1_2-C1_2	1.441(8)	C1_2-C2_2	1.465(9)
C2_2-C3_2	1.488(9)	C3_2-C4_2	1.464(9)
O1_3-C4_3	1.399(8)	O1_3-C1_3	1.423(9)
C1_3-C2_3	1.447(9)	C2_3-C3_3	1.468(9)
C3_3-C4_3	1.468(9)	O1_4-C1_4	1.420(9)
O1_4-C4_4	1.45(1)	C1_4-C2_4	1.53(1)
C2_4-C3_4	1.39(1)	C3_4-C4_4	1.46(1)
O1_5-C4B_5	1.34(3)	O1_5-C1_5	1.428(8)
O1_5-C4A_5	1.57(5)	C1_5-C2_5	1.459(8)
C2_5-C3_5	1.495(9)	C3_5-C4A_5	1.35(3)
C3_5-C4B_5	1.56(4)	O1_6-C4_6	1.442(9)
O1_6-C1_6	1.444(9)	C1_6-C2_6	1.44(1)
C2_6-C3_6	1.45(1)	C3_6-C4_6	1.48(1)
O1_7-C4_7	1.380(8)	O1_7-C1_7	1.451(8)
C1_7-C2_7	1.423(9)	C2_7-C3_7	1.478(9)
C3_7-C4_7	1.447(9)		

Angles (°)

N1-Cr1-N2	80.6(2)	N1-Cr1-C1A	117.8(4)
N2-Cr1-C1A	114.8(3)	N1-Cr1-C1B	142.7(3)
N2-Cr1-C1B	97.2(3)	N1-Cr1-Cr2	140.5(1)
N2-Cr1-Cr2	138.5 (1)	C1A-Cr1-Cr2	58.9(2)
C1B-Cr1-Cr2	55.8(2)	N4-Cr2-N3	80.6(2)
N4-Cr2-C1B	116.4(4)	N3-Cr2-C1B	115.5(3)
N4-Cr2-C1A	141.4(3)	N3-Cr2-C1A	97.8(3)
N4-Cr2-Cr1	139.7 (1)	N3-Cr2-Cr1	139.4 (1)
C1B-Cr2-Cr1	58.9(2)	C1A-Cr2-Cr1	56.1(2)
Cr1-C1A-Cr2	65.0(3)	Cr2-C1B-Cr1	65.3(3)
C1-N1-C8	117.0(4)	C1-N1-Cr1	113.2(3)
C8-N1-Cr1	128.6(3)	C2-N2-C20	116.3(4)
C2-N2-Cr1	113.8(3)	C20-N2-Cr1	128.9(3)
C27-N3-C34	117.1(4)	C27-N3-Cr2	113.5(3)
C34-N3-Cr2	128.8(3)	C28-N4-C46	116.9(4)
C28-N4-Cr2	113.3(3)	C46-N4-Cr2	128.8(3)
C2-C1-N1	117.1(4)	C1-C2-N2	115.0(4)
C4-C3-C8	119.0(5)	C4-C3-C10	119.6(5)
C8-C3-C10	121.4(4)	C5-C4-C3	120.8(5)
C6-C5-C4	120.1(5)	C5-C6-C7	121.2(5)
C6-C7-C8	118.9(5)	C6-C7-C13	120.0(5)
C8-C7-C13	121.1(4)	C7-C8-C3	120.0(4)
C7-C8-N1	121.3(4)	C3-C8-N1	118.7(4)
C11-C10-C3	113.7(5)	C11-C10-C9	111.5(6)

C3-C10-C9	109.8(5)	C14-C13-C7	111.3(5)
C14-C13-C12	110.8(6)	C7-C13-C12	111.6(5)
C16-C15-C20	118.4(5)	C16-C15-C22	120.3(5)
C20-C15-C22	121.3(4)	C17-C16-C15	120.8(5)
C18-C17-C16	120.5(5)	C17-C18-C19	121.5(5)
C20-C19-C18	118.0(5)	C20-C19-C25	122.4(4)
C18-C19-C25	119.5(5)	C19-C20-C15	120.7(4)
C19-C20-N2	118.8(4)	C15-C20-N2	120.4(4)
C21-C22-C15	111.2(5)	C21-C22-C23	110.8(7)
C15-C22-C23	111.0(6)	C26-C25-C19	112.7(5)
C26-C25-C24	111.1(5)	C19-C25-C24	112.0(4)
C28-C27-N3	115.9(4)	C27-C28-N4	116.5(4)
C30-C29-C34	118.4(6)	C30-C29-C36	119.7(6)
C34-C29-C36	121.8(5)	C31-C30-C29	121.1(6)
C32-C31-C30	121.2(6)	C31-C32-C33	120.0(6)
C34-C33-C32	118.3(6)	C34-C33-C39	122.5(5)
C32-C33-C39	119.2(6)	C29-C34-C33	120.9(5)
C29-C34-N3	118.9(5)	C33-C34-N3	120.3(5)
C35-C36-C29	113.6(7)	C35-C36-C37	111.5(7)
C29-C36-C37	112.7(6)	C40-C39-C33	113.1(6)
C40-C39-C38	110.9(9)	C33-C39-C38	112.2(7)
C42-C41-C46	117.9(5)	C42-C41-C48	120.1(5)
C46-C41-C48	122.0(4)	C43-C42-C41	121.8(5)
C42-C43-C44	120.0(5)	C43-C44-C45	121.1(5)
C46-C45-C44	118.3(5)	C46-C45-C51	121.7(4)
C44-C45-C51	120.0(5)	C45-C46-C41	120.9(4)
C45-C46-N4	120.6(4)	C41-C46-N4	118.5(4)
C49-C48-C47	111.5(7)	C49-C48-C41	110.7(5)
C47-C48-C41	111.6(5)	C45-C51-C50	111.7(5)
C45-C51-C52	111.4(5)	C50-C51-C52	110.8(6)
O1_3-Li1-O1_2	109(1)	O1_3-Li1-O1_4	103.8(9)
O1_2-Li1-O1_4	112(1)	O1_3-Li1-C11_1	114.0(9)
O1_2-Li1-C11_1	109.4(8)	O1_4-Li1-C11_1	108.7(9)
O1_5-Li2-O1_7	109.7(9)	O1_5-Li2-O1_6	104.4(8)
O1_7-Li2-O1_6	111.4(8)	O1_5-Li2-C11_1	116.3(8)
O1_7-Li2-C11_1	108.4(7)	O1_6-Li2-C11_1	106.7(7)
Li2-C11_1-Li1	167.3(6)	C4_2-O1_2-C1_2	110.0(6)
C4_2-O1_2-Li1	129.0(7)	C1_2-O1_2-Li1	121.0(7)
O1_2-C1_2-C2_2	105.7(6)	C1_2-C2_2-C3_2	103.8(6)
C4_2-C3_2-C2_2	105.1(7)	O1_2-C4_2-C3_2	106.6(6)
C4_3-O1_3-C1_3	105.3(7)	C4_3-O1_3-Li1	126.0(8)
C1_3-O1_3-Li1	120.6(8)	O1_3-C1_3-C2_3	105.1(7)
C1_3-C2_3-C3_3	105.7(7)	C2_3-C3_3-C4_3	105.0(7)

O1_3-C4_3-C3_3	106.3(7)	C1_4-O1_4-C4_4	111.5(8)
C1_4-O1_4-Li1	126.1(9)	C4_4-O1_4-Li1	112.6(9)
O1_4-C1_4-C2_4	99.8(7)	C3_4-C2_4-C1_4	107.6(7)
C2_4-C3_4-C4_4	110.3(8)	O1_4-C4_4-C3_4	98.4(7)
C4B_5-O1_5-C1_5	105(1)	C1_5-O1_5-C4A_5	107(1)
C4B_5-O1_5-Li2	127 (2)	C1_5-O1_5-Li2	123.5(7)
C4A_5-O1_5-Li2	118 (2)	O1_5-C1_5-C2_5	105.8(6)
C1_5-C2_5-C3_5	105.4(6)	C4A_5-C3_5-C2_5	112.(2)
C2_5-C3_5-C4B_5	101 (2)	C3_5-C4A_5-O1_5	104 (2)
O1_5-C4B_5-C3_5	105 (2)	C4_6-O1_6-C1_6	105.9(7)
C4_6-O1_6-Li2	119.0(7)	C1_6-O1_6-Li2	120.7(7)
C2_6-C1_6-O1_6	106.8(7)	C1_6-C2_6-C3_6	106.2(7)
C2_6-C3_6-C4_6	107.4(7)	O1_6-C4_6-C3_6	103.8(7)
C4_7-O1_7-C1_7	108.8(6)	C4_7-O1_7-Li2	131.2(7)
C1_7-O1_7-Li2	118.7(7)	C2_7-C1_7-O1_7	107.0(6)
C1_7-C2_7-C3_7	105.7(6)	C4_7-C3_7-C2_7	105.9(6)
O1_7-C4_7-C3_7	108.7(6)		

Due to the fact that **5** often crystallized in long needle or thin plate form, crystal that is suitable for X-ray diffraction was hard to obtain. The structure in Figure 3.4 and data in Table 3.3 are the best results from many trials. **5** crystallized in triclinic space group *P*-1, and the methyl group has added across the two Cr centers resulting in a bridging methyl di(hydrido) complex. The crystal structure contained a Li(THF)₃CiLi(THF)₃ cation, which was unexpected. The products of alkyl lithium and α -diimine Cr complexes typically pair with a Li(THF)₄ or Li(THF)₃(Et₂O) counterion as shown in literatures.¹⁶ The LiCl contamination was likely from impure (^HL^{iPr}Cr)₂(μ -H)₂ precursor. Thus the formula of **5** is still best described as [(^HL^{iPr}Cr)₂(μ -Me)(μ -H)₂][Li(THF)₄]. The bridging methyl was split into C1A and C1B positions due to disorder of the crystal structure. The bridging hydrides H1 and H2 were localized by difference map, yet the methyl protons were unable to be refined due to disorder of methyl carbon. The ligand backbone average C-C length of 1.330(7) Å and C-N length of 1.368(6) Å indicate that both diimine ligands are dianionic, thus **5** is best described

as a Cr(III)-Cr(III) complex. Due to binding of the three bridging ligand, the geometry around each Cr is distorted from ideal form. In order to address this issue, the τ_5 parameter was used. This was first proposed by Addison *et al.*, to distinguish coordination geometries of 5-coordinate compounds.¹⁴ τ_5 equals the difference of the two greatest valence angles of the coordination center divided by 60° . When τ_5 is close to 0 the geometry is similar to square pyramidal, while if τ_5 is close to 1 the geometry is similar to trigonal bipyramidal. Thus, the geometry around Cr1 is closer to trigonal bipyramidal with axis of H2-Cr1-N2 and τ_5 value of 0.56, and the Cr2 shows a twisted square pyramidal geometry with a tilted axis of Cr2-C1A and τ_5 value of 0.26. The Cr-C distances are 2.236(9) Å and 2.308(9) Å. The bridging ligands held the chromium atoms at a short distance of 2.4420(10) Å from one to another, suggesting the possibility of an unusual metal-metal bonding of Cr(III)-Cr(III). The THF solvated lithium cation does not exhibit any close contact with the anion. Room temperature magnetic measurement of **5** gave low μ_{eff} values of 2.1(1) μ_{B} per Cr, likely due to antiferromagnetic coupling between the chromium ions. The complex showed broadened paramagnetic $^1\text{H-NMR}$ resonances at 7.78, 5.60, 3.39 and 1.67 ppm in C_6D_6 .

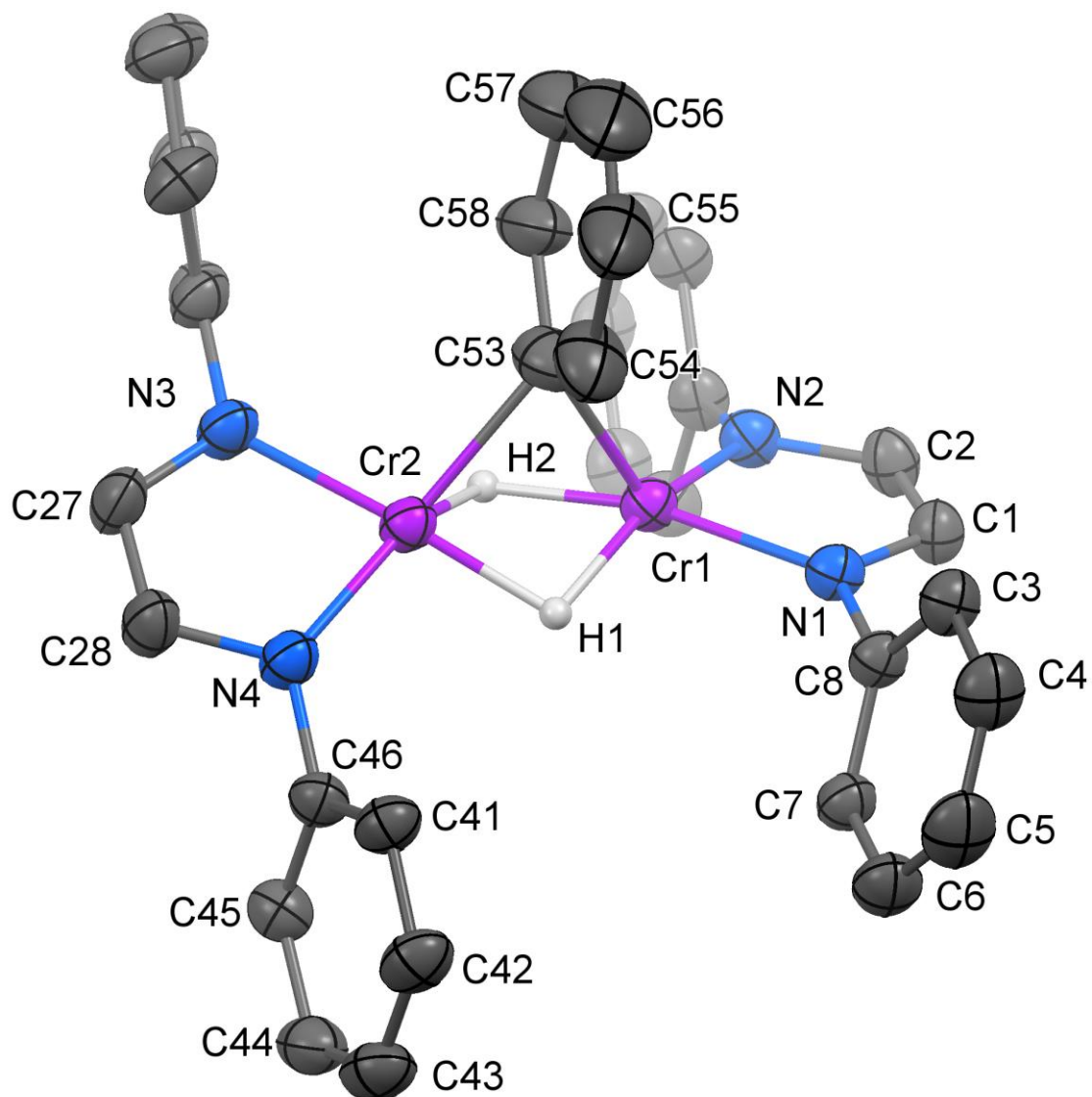


Figure 3.5 Molecular structure of $[(^{\text{H}}\text{Li}^{\text{iPr}}\text{Cr})_2(\mu\text{-Ph})(\mu\text{-H})_2][\text{Li}(\text{THF})_4]^+$ (**6**) with thermal ellipsoids at the 30% probability level. H1 has been located on a difference map. Isopropyl groups and hydrogen atoms have been omitted for clarity.

Table 3.3 Interatomic distances (Å) and angles (°) for [(^HL^{iPr}Cr)₂(μ-Ph)(μ-H)₂]⁻ [Li(THF)₄]⁺ (6)

Distance (Å)			
Cr1-N2	1.965(3)	Cr1-N1	1.965(3)
Cr1-C53	2.216(5)	Cr1-Cr2	2.4823(7)
Cr1-H1	1.71(3)	Cr1-H2	1.70(3)
Cr2-N4	1.948(3)	Cr2-N3	1.977(3)
Cr2-C53	2.181(4)	Cr2-H1	1.67(3)
Cr2-H2	1.61(3)	N1-C1	1.377(4)
N1-C8	1.430(4)	N2-C2	1.382(4)
N2-C20	1.433(4)	N3-C27	1.375(5)
N3-C34	1.427(4)	N4-C28	1.382(4)
N4-C46	1.434(4)	C1-C2	1.360(4)
C3-C10	1.517(5)	C3-C4	1.402(5)
C3-C8	1.400(4)	C4-C5	1.364(6)
C7-C13	1.504(5)	C5-C6	1.376(6)
C12-C13	1.496(6)	C6-C7	1.394(5)
C13-C14	1.539(6)	C7-C8	1.407(4)
C15-C20	1.409(5)	C9-C10	1.523(6)
C16-C17	1.396(6)	C10-C11	1.522(6)
C17-C18	1.363(6)	C15-C16	1.394(5)
C18-C19	1.413(4)	C15-C22	1.509(5)
C19-C20	1.403(5)	C19-C25'	1.503(5)
C19-C25	1.503(5)	C21-C22	1.521(7)
C24-C25	1.53(1)	C22-C23	1.527(7)
C25-C26	1.57(1)	C24'-C25'	1.582(8)
C27-C28	1.350(5)	C25'-C26'	1.526(8)
C29-C30	1.403(6)	C29-C34	1.393(5)
C29-C36	1.540(7)	C29-C36'	1.540(7)
C33-C39	1.520(5)	C30-C31	1.357(7)
C35'-C36'	1.535(9)	C31-C32	1.361(6)
C36'-C37'	1.57(1)	C32-C33	1.386(5)
C41-C42	1.394(5)	C33-C34	1.407(5)
C41-C48'	1.507(5)	C35-C36	1.56(2)
C42-C43	1.373(6)	C36-C37	1.56(2)
C43-C44	1.374(6)	C38-C39	1.508(6)
C44-C45	1.399(5)	C39-C40	1.518(6)
C45-C46	1.408(5)	C41-C46	1.404(5)
C45-C51	1.512(5)	C41-C48	1.507(5)

C47'-C48'	1.524(7)	C45-C51'	1.512(5)
C48'-C49'	1.537(8)	C47-C48	1.49(1)
C50'-C51'	1.535(7)	C48-C49	1.52(1)
C51'-C52'	1.580(7)	C50-C51	1.53(1)
C53-C58	1.426(6)	C51-C52	1.52(1)
C59-C60	1.47(2)	C53-C54	1.358(7)
C60'-C61'	1.416(9)	C54-C55	1.437(7)
C61-C62	1.47(2)	C55-C56	1.29(1)
C63-C64	1.51(1)	C56-C57	1.38(1)
C65-C66	1.45(1)	C57-C58	1.392(8)
C67'-C68'	1.48(1)	C59'-C60'	1.43(1)
C68-C69	1.51(2)	C60-C61	1.46(1)
C69'-C70'	1.47(1)	C61'-C62'	1.47(1)
C72-C73	1.470(9)	C64-C65	1.40(1)
Li1-O1'	1.905(9)	C67-C68	1.50(2)
Li1-O3'	1.915(9)	C68'-C69'	1.47(1)
Li1-O4	1.921(8)	C69-C70	1.51(2)
O1'-C62'	1.447(8)	C71-C72	1.482(8)
O1-C62	1.43(2)	C73-C74	1.417(9)
O2-C66	1.425(7)	Li1-O1	1.905(9)
O3'-C67'	1.420(9)	Li1-O2	1.919(8)
O3-C70	1.44(2)	Li1-O3	1.915(9)
O4-C74	1.434(7)	O1'-C59'	1.424(8)
O3-C67	1.44(2)	O1-C59	1.45(1)
O3'-C70'	1.421(9)	O2-C63	1.429(7)
O4-C71	1.413(6)		

Angles (°)

N2-Cr1-N1	80.7 (1)	N2-Cr1-C53	121.6(2)
N1-Cr1-C53	117.4(2)	N2-Cr1-Cr2	139.94(8)
N1-Cr1-Cr2	138.79(8)	C53-Cr1-Cr2	55.0(1)
N2-Cr1-H1	159(1)	N1-Cr1-H1	98(1)
C53-Cr1-H1	77(1)	Cr2-Cr1-H1	42(1)
N2-Cr1-H2	100(1)	N1-Cr1-H2	166(1)
C53-Cr1-H2	74(1)	Cr2-Cr1-H2	40(1)
H1-Cr1-H2	76(2)	N4-Cr2-N3	80.4(1)
N4-Cr2-C53	138.1(2)	N3-Cr2-C53	103.7(2)
N4-Cr2-Cr1	139.32(8)	N3-Cr2-Cr1	139.16(9)
C53-Cr2-Cr1	56.3(1)	N4-Cr2-H1	96(1)
N3-Cr2-H1	176(1)	C53-Cr2-H1	79(1)

Cr1-Cr2-H1	43(1)	N4-Cr2-H2	144(1)
N3-Cr2-H2	102(1)	C53-Cr2-H2	77(1)
Cr1-Cr2-H2	43(1)	H1-Cr2-H2	79(2)
C1-N1-C8	116.3(3)	C1-N1-Cr1	114.1(2)
C8-N1-Cr1	129.5(2)	C2-N2-C20	114.6(3)
C2-N2-Cr1	114.0(2)	C20-N2-Cr1	129.9(2)
C27-N3-C34	118.2(3)	C27-N3-Cr2	113.8(2)
C34-N3-Cr2	128.0(2)	C28-N4-C46	114.9(3)
C28-N4-Cr2	114.9(2)	C46-N4-Cr2	129.5(2)
C11-C10-C9	110.1(3)	C12-C13-C14	110.9(4)
C12-C13-C7	115.0(4)	C15-C16-C17	120.4(4)
C15-C22-C21	112.0(4)	C15-C20-N2	118.4(3)
C16-C15-C20	118.9(3)	C15-C22-C23	111.8(4)
C18-C17-C16	120.2(3)	C16-C15-C22	119.6(3)
C18-C19-C25	120.3(3)	C17-C18-C19	121.7(4)
C18-C19-C25'	120.3(3)	C19-C20-C15	121.1(3)
C19-C20-N2	120.5(3)	C19-C25'-C24'	107.1(8)
C19-C25-C24	116.(2)	C19-C25-C26	104(1)
C19-C25'-C26'	116.0(5)	C1-C2-N2	115.5(3)
C20-C15-C22	121.5(3)	C20-C19-C25	121.9(3)
C20-C19-C18	117.7(3)	C20-C19-C25'	121.9(3)
C21-C22-C23	110.3(4)	C27-C28-N4	115.1(3)
C24-C25-C26	110(1)	C29-C34-C33	120.2(3)
C26'-C25'-C24'	109.4(5)	C29-C36'-C37'	110(1)
C28-C27-N3	115.7(3)	C31-C30-C29	122.4(4)
C29-C34-N3	120.8(3)	C31-C32-C33	121.9(4)
C29-C36'-C35'	117.2(7)	C32-C33-C39	120.4(4)
C2-C1-N1	115.4(3)	C33-C34-N3	118.8(3)
C30-C29-C36	121.4(4)	C34-C29-C36	120.8(4)
C30-C29-C36'	121.4(4)	C34-C29-C36'	120.8(4)
C30-C31-C32	119.2(4)	C37-C36-C29	115.(3)
C32-C33-C34	118.6(4)	C38-C39-C33	114.7(4)
C34-C29-C30	117.7(4)	C3-C10-C9	112.1(3)
C34-C33-C39	120.9(3)	C3-C8-C7	121.3(3)
C35-C36-C29	101 (2)	C41-C46-C45	120.5(3)
C35'-C36'-C37'	108.2(7)	C41-C48'-C49'	109.3(5)
C37-C36-C35	108(2)	C42-C41-C48	120.0(3)
C38-C39-C40	109.9(4)	C42-C41-C48'	120.0(3)
C3-C10-C11	111.3(4)	C43-C42-C41	121.8(4)
C3-C8-N1	119.9(3)	C43-C44-C45	122.0(4)
C40-C39-C33	109.4(4)	C44-C45-C51	120.7(3)

C41-C46-N4	119.7(3)	C44-C45-C51'	120.7(3)
C41-C48'-C47'	111.4(4)	C45-C46-N4	119.7(3)
C41-C48-C49	111(1)	C45-C51-C50	115 (1)
C42-C41-C46	118.5(3)	C45-C51'-C52'	111.4(4)
C42-C43-C44	119.2(3)	C47-C48-C49	112(1)
C44-C45-C46	118.0(3)	C54-C53-Cr1	118.3(4)
C45-C51'-C50'	108.5(5)	C54-C53-Cr2	114.7(4)
C45-C51-C52	115(1)	C56-C55-C54	117.5(8)
C46-C41-C48	121.5(3)	C56-C57-C58	117.9(7)
C46-C41-C48'	121.5(3)	C59'-O1'-C62'	111.2(7)
C46-C45-C51	121.2(3)	C5-C4-C3	121.2(4)
C46-C45-C51'	121.2(3)	C5-C6-C7	121.0(4)
C47-C48-C41	116.7(9)	C60-C61-C62	103(1)
C47'-C48'-C49'	110.5(6)	C61-C60-C59	102(1)
C4-C3-C10	119.6(3)	C62'-O1'-Li1	127.2(5)
C4-C5-C6	120.5(4)	C62-O1-Li1	123(1)
C50'-C51'-C52'	108.0(5)	C64-C65-C66	101.1(8)
C52-C51-C50	113(1)	C65-C64-C63	111.9(8)
C53-C54-C55	121.9(6)	C66-O2-Li1	125.2(5)
C54-C53-C58	117.4(5)	C67-O3-C70	100(2)
C55-C56-C57	124.8(7)	C67'-O3'-Li1	130.8(5)
C57-C58-C53	120.2(6)	C68'-C69'-C70'	99.9(8)
C58-C53-Cr1	109.7(3)	C69'-C68'-C67'	103.7(8)
C58-C53-Cr2	118.6(4)	C6-C7-C13	119.9(3)
C59'-O1'-Li1	120.8(6)	C70-O3-Li1	119.2(9)
C59-O1-Li1	132(1)	C71-O4-C74	108.6(4)
C60'-C61'-C62'	109.1(8)	C74-O4-Li1	122.9(4)
C61'-C60'-C59'	108.9(7)	C7-C8-N1	118.8(3)
C62-O1-C59	95(2)	C8-C3-C10	122.4(3)
C63-O2-Li1	126.7(4)	Cr2-C53-Cr1	68.7(1)
C66-O2-C63	108.0(5)	O1-C59-C60	107(2)
C67-C68-C69	98(1)	O1-C62-C61	109(2)
C67'-O3'-C70'	106.6(7)	O1'-Li1-O2	111.1(4)
C67-O3-Li1	133(1)	O1'-Li1-O3'	110.9(4)
C68-C69-C70	96(1)	O1'-Li1-O4	107.9(4)
C6-C7-C8	118.0(3)	O2-C63-C64	102.6(7)
C70'-O3'-Li1	121.5(5)	O2-C66-C65	111.0(7)
C71-O4-Li1	127.4(4)	O3'-C67'-C68'	106.1(7)
C73-C72-C71	105.6(5)	O3'-C70'-C69'	108.2(8)
C73-C74-O4	108.9(6)	O3'-Li1-O2	110.4(4)
C74-C73-C72	107.1(6)	O3'-Li1-O4	107.7(4)

C7-C13-C14	110.4(3)	O4-Li1-O2	108.7(4)
C8-C3-C4	118.0(3)	O1-Li1-O4	107.9(4)
C8-C7-C13	122.1(3)	O3-C67-C68	108(1)
O1'-C59'-C60'	106.2(7)	O3-C70-C69	95.4(18)
O1'-C62'-C61'	103.7(7)	O3-Li1-O2	110.4(4)
O1-Li1-O2	111.1(4)	O3-Li1-O4	107.7(4)
O1-Li1-O3	110.9(4)	O4-C71-C72	107.7(5)

Phenylation of $(^{\text{H}}\text{L}^{\text{iPr}}\text{Cr})_2(\mu\text{-H})_2$ in a mixed solvent of pentane and a few drops of THF gave a purple to violet slurry. After washing with pentane and extraction with THF, $[(^{\text{H}}\text{L}^{\text{iPr}}\text{Cr})_2(\mu\text{-Ph})(\mu\text{-H})_2][\text{Li}(\text{THF})_4]^+$ (**6**) was crystallized by layering with pentane at -30°C . Complex **6** crystallized in the monoclinic space group $P2_1/n$ as an asymmetric dinuclear complex with two diimine chromium fragments, two bridging hydrides and one bridging phenyl ligand. The coordination geometry around each Cr is best described as square pyramidal with two severely tilted axial vectors of Cr1-C53 and Cr2-C53. The τ_5 values of two Cr centers are 0.11 for Cr1 and 0.54 for Cr2. The distances from the chromium to the bridging phenyl's ipso carbon are 2.216(5) and 2.181(4) Å, and fall within the range of other bridging aryl complexes of chromium.¹⁵ The Cr-H bond lengths ranged from 1.61(3) to 1.71(3) Å and are similar to the analogous $\text{Cr}_2(\mu\text{-H})_3$ complex.¹⁶ The Cr-N distances in **6** (1.948(3) – 1.977(3) Å) are close to those in **5**. The ligand backbone's average C-N bond length of 1.379(4) Å and average C-C bond length of 1.355(5) Å suggested that the α -diimine ligands have formal charge of -2. Combining of three bridging ligand and one lithium counterion, the two chromium centers are best described as Cr(III)-Cr(III). The $^1\text{H-NMR}$ shows four broad shifts in THF- d_8 solution at 7.86, 6.70, 4.13 and 1.19 ppm, which are considered as the α -diimine ligand proton signals. No bridging ligand close to the core area could be observed on the resonance from 120 to -110 ppm. The magnetic moment

measurement of **6** at room temperature was $3.4(1) \mu_B$. The lower value was presumably due to antiferromagnetic coupling between chromium atoms.

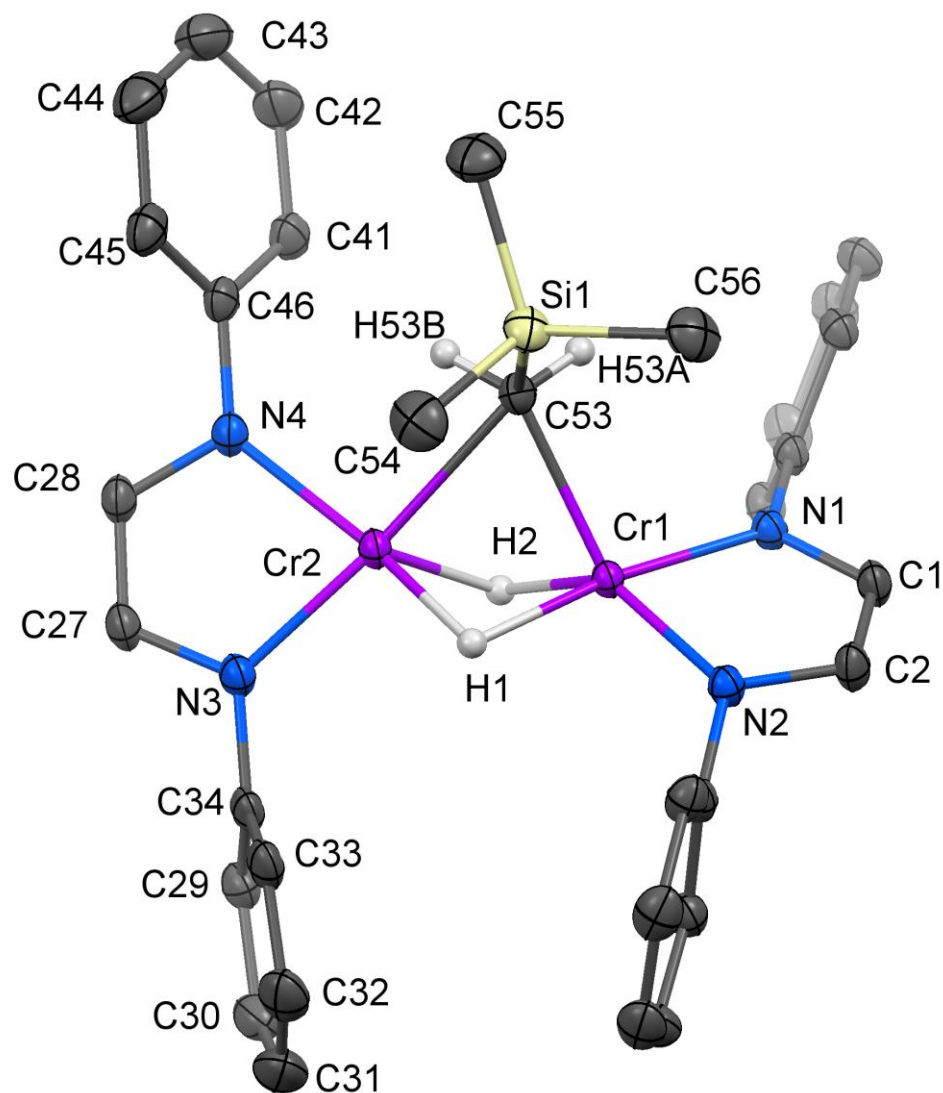


Figure 3.6 Molecular structure of $[(^H\text{L}^{\text{iPr}}\text{Cr})_2(\mu\text{-CH}_2\text{TMS})(\mu\text{-H})_2]^- [\text{Li}(\text{THF})_3(\text{Et}_2\text{O})]^+$ (**7**) with thermal ellipsoids at the 30% probability level. Lithium atoms, isopropyl groups, most of the hydrogen atoms and solvent molecules have been omitted for clarity. H1, H2, H53A and H53B have been located on a difference map.

Table 3.4 Interatomic distances (Å) and angles (°) for [(^HL^{iPr}Cr)₂(μ-CH₂TMS)(μ-H)₂][Li(THF)₃(Et₂O)]⁺ (7)

Distance (Å)			
Cr1-N2	1.958(1)	Cr1-N1	2.000(1)
Cr1-C53	2.197(2)	Cr1-Cr2	2.4850(3)
Cr1-H1	1.74(1)	Cr1-H2	1.73(1)
Cr2-N3	1.970(1)	Cr2-N4	2.000(1)
Cr2-C53	2.304(2)	Cr2-H1	1.73(1)
Cr2-H2	1.74(1)	Si1-C53	1.847(2)
Si1-C56	1.870(2)	Si1-C54	1.869(2)
Si1-C55	1.886(2)	N1-C1	1.371(2)
N1-C8	1.429(2)	N3-C27	1.372(2)
N3-C34	1.420(2)	N2-C2	1.378(2)
N2-C20	1.433(2)	N4-C28	1.378(2)
N4-C46	1.420(2)	C1-C2	1.352(2)
C3-C4	1.391(2)	C3-C8	1.408(2)
C3-C10	1.519(2)	C4-C5	1.380(3)
C7-C13	1.511(2)	C5-C6	1.376(3)
C12-C13	1.526(3)	C6-C7	1.393(2)
C13-C14	1.530(3)	C7-C8	1.409(2)
C15-C20	1.404(2)	C9-C10	1.509(3)
C16-C17	1.374(3)	C10-C11	1.519(3)
C17-C18	1.375(3)	C15-C16	1.400(2)
C18-C19	1.397(3)	C15-C22	1.512(2)
C19-C20	1.408(2)	C19-C25	1.511(3)
C21-C22	1.524(3)	C24-C25	1.507(3)
C22-C23	1.513(3)	C25-C26	1.523(3)
C27-C28	1.345(2)	C29-C34	1.400(2)
C29-C30	1.402(3)	C29-C36	1.516(3)
C30-C31	1.372(3)	C33-C39	1.511(3)
C31-C32	1.375(3)	C38-C39	1.527(3)
C32-C33	1.388(3)	C39-C40	1.526(3)
C33-C34	1.417(2)	C41-C46	1.413(2)
C35-C36	1.501(3)	C42-C43	1.362(4)
C36-C37	1.535(3)	C43-C44	1.372(4)
C41-C42	1.385(3)	C44-C45	1.398(3)
C41-C48	1.509(3)	C45-C46	1.404(2)
C45-C51	1.514(3)	C47-C48	1.520(3)
C50-C51	1.528(3)	C48-C49	1.511(4)

C51-C52	1.544(3)	C53-H53A	0.96(2)
C53-H53B	0.95(2)		

Angles (°)

N2-Cr1-N1	80.68(5)	N2-Cr1-C53	134.47(6)
N1-Cr1-C53	102.38(6)	N2-Cr1-Cr2	139.11(4)
N1-Cr1-Cr2	139.46(4)	C53-Cr1-Cr2	58.56(4)
N2-Cr1-H1	95.0(4)	N1-Cr1-H1	172.1(5)
C53-Cr1-H1	85.4(5)	Cr2-Cr1-H1	44.2(4)
N2-Cr1-H2	139.8(5)	N1-Cr1-H2	103.2(5)
C53-Cr1-H2	84.5(5)	Cr2-Cr1-H2	44.5(4)
H1-Cr1-H2	75.8(7)	N3-Cr2-N4	80.16(5)
N3-Cr2-C53	167.45(6)	N4-Cr2-C53	97.83(6)
N3-Cr2-Cr1	130.20(4)	N4-Cr2-Cr1	148.64(4)
C53-Cr2-Cr1	54.45(4)	N3-Cr2-H1	95.0(5)
N4-Cr2-H1	158.3(5)	C53-Cr2-H1	82.3(5)
Cr1-Cr2-H1	44.5(4)	N3-Cr2-H2	110.2(5)
N4-Cr2-H2	125.8(5)	C53-Cr2-H2	81.1(5)
Cr1-Cr2-H2	44.2(4)	H1-Cr2-H2	75.7(7)
C53-Si1-C56	111.64(9)	C53-Si1-C54	110.01(9)
C56-Si1-C54	109.9(1)	C53-Si1-C55	109.27(9)
C56-Si1-C55	107.1(1)	C54-Si1-C55	108.9(1)
C1-N1-C8	116.7(1)	N4-C46-C41	119.3(2)
C8-N1-Cr1	130.6(1)	Si1-C53-Cr2	122.95(8)
C27-N3-Cr2	114.3(1)	Si1-C53-H53A	109(1)
C2-N2-C20	115.6(1)	C1-N1-Cr1	112.6(1)
C20-N2-Cr1	128.05(9)	C27-N3-C34	117.2(1)
C28-N4-Cr2	113.0(1)	C34-N3-Cr2	127.8(1)
C7-C13-C12	111.1(2)	C2-N2-Cr1	114.2(1)
Cr1-C53-Cr2	66.98(4)	C28-N4-C46	115.5(1)
Cr1-C53-H53A	91(1)	C46-N4-Cr2	131.5(1)
Cr2-C53-H53B	71(1)	C1-C2-N2	115.7(1)
Si1-C53-Cr1	117.07(8)	C4-C3-C10	120.1(2)
Si1-C53-H53B	105(1)	C5-C4-C3	121.7(2)
C2-C1-N1	116.5(1)	C5-C6-C7	121.6(2)
C4-C3-C8	118.7(2)	C6-C7-C13	119.3(2)
C8-C3-C10	121.2(2)	C3-C8-C7	120(12)
C4-C5-C6	119.3(2)	C7-C8-N1	120.7(2)
C6-C7-C8	118.8(2)	C9-C10-C3	111.2(2)
C8-C7-C13	122.0(1)	C7-C13-C14	111.5(2)

C3-C8-N1	119.4(1)	C15-C20-C19	120.6(2)
C9-C10-C11	110.5(2)	C16-C15-C22	120.2(2)
C11-C10-C3	113.3(2)	C17-C16-C15	121.4(2)
C12-C13-C14	110.8(2)	C17-C18-C19	121.4(2)
C15-C20-N2	118.3(1)	C18-C19-C25	120.9(2)
C15-C22-C21	111.6(2)	C19-C20-N2	121.1(2)
C16-C15-C20	118.3(2)	C23-C22-C21	110.6(2)
C16-C17-C18	119.8(2)	C24-C25-C26	110.3(2)
C18-C19-C20	118.4(2)	C27-C28-N4	116.2(2)
C19-C25-C26	113.9(2)	C29-C34-C33	121(2)
C20-C15-C22	121.4(2)	C31-C30-C29	121.3(2)
C20-C19-C25	120.7(2)	C31-C32-C33	121.6(2)
C23-C22-C15	112.1(2)	C32-C33-C39	121.7(2)
C24-C25-C19	111.2(1)	C33-C34-N3	118.6(2)
C28-C27-N3	116.0(2)	C33-C39-C38	111.4(2)
C29-C34-N3	120.4(2)	C34-C29-C36	122.6(2)
C29-C36-C37	111.1(2)	C35-C36-C37	111.9(2)
C30-C29-C36	119.4(2)	C41-C48-C47	113.5(2)
C30-C31-C32	120.1(2)	C42-C41-C48	120(2)
C32-C33-C34	118.0(2)	C43-C42-C41	121.4(2)
C33-C39-C40	114.0(2)	C43-C44-C45	121.4(2)
C34-C29-C30	118.0(2)	C44-C45-C51	119.5(2)
C34-C33-C39	120.3(2)	C45-C46-N4	120.9(2)
C35-C36-C29	112.1(3)	C45-C51-C52	111.8(2)
C40-C39-C38	109.3(2)	Cr1-C53-H53B	132(1)
C41-C48-C49	109.8(2)	Cr2-C53-H53A	128(1)
C42-C41-C46	119.0(2)	H53A-C53-H53B	96(2)
C42-C43-C44	120.1(2)	C46-C41-C48	121.0(2)
C44-C45-C46	118.4(2)	C46-C45-C51	122.1(2)
C45-C46-C41	119.8(2)	C49-C48-C47	109.7(2)
C45-C51-C50	112.2(2)	C50-C51-C52	109.5(2)

The TMS(CH₂) ligand bridging complex [(^HL^{iPr}Cr)₂(μ-CH₂TMS)(μ-H)₂]⁻ [Li(THF)₃(Et₂O)]⁺ (**7**) was synthesized via a similar procedure as **6**. Dark violet solid of **7** precipitated out of pentane/THF mixed solvent. Complex **7** was crystallized from a THF solution layered with pentane at -30°C in 70% yield. The solid state structure of **7** shows an asymmetric dinuclear complex with one TMS(CH₂) bridging alkyl ligand and two bridging hydrides. The asymmetry is presumably introduced by the repulsion

between bridging TMS(CH₂) ligand and aryl groups on diimine ligands. The τ_5 values of Cr1 and Cr2 are 0.55 and 0.15 respectively. Thus, Cr2 is best described as strongly distorted square pyramidal with tilted axial vector of Cr2-H2, while Cr1 barely shows a square pyramidal geometry with axial vector of Cr1-C53. The Cr-H bond length ranged from 1.73(1) to 1.74(1) Å and are slightly longer than those in **6**, but still in the range of chromium bridging hydrides.^{9,10,16} The longer distances between Cr and hydride presumably come from the larger size of TMS(CH₂) ligand. Likewise, the average Cr-N bond length of 1.981(1) Å is mildly longer than those in **6**. Two chromium centers are 2.4850(3) Å away from each other. The ¹H-NMR spectrum showed the ligand chemical shifts at 8.52, 4.65, 3.55, 1.84 and 1.32 ppm. No bridging hydride or methylene signal can be observed in the spectrum from 120 to -110 ppm. The C-N bond lengths of ligand backbone ranged from 1.371(2) to 1.378(2) Å and the C-C bond lengths are 1.352 (2) and 1.345(2) Å respectively. The C-C double bond order and C-N single bond order clearly indicated that both ligands are dianionic and gave a Cr(III)-Cr(III) core. Due to the antiferromagnetic coupling between two Cr centers, in solid state complex **7** showed a low magnetism measurement of 2.1(1) μ_B at room temperature.

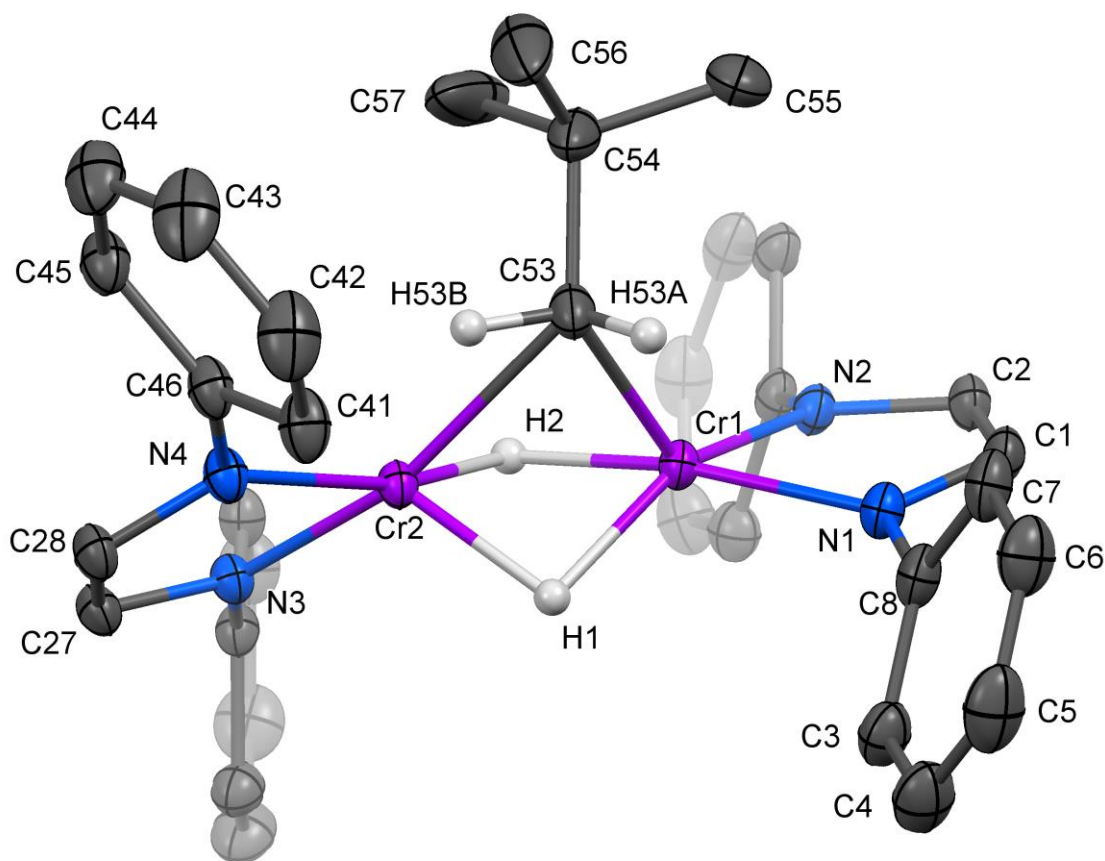


Figure 3.7 Molecular structure of $[(^{\text{H}}\text{L}^{\text{iPr}}\text{Cr})_2(\mu\text{-CH}_2^{\text{tBu}})(\mu\text{-H})_2][\text{Li}(\text{THF})_3(\text{Et}_2\text{O})]^+$ (**8**) with thermal ellipsoids at the 30% probability level. Lithium atoms, isopropyl groups, most of the hydrogen atoms and solvent molecules have been omitted for clarity. H1, H2, H53A and H53B have been located on a difference map.

Table 3.5 Interatomic distances (Å) and angles (°) for $[(^{\text{H}}\text{L}^{\text{iPr}}\text{Cr})_2(\mu\text{-CH}_2^{\text{tBu}})(\mu\text{-H})_2][\text{Li}(\text{THF})_3(\text{Et}_2\text{O})]^+$ (**8**)

Distance (Å)			
Cr1-N2	1.960(1)	Cr1-N1	1.992(1)
Cr1-C53	2.170(2)	Cr1-Cr2	2.4763(3)
Cr1-H1	1.76(2)	Cr1-H2	1.72(2)
Cr2-N3	1.954(1)	Cr2-N4	2.003(1)

Cr2-C53	2.337(2)	Cr2-H1	1.67(2)
Cr2-H2	1.69(2)	Cr2-H53B	2.03(2)
N1-C1	1.381(2)	N1-C8	1.420(2)
N2-C2	1.387(2)	N2-C20	1.430(2)
N3-C27	1.377(2)	N3-C34	1.425(2)
N4-C28	1.374(2)	N4-C46	1.429(2)
C1-C2	1.347(2)	C3-C4	1.399(2)
C3-C8	1.411(2)	C3-C10	1.523(3)
C4-C5	1.378(3)	C7-C13	1.514(3)
C5-C6	1.366(3)	C12-C13	1.541(3)
C6-C7	1.393(2)	C13-C14	1.535(3)
C7-C8	1.417(2)	C15-C20	1.411(2)
C9-C10	1.517(4)	C16-C17	1.373(3)
C10-C11	1.520(4)	C17-C18	1.365(3)
C15-C16	1.397(2)	C18-C19	1.397(3)
C15-C22	1.518(2)	C19-C20	1.410(2)
C19-C25	1.513(3)	C21-C22	1.516(3)
C24-C25	1.526(3)	C22-C23	1.522(3)
C25-C26	1.535(3)	C27-C28	1.355(2)
C29-C30	1.394(2)	C29-C34	1.412(2)
C29-C36	1.512(2)	C30-C31	1.376(3)
C33-C39	1.520(2)	C31-C32	1.372(3)
C38-C39	1.533(3)	C32-C33	1.396(2)
C39-C40	1.512(3)	C33-C34	1.408(2)
C41-C46	1.411(2)	C35-C36	1.528(2)
C42-C43	1.373(3)	C36-C37	1.521(2)
C43-C44	1.373(3)	C41-C42	1.401(3)
C44-C45	1.397(2)	C41-C48	1.509(3)
C45-C46	1.414(2)	C45-C51	1.515(3)
C47-C48	1.506(3)	C50-C51	1.535(3)
C48-C49	1.529(3)	C51-C52	1.534(3)
C53-C54	1.544(3)	C53-H53A	1.00(2)
C53-H53B	0.99(2)	C54-C57	1.517(3)
C54-C55	1.532(3)	C54-C56	1.550(3)

Angles (°)

N2-Cr1-N1	81.31(5)	N2-Cr1-C53	127.98(6)
N1-Cr1-C53	102.13(6)	N2-Cr1-Cr2	138.21(4)
N1-Cr1-Cr2	140.32(4)	C53-Cr1-Cr2	59.97(4)
N2-Cr1-H1	149.8(5)	N1-Cr1-H1	103.5(5)

C53-Cr1-H1	80.8(5)	Cr2-Cr1-H1	42.5(5)
N2-Cr1-H2	95.7(5)	N1-Cr1-H2	169.6(5)
C53-Cr1-H2	87.6(5)	Cr2-Cr1-H2	42.8(5)
H1-Cr1-H2	74.2(7)	N3-Cr2-N4	80.47(5)
N3-Cr2-C53	164.52(6)	N4-Cr2-C53	99.81(5)
N3-Cr2-Cr1	130.06(3)	N4-Cr2-Cr1	148.31(4)
C53-Cr2-Cr1	53.51(4)	N3-Cr2-H1	116.0(5)
N4-Cr2-H1	119.6(5)	C53-Cr2-H1	77.5(5)
Cr1-Cr2-H1	45.2(5)	N3-Cr2-H2	92.3(5)
N4-Cr2-H2	163.1(5)	C53-Cr2-H2	83.1(5)
Cr1-Cr2-H2	44.0(5)	H1-Cr2-H2	77.3(8)
N3-Cr2-H53B	149.9(6)	N4-Cr2-H53B	74.8(6)
C53-Cr2-H53B	25.1(6)	Cr1-Cr2-H53B	77.9(6)
H1-Cr2-H53B	91.3(8)	H2-Cr2-H53B	106.6(8)
C1-N1-C8	117.7(1)	C1-N1-Cr1	111.40(9)
C8-N1-Cr1	130.69(9)	C2-N2-C20	118.0(1)
C2-N2-Cr1	112.95(9)	C20-N2-Cr1	128.52(9)
C27-N3-C34	117.3(1)	C27-N3-Cr2	114.38(9)
C34-N3-Cr2	128.12(9)	C28-N4-C46	116.2(1)
C28-N4-Cr2	112.47(9)	C46-N4-Cr2	130.89(9)
C2-C1-N1	117.0(1)	C1-C2-N2	115.7(1)
C4-C3-C8	118.6(2)	C4-C3-C10	118.7(2)
C8-C3-C10	122.7(2)	C5-C4-C3	121.4(2)
C6-C5-C4	120.0(2)	C5-C6-C7	121.6(2)
C6-C7-C8	118.8(2)	C6-C7-C13	118.3(2)
C8-C7-C13	122.95(15)	C3-C8-C7	119.8(2)
C3-C8-N1	119.48(14)	C7-C8-N1	120.8(2)
C9-C10-C11	111.0(3)	C9-C10-C3	111.0(2)
C11-C10-C3	112.3(2)	C7-C13-C12	112.4(2)
C7-C13-C14	111.5(2)	C16-C15-C22	120.2(2)
C14-C13-C12	109.7(2)	C17-C16-C15	121.5(2)
C16-C15-C20	118.6(2)	C17-C18-C19	121.8(2)
C20-C15-C22	121.2(1)	C18-C19-C25	119.3(2)
C18-C17-C16	119.7(2)	C19-C20-C15	119.7(2)
C18-C19-C20	118.6(2)	C15-C20-N2	118.4(2)
C20-C19-C25	122.1(2)	C21-C22-C23	108.5(2)
C19-C20-N2	121.9(1)	C19-C25-C26	112.2(2)
C21-C22-C15	112.1(2)	C27-C28-N4	116.3(2)
C15-C22-C23	114.7(2)	C30-C29-C36	121.3(2)
C19-C25-C24	111.3(2)	C31-C30-C29	121.1(2)
C24-C25-C26	110.0(2)	C31-C32-C33	121.4(2)

C28-C27-N3	115.4(2)	C32-C33-C39	120.1(2)
C30-C29-C34	118.4(2)	C33-C34-C29	120.7(2)
C34-C29-C36	120.2(2)	C29-C34-N3	118.5(2)
C32-C31-C30	120.2(2)	C29-C36-C35	114.0(2)
C32-C33-C34	118.2(2)	C40-C39-C38	110.5(2)
C34-C33-C39	121.7(2)	C42-C41-C48	120.8(2)
C33-C34-N3	120.8(2)	C43-C42-C41	121.6(2)
C29-C36-C37	111.0(2)	C43-C44-C45	121.0(2)
C37-C36-C35	110.8(2)	C44-C45-C51	118.3(2)
C40-C39-C33	112.6(2)	C41-C46-C45	120.5(2)
C33-C39-C38	109.3(2)	C45-C46-N4	120.0(2)
C42-C41-C46	117.9(2)	C47-C48-C49	111.0(2)
C46-C41-C48	121.3(2)	C45-C51-C50	111.9(2)
C42-C43-C44	120.4(2)	C54-C53-Cr2	124.3(1)
C44-C45-C46	118.6(2)	C54-C53-H53A	109(1)
C46-C45-C51	123.1(2)	Cr2-C53-H53A	126(1)
C41-C46-N4	119.4(2)	Cr1-C53-H53B	124(1)
C47-C48-C41	111.2(2)	H53A-C53-H53B	105(2)
C41-C48-C49	114.2(2)	C57-C54-C53	109.5(2)
C45-C51-C52	111.7(2)	C57-C54-C56	111.1(2)
C52-C51-C50	109.9(2)	C53-C54-C56	108.1(2)
C54-C53-Cr1	118.4(2)	Cr2-C53-H53B	60.0(11)
Cr1-C53-Cr2	66.53(4)	C57-C54-C55	109.3(2)
Cr1-C53-H53A	94(1)	C55-C54-C53	110.7(2)
C54-C53-H53B	103(1)	C55-C54-C56	108.1(2)

Complex $[(^H\text{L}^{\text{iPr}}\text{Cr})_2(\mu\text{-CH}_2^{\text{tBu}})(\mu\text{-H})_2][\text{Li}(\text{THF})_3(\text{Et}_2\text{O})]^+$ (**8**) as the analog **7** could be prepared by reacting **4** with neopentyl lithium reagent in the same manner as described above. The dark violet solid of **8** was crystallized out of THF solution by layering with pentane. As an analog of **7** with only one atom different from each other, **7** and **8** shares many similarities in solid state structure. Both Cr centers showed a square pyramidal geometry with τ_5 values of 0.33 for Cr1 and 0.01 for Cr2. The axial vectors of Cr1-C53 and Cr2-H1 are tilted because C53 and H1 are bridging atoms. The bridging methylene centered on C53 is slightly closer to Cr1 (Cr1-C53 = 2.170(2) Å) than Cr2 (Cr2-C53 = 2.337(2) Å), which may be the result of the combination of

distorted coordination geometry and trans influence of N3. It's noticeable that the C53 is on the axis of square pyramid of Cr1 and is on the edge of square pyramid of Cr2. Both the bridging hydrides and bridging methylene protons were located on a X-ray difference map. The Cr-H distances range from 1.67(2) to 1.76(2) Å and are slightly shorter than those in **7** (1.73(1) – 1.74(1) Å). Yet, they do not bring two Cr centers (Cr1-Cr2 = 2.4763(3) Å) noticeably closer. The Cr-N distances are in the expected range of 1.961(1) to 2.003(1) Å. The two dianionic α -diimine ligands showed backbone average C-N bond length of 1.380(2) Å and average C-C bond length of 1.351(2) Å. The ¹H-NMR also only showed α -diimine chemical shifts at 8.53, 4.81, 3.55 and 1.81 ppm. The room temperature magnetic moment of 3.1(1) μ_B is higher than **7** of 2.1(1) μ_B , but still showed antiferromagnetic coupling between two Cr atoms.

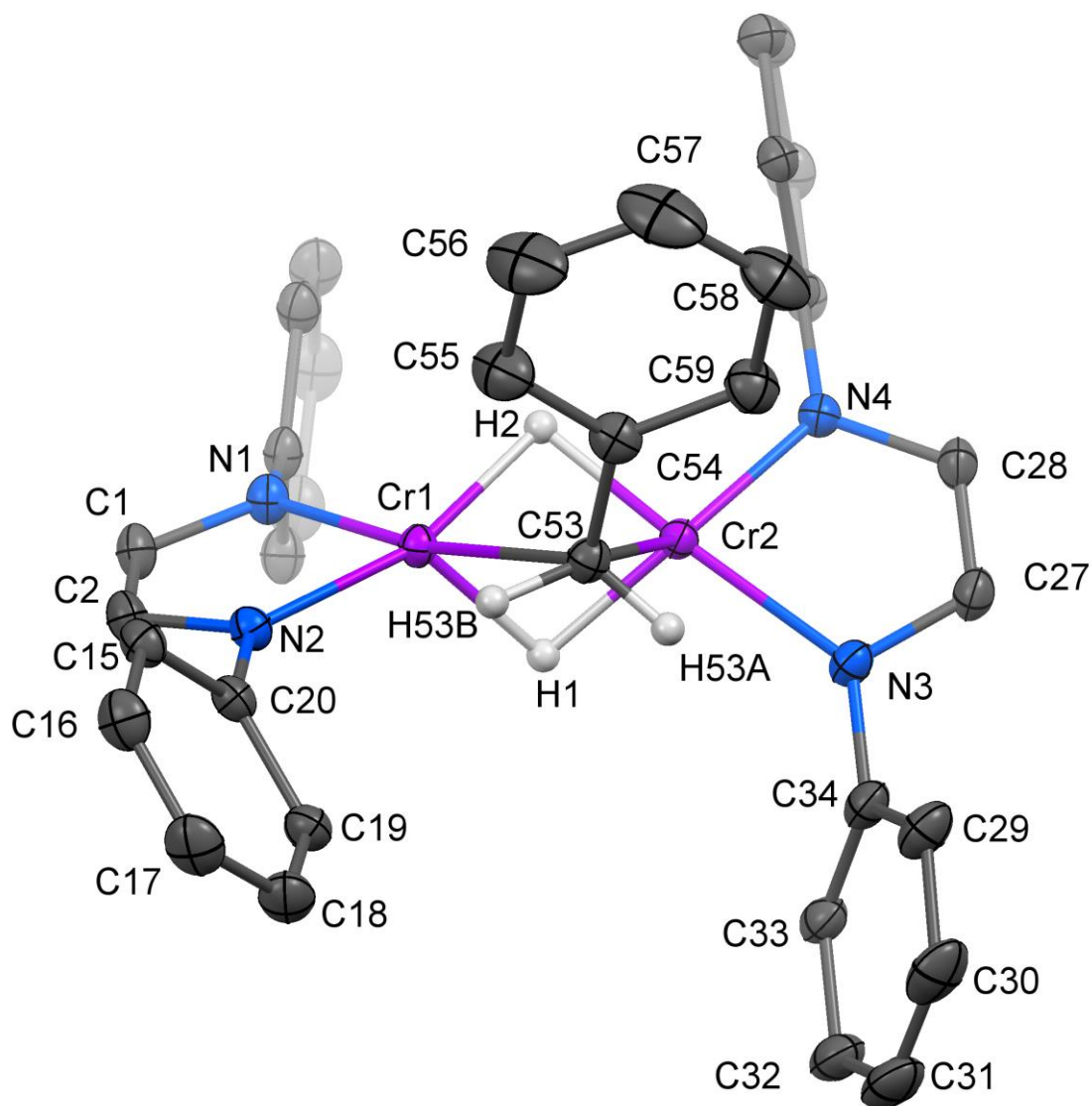


Figure 3.8 Molecular structure of $[(\text{HLi}^{\text{iPr}}\text{Cr})_2(\mu\text{-CH}_2\text{Ph})(\mu\text{-H})_2]^+[\text{Li}(\text{THF})_4]^+$ (**9**) with thermal ellipsoids at the 30% probability level. Lithium atoms, isopropyl groups, most of the hydrogen atoms and solvent molecules have been omitted for clarity. H1, H2, H53A and H53B have been located on a difference map.

Table 3.6 Interatomic distances (Å) and angles (°) for $[(^{\text{H}}\text{L}^{\text{iPr}}\text{Cr})_2(\mu\text{-CH}_2\text{Ph})(\mu\text{-H})_2][\text{Li}(\text{THF})_4]^+$ (9)

Distances (Å)			
Cr1-N1	1.958(2)	Cr1-N2	2.017(2)
Cr1-C53	2.325(2)	Cr1-Cr2	2.4948(4)
Cr1-H1	1.75(2)	Cr1-H2	1.75(2)
Cr2-N4	1.951(2)	Cr2-N3	2.010(2)
Cr2-C53	2.251(2)	Cr2-H1	1.73(2)
Cr2-H2	1.70(2)	Li1-O1	1.927(5)
Li1-O3'	1.935(5)	Li1-O3	1.935(5)
Li1-O4	1.944(5)	Li1-O2	1.940(5)
N1-C1	1.373(2)	N1-C8	1.430(2)
N2-C2	1.380(2)	N2-C20	1.432(2)
N3-C27	1.377(3)	N3-C34	1.430(2)
N4-C28	1.382(2)	N4-C46	1.432(2)
O1-C63	1.435(3)	O1-C60	1.428(3)
O2-C67	1.396(4)	O2-C64	1.419(4)
O4-C72	1.424(4)	O4-C75	1.444(4)
C1-C2	1.357(3)	C3-C4	1.397(3)
C3-C8	1.402(3)	C3-C10	1.523(3)
C4-C5	1.374(4)	C7-C13	1.511(3)
C5-C6	1.382(4)	C12-C13	1.534(4)
C6-C7	1.399(3)	C13-C14	1.527(3)
C7-C8	1.411(3)	C15-C20	1.407(3)
C9-C10	1.531(3)	C16-C17	1.373(3)
C10-C11	1.527(3)	C17-C18	1.380(4)
C15-C16	1.401(3)	C18-C19	1.392(3)
C15-C22	1.518(3)	C19-C20	1.422(3)
C19-C25	1.511(3)	C21-C22	1.534(3)
C24-C25	1.523(4)	C22-C23	1.535(3)
C25-C26	1.528(4)	C27-C28	1.348(3)
C29-C30	1.406(3)	C29-C34	1.409(3)
C29-C36	1.512(4)	C30-C31	1.359(4)
C33-C39	1.523(3)	C31-C32	1.373(4)
C38-C39	1.527(3)	C32-C33	1.394(3)
C39-C40	1.526(3)	C33-C34	1.410(3)
C41-C46	1.400(3)	C35-C36	1.533(4)
C42-C43	1.375(3)	C36-C37	1.524(4)
C43-C44	1.375(3)	C41-C42	1.402(3)

C44-C45	1.398(3)	C41-C48	1.514(3)
C45-C46	1.415(3)	C45-C51	1.518(3)
C47-C48	1.520(3)	C50-C51	1.526(3)
C48-C49	1.516(4)	C51-C52	1.539(3)
C53-C54	1.490(3)	C53-H53A	0.99(3)
C53-H53B	1.04(3)	C54-C59	1.398(3)
C54-C55	1.402(3)	C55-C56	1.381(4)
C60-C61	1.511(4)	C56-C57	1.371(5)
C62-C63	1.418(5)	C57-C58	1.390(5)
C65-C66	1.395(6)	C58-C59	1.395(3)
C72-C73	1.485(5)	C61-C62	1.487(5)
C74-C75	1.484(5)	C64-C65	1.442(5)
O3-C71	1.529(5)	C66-C67	1.390(6)
C69-C70	1.377(7)	C73-C74	1.484(5)
O3'-C71'	1.430(8)	O3-C68	1.431(7)
C68'-C69'	1.44(1)	C68-C69	1.403(8)
C70'-C71'	1.42(1)	C70-C71	1.412(6)
C69'-C70'	1.31(1)	O3'-C68'	1.45(1)

Angles (°)

N1-Cr1-N2	80.87(6)	N1-Cr1-C53	169.48(7)
N2-Cr1-C53	99.43(7)	N1-Cr1-Cr2	127.21(5)
N2-Cr1-Cr2	149.22(5)	C53-Cr1-Cr2	55.54(5)
N1-Cr1-H1	109.6(7)	N2-Cr1-H1	121.1(7)
C53-Cr1-H1	79.3(7)	Cr2-Cr1-H1	43.8(7)
N1-Cr1-H2	94.8(7)	N2-Cr1-H2	162.7(7)
C53-Cr1-H2	81.7(7)	Cr2-Cr1-H2	42.9(7)
H1-Cr1-H2	76(1)	N4-Cr2-N3	80.53(7)
N4-Cr2-C53	134.77(7)	N3-Cr2-C53	100.07(7)
N4-Cr2-Cr1	138.99(5)	N3-Cr2-Cr1	140.19(5)
C53-Cr2-Cr1	58.41(5)	N4-Cr2-H1	142.3(7)
N3-Cr2-H1	104.4(7)	C53-Cr2-H1	81.9(7)
Cr1-Cr2-H1	44.4(7)	N4-Cr2-H2	94.7(7)
N3-Cr2-H2	174.6(7)	C53-Cr2-H2	85.0(7)
Cr1-Cr2-H2	44.4(7)	H1-Cr2-H2	77.9(10)
O1-Li1-O3'	106.3(3)	O1-Li1-O3	106.3(3)
O1-Li1-O4	103.4(2)	O3'-Li1-O4	117.3(3)
O3-Li1-O4	117.3(3)	O1-Li1-O2	110.9(3)
O3'-Li1-O2	113.4(2)	O3-Li1-O2	113.4(2)
O4-Li1-O2	105.0(2)	C1-N1-C8	115.8(2)

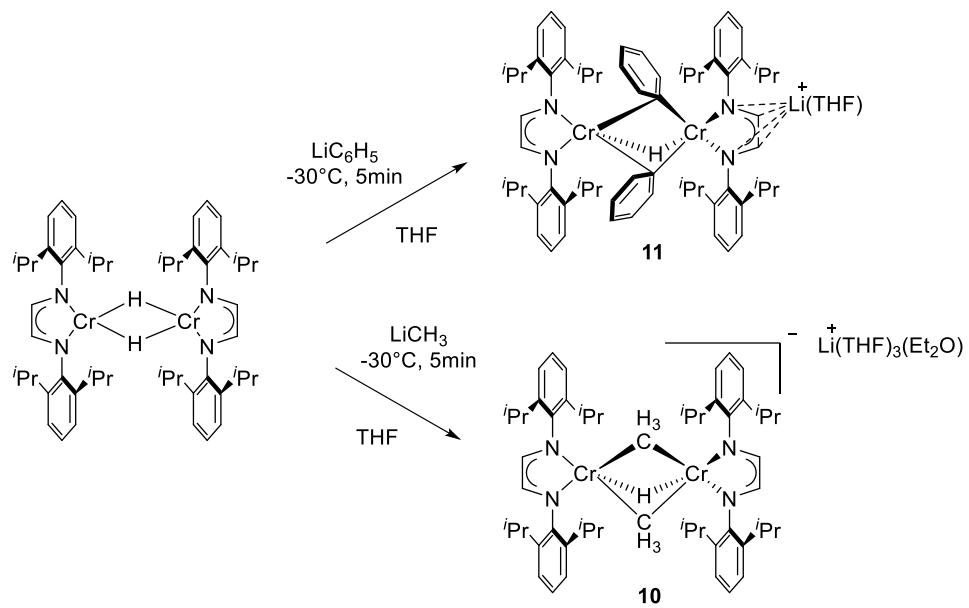
C1-N1-Cr1	114.2(1)	C8-N1-Cr1	127.8(2)
C2-N2-C20	113.7(2)	C2-N2-Cr1	112.0(2)
C20-N2-Cr1	134.3(2)	C27-N3-C34	116.6(2)
C27-N3-Cr2	112.3(2)	C34-N3-Cr2	131.1(2)
C28-N4-C46	115.6(3)	C28-N4-Cr2	114.4(2)
C46-N4-Cr2	129.9(2)	C63-O1-C60	106.9(2)
C63-O1-Li1	126.5(3)	C60-O1-Li1	123.8(2)
C67-O2-C64	107.2(3)	C67-O2-Li1	128.4(3)
C64-O2-Li1	124.1(2)	C72-O4-C75	105.3(2)
C72-O4-Li1	125.7(3)	C75-O4-Li1	126.3(2)
C2-C1-N1	116.4(2)	C1-C2-N2	116.3(2)
C4-C3-C8	118.6(2)	C4-C3-C10	119.3(2)
C8-C3-C10	122.2(2)	C5-C4-C3	121.0(2)
C4-C5-C6	120.3(2)	C5-C6-C7	121.1(2)
C6-C7-C8	118.0(2)	C6-C7-C13	121.2(2)
C8-C7-C13	120.7(2)	C3-C8-C7	121.0(2)
C3-C8-N1	119.2(2)	C7-C8-N1	119.8(2)
C9-C10-C11	110.2(2)	C9-C10-C3	111.1(2)
C11-C10-C3	111.6(2)	C7-C13-C12	110.3(2)
C7-C13-C14	114.0(2)	C16-C15-C22	118.1(2)
C14-C13-C12	110.0(2)	C17-C16-C15	121.7(2)
C16-C15-C20	118.6(2)	C17-C18-C19	121.8(2)
C20-C15-C22	123.3(2)	C18-C19-C25	120.4(2)
C16-C17-C18	119.5(2)	C15-C20-C19	120.0(2)
C18-C19-C20	118.4(2)	C19-C20-N2	119.1(2)
C20-C19-C25	121.1(2)	C15-C22-C23	111.8(2)
C15-C20-N2	120.9(2)	C19-C25-C24	114.0(2)
C15-C22-C21	111.6(2)	C27-C28-N4	115.8(2)
C21-C22-C23	109.0(2)	C30-C29-C36	120.1(2)
C19-C25-C26	110.8(2)	C31-C30-C29	122.3(2)
C26-C25-C24	110.8(2)	C31-C32-C33	121.3(2)
C28-C27-N3	116.3(2)	C32-C33-C39	120.3(2)
C30-C29-C34	117.8(2)	C33-C34-C29	119.9(2)
C34-C29-C36	122.1(2)	C29-C34-N3	120.6(2)
C30-C31-C32	119.7(2)	C29-C36-C35	111.5(2)
C32-C33-C34	119.0(2)	C40-C39-C33	110.4(2)
C34-C33-C39	120.6(2)	C42-C41-C48	120.2(2)
C33-C34-N3	119.5(2)	C43-C42-C41	121.1(2)
C29-C36-C37	112.2(3)	C43-C44-C45	121.3(2)
C37-C36-C35	110.5(2)	C44-C45-C51	121.1(2)
C40-C39-C38	109.8(2)	C41-C46-C45	120.7(2)

C38-C39-C33	114.3(2)	C45-C46-N4	119.3(2)
C42-C41-C46	118.6(2)	C41-C48-C49	111.4(2)
C46-C41-C48	121.2(2)	C45-C51-C52	113.6(2)
C44-C43-C42	120.2(2)	C54-C53-Cr1	121.0(2)
C44-C45-C46	118.2(2)	C54-C53-H53A	110(2)
C46-C45-C51	120.7(2)	Cr1-C53-H53A	127(2)
C41-C46-N4	120.0(2)	Cr2-C53-H53B	131(2)
C41-C48-C47	112.3(2)	H53A-C53-H53B	113.(2)
C47-C48-C49	110.4(2)	C59-C54-C53	122.4(2)
C45-C51-C50	109.5(2)	C56-C55-C54	121.4(3)
C50-C51-C52	109.6(2)	C56-C57-C58	118.5(3)
C54-C53-Cr2	115.5(2)	C58-C59-C54	121.0(2)
Cr2-C53-Cr1	66.06(5)	C68-O3-Li1	125.5(4)
Cr2-C53-H53A	80(2)	C69-C68-O3	109.3(5)
C54-C53-H53B	105(2)	C70-C69-C68	111.3(5)
Cr1-C53-H53B	69(2)	C69-C70-C71	106.5(5)
C59-C54-C55	116.9(2)	C70-C71-O3	107.9(4)
C55-C54-C53	120.7(2)	C71'-O3'-C68'	98.0(7)
C57-C56-C55	121.4(3)	C68'-O3'-Li1	130.8(5)
C57-C58-C59	120.7(3)	C74-C73-C72	105.6(3)
O1-C60-C61	106.2(2)	C73-C74-C75	105.4(3)
C62-C61-C60	103.5(3)	O4-C75-C74	104.3(3)
C63-C62-C61	108.4(3)	C68-O3-C71	101.7(4)
C62-C63-O1	108.5(3)	C71-O3-Li1	122.4(3)
O2-C64-C65	106.5(3)	C71'-O3'-Li1	123.1(4)
C66-C65-C64	108.6(4)	C69'-C68'-O3'	109.5(8)
C67-C66-C65	107.2(4)	C70'-C69'-C68'	105.5(8)
C66-C67-O2	110.5(4)	C69'-C70'-C71'	109.5(7)
O4-C72-C73	104.0(3)	O3'-C71'-C70'	108.9(7)

The benzyl group can also be added to the Cr_2H_2 core by treating $(^{\text{H}}\text{L}^{\text{iPr}}\text{Cr})_2(\mu\text{-H})_2$ (**4**) with benzyl lithium in pentane/THF. After standard work up, $[(^{\text{H}}\text{L}^{\text{iPr}}\text{Cr})_2(\mu\text{-CH}_2\text{Ph})(\mu\text{-H})_2][\text{Li}(\text{THF})_4]^+$ (**9**) crystallized out of THF solution layered with pentane. In the solid state, **9** exhibits an asymmetric dinuclear structure of two Cr diimine fragments and three bridging ligands in monoclinic $P2_1/n$ space group. The bridging hydrides and methylene protons were located on a X-ray difference map. The

distances of bridging methylene carbon to chromium atoms are Cr1-C53 2.325(2) Å and Cr2-C53 2.251(2) Å. The distances between Cr and the bridging hydrides range from 1.70(2) to 1.75(2) Å and fall in the typical range of Cr bridging hydride complexes. The three bridging ligands strongly twisted the square pyramidal coordination geometry around both Cr centers, and gave τ_5 value of 0.12 for Cr1 with axial vector of Cr1-H1 and τ_5 value of 0.53 for Cr2 with axial vector of Cr2-C53. The Cr1-Cr2 distance of 2.4948(4) Å is only a little longer than the other five complexes. The chromium nitrogen bond lengths range from 1.951(2) to 2.0017(2) Å, as expected. And the ligand backbone average C-N bond length of 1.378(3) Å and average C-C bond length of 1.3552(3) Å implied dianionic charge for both diimine ligand. The low magnetic moment of 2.5(1) μ_B per complex at room temperature was presumably due to strong Cr-Cr antiferromagnetic coupling. The paramagnetic feature of **9** also exhibits broad $^1\text{H-NMR}$ peaks at 8.21, 5.34, 3.53 and 1.75 ppm.

The reaction of $(^{\text{H}}\text{L}^{\text{iPr}}\text{Cr})_2(\mu\text{-H})_2$ with methyl lithium or phenyl lithium in pure THF yielded a complementary series of hydrido-bis(alkyl) chromium complexes, namely $[(^{\text{H}}\text{L}^{\text{iPr}}\text{Cr})_2(\mu\text{-Me})_2(\mu\text{-H})]^-[\text{Li}(\text{THF})_3(\text{Et}_2\text{O})]^+$ (**10**) and $[(^{\text{H}}\text{L}^{\text{iPr}}\text{Cr})_2(\mu\text{-Ph})_2(\mu\text{-H})]^-[\text{Li}(\text{THF})]^+$ (**11**) (Scheme 3.7). After standard work up, **10** and **11** were crystallized from pentane/THF solution at -30°C in 40% and 30% yield. To our surprise, X-ray crystallography revealed that both **10** and **11** gave a $\text{Cr}_2(\mu\text{-R})_2(\mu\text{-H})$ core, yet their $^1\text{H-NMR}$ spectra are identical to those of **5** and **6**. The solid state structures, bond distances, and angles of **10** and **11** are displayed in Figures 3.7 and 3.8 and Tables 3.7 and 3.8 respectively.



Scheme 3.7 Reaction of $(\text{HL}^{\text{iPr}}\text{Cr})_2(\mu\text{-H})_2$ with lithium reagent in THF

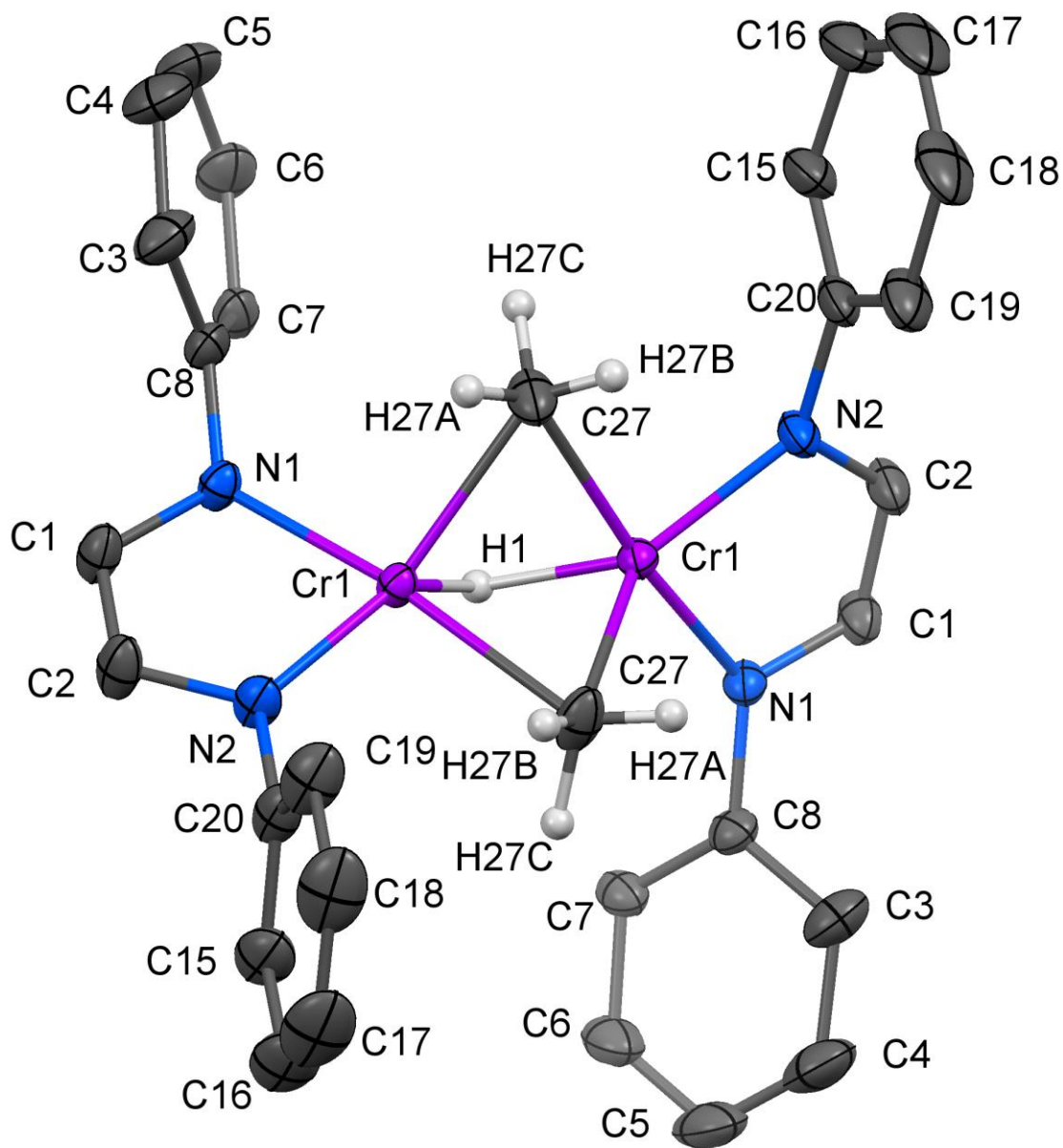


Figure 3.9 Molecular structure of $[(\text{H}^{\text{iPr}}\text{Cr})_2(\mu\text{-Me})_2(\mu\text{-H})]\text{-}[\text{Li}(\text{THF})_3(\text{Et}_2\text{O})]^+$ (**10**) with thermal ellipsoids at the 30% probability level. Lithium atoms, isopropyl groups, most of the hydrogen atoms and solvent molecules have been omitted for clarity. H1, H27A, H27B and H27C have been located on a difference map.

Table 3.7 Interatomic distances (Å) and angles (°) for $[(^{\text{H}}\text{L}^{\text{iPr}}\text{Cr})_2(\mu\text{-Me})_2(\mu\text{-H})]^-$ $[\text{Li}(\text{THF})_3(\text{Et}_2\text{O})]^+$ (10)

Distance (Å)			
Cr1-N2	1.968(2)	Cr1-N1	1.994(2)
Cr1-C27	2.220(4)	Cr1-C27	2.231(4)
Cr1-Cr1	2.4542(8)	Cr1-H1	1.65(3)
Li1-O1'	1.942(6)	Li1-O1	1.942(6)
Li1-O1	1.942(6)	Li1-O1'	1.942(6)
Li1-O2	1.956(6)	Li1-O2'	1.956(6)
Li1-O2'	1.956(6)	Li1-O2	1.956(6)
N1-C1	1.372(4)	N1-C8	1.411(4)
N2-C2	1.374(4)	N2-C20	1.431(4)
C1-C2	1.342(5)	C3-C4	1.406(6)
C3-C8	1.419(5)	C3-C10	1.508(7)
C4-C5	1.366(8)	C7-C13	1.508(5)
C5-C6	1.365(7)	C12-C13	1.533(5)
C6-C7	1.397(5)	C13-C14	1.538(5)
C7-C8	1.408(5)	C15-C20	1.403(6)
C9-C10	1.530(9)	C16-C17	1.361(7)
C10-C11	1.543(9)	C17-C18	1.364(8)
C15-C16	1.395(5)	C18-C19	1.408(6)
C15-C22	1.518(7)	C19-C20	1.409(6)
C19-C25	1.514(7)	C21-C22	1.530(8)
C24-C25	1.518(8)	C22-C23	1.523(8)
C25-C26	1.504(8)	C27-Cr1	2.219(4)
C27-H27A	0.87(5)	C27-H27B	0.87(5)
C27-H27C	1.04(5)	O1-C28	1.44(2)
O1-C31	1.52(1)	C28-C29	1.46(2)
C29-C30	1.52(2)	C30-C31	1.47(2)
O1'-C31'	1.41(1)	O1'-C28'	1.47(2)
C28'-C29'	1.48(2)	C29'-C30'	1.54(2)
C30'-C31'	1.46(2)	O2-C32	1.379(9)
O2-C35	1.428(9)	C33-C34	1.43(2)
C33-C32	1.44(2)	C34-C35	1.45(2)
O2'-C35'	1.38(2)	O2'-C32'	1.44(2)
C33'-C32'	1.42(2)	C33'-C34'	1.41(2)
C34'-C35'	1.45(2)		

Angles (°)

N2-Cr1-N1	80.0(1)	N2-Cr1-C27	138.1(2)
N1-Cr1-C27	98.9(2)	N2-Cr1-C27	93.5(2)
N1-Cr1-C27	173.1(2)	C27-Cr1-C27	87.6(2)
N2-Cr1-Cr1	148.71(8)	N1-Cr1-Cr1	129.59(7)
C27-Cr1-Cr1	56.8(1)	C27-Cr1-Cr1	56.3(1)
N2-Cr1-H1	137.3(8)	N1-Cr1-H1	99(1)
C27-Cr1-H1	84.5(9)	C27-Cr1-H1	84.1(9)
Cr1-Cr1-H1	42(2)	O1-Li1-O1	113.1(5)
O1'-Li1-O1'	113.1(5)	O1-Li1-O2	108.4(2)
O1-Li1-O2	108.3(2)	O1'-Li1-O2'	108.4(2)
O1'-Li1-O2'	108.3(2)	O1'-Li1-O2'	108.3(2)
O1'-Li1-O2'	108.4(2)	O2'-Li1-O2'	110.3(5)
O1-Li1-O2	108.3(2)	O1-Li1-O2	108.4(2)
O2-Li1-O2	110.3(5)	C1-N1-C8	118.3(2)
C1-N1-Cr1	113.3(2)	C8-N1-Cr1	126.9(2)
C2-N2-C20	115.7(3)	C2-N2-Cr1	114.0(2)
C20-N2-Cr1	130.3(2)	C2-C1-N1	115.9(3)
C1-C2-N2	116.2(3)	C4-C3-C8	117.7(4)
C4-C3-C10	120.4(4)	C8-C3-C10	121.8(4)
C5-C4-C3	121.9(4)	C6-C5-C4	120.2(4)
C5-C6-C7	121.2(4)	C6-C7-C8	119.0(4)
C6-C7-C13	119.5(3)	C8-C7-C13	121.5(3)
N1-C8-C7	121.2(3)	N1-C8-C3	118.9(3)
C7-C8-C3	119.9(3)	C9-C10-C3	111.5(6)
C9-C10-C11	111.8(5)	C3-C10-C11	111.7(4)
C7-C13-C12	112.9(3)	C7-C13-C14	111.4(3)
C16-C15-C22	119.8(4)	C14-C13-C12	109.0(3)
C17-C16-C15	121.7(5)	C16-C15-C20	118.5(4)
C17-C18-C19	121.7(5)	C20-C15-C22	121.7(3)
C18-C19-C25	120.9(4)	C16-C17-C18	119.9(4)
C15-C20-C19	120.5(3)	C18-C19-C20	117.7(5)
C19-C20-N2	118.6(4)	C20-C19-C25	121.3(3)
C15-C22-C21	112.0(5)	C15-C20-N2	120.9(3)
C19-C25-C24	113.2(5)	C15-C22-C23	111.6(4)
Cr1-C27-H27A	78.(3)	C23-C22-C21	111.5(5)
Cr1-C27-H27B	140.(3)	C19-C25-C26	112.8(6)
H27A-C27-H27B	108.(4)	C26-C25-C24	110.0(5)
Cr1-C27-H27C	107.(3)	Cr1-C27-Cr1	66.9(1)
H27B-C27-H27C	98.(4)	Cr1-C27-H27A	140.(3)

C28-O1-Li1	132.7(9)	Cr1-C27-H27B	90.(3)
O1-C28-C29	103(1)	Cr1-C27-H27C	119.(3)
C28-C29-C30	110(1)	H27A-C27-H27C	105.(4)
C31-C30-C29	105(1)	C28-O1-C31	107(1)
C30-C31-O1	106(1)	C31-O1-Li1	119.4(5)
C31'-O1'-C28'	110(1)	C31'-O1'-Li1	125.4(5)
C28'-O1'-Li1	121.2(8)	O1'-C28'-C29'	104(1)
C32-O2-Li1	139.6(5)	C28'-C29'-C30'	106(1)
C34-C33-C32	104.8(7)	C31'-C30'-C29'	103(1)
O2-C32-C33	114.4(8)	O1'-C31'-C30'	105(1)
C33-C34-C35	105.7(8)	C32-O2-C35	102.9(6)
O2-C35-C34	111.3(7)	C35-O2-Li1	117.4(5)
C35'-O2'-C32'	118(2)	C35'-O2'-Li1	123(1)
C32'-O2'-Li1	113.2(9)	C32'-C33'-C34'	109(2)
C33'-C34'-C35'	109(2)	O2'-C32'-C33'	99(2)
O2'-C35'-C34'	98(2)		

Complex **10** crystallized in the orthorhombic space group $C222_1$ and contains a crystallographic C_2 axis going through hydride H1 and perpendicular to the Cr1-Cr1 vector. Due to the symmetry, the coordination geometry around the Cr is best described as trigonal bipyramidal with axial vector of N1-Cr1-C27 and the calculated τ_5 value is 0.58. Complex **10** has two bridging methyl groups and one bridging hydride in between two α -diimine chromium fragments. The bridging hydride and methyl protons were located by X-ray difference map. The Cr-C bond lengths are 2.220(4) and 2.231(4) Å respectively. The Cr-H distance of 1.65(3) Å is within the range of bridging hydride complex of chromium. Unexceptionally, the Cr-N bond lengths are 1.968(2) Å for Cr1-N1 and 1.994(2) Å for Cr1-N2. The dianionic assignment for α -diimine ligand agrees with the C-N single bond length of 1.372(4) and 1.374(4) Å and C-C double bond length of 1.342(5) Å. The Cr-Cr distance of 2.4542(8) Å in **10** is lightly longer than that in **5**. The room temperature magnetic moment of **10** was 3.1(1) μ_B per complex, presumably due to antiferromagnetic coupling. Because only diimine

ligand signals can be observed in $^1\text{H-NMR}$, **10** shows an identical spectrum to that of **5** with broad resonance and chemical shifts at 7.78, 5.60, 3.39 and 1.67 ppm.

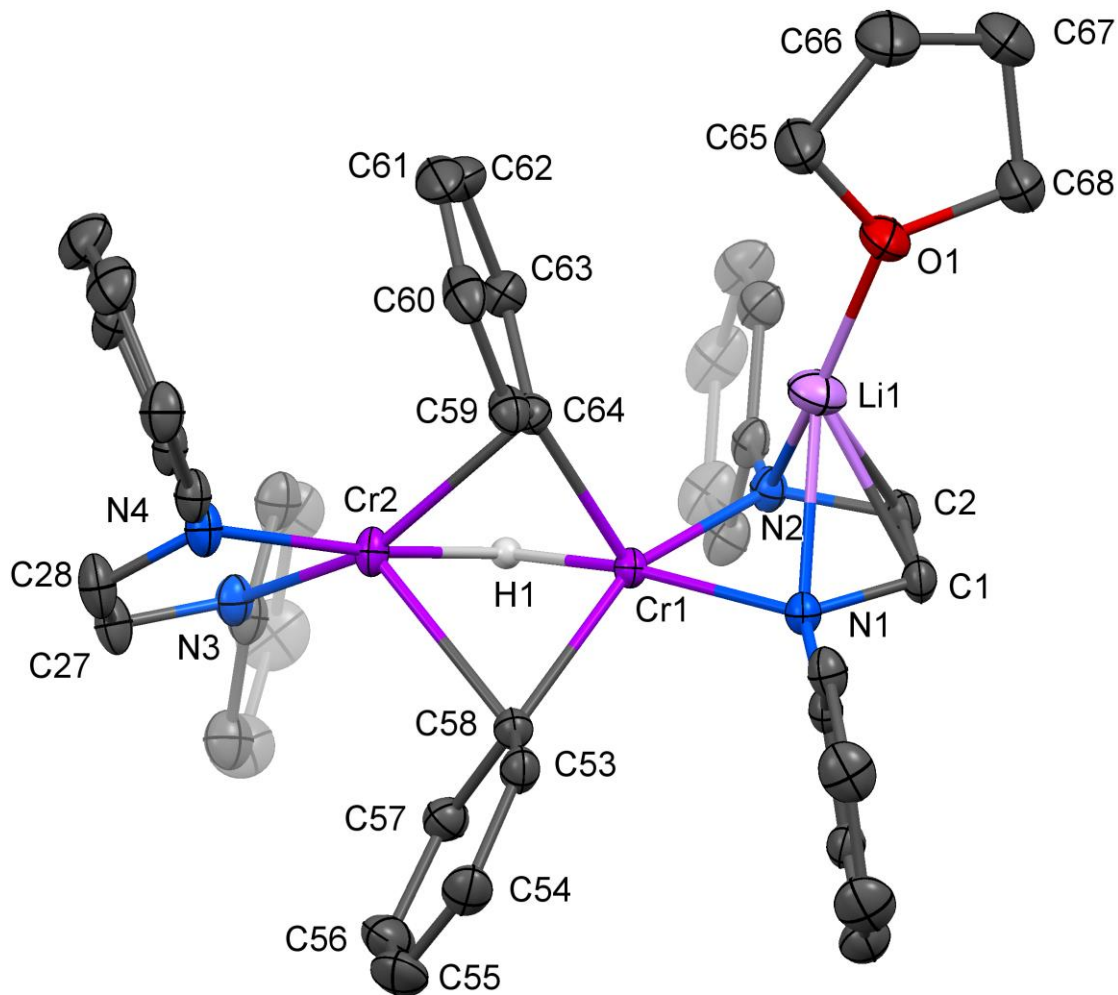


Figure 3.10 Molecular structure of $[(^{\text{H}}\text{Li}^{\text{iPr}}\text{Cr})_2(\mu\text{-Ph})_2(\mu\text{-H})][\text{Li}(\text{THF})]^+$ (**11**) with thermal ellipsoids at the 30% probability level. H1 has been located on a difference map. Isopropyl groups and hydrogen atoms have been omitted for clarity.

Table 3.8 Interatomic distances (Å) and angles (°) for [(^HL^{iPr}Cr)₂(μ-Ph)₂(μ-H)]⁻ [Li(THF)]⁺ (11)

Distance (Å)			
Cr1-N2	2.005(2)	Cr1-N1	2.038(2)
Cr1-C64	2.091(2)	Cr1-C58	2.121(2)
Cr1-Cr2	2.5852(4)	Cr1-Li1	2.679(4)
Cr1-H1	1.68(2)	Cr2-N3	2.004(2)
Cr2-N4	2.025(2)	Cr2-C64	2.343(2)
Cr2-C58	2.384(2)	Cr2-H1	1.74(2)
Li1-O1	1.880(4)	Li1-C1	2.184(5)
Li1-N1	2.213(4)	Li1-C2	2.233(5)
Li1-N2	2.300(4)	N1-C1	1.395(2)
N1-C8	1.435(2)	N2-C2	1.396(2)
N2-C20	1.434(2)	N3-C27	1.348(3)
N3-C34	1.434(3)	N4-C28	1.355(3)
N4-C46	1.439(3)	O1-C65	1.444(3)
O1-C68	1.449(3)	C1-C2	1.342(3)
C3-C4	1.394(3)	C3-C8	1.409(3)
C3-C10	1.518(3)	C4-C5	1.374(4)
C7-C13	1.517(3)	C5-C6	1.371(4)
C12-C13	1.535(4)	C6-C7	1.399(3)
C13-C14	1.530(4)	C7-C8	1.405(3)
C15-C20	1.406(3)	C9-C10	1.533(3)
C16-C17	1.387(4)	C10-C11	1.534(3)
C17-C18	1.369(4)	C15-C16	1.396(3)
C18-C19	1.402(3)	C15-C22	1.517(3)
C19-C20	1.410(3)	C19-C25	1.510(4)
C21-C22	1.514(4)	C24-C25	1.533(4)
C22-C23	1.523(4)	C25-C26	1.531(4)
C27-C28	1.366(3)	C29-C30	1.393(3)
C29-C34	1.410(3)	C29-C36	1.519(4)
C30-C31	1.377(4)	C33-C39	1.530(4)
C31-C32	1.369(4)	C38-C39	1.533(4)
C32-C33	1.407(3)	C39-C40	1.528(4)
C33-C34	1.396(3)	C41-C46	1.408(3)
C35-C36	1.530(3)	C42-C43	1.375(4)
C36-C37	1.524(4)	C43-C44	1.374(4)
C41-C42	1.395(4)	C44-C45	1.398(3)

C41-C48	1.525(3)	C45-C46	1.408(3)
C45-C51	1.507(3)	C47-C48	1.528(5)
C50-C51	1.522(4)	C48-C49	1.550(4)
C51-C52	1.530(4)	C53-C54	1.386(3)
C53-C58	1.417(3)	C59-C64	1.406(3)
C54-C55	1.370(4)	C60-C61	1.374(4)
C55-C56	1.391(4)	C61-C62	1.378(4)
C56-C57	1.394(3)	C62-C63	1.384(3)
C57-C58	1.411(3)	C63-C64	1.413(3)
C59-C60	1.394(3)	C65-C66	1.480(4)
C66-C67	1.491(5)	C67-C68	1.506(4)

Angles (°)

N2-Cr1-N1	78.56(6)	N2-Cr1-C64	109.58(7)
N1-Cr1-C64	108.96(7)	N2-Cr1-C58	152.82(8)
N1-Cr1-C58	97.34(7)	C64-Cr1-C58	97.22(8)
N2-Cr1-Cr2	131.32(5)	N1-Cr1-Cr2	149.25(5)
C64-Cr1-Cr2	59.02(5)	C58-Cr1-Cr2	59.90(5)
N2-Cr1-Li1	56.7(1)	N1-Cr1-Li1	53.9(1)
C64-Cr1-Li1	72.6(1)	C58-Cr1-Li1	140.5(1)
Cr2-Cr1-Li1	130.9(1)	N2-Cr1-H1	93.7(8)
N1-Cr1-H1	165.6(8)	C64-Cr1-H1	85.0(8)
C58-Cr1-H1	83.9(8)	Cr2-Cr1-H1	41.8(8)
Li1-Cr1-H1	131.1(8)	N3-Cr2-N4	80.41(7)
N3-Cr2-C64	155.51(7)	N4-Cr2-C64	104.96(7)
N3-Cr2-C58	116.31(7)	N4-Cr2-C58	113.70(7)
C64-Cr2-C58	83.90(7)	N3-Cr2-Cr1	132.23(5)
N4-Cr2-Cr1	146.41(5)	C64-Cr2-Cr1	49.91(5)
C58-Cr2-Cr1	50.34(5)	N3-Cr2-H1	95.0(7)
N4-Cr2-H1	171.2(7)	C64-Cr2-H1	76.3(7)
C58-Cr2-H1	75.0(7)	Cr1-Cr2-H1	40.1(7)
O1-Li1-C1	129.4(2)	O1-Li1-N1	143.0(2)
C1-Li1-N1	36.99(9)	O1-Li1-C2	130.1(2)
C1-Li1-C2	35.3(1)	N1-Li1-C2	63.1(2)
O1-Li1-N2	144.6(2)	C1-Li1-N2	62.9(2)
N1-Li1-N2	69.1(2)	C2-Li1-N2	35.82(9)
O1-Li1-Cr1	156.8(2)	C1-Li1-Cr1	72.4(2)
N1-Li1-Cr1	48.08(9)	C2-Li1-Cr1	71.5(2)
N2-Li1-Cr1	46.71(8)	C1-N1-C8	113.3(2)
C1-N1-Cr1	113.9(2)	C8-N1-Cr1	129.3(2)

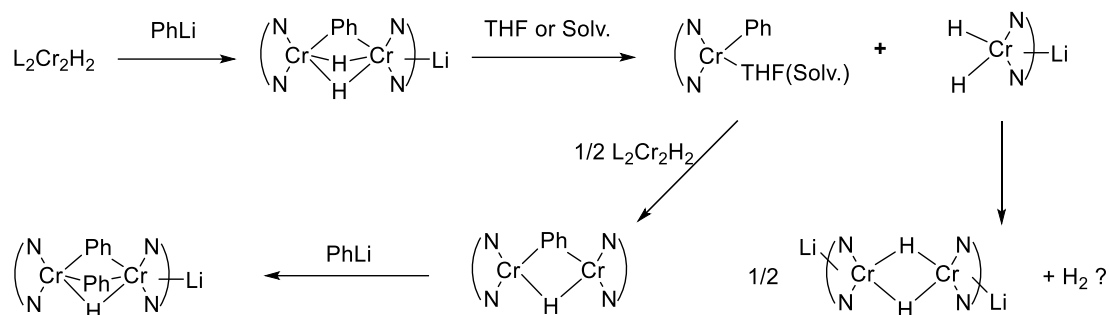
C1-N1-Li1	70.4(2)	C8-N1-Li1	136.0(2)
Cr1-N1-Li1	78.0(2)	C2-N2-C20	114.6(2)
C2-N2-Cr1	115.5(2)	C20-N2-Cr1	127.8(2)
C2-N2-Li1	69.5(2)	C20-N2-Li1	136.0(2)
Cr1-N2-Li1	76.6(2)	C27-N3-C34	118.1(2)
C27-N3-Cr2	111.9(2)	C34-N3-Cr2	130.0(2)
C28-N4-C46	114.8(2)	C28-N4-Cr2	110.4(2)
C46-N4-Cr2	133.7(2)	C65-O1-C68	108.9(2)
C65-O1-Li1	122.3(2)	C68-O1-Li1	128.7(2)
C2-C1-N1	116.3(2)	C2-C1-Li1	74.3(2)
N1-C1-Li1	72.6(2)	C1-C2-Li1	70.3(2)
C1-C2-N2	115.4(2)	C4-C3-C10	119.6(2)
N2-C2-Li1	74.7(2)	C5-C4-C3	121.4(2)
C4-C3-C8	118.9(2)	C5-C6-C7	121.6(2)
C8-C3-C10	121.5(2)	C6-C7-C13	119.2(2)
C6-C5-C4	119.6(2)	C7-C8-C3	119.9(2)
C6-C7-C8	118.6(2)	C3-C8-N1	121.4(2)
C8-C7-C13	122.2(2)	C3-C10-C11	109.4(2)
C7-C8-N1	118.7(2)	C7-C13-C12	110.9(2)
C3-C10-C9	114.1(2)	C16-C15-C22	119.3(2)
C9-C10-C11	110.1(2)	C17-C16-C15	121.4(3)
C7-C13-C14	112.6(2)	C17-C18-C19	121.8(2)
C14-C13-C12	110.1(2)	C18-C19-C25	118.9(2)
C16-C15-C20	118.9(2)	C15-C20-C19	120.0(2)
C20-C15-C22	121.7(2)	C19-C20-N2	121.5(2)
C18-C17-C16	119.3(2)	C21-C22-C23	111.4(2)
C18-C19-C20	118.6(2)	C19-C25-C24	113.2(2)
C20-C19-C25	122.4(2)	N4-C28-C27	117.8(2)
C15-C20-N2	118.5(2)	C30-C29-C36	119.7(2)
C21-C22-C15	113.3(2)	C31-C30-C29	121.2(3)
C15-C22-C23	110.0(2)	C31-C32-C33	121.3(3)
C19-C25-C26	109.9(2)	C34-C33-C39	123.9(2)
C26-C25-C24	110.1(2)	C33-C34-C29	120.5(2)
N3-C27-C28	116.6(2)	C29-C34-N3	117.3(2)
C30-C29-C34	118.7(2)	C29-C36-C35	109.8(2)
C34-C29-C36	121.3(2)	C40-C39-C38	109.9(2)
C32-C31-C30	119.9(3)	C42-C41-C48	119.5(2)
C34-C33-C32	118.4(2)	C43-C42-C41	121.6(2)
C32-C33-C39	117.8(2)	C43-C44-C45	121.1(2)
C33-C34-N3	122.2(2)	C44-C45-C51	121.1(2)
C29-C36-C37	113.7(2)	C45-C46-C41	120.6(2)

C37-C36-C35	110.4(2)	C41-C46-N4	118.9(2)
C40-C39-C33	112.5(2)	C41-C48-C49	110.1(2)
C33-C39-C38	110.5(2)	C45-C51-C52	111.0(2)
C42-C41-C46	118.2(2)	C55-C54-C53	120.6(2)
C46-C41-C48	122.3(2)	C55-C56-C57	119.9(2)
C44-C43-C42	119.9(2)	C57-C58-C53	114.6(2)
C44-C45-C46	118.5(2)	C53-C58-Cr1	121.8(2)
C46-C45-C51	120.4(2)	C53-C58-Cr2	122.8(2)
C45-C46-N4	120.5(2)	C60-C59-C64	122.1(2)
C41-C48-C47	113.6(3)	C60-C61-C62	120.0(2)
C47-C48-C49	109.4(3)	C62-C63-C64	122.1(2)
C45-C51-C50	113.4(2)	C59-C64-Cr1	125.2(2)
C50-C51-C52	110.1(2)	C59-C64-Cr2	110.0(2)
C54-C53-C58	122.7(2)	Cr1-C64-Cr2	71.07(6)
C54-C55-C56	119.3(2)	C59-C64-C63	115.7(2)
C56-C57-C58	122.8(2)	C63-C64-Cr1	118.3(2)
C57-C58-Cr1	122.4(2)	C63-C64-Cr2	98.4(2)
C57-C58-Cr2	90.1(2)	O1-C65-C66	106.8(2)
Cr1-C58-Cr2	69.76(6)	C65-C66-C67	104.0(3)
C61-C60-C59	120.0(2)	C66-C67-C68	102.9(2)
C61-C62-C63	120.1(2)	O1-C68-C67	104.6(2)

Complex **11** crystallized in monoclinic space group $P2_1/n$ and gave an unexpected crystal structure compared to the other six complexes. Other than two bridging phenyl rings and one bridging hydride in between diimine chromium fragments, there is a direct interaction between the lithium counterion and one of the diimine ligand. This diimine-lithium interaction was unusual in our chemistry, yet examples of similar coordination exist.^{16,17} The Li(THF) fragment is coordinated to the diimine ligand in a η^4 -manner with an average Li-N distance of 2.2565(4) Å and average Li-C distance of 2.2085(4) Å. The lithium coordinated diimine ligand is extremely reduced and exhibits an average C-N bond length of 1.395(2) Å and C-C bond length of 1.342(3) Å. The other diimine ligand shows a less reduced feature with average C-N bond length of 1.3515(3) Å and C-C bond length of 1.366(3) Å. Yet the

Cr-N distances in the two diimine chromium fragments are not noticeable different and range from 2.004(2) to 2.038(2) Å. The Cr1-Cr2 distance of 2.5852(4) Å is the longest among those seven molecules (**5-11**). The two bridging phenyl rings are obviously leaning toward Cr2 and have shorter Cr1-C_{ipso} bond length. The bridging carbon are about 0.2 Å closer to Cr1 than Cr2 with 2.121(2) Å, 2.091(2) Å for Cr1-C53, Cr1-C64 and 2.384(2) Å, 2.343(2) Å for Cr2-C53, Cr2-C64. On the other hand, the Cr2-H1 bond length of 1.68(2) Å is slightly shorter than Cr1-H1 bond length of 1.74(2) Å. Despite the structural differences between **5** and **11**, they share identical ¹H-NMR spectra with broad resonance and chemical shifts at 7.86, 6.70, 4.13 and 1.19 ppm in THF-d₈. Presumably, the lithium-diimine coordination only exist in solid state **11**, while in THF solvent, **11** will share the similar structure of **5** as lithium cation coordinated by four THF molecules. Thus, complex **11** is also assigned as Cr(III)-C(III) dinuclear complex. The low room temperature magnetism of 3.4(1) μ_B is also due to antiferromagnetic coupling between two Cr(III) ions.

Similar reactions did not happen with the other lithium reagents mentioned earlier (CH₂SiMe₃, Np, Bz.). The yields of **10** and **11** are significantly lower than **5** and **6**. Possibly, the formation of dialkyl(diaryl) hydrides could go through a dissociation-association-alkylation process after **5** or **6** were generated (Scheme **3.8**).



Scheme 3.8 Plausible mechanism of formation of chromium di-phenyl hydride complex

Presumably, the smaller bridging ligands of methyl and phenyl would leave a coordination site open on the chromium center for coordinating solvent, such as THF. After the coordination of one or more THF molecules, complex **5** would dissociate into two monomers in a weak dissociation equilibrium. The re-association of chromium mono-phenyl and chromium hydride would give a neutral binuclear chromium aryl hydride, which would be captured by another equivalent of PhLi to generate the final chromium bis(aryl)hydrido complex **11**. While in a less polar solvent system (e.g. pentane), the anionic complex **5** and **6** would precipitate out and prevent any further reaction. In addition, no such bis(alkyl) hydride was observed in reactions with TMS(CH₂)Li, t-Bu(CH₂)Li or Ph(CH₂)Li, plausibly due to stronger steric hindrance preventing solvent coordination.

Table 3.9 Selected bond distances (Å) of the diimine backbone, Cr-Cr distances, intramolecular bond distances, τ_5 values and room temperature magnetic moment per Cr (μ_B) for complexes 5-11

Compound	5	6	7	8
Cr-Cr	2.4420(1)	2.4823(7)	2.4850(3)	2.4763(3)
Cr-C	2.236(9) 2.31(1)	2.216(5) 2.181(4)	2.197(2) 2.304(2)	2.170(2) 2.337(2)
Cr-H	1.69(3) 1.68(3) 1.69(2) 1.68(4)	1.71(3) 1.70(3) 1.67(3) 1.61(3)	1.74(2) 1.73(2) 1.74(2) 1.73(2)	1.76(2) 1.72(2) 1.67(2) 1.69(2)
Cr-N	1.956(4) 1.959(4) 1.966(4) 1.960(4)	1.965(3) 1.965(3) 1.948(3) 1.977(3)	1.958(2) 1.999(2) 1.970(2) 2.000(2)	1.961(2) 1.992(2) 1.954(2) 2.003(2)
C-N	1.364(6) 1.373(6) 1.367(6) 1.369(6)	1.377(4) 1.382(4) 1.375(5) 1.382(4)	1.371(2) 1.372(2) 1.378(2) 1.378(2)	1.381(2) 1.387(2) 1.377(2) 1.374(2)
C-C	1.330(7) 1.331(7)	1.360(4) 1.350(5)	1.352(2) 1.345(2)	1.347(2) 1.355(2)
τ_5 (Cr1)	0.56	0.11	0.55	0.33
τ_5 (Cr2)	0.26	0.54	0.15	0.01
μ_{eff}	2.9(1)	3.4(1)	2.1(1)	3.1(1)

Table 3.9 Selected bond distances (Å) of the diimine backbone, Cr-Cr distances, intramolecular bond distances, τ_5 values and room temperature magnetic moment per Cr (μ_B) for complexes 5-11 (continue)

Compound	9	10	11
Cr-Cr	2.4948(4)	2.4542(8)	2.5852(4)
Cr-C	2.325(2)	2.220(4)	2.121(2)
	2.251(2)	2.231(4)	2.091(2)
			2.384(2)
			2.343(2)
Cr-H	1.75(2)	1.65(3)	1.68(2)
	1.75(2)		1.74(2)
	1.70(2)		
	1.73(2)		
Cr-N	1.958(2)	1.968(2)	2.005(2)
	2.017(2)	1.994(2)	2.038(2)
	1.951(2)		2.025(2)
	2.010(2)		2.004(2)
C-N	1.373(2)	1.372(4)	1.395(2)
	1.380(2)	1.374(4)	1.396(2)
	1.377(2)		1.348(3)
	1.382(2)		1.355(3)
C-C	1.357(3)	1.342(5)	1.342(3)
	1.348(3)		1.366(3)
τ_5 (Cr1)	0.12	0.58	0.22
τ_5 (Cr2)	0.53	0.58	0.27
μ_{eff}	2.5(1)	3.1(1)	3.4(1)

With a series of α -diimine chromium alkyl hydride complexes in hand, it is interesting to make a solid state structural comparison of all first row transition metal alkyl hydrides we know so far. Among α -diimine supported chromium alkyl hydride complexes series, complexes **6**, **9**, **11** crystallized in the monoclinic space group $P2_1/n$ while **5**, **7** and **8** crystallized in the triclinic space group $P-1$. Complex **10** crystallized in the monoclinic space group $C222_1$. Similarly, the bridging alkyl or aryl group sits between two chromium centers, and forms a Cr₂ binuclear core. All diimine ligands are in dianionic form according to bond length of C-N (average 1.378(5) Å) and C-C

(average 1.352(5) Å) bonds on the ligand backbones. Therefore, complexes **5-11** are all Cr(III)-Cr(III) dinuclear complexes and share similar distorted trigonal bipyramidal / square pyramidal coordination geometry around two chromium ions. Mindful of the limitations of X-ray crystallography for locating hydrogen atoms, the bridging hydride ligand range from 1.61(3) Å to 1.75(2) Å and are comparable to other reported bridging hydride chromium complexes. Likewise, antiferromagnetic coupling between chromium ions gave complex **5-11** magnetic moment measurement of 2.9(1), 3.4(1), 2.1(1), 3.1(1), 2.5(1), 3.1(1) and 3.4(1) μ_B respectively at room temperature. Because of the structural similarity of **5-11**, they show similar $^1\text{H-NMR}$ spectra (Figure 3.11).

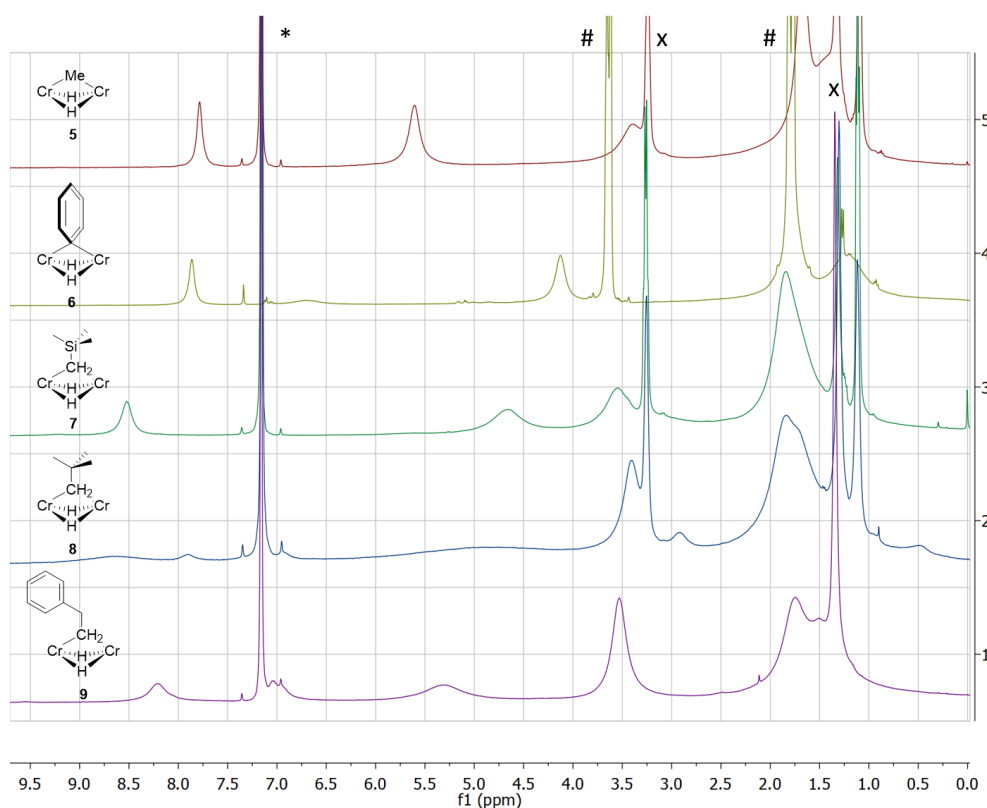
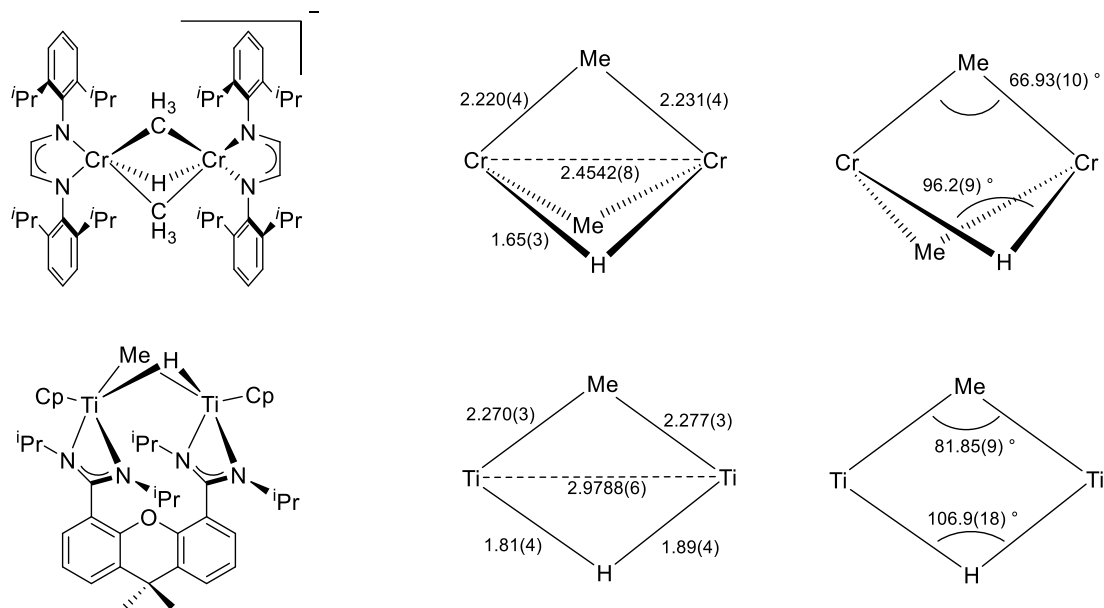


Figure 3.11 $^1\text{H-NMR}$ spectra of **5,7,8,9** in C_6D_6 and **6** in THF-d_8 due to poor solubility in C_6D_6 .

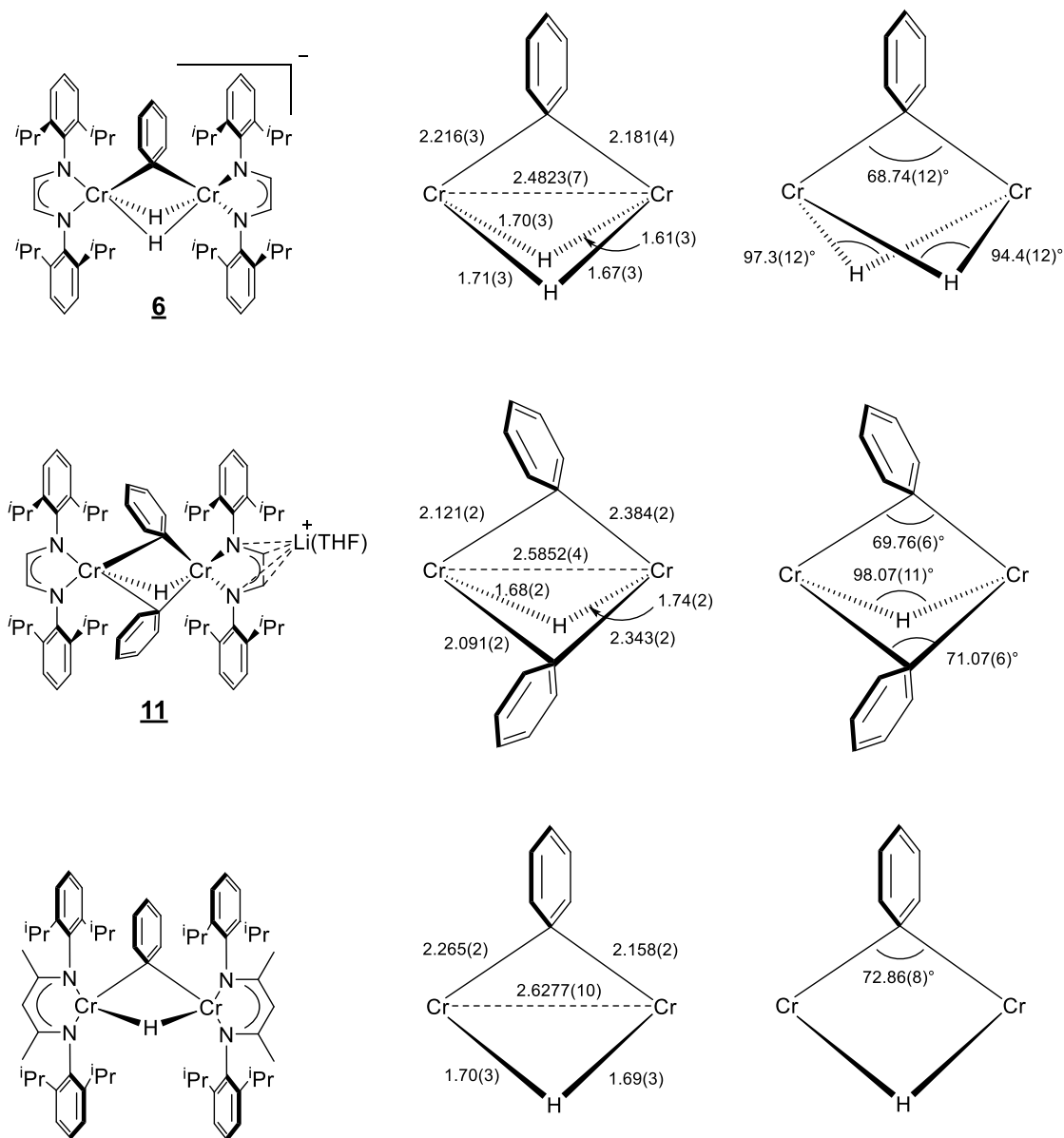
In order to make a comparison of complexes with similar alkyl hydride systems, complex **10** is selected to make a comparison to McNevin's [bis(amidinate)]Ti₂Cp₂(μ-Me)(μ-H) complex. Complex **6** and **11** are compared to Monillas' (nacnac^{iPr}Cr)₂(μ-Ph)(μ-H) complex. And complex **7** is compared to McAdams' (nacnac^{Me}Cr)₂(μ-CH₂TMS)(μ-H) complex. For both titanium methyl hydride and chromium methyl hydride complexes, each metal ion has the same oxidation state of +3 and five coordinated ligands. Presumably due to difference of ligand systems and covalent radii (covalent radii: Ti = 1.60(8) Å v.s. Cr = 1.39(5) Å), the Cr-Cr distance of 2.4542(8) Å in **10** is significantly shorter than the Ti-Ti distance of 2.9788(6) Å in titanium complex.¹⁸ The bridging methyl is also closer to Cr center (average Cr-C = 2.225(4) Å) with smaller metal-C-metal angle (Cr1-C27-Cr2 = 66.9(1)°) than those in Ti₂(μ-Me)(μ-H) complex (average Ti-C = 2.273(3) Å, Ti-C-Ti = 81.85(9)°). The Cr-H bond length of 1.65(3) Å is shorter than Ti-H average bond length of 1.85(4) Å. The Cr1-H1-Cr1 angle of 96.2(9)° is sharper than Ti-H-Ti angle of 107(2)° as well. The bond distances and angles are summed up in Scheme **3.9**.



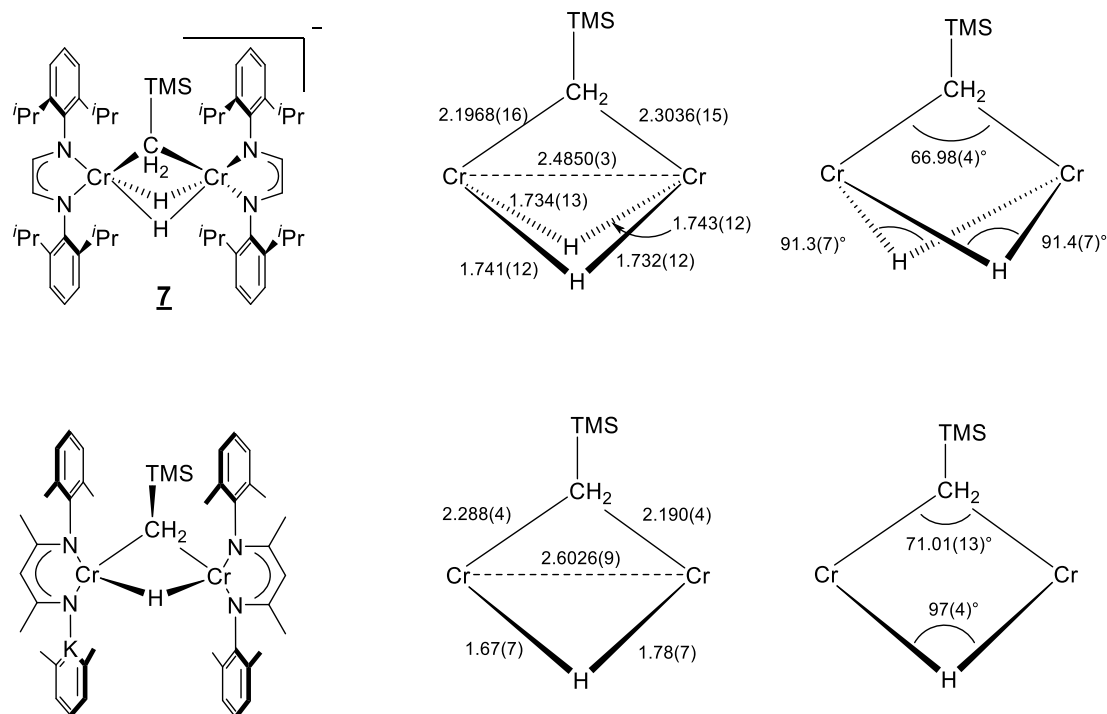
Scheme 3.9 Selected bond distances and angles in $\text{Cr}_2(\mu\text{-Me})_2(\mu\text{-H})$ and $\text{Ti}_2(\mu\text{-Me})(\mu\text{-H})$ core

The solid state structures of **6** and **11** are more comparable to $(\text{nacnacCr})_2(\mu\text{-Ph})(\mu\text{-H})$, due to their closely related ligand system. The bidentate *nacnac* ligand has a fixed formal charge of -1. Thus, $(\text{nacnac}^{\text{iPr}}\text{Cr})_2(\mu\text{-Ph})(\mu\text{-H})$ exhibit a Cr(II)-Cr(II) core with Cr-Cr distance of 2.68(1) Å. The Cr(III)-Cr(III) complex **6** and **11** show shorter distances between two chromium ions of 2.4823(7) and 2.5852(4) Å respectively, presumably due to the face-sharing geometry in **6** and **11**. The bridging ipso carbon of phenyl ligands keep about the same distances to chromium centers in both ligand systems with average Cr- C_{ipso} bond length of 2.198(5) Å for **6**, 2.234(2) Å for **11** and 2.211(2) Å for $\text{nacnac}^{\text{iPr}}\text{Cr}$ complex. The Cr-H bond length are even similar and range from 1.61(3) to 1.71(3) Å for **6**, from 1.68(2) to 1.74(2) Å for **11** and from 1.70(3) to 1.69(3) Å for $\text{nacnac}^{\text{iPr}}\text{Cr}$ complex. The bridging carbon angles are slightly sharper in

6 ($68.7(1)^\circ$) and **11** ($69.76(6)^\circ$, $71.07(6)^\circ$) than that in $(\text{nacnac}^{\text{iPr}}\text{Cr})_2(\mu\text{-Ph})(\mu\text{-H})$ ($72.86(8)^\circ$). The selected atom distances and angles are summed up in Scheme **2.10**.



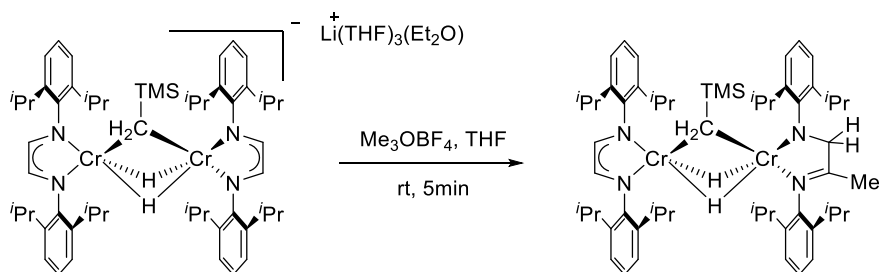
Scheme 3.10 Selected bond distances and angles in $\text{Cr}_2(\mu\text{-Ph})(\mu\text{-H})_2$, $\text{Cr}_2(\mu\text{-Ph})_2(\mu\text{-H})$ and $\text{Cr}_2(\mu\text{-Ph})(\mu\text{-H})$ core



Scheme 3.11 Selected bond distances and angles in Cr₂(μ-CH₂TMS)(μ-H)₂ and Cr₂(μ-CH₂TMS)(μ-H) core

Similarly, the Cr-Cr distance of 2.4850(3) Å in **7** is shorter than that of 2.6026(9) Å in MacAdams' (nacnac^{Me}Cr)₂(μ-CH₂TMS)(μ-H). The difference might result from the combination of the face-sharing geometry of Cr(III)-Cr(III) core in **7** and the edge-sharing geometry of Cr(II)-Cr(II) core in (nacnac^{Me}Cr)₂(μ-CH₂TMS)(μ-H). The chromium bridging carbon distances are very close in both ligand systems with average Cr-C bond length of 2.250(2) Å for **7** and 2.239(4) Å for nacnac^{Me}Cr complex. The Cr-H bond lengths are also very similar and range from 1.73(1) to 1.74(1) Å in **7** and from 1.67(7) to 1.78(7) Å in (nacnac^{Me}Cr)₂(μ-CH₂TMS)(μ-H). Presumably, due to the face-sharing geometry of **7**, all the angles of bridging ligands are more acute in **7** than those in nacnac^{iPr} system (Scheme **3.11**).

The synthesis and isolation of neutral chromium alkyl-hydride supported by diimine ligand is still outstanding. Attempts of mixing bis-alkyl hydride with $(^{\text{H}}\text{L}^{\text{iPr}}\text{Cr})_2(\mu\text{-Cl})_2$ did not give any desired complex, but only unidentifiable chromium diimine fragments and free ligands. Similar decomposition results also were observed when **7** was oxidized by lead(II) chloride, silver triflate, ferrocenium triflate or aminium radical cation (magic blue). Serval cationic carbon reagents and stable radicals, like triphenylmethyl halide, trimethyloxonium, (2,2,6,6-tetramethylpiperidin-1-yl)oxyl (TEMPO), were tested to generate neutral chromium alkyl(aryl)-hydride complexes via hydride abstraction. Only trimethyloxonium tetrafluoroborate reacted with $[(^{\text{H}}\text{L}^{\text{iPr}}\text{Cr})_2(\mu\text{-CH}_2\text{TMS})(\mu\text{-H})_2][\text{Li}(\text{THF})_3(\text{Et}_2\text{O})]^+$ (**7**) resulting a clean product (Scheme 3.12). 1 eq. of Me_3OBF_4 was added to a THF solution of **7** at -30°C . After 5 min stirring, the reaction was complete and changed color from violet to brown. The THF was removed under vacuum and the remaining solid was extracted with pentane. Complex **12** was recrystallized out of pentane solution at -30°C in 79% yield. Instead of getting a neutral alkyl-hydride $\text{L}_2\text{Cr}_2(\mu\text{-CH}_2\text{TMS})(\mu\text{-H})$, X-ray crystallography revealed that the methyl cation attacked one carbon on the diimine ligand backbone and left the $\text{Cr}_2(\mu\text{-H})(\mu\text{-CH}_2\text{TMS})$ core intact. The solid state structure, bond distances, and angles of **12** are displayed in Figure 3.12 and Table 3.9 respectively.



Scheme 3.12 Reaction of $[(^{\text{H}}\text{L}^{\text{iPr}}\text{Cr})_2(\mu\text{-CH}_2\text{TMS})(\mu\text{-H})_2]^+$ with Me_3OBF_4

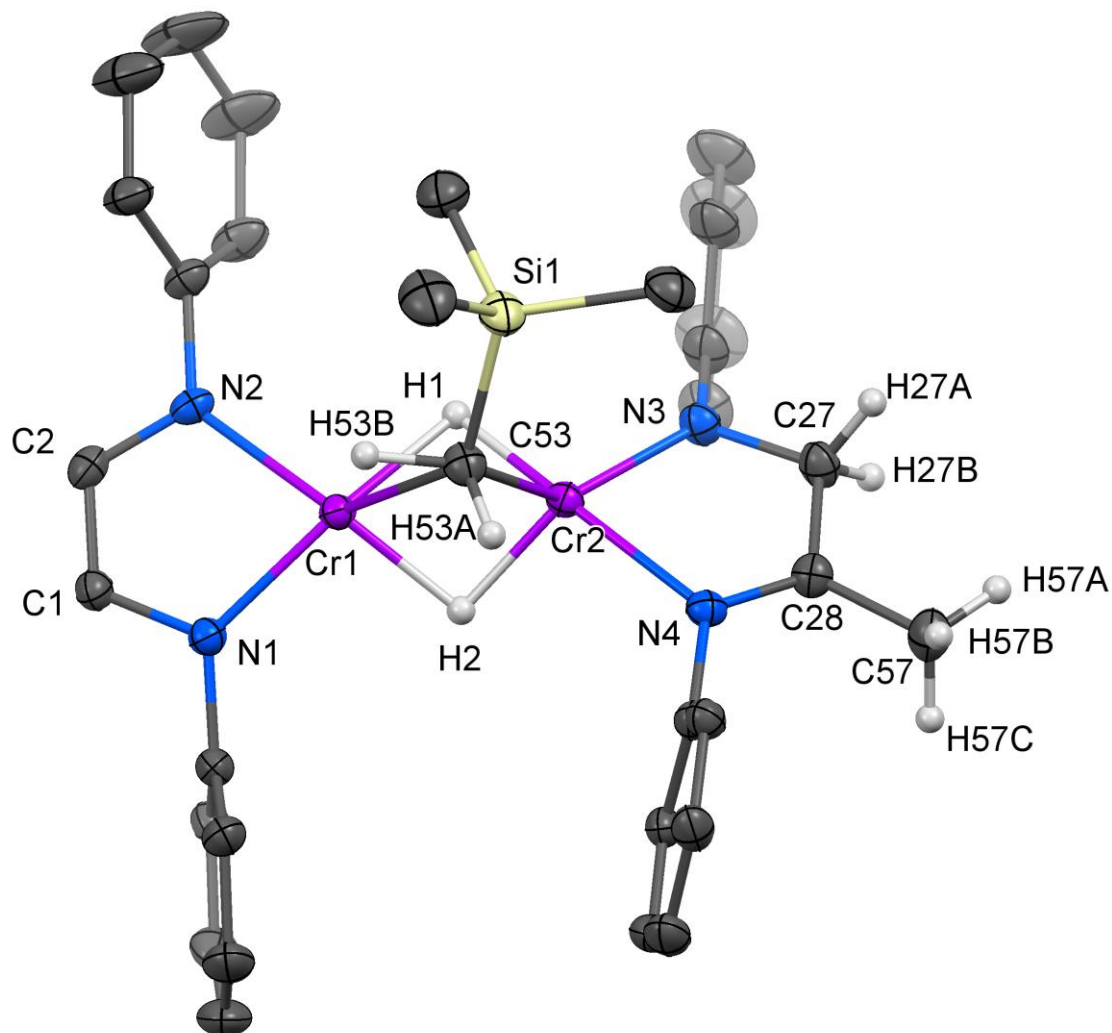


Figure 3.12 Molecular structure of $(\text{H}^{\text{L}}\text{iPrCr})(\text{Me},\text{H}^2\text{L}^{\text{iPrCr}})(\mu\text{-CH}_2\text{TMS})(\mu\text{-H})_2$ (12) with thermal ellipsoids at the 30% probability level. H1, H2, H27A, H27B, H53A, H53B, H57A, H57B and H57C have been located on a difference map. Isopropyl groups and hydrogen atoms have been omitted for clarity.

Table 3.10 Interatomic distances (Å) and angles (°) for (HL^{iPr}Cr) (Me₂H²L^{iPr}Cr)(μ-CH₂TMS)(μ-H)₂ (12)

Distances (Å)			
Cr1-N1	1.986(2)	Cr1-N2	2.020(2)
Cr1-C53	2.424(2)	Cr1-Cr2	2.5100(5)
Cr1-H1	1.82(2)	Cr1-H2	1.75(2)
Cr2-N3	1.917(2)	Cr2-N4	2.107(2)
Cr2-C53	2.130(2)	Cr2-H1	1.70(2)
Cr2-H2	1.71(2)	Si1-C56	1.865(3)
Si1-C53	1.867(2)	Si1-C55	1.878(3)
Si1-C54	1.884(3)	N1-C1	1.361(3)
N1-C8	1.440(3)	N2-C2	1.333(3)
N2-C20	1.438(3)	N3-C34	1.444(3)
N3-C27	1.445(3)	N4-C28	1.271(3)
N4-C46	1.463(3)	C1-C2	1.368(3)
C3-C4	1.404(4)	C3-C8	1.408(3)
C3-C10	1.520(4)	C4-C5	1.359(4)
C7-C13	1.520(4)	C5-C6	1.376(4)
C12-C13	1.530(4)	C6-C7	1.401(4)
C13-C14	1.521(4)	C7-C8	1.396(3)
C15-C20	1.402(3)	C9-C10	1.522(4)
C16-C17	1.363(5)	C10-C11	1.524(4)
C17-C18	1.374(5)	C15-C16	1.396(4)
C18-C19	1.390(4)	C15-C22	1.512(4)
C19-C20	1.410(3)	C19-C25	1.521(4)
C21-C22	1.524(4)	C24-C25	1.534(3)
C22-C23	1.527(4)	C25-C26	1.535(4)
C27-C28	1.503(3)	C27-H27A	0.94(3)
C27-H27B	0.97(3)	C28-C57	1.498(3)
C29-C30	1.401(4)	C29-C34	1.402(4)
C29-C36	1.519(4)	C30-C31	1.363(5)
C33-C39	1.521(4)	C31-C32	1.361(5)
C38-C39	1.494(5)	C32-C33	1.404(4)
C39-C40	1.535(4)	C33-C34	1.408(4)
C41-C46	1.407(3)	C35-C36	1.528(4)
C42-C43	1.370(4)	C36-C37	1.528(4)
C43-C44	1.378(4)	C41-C42	1.392(3)
C44-C45	1.391(3)	C41-C48	1.522(3)
C45-C46	1.398(3)	C45-C51	1.518(3)

C47-C48	1.530(4)	C50-C51	1.536(4)
C48-C49	1.519(4)	C51-C52	1.529(4)
C53-H53A	0.99(3)	C53-H53B	1.05(3)

Angles (°)

N1-Cr1-N2	79.97(7)	N1-Cr1-C53	124.66(8)
N2-Cr1-C53	119.24(8)	N1-Cr1-Cr2	139.25(5)
N2-Cr1-Cr2	140.32(6)	C53-Cr1-Cr2	51.12(6)
N1-Cr1-H1	157.9(7)	N2-Cr1-H1	99.5(7)
C53-Cr1-H1	75.1(7)	Cr2-Cr1-H1	42.6(7)
N1-Cr1-H2	96.7(8)	N2-Cr1-H2	165.7(7)
C53-Cr1-H2	74.1(7)	Cr2-Cr1-H2	42.9(8)
H1-Cr1-H2	78(1)	N3-Cr2-N4	80.42(7)
N3-Cr2-C53	134.98(8)	N4-Cr2-C53	100.89(8)
N3-Cr2-Cr1	140.98(6)	N4-Cr2-Cr1	136.33(5)
C53-Cr2-Cr1	62.35(6)	N3-Cr2-H1	95.5(8)
N4-Cr2-H1	173.1(8)	C53-Cr2-H1	85.9(8)
Cr1-Cr2-H1	46.4(8)	N3-Cr2-H2	141.6(7)
N4-Cr2-H2	97.0(8)	C53-Cr2-H2	83.3(7)
Cr1-Cr2-H2	44.1(8)	H1-Cr2-H2	83(2)
C56-Si1-C53	107.7(2)	C56-Si1-C55	109.5(2)
C53-Si1-C55	109.9(2)	C56-Si1-C54	109.2(2)
C53-Si1-C54	113.5(2)	C55-Si1-C54	107.0(2)
C1-N1-C8	114.8(2)	C1-N1-Cr1	113.8(2)
C8-N1-Cr1	130.6(2)	C2-N2-C20	117.6(2)
C2-N2-Cr1	112.9(2)	C20-N2-Cr1	129.4(2)
C34-N3-C27	111.3(2)	C34-N3-Cr2	130.8(2)
C27-N3-Cr2	116.6(2)	C28-N4-C46	118.9(2)
C28-N4-Cr2	114.7(2)	C46-N4-Cr2	126.3(2)
N1-C1-C2	115.8(2)	N2-C2-C1	117.4(2)
C4-C3-C8	117.4(2)	C4-C3-C10	120.3(2)
C8-C3-C10	122.3(2)	C5-C4-C3	121.4(2)
C4-C5-C6	120.6(3)	C5-C6-C7	120.9(3)
C8-C7-C6	118.0(2)	C8-C7-C13	121.9(2)
C6-C7-C13	120.1(2)	C7-C8-C3	121.6(2)
C7-C8-N1	120.3(2)	C3-C8-N1	118.0(2)
C3-C10-C11	112.2(2)	C3-C10-C9	111.7(2)
C11-C10-C9	110.5(2)	C7-C13-C12	113.4(2)
C7-C13-C14	110.3(2)	C16-C15-C22	120.1(3)
C14-C13-C12	109.5(2)	C17-C16-C15	121.9(3)

C16-C15-C20	117.8(3)	C17-C18-C19	121.3(3)
C20-C15-C22	122.1(2)	C18-C19-C25	118.3(2)
C16-C17-C18	119.9(3)	C15-C20-C19	120.7(2)
C18-C19-C20	118.3(3)	C19-C20-N2	121.0(2)
C20-C19-C25	123.4(2)	C15-C22-C21	114.0(3)
C15-C20-N2	118.2(2)	C19-C25-C26	111.3(2)
C15-C22-C23	110.5(2)	N3-C27-H27A	117(2)
C23-C22-C21	110.8(2)	N3-C27-H27B	114(2)
C19-C25-C24	112.4(2)	H27A-C27-H27B	98.(2)
C24-C25-C26	108.9(2)	N4-C28-C27	116.2(2)
N3-C27-C28	111.4(2)	C30-C29-C34	118.5(3)
C28-C27-H27A	107(2)	C34-C29-C36	121.8(2)
C28-C27-H27B	108(2)	C32-C31-C30	120.5(3)
N4-C28-C57	127.2(2)	C32-C33-C34	118.1(3)
C57-C28-C27	116.6(2)	C34-C33-C39	122.4(2)
C30-C29-C36	119.6(3)	C29-C34-N3	121.2(2)
C31-C30-C29	121.2(3)	C37-C36-C29	111.3(3)
C31-C32-C33	121.3(3)	C29-C36-C35	113.2(3)
C32-C33-C39	119.5(3)	C38-C39-C33	111.5(3)
C29-C34-C33	120.3(2)	C33-C39-C40	112.2(3)
C33-C34-N3	118.5(2)	C42-C41-C46	116.8(2)
C37-C36-C35	109.7(2)	C46-C41-C48	122.2(2)
C38-C39-C40	109.7(3)	C42-C43-C44	120.1(2)
C42-C41-C48	121.0(2)	C44-C45-C46	118.1(2)
C43-C42-C41	122.1(2)	C46-C45-C51	123.3(2)
C43-C44-C45	120.8(2)	C45-C46-N4	120.6(2)
C44-C45-C51	118.6(2)	C49-C48-C41	112.1(2)
C45-C46-C41	122.1(2)	C41-C48-C47	111.7(2)
C41-C46-N4	117.3(2)	C45-C51-C52	111.8(2)
C49-C48-C47	111.4(2)	C52-C51-C50	109.0(2)
C45-C51-C50	111.2(2)	Si1-C53-Cr2	112.3(2)
Si1-C53-Cr1	129.2(2)	Cr2-C53-Cr1	66.53(6)
Si1-C53-H53A	110(2)	Cr2-C53-H53A	105(2)
Cr1-C53-H53A	120(2)	Si1-C53-H53B	99(2)
Cr2-C53-H53B	125(2)	Cr1-C53-H53B	59(2)
H53A-C53-H53B	105(2)		

12 crystallized in monoclinic space group *C2/c*. The bridging alkyl group, two bridging hydrides and one diimine-chromium fragment remained the same as those in

complex **7**, while the other diimine ligand is methylated on a backbone carbon. The square pyramidal geometry around Cr1 with τ_5 value of 0.15 has a tilted axial vector of Cr1-C53. The coordination geometry around Cr2 is best described as distorted trigonal bipyramidal with axial vector of N4-Cr2-H1 and τ_5 value of 0.50. The bridging hydrides, methylene protons and protons on the methylated ligand backbone were located on a X-ray difference map. Compared to complex **7**, the bridging carbon C53 moves even further away from Cr1 with Cr1-C53 bond length of 2.424(2) Å and closer toward Cr2 with Cr2-C53 bond length of 2.130(2) Å. The Cr-H distances of the bridging hydrides range from 1.70(2) Å to 1.82(2) Å. The distance between two chromium atoms (Cr1-Cr2 = 2.5100(5) Å) is slightly shorter than that in **7** (Cr1-Cr2 = 2.4850(3) Å). The unreacted ligand is still dianionic with average C-N bond length of 1.347(3) Å and C-C bond length of 1.368(3) Å. Instead, the other ligand has a methyl group on C28 and two protons on C27. Thus, the $\text{Me,H}^2\text{L}^{\text{iPr}}$ was functionalized and became a monoanionic amine-imine ligand with a N3-C27 single bond of 1.445(3) Å, a C27-C28 single bond of 1.503(3) Å and a N4-C28 double bond of 1.271(3) Å. Presumably, after the bond formation of methylene carbon C28 and methyl C57, the proton migrated onto adjacent C27. Therefore, complex **11** has one dianionic diimine ligand, one monoanionic amine-imine ligand, one bridging alkyl ligand and two bridging hydrides for two Cr(III) ions. The ligand activation is similar to CO_2 and $(\text{F}_3\text{C})\text{C}\equiv\text{C}(\text{CF}_3)$ addition onto the ligand of $(\mu\text{-}\eta^1\text{:}\eta^1\text{-H}^{\text{iPr}})_2\text{Cr}_2$. The electron rich ligand backbone is more attractive to the electron deficient Me^+ . The brown C_6D_6 solution of **12** showed a very similar $^1\text{H-NMR}$ spectrum as **7** with broad resonance and chemical shift at 21.26, 9.33, 3.87 and 1.54-1.25 ppm. The room temperature magnetic

moment of $3.6(1) \mu_B$ per complex is consistent with antiferromagnetic coupling of chromium atoms in α -diimine chromium alkyl-hydride series.

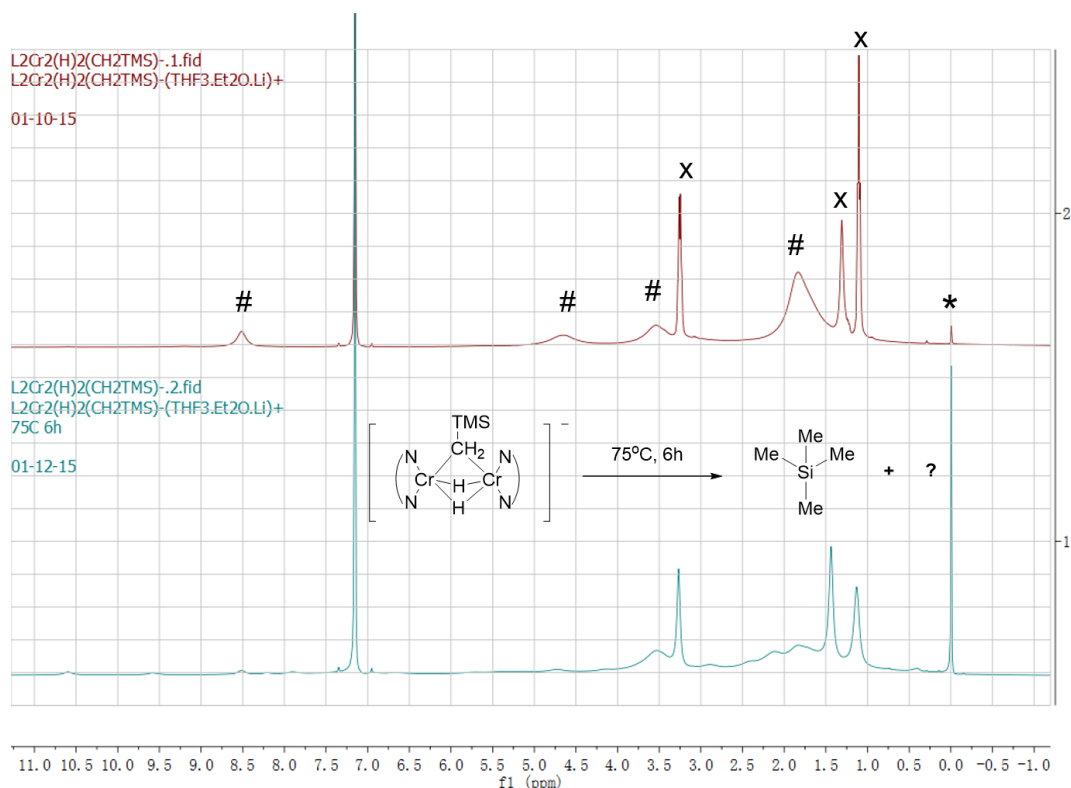
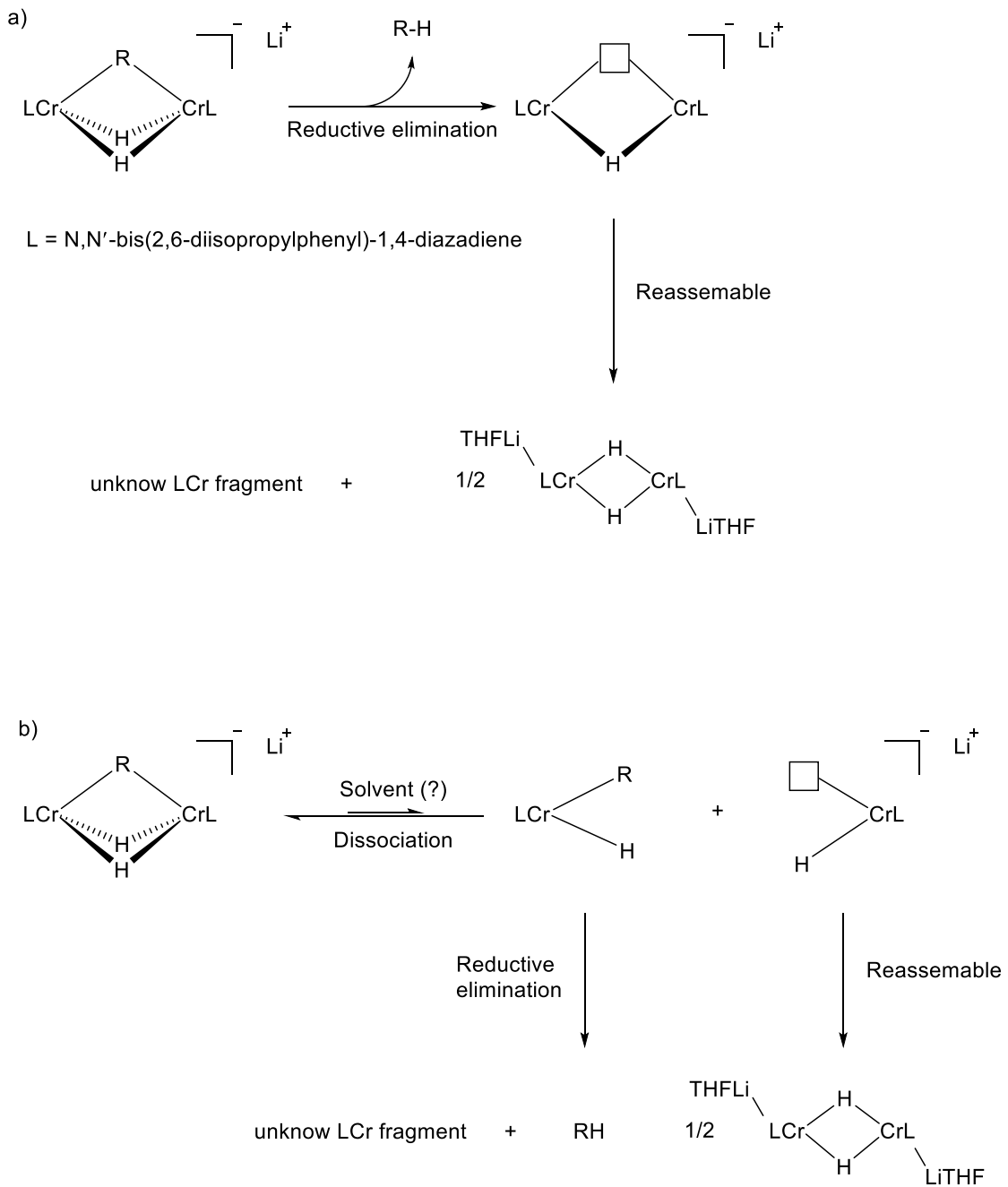


Figure 3.13 $^1\text{H-NMR}$ spectra of reductive elimination of **7**. The (#) denotes the characteristic peak belong to **7**, the (*) denotes the chemical shift of tetramethylsilane and (x) denotes the coordinated solvent of **7**

Given the successful synthesis and isolation of those first row transition metal alkyl(aryl) hydride complexes, the question about their stability/reactivity becomes more pressing, as the reductive elimination reaction is expected to be thermodynamically favorable and kinetically facile. As a series of chromium alkyl(aryl) hydride complexes supported by redox non-innocent diimine ligands were

synthesized successfully and isolated in good yield, the study of the reactivity of those complex **5-11** become possible. Monitored by $^1\text{H-NMR}$ spectroscopy, all anionic alkyl(aryl) hydride complexes would undergo reductive elimination at certain temperature and gave corresponding alkane/arene as the major organic product (take **7** for example as shown in Figure **3.13**). Due to the paramagnetism of the chromium α -diimine complexes, the inorganic product could not be easily identified. With the help of crystallization and X-ray crystallography, a dianionic $(^{\text{H}}\text{L}^{\text{iPr}}\text{Cr})_2(\mu\text{-H})_2(\text{LiTHF})_2$ complex was identified as a major inorganic product. However, no meaningful inorganic product could be isolated or identified for **10** and **11**. One possible mechanism of the thermal decomposition reaction of complex **5-9** is best described as reductive elimination followed reassembly of inorganic fragments (Scheme **3.12 a**). It is also possible that the reductive elimination occurs after the dissociation of Cr alkyl(aryl) hydride complex (Scheme **3.12 b**).



Scheme 3.13 Plausible mechanisms of decomposition reaction of 5-9

According to the hypothesis a) stated above, the decomposition rates of α -diimine Cr alkyl/aryl hydride complexes should be controlled by the reductive elimination step. Therefore, the observed decomposition rate of alkyl/aryl hydrides may represent the rate of reductive elimination and was predicted to be first order reaction. If mechanism b) is operative, the observed rate law of decomposition could be more complicated. The thermal stability of complexes **5-11** was monitored by $^1\text{H-NMR}$ in C_6D_6 (**5**, **7**, **8**, **9**, **10**) and THF-d₈ (**6**, **11**) in sealed J-Young tubes. The bridging alkyl/aryl ligands show strong impact on the thermal stability of Cr alkyl/aryl hydride complexes. Complex **5** and **10** have the same thermal stability and would not undergo reductive elimination or any reaction until heated up to 85°C. Judged by the integration of $^1\text{H-NMR}$ spectra, even at that high temperature, both complexes remain remarkable inert and only show <5% decomposition over 48h. Complex **6** and **11** are the second most stable with <20% decomposition at 75°C over 6 h in THF-d₈. At the same temperature over 70% of **7** decomposed within 6 h in C_6D_6 . The most reactive two are complex **8** and **9**. At room temperature, less than 30% of **8** and over 60% of **9** had decomposed in C_6D_6 solution after 6 days. The other Cr alkyl hydrides did not decompose at room temperature.

The most interesting comparison lies in the big difference of decomposition rates between complex **7** and **8**, despite their difference of only one atom. Due to the inaccuracy of integration of broad and overlapping $^1\text{H-NMR}$ resonances, the decomposition rates were measured by UV-Vis spectroscopy. A THF solution (3ml) of **7** ($8.06 \times 10^{-5}\text{M}$) or **8** ($8.16 \times 10^{-5}\text{M}$) were warmed up to 40 °C and were measured by UV-Vis. The decay of samples were monitored by the absorption band at 530 nm.

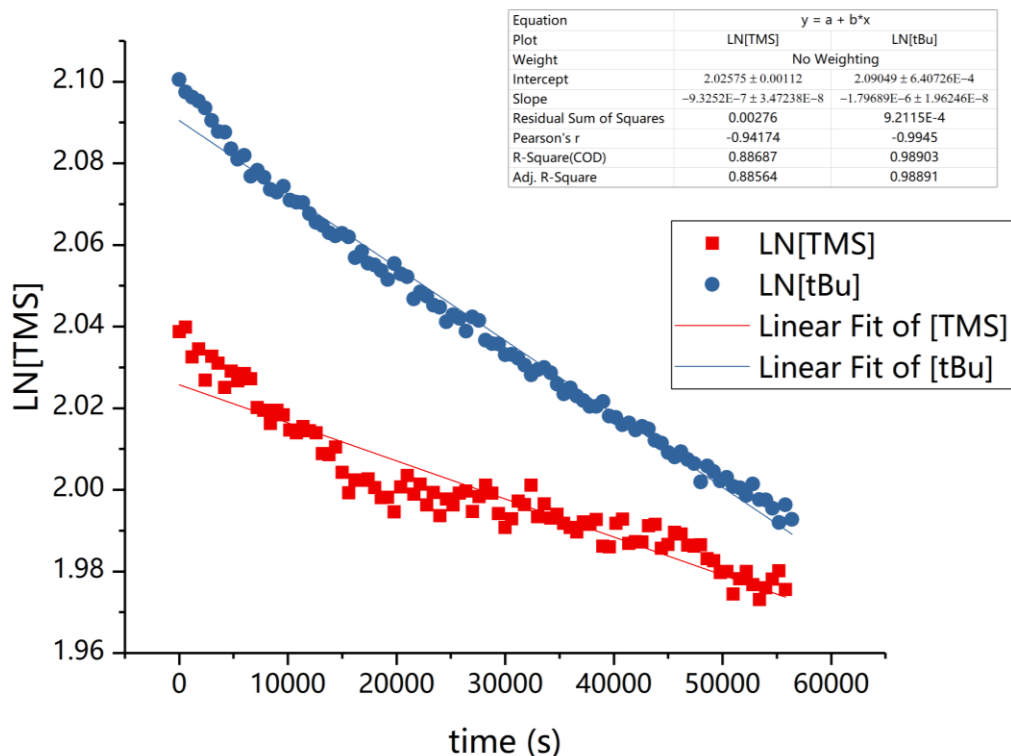


Figure 3.14 First order decay of 7 and 8 in THF

Figure 3.14. shows the best fitting for first order reaction, and the decomposition rates for **7** and **8** are $9.3 \times 10^{-7} \text{ s}^{-1}$ and $18.0 \times 10^{-7} \text{ s}^{-1}$ respectively. The linear fitting for 0 order or 2nd order reaction were less correlated. Despite the poor linear fitting, the decomposition of α -diimine alkylhydrido chromium is best described as 1st order reaction and implied that hypothesis a) is more likely. The faster decomposition rate of **7** than that of **8** is plausibly due to the beta-silicon effect via silicon hyperconjugation. It has been established that a β -silyl group can efficiently stabilize cationic carbon in organic chemistry.^{19,20,21} But no such argument has been discussed in inorganic chemistry based on literature investigation. Hypothetically, the

trimethylsilyl group stabilized the Cr(III) cation and lower the energy state of **7**. Thus the reductive elimination activation energy of **7** is slightly higher than **8**, which results in higher stability of **7**.

In conclusion, alkylation of $(^{\text{H}}\text{L}^{\text{iPr}}\text{Cr})_2(\mu\text{-H})_2$ as a new strategy of synthesizing alkyl hydrides was explored and a series of hydridoalkyl Cr complexes supported by α -diimine ligand were synthesized, namely $[(^{\text{H}}\text{L}^{\text{iPr}}\text{Cr})_2(\mu\text{-Me})(\mu\text{-H})_2][\text{Li}(\text{THF})_4]^+$ (**5**), $[(^{\text{H}}\text{L}^{\text{iPr}}\text{Cr})_2(\mu\text{-Ph})(\mu\text{-H})_2][\text{Li}(\text{THF})_4]^+$ (**6**), $[(^{\text{H}}\text{L}^{\text{iPr}}\text{Cr})_2(\mu\text{-CH}_2\text{TMS})(\mu\text{-H})_2][\text{Li}(\text{THF})_3(\text{Et}_2\text{O})]^+$ (**7**), $[(^{\text{H}}\text{L}^{\text{iPr}}\text{Cr})_2(\mu\text{-CH}_2^{\text{tBu}})(\mu\text{-H})_2][\text{Li}(\text{THF})_3(\text{Et}_2\text{O})]^+$ (**8**), $[(^{\text{H}}\text{L}^{\text{iPr}}\text{Cr})_2(\mu\text{-CH}_2\text{Ph})(\mu\text{-H})_2][\text{Li}(\text{THF})_4]^+$ (**9**), $[(^{\text{H}}\text{L}^{\text{iPr}}\text{Cr})_2(\mu\text{-Me})_2(\mu\text{-H})][\text{Li}(\text{THF})_3(\text{Et}_2\text{O})]^+$ (**10**), $[(^{\text{H}}\text{L}^{\text{iPr}}\text{Cr})_2(\mu\text{-Ph})_2(\mu\text{-H})][\text{Li}(\text{THF})]^+$ (**11**) and $(^{\text{Me,H}_2}\text{L}^{\text{iPr}}\text{Cr})(\mu\text{-CH}_2\text{TMS})(\mu\text{-H})_2$ (**12**). Those new complexes are the first examples of first row transition metal alkyl hydride complexes supported by redox noninnocent ligand. The bridging alkyl ligand shown significant impact on the stability of hydridobisalkyl chromium. And the decomposition of **7** and **8** were measured by UV-Vis spectroscopy.

3.3 Experimental

3.3.1 General Considerations

All manipulations were carried out with standard Schlenk, high vacuum line, and glovebox techniques. Pentane, diethyl ether, tetrahydrofuran, and toluene were dried by passing the solvent through activated aluminum columns followed by a nitrogen purge to remove dissolved oxygen. THF- d_8 was predried over potassium metal and stored under vacuum over Na/K. CD_2Cl_2 was predried with P_2O_5 and stored under vacuum over 4 Å molecular sieves. C_6D_6 was predried with sodium metal and

stored under vacuum over Na/K. CrCl₃ (anhydrous) and sodium metal were purchased from Strem Chemical Co.. CrCl₃(THF)₃, and diimine ligand was prepared by literature procedures. All other reagents were purchased from Aldrich or Acros and dried using standard procedures when necessary.

NMR spectra were recorded on a Bruker DRX-400 spectrometer and were referenced to the residual protons of the solvent (THF-d₈, 1.73 and 3.58 ppm; CD₂Cl₂, 5.32 ppm; CDCl₃, 7.27 ppm; C₆D₆, 7.15 ppm). FTIR spectra were taken on a Magna-IR E. S. P. 560 spectrometer. UV/vis spectra were taken on a Thermo UV-1 spectrophotometer. Mass spectral data were collected at the University of Delaware Mass Spectrometry Facility in electron ionization mode (+15eV); however no chromium containing fragments were detected for any of the complexes. Elemental analyses were performed by Robertson Microlit Laboratories Inc. (in Ledgewood, NJ). Room-temperature magnetic susceptibility (χ_m) measurements were carried out using a Johnson Matthey magnetic susceptibility balance unless otherwise stated. Molar magnetic susceptibilities were corrected for diamagnetism using Pascal constants and converted into effective magnetic moments (μ_{eff}).

3.3.2 Preparation of (H^LiPrCr)₂(μ -H)₂ (4)

(H^LiPr)Cr(CH₂TMS)(THF) (0.500 g, 0.852 mmol) was placed in an ampoule with a stir bar and 25mL diethyl ether and attached to a vacuum manifold. Three freeze-pump-thaw cycles were performed and then 1 atm of dry hydrogen was admitted to the ampoule. The remaining hydrogen and diethyl ether were removed after stirring overnight and the ampoule was brought back into the dry box, where the residue was extracted with pentane. The solution was filtered, concentrated and cooled to -30 °C to yield green crystals of 4 (0.292 g, 80 %). ¹H NMR (C₆D₆): 27.90 (4H,

CH=CH), 9.48 (12H, aromatic), 4.47 (8H, iPr), 2.17, 2.15, 0.20 (48H, iPr) ppm. IR (KBr; cm^{-1}): 3064(w), 2962 (s), 2927 (m), 2867 (m), 1627 (w), 1579 (w), 1463 (m), 1438 (m), 1382 (m), 1361 (m), 1322 (m), 1261 (m), 1222 (w), 1178 (w), 1110 (w), 1058 (w), 1041 (w), 935 (w), 883 (w), 867 (w), 798 (m), 757 (m). Anal. Calcd. for $\text{C}_{52}\text{H}_{74}\text{Cr}_2\text{N}_4$: C, 72.69; H, 8.68; N, 6.52. Found: C, 66.86; H, 7.91; N, 6.33. UV/Vis (ϵ , $\text{M}^{-1}\text{cm}^{-1}$) 426 (3124), 506 (1862), 647 (1006). $\mu_{\text{eff}}(294\text{K}) = 2.3(1) \mu_{\text{B}}$. M.p.: 158 °C. Elemental analysis consistently gave values that were significantly low in carbon and hydrogen and high in nitrogen. The exact cause is unknown, but could be due to decomposition of the complex.

3.3.3 Preparation of $[(^{\text{H}}\text{L}^{\text{iPr}}\text{Cr})_2(\mu\text{-Me})(\mu\text{-H})_2][\text{Li}(\text{THF})_4]^+$ (5)

$(^{\text{H}}\text{L}^{\text{iPr}}\text{Cr})_2(\mu\text{-H})_2$ (0.100 g, 0.116 mmol) was dissolved in mix solvent of Et_2O (10 ml) with 3 drops of THF and cooled to -30°C . LiMe (0.5 M in Et_2O , 0.232 ml, 0.116 mmol) was then added and the solution was stirred at room temp. for 10 min. The solvent was removed, and the residue was washed with pentane and extracted into THF. The THF solution was concentrated by vacuum and layered with pentane to give $[(^{\text{H}}\text{L}^{\text{iPr}}\text{Cr})_2(\mu\text{-Me})(\mu\text{-H})_2][\text{Li}(\text{THF})_4]^+$ in 63% yield. ^1H NMR (C_6D_6): 7.78 (12H, aromatic), 5.60 (4H, HC=CH), 3.39 (8H, iPr), 3.26 (THF), 1.67 (48H, iPr), 1.29 (THF) ppm. IR (KBr; cm^{-1}): 3051 (m), 2960 (s), 2928 (m), 2866 (m), 1622 (m), 1579 (m), 1460 (m), 1429 (m), 1380 (w), 1353 (w), 1245 (m), 1188 (m), 1175 (w), 1035 (m), 837 (w), 797 (m), 765 (m). UV/Vis (THF, λ_{max} , nm (ϵ , $\text{M}^{-1}\text{cm}^{-1}$)) 461 (4973), 527 (6382), 612 (6879). $\mu_{\text{eff}}(294\text{K}) = 2.9(1) \mu_{\text{B}}$. M.p.: 253 °C

3.3.4 Preparation of $[(^{\text{H}}\text{L}^{\text{iPr}}\text{Cr})_2(\mu\text{-Ph})(\mu\text{-H})_2][\text{Li}(\text{THF})_4]^+$ (6)

$(^{\text{H}}\text{L}^{\text{iPr}}\text{Cr})_2(\mu\text{-H})_2$ (0.100 g, 0.116 mmol) was dissolved in pentane (10 ml) with 3 drops of THF and cooled to -30°C . PhLi (1.8 M in Bu_2O , 0.065 ml, 0.116 mmol) was then added and the solution was stirred at room temp. for 10 min. The solvent was removed, and the residue was washed with pentane and extracted into THF. The THF solution was concentrated by vacuum and layered with pentane to give $[(^{\text{H}}\text{L}^{\text{iPr}}\text{Cr})_2(\mu\text{-Ph})(\mu\text{-H})_2][\text{Li}(\text{THF})_4]^+$ in 60% yield. ^1H NMR (THF-d_8): 7.86 (12H, aromatic), 6.70 (4H, HC=CH), 4.13 (8H, iPr), 1.19 (48H, iPr) ppm. IR (KBr; cm^{-1}): 3050 (w), 2956 (s), 2925 (m), 2867 (m), 1622 (m), 1571 (m), 1462 (m), 1435 (m), 1384 (m), 1361 (m), 1314 (m), 1252 (m), 1178 (m), 1104 (m), 1042 (m), 796 (m), 754 (m). UV/Vis (THF , λ_{max} , nm (ϵ , $\text{M}^{-1}\text{cm}^{-1}$)) 463 (5133), 530 (5981), 617 (5240). $\mu_{\text{eff}}(294\text{K}) = 3.4(1)$ μ_{B} . M.p.: 226°C

3.3.5 Preparation of $[(^{\text{H}}\text{L}^{\text{iPr}}\text{Cr})_2(\mu\text{-CH}_2\text{TMS})(\mu\text{-H})_2][\text{Li}(\text{THF})_3(\text{Et}_2\text{O})]^+$ (7)

$(^{\text{H}}\text{L}^{\text{iPr}}\text{Cr})_2(\mu\text{-H})_2$ (0.100 g, 0.116 mmol) was dissolved in pentane (10 ml) with 3 drops of THF and cooled to -30°C . $\text{LiCH}_2\text{SiMe}_3$ (0.7 M in hexane, 0.166 ml, 0.116 mmol) was then added and the solution was stirred at room temp. for 10 min. The solvent was removed, and the residue was washed with pentane and extracted into THF. The THF solution was concentrated by vacuum and layered with pentane to give $[(^{\text{H}}\text{L}^{\text{iPr}}\text{Cr})_2(\mu\text{-CH}_2\text{TMS})(\mu\text{-H})_2][\text{Li}(\text{THF})_3(\text{Et}_2\text{O})]^+$ in 70% yield. ^1H NMR (C_6D_6): 8.52 (12H, aromatic), 4.65 (4H, HC=CH), 3.55 (8H, iPr), 3.26 (THF), 1.84 (48H, iPr), 1.32 (THF), 1.10 (Et_2O) ppm. IR (KBr; cm^{-1}): 3050 (m), 2960 (s), 2927 (m), 2867 (m), 1622 (m), 1579 (m), 1462 (m), 1431 (m), 1380 (w), 1357 (w), 1240 (m), 1197 (m), 1170 (w), 1112 (m), 1034 (m), 839 (m), 796 (m), 765 (m), 695 (w). Anal. Calcd. for $\text{C}_{72}\text{H}_{116}\text{Cr}_2\text{LiN}_4\text{O}_4\text{Si}$: C, 69.7; H, 9.42; N, 4.52. Found: C, 55.88; H, 7.56; N, 5.83.

UV/Vis (THF, λ_{\max} , nm (ϵ , $M^{-1}cm^{-1}$)) 465 (5349), 527 (6334), 621 (5282). μ_{eff} (294K) = 2.1(1) μ_B . M.p.: 170 °C. Elemental analysis consistently gave values that were significantly low in carbon and hydrogen and high in nitrogen. The exact cause is unknown, but could be due to incomplete combustion of the cation/anion pair.

3.3.6 Preparation of $[(^H\text{L}^{\text{iPr}}\text{Cr})_2(\mu\text{-CH}_2^t\text{Bu})(\mu\text{-H})_2][\text{Li}(\text{THF})_3(\text{Et}_2\text{O})]^+$ (**8**)

$(^H\text{L}^{\text{iPr}}\text{Cr})_2(\mu\text{-H})_2$ (0.100 g, 0.116 mmol) was dissolved in pentane (10 ml) with 3 drops of THF and cooled to -30°C. $\text{LiCH}_2\text{CMe}_3$ (0.2 M in Et_2O , 0.580 ml, 0.116 mmol) was then added and the solution was stirred at room temp. for 10 min. The solvent was removed under vacuum, and the residue was washed with pentane and extracted into THF. The THF solution was concentrated by vacuum and layered with pentane to give $[(^H\text{L}^{\text{iPr}}\text{Cr})_2(\mu\text{-CH}_2^t\text{Bu})(\mu\text{-H})_2][\text{Li}(\text{THF})_3(\text{Et}_2\text{O})]^+$ in 60% yield. ^1H NMR (C_6D_6): 8.53 (12H, aromatic), 4.81 (4H, $\text{HC}=\text{CH}$), 3.55 (8H, iPr), 3.26 (THF), 1.81 (48H, iPr), 1.32 (THF), 1.10 (Et_2O) ppm. IR (KBr; cm^{-1}): 3050 (m), 2960 (s), 2927 (m), 2867 (m), 1622 (m), 1579 (m), 1460 (m), 1431 (m), 1380 (w), 1353 (w), 1240 (m), 1200 (m), 1171 (w), 1112 (m), 1035 (m), 839 (m), 797 (m), 765 (m), 695 (w). UV/Vis (THF, λ_{\max} , nm (ϵ , $M^{-1}cm^{-1}$)) 470 (4612), 534 (6149), 614 (5167). μ_{eff} (294K) = 3.1(1) μ_B . M.p.: 143 °C.

3.3.7 Preparation of $[(^H\text{L}^{\text{iPr}}\text{Cr})_2(\mu\text{-CH}_2\text{Ph})(\mu\text{-H})_2][\text{Li}(\text{THF})_4]^+$ (**9**)

$(^H\text{L}^{\text{iPr}}\text{Cr})_2(\mu\text{-H})_2$ (0.100 g, 0.116 mmol) was dissolved in mix solvent of pentane (10 ml) with 3 drops of THF and cooled to -30°C. LiCH_2Ph (0.5 M in Et_2O , 0.232 ml, 0.116 mmol) was then added and the solution was stirred at room temp. for 10 min. The solvent was removed, and the residue was washed with pentane and extracted into THF. The THF solution was concentrated by vacuum and layered with

pentane to give $[(^{\text{H}}\text{L}^{\text{iPr}})\text{Cr}_2(\mu\text{-Bz})(\mu\text{-H})_2]^{-}\text{Li}^+(\text{THF})_4$ in 65% yield. ^1H NMR (C_6D_6): 8.21 (12H, aromatic), 5.34 (4H, HC=CH), 3.53 (8H, iPr), 3.26 (THF), 1.75 (48H, iPr), 1.32 (THF) ppm. IR (KBr; cm^{-1}): 3050 (w), 2954 (s), 2925 (m), 2866 (m), 1624 (m), 1570 (m), 1465 (m), 1433 (m), 1384 (m), 1360 (m), 1314 (m), 1256 (m), 1178 (m), 1105 (m), 1042 (m), 796 (m), 754 (m). Anal. Calcd. for $\text{C}_{76}\text{H}_{111}\text{Cr}_2\text{Li}_4\text{O}_4$: C, 72.7; H, 8.91; N, 4.46. Found: C, 60.24; H, 7.33; N, 5.17. UV/Vis (THF, λ_{max} , nm (ϵ , $\text{M}^{-1}\text{cm}^{-1}$)) 470 (4583), 528 (5743), 617 (4858). $\mu_{\text{eff}}(294\text{K}) = 2.5(1) \mu_{\text{B}}$. M.p.: 163 °C. Elemental analysis consistently gave values that were significantly low in carbon and hydrogen and high in nitrogen. The exact cause is unknown, but could be due to incomplete combustion of the cation/anion pair.

3.3.8 Preparation of $[(^{\text{H}}\text{L}^{\text{iPr}}\text{Cr})_2(\mu\text{-Me})_2(\mu\text{-H})]^{-}[\text{Li}(\text{THF})_3(\text{Et}_2\text{O})]^{+}$ (10)

$(^{\text{H}}\text{L}^{\text{iPr}}\text{Cr})_2(\mu\text{-H})_2$ (0.100 g, 0.116 mmol) was dissolved in THF (10 ml) and cooled to -30°C . LiMe (0.5 M in Et_2O , 0.464 ml, 0.232 mmol) was then added and the solution was stirred at room temp. for 10 min. The THF was removed, and the residue was washed with pentane and extracted into THF. The THF solution was concentrated by vacuum and layered with pentane to give $[(^{\text{H}}\text{L}^{\text{iPr}}\text{Cr})_2(\mu\text{-Me})_2(\mu\text{-H})]^{-}[\text{Li}(\text{THF})_3(\text{Et}_2\text{O})]^{+}$ in 40% yield. ^1H NMR (C_6D_6): 7.78 (12H, aromatic), 5.60 (4H, HC=CH), 3.39 (8H, iPr), 3.26 (THF), 1.67 (48H, iPr), 1.32 (THF) ppm. IR (KBr; cm^{-1}): 3050 (m), 2960 (s), 2927 (m), 2867 (m), 1622 (m), 1579 (m), 1460 (m), 1431 (m), 1380 (w), 1353 (w), 1245 (m), 1191 (m), 1177 (w), 1035 (m), 839 (w), 797 (m), 765 (m). UV/Vis (THF, λ_{max} , nm (ϵ , $\text{M}^{-1}\text{cm}^{-1}$)) 462 (4476), 527 (5807), 612 (5984). $\mu_{\text{eff}}(294\text{K}) = 3.1(1) \mu_{\text{B}}$. M.p.: 249 °C

3.3.9 Preparation of $[(^{\text{H}}\text{L}^{\text{iPr}}\text{Cr})_2(\mu\text{-Ph})_2(\mu\text{-H})]^{-}[\text{Li}(\text{THF})]^{+}$ (11)

$(^{\text{H}}\text{L}^{\text{iPr}}\text{Cr})_2(\mu\text{-H})_2$ (0.100 g, 0.116 mmol) was dissolved in THF (10 ml) and cooled to -30°C . PhLi (1.8 M in Bu_2O , 0.065 ml, 0.116 mmol) was then added and the solution was stirred at room temp. for 10 min. The THF was removed, and the residue was washed with pentane and extracted into THF. The THF solution was concentrated by vacuum and layered with pentane to give $[(^{\text{H}}\text{L}^{\text{iPr}}\text{Cr})_2(\mu\text{-Ph})_2(\mu\text{-H})]^{-}[\text{Li}(\text{THF})]^{+}$ in 30% yield. ^1H NMR (THF- d_8): 7.86 (8H, iPr), 6.70 (4H, HC=CH), 4.13 (12H, aromatic), 1.19 (48H, iPr) ppm. IR (KBr; cm^{-1}): 3050 (w), 2957 (s), 2927 (m), 2867 (m), 1620 (m), 1571 (m), 1462 (m), 1435 (m), 1384 (m), 1361 (m), 1314 (m), 1252 (m), 1178 (m), 1103 (m), 1042 (m), 796 (m), 754 (m). UV/Vis (THF, λ_{max} , nm (ϵ , $\text{M}^{-1}\text{cm}^{-1}$)) 463 (4876), 528 (5801), 617 (4873). $\mu_{\text{eff}}(294\text{K}) = 3.4(1) \mu_{\text{B}}$. M.p.: 224°C .

3.3.10 Preparation of $(^{\text{H}}\text{L}^{\text{iPr}}\text{Cr})(^{\text{Me,H}_2}\text{L}^{\text{iPr}}\text{Cr})(\mu\text{-CH}_2\text{TMS})(\mu\text{-H})_2$ (12)

$[(^{\text{H}}\text{L}^{\text{iPr}}\text{Cr})_2(\mu\text{-CH}_2\text{TMS})(\mu\text{-H})_2]^{-}[\text{Li}(\text{THF})_3(\text{Et}_2\text{O})]^{+}$ (0.050 g, 0.040 mmol) and Me_3OBF_4 (0.006 g, 0.040 mmol) were dissolved in 20 ml of THF. The mixture was allowed to stir at room temp. for 20 min. The THF was removed by vacuum and the residue was extracted by pentane. The pentane solution was concentrated and cool into -30°C to give $(^{\text{H}}\text{L}^{\text{iPr}}\text{Cr})(^{\text{Me,H}_2}\text{L}^{\text{iPr}}\text{Cr})(\mu\text{-CH}_2\text{TMS})(\mu\text{-H})_2$ in 79 % yield. ^1H NMR (C_6D_6): 21.26 (2H, $\text{H}_2\text{C-CMe}$), 9.33 (2H, HC=CH), 3.87 (4H, iPr), 1.54-1.25 (48H, iPr) ppm. IR (KBr; cm^{-1}): 3051 (m), 2962 (s), 2927 (m), 2867 (m), 1622 (m), 1579 (m), 1462 (m), 1431 (m), 1380 (w), 1356 (w), 1240 (m), 1197 (m), 1171 (w), 1112 (m), 1036 (m), 839 (m), 796 (m), 767 (m), 696 (w). UV/Vis (ϵ , $\text{M}^{-1}\text{cm}^{-1}$). $\mu_{\text{eff}}(294\text{K}) = 3.6(1) \mu_{\text{B}}$. M.p.: 155°C .

3.3.11 General considerations for X-ray diffraction

Single crystal X-ray diffraction studies were performed under the following conditions. Crystals were selected, sectioned as required, and mounted on MiTeGen™ plastic mesh with viscous oil and flash-cooled to the data collection temperature. Diffraction data were collected on a Bruker-AXS APEX CCD diffractometer with graphite-monochromated Mo-K α radiation ($\lambda=0.71073$ Å). The data-sets were treated with SADABS absorption corrections based on redundant multiscan²².

The structures were solved using direct methods and refined with full-matrix, leastsquares procedures on F^2 . Unit cell parameters were determined by sampling three different sections of the Ewald sphere. Nonhydrogen atoms were refined with anisotropic displacement parameters. Hydrogen atoms were treated as idealized contributions. Structure factors and anomalous dispersion coefficients are contained in the SHELXTL 6.12 program library²¹

3.3.12 Single crystal X-ray diffraction studies

The unit cell parameters and systematic absences in the diffraction data were consistent for space groups $P2_1/n$ for **4**; $P2_1/c$ for **6, 9, 11**; $P-1$ for **5, 7, 8**; $C222_1$ for **10** and $C2/c$ for **12**. No symmetry higher than triclinic was observed in the diffraction data for **7, 8**. Structural solution in the centrosymmetric space group options yielded chemically reasonable and computationally stable results of refinement. The data for **7** and **8** were treated with Squeeze²³ to model, as diffused contributions, the severely disordered Li(THF)₃(Et₂O) counterion in **7** and **8**. The data for **5, 6** and **12** were treated with Squeeze²² to model, as diffused contributions, the severely disordered THF solvent molecule in **5, 6** and **12**.

Table 3.11 Crystallographic data for complexes 4-12

	4 (kla0641)	5 (kla0863)	6 (kla0858)
Formula	C ₅₉ H ₈₂ Cr ₂ N ₄	C ₇₇ H ₁₂₅ ClCr ₂ Li ₂ N ₄ O ₆	C ₈₂ H ₁₂₇ Cr ₂ LiN ₄ O ₆
Formula Wt.	951.28	1356.13	1375.81
Space group	<i>P2₁/c</i>	<i>P-1</i>	<i>P2₁/n</i>
Color	Green	Blue	Purple
a, Å	13.1344(7)	15.076(2)	19.6142(3)
b, Å	14.5821(8)	16.199(2)	13.2598(2)
c, Å	14.8733(8)	18.166(3)	32.4828(5)
α, deg	90	83.567(3)	90
β, deg	97.111(1)	73.110(3)	104.267(1)
γ, deg	90	89.282(4)	90
V, Å ³	2826.7(3)	4217.4(10)	8187.6(2)
Z	2	2	4
D(calcd), g•cm ⁻³	1.118	1.066	0.999
μ(Mo Kα), mm ⁻¹	0.422	0.336	2.503 (Cu Kα)
Temp., K	200	200	200
T _{max} /T _{min}	0.746/0.628	0.745/0.667	0.754/0.542
no. data/params	5549/323	17433/844	16934/822
GOF on F ₂	1.014	1.079	0.995
R(F), % ^a	4.44	9.61	8.78
Rw(F ₂), % ^a	13.21	31.44	25.99

Table 3.11 Crystallographic data for complexes 4-12 (continued)

	7 (kla0688)	8 (kla0716)	9 (kla0727)
Formula	C ₇₂ H ₁₁₉ Cr ₂ LiN ₄ O ₄ Si	C ₇₃ H ₁₁₉ Cr ₂ LiN ₄ O ₄	C ₇₅ H ₁₁₃ Cr ₂ LiN ₄ O ₄
Formula Wt.	1243.73	1227.65	1245.63
Space group	<i>P</i> -1	<i>P</i> -1	<i>P</i> 2 ₁ / <i>n</i>
Color	Purple	Purple	Purple
a, Å	11.7897(6)	11.9078(5)	12.9493(6)
b, Å	18.0621(10)	17.2068(7)	28.9770(14)
c, Å	18.119(1)	18.4228(8)	19.8543(10)
α, deg	84.658(2)	82.262(1)	90
β, deg	78.063(2)	78.716(1)	103.160(1)
γ, deg	86.270(2)	82.763(1)	90
V, Å ³	3754.4(4)	3648.7(3)	7254.3(6)
Z	2	2	4
D(calcd), g•cm ⁻³	0.837	0.847	1.140
μ(Mo Kα), mm ⁻¹	0.333	0.326	0.348
Temp., K	200	200	200
T _{max} /T _{min}	0.746/0.690	0.746/0.701	0.746/0.680
no. data/params	17458/580	18308/599	18177/800
GOF on F ₂	1.011	1.023	1.005
R(F), % ^a	3.89	3.95	5.44
Rw(F ₂), % ^a	11.84	11.88	15.85

Table 3.11 Crystallographic data for complexes 4-12 (continued)

	10 (kla0706)	11 (kla0672)	12 (kla0731)
Formula	C ₇₀ H ₁₁₁ Cr ₂ LiN ₄ O ₄	C ₇₈ H ₁₁₅ Cr ₂ LiN ₄ O	C ₁₁₈ H ₁₈₄ Cr ₄ N ₈ O ₂ Si ₂
Formula Wt.	1183.56	1235.67	2010.90
Space group	C222 ₁	P2 ₁ /n	C2/c
Color	Purple	Purple	Brown
a, Å	15.3314(9)	13.3399(16)	39.728(3)
b, Å	21.2363(12)	24.602(3)	13.3684(10)
c, Å	1.8467(13)	23.247(3)	22.3141(16)
α, deg	90	90	90
β, deg	90	101.502(2)	103.423(2)
γ, deg	90	90	90
V, Å ³	7112.9(7)	7476.2(16)	5472.1(14)
Z	4	4	8
D(calcd), g•cm ⁻³	1.105	1.098	1.108
μ(Mo Kα), mm ⁻¹	0.351	0.334	0.434
Temp., K	200	200	200
T _{max} /T _{min}	0.746/0.678	0.746/0.677	0.746/0.670
no. data/params	8162/402	17355/776	13366/595
GOF on F ₂	1.020	1.046	1.023
R(F), % ^a	4.25	5.01	5.12
Rw(F ₂), % ^a	12.06	15.32	15.06

a Quantity minimized: $R_w(F^2) = \sum[w(F_o^2 - F_c^2)^2] / \sum[(wF_o^2)^2]^{1/2}$; $R = \sum \Delta / \sum(F_o)$, $\Delta = |(F_o - F_c)|$

REFERENCES

1. S. Murahashi, *J. Am. Chem. Soc.* **1955**, *77*, 6403-6404.
2. J. Chatt, J. M. Davidson, *J. Chem. Soc.* **1965**.
3. A. H. Janowicz, R. G. Bergman, *J. Am. Chem. Soc.* **1982**, *104*, 352-354.
4. J. K. Hoyano, W. A. G. Graham, *J. Am. Chem. Soc.* **1982**, *104*, 3723-3725.
5. (a) L. Ackermann, *Chem. Rev.* **2011**, *111*, 1315-1345; (b) P. B. Arockiam, C. Bruneau, P. H. Dixneuf, *Chem. Rev.* **2012**, *112*, 5879-5918; (c) D. A. Colby, A. S. Tsai, R. G. Bergman, J. A. Ellman, *Acc. Chem. Res.* **2012**, *45*, 814-825; (d) K. M. Engle, J. Q. Yu, *J. Org. Chem.* **2013**, *78*, 8927-8955; (e) N. Kuhl, M. N. Hopkinson, J. Wencel-Delord, F. Glorius, *Angew. Chem. Int. Ed. Engl.* **2012**, *51*, 10236-10254; (f) N. Kuhl, N. Schröder, F. Glorius, *Adv. Synth. Catal.* **2014**, *356*, 1443-1460; (g) T. W. Lyons, M. S. Sanford, *Chem. Rev.* **2010**, *110*, 1147-1169; (h) C. S. Yeung, V. M. Dong, *Chem. Rev.* **2011**, *111*, 1215-1292.
6. T. Gensch, M. N. Hopkinson, F. Glorius, J. Wencel-Delord, *Chem. Soc. Rev.* **2016**, *45*, 2900-2936.
7. J. Wencel-Delord, T. Droge, F. Liu, F. Glorius, *Chem. Soc. Rev.* **2011**, *40*, 4740-4761.
8. J. R. Hagadorn, M. J. McNevin, *Organomet.* **2003**, *22*, 609-611.
9. L. A. MacAdams, G. P. Buffone, C. D. Incarvito, J. A. Golen, A. L. Rheingold, K. H. Theopold, *Chem. Commun. (Camb.)* **2003**, 1164-1165.
10. W. H. Monillas, G. P. Yap, K. H. Theopold, *Angew. Chem. Int. Ed. Engl.* **2007**, *46*, 6692-6694.
11. A. Lennartson, M. Hakansson, S. Jagner, *Angew. Chem. Int. Ed. Engl.* **2007**, *46*, 6678-6680.
12. P. Cui, T. P. Spaniol, L. Maron, J. Okuda, *Chem. Commun. (Camb.)* **2014**, *50*, 424-426.
13. M. D. Fryzuk, D. B. Leznoff, S. J. Rettig, R. C. Thompson, *Inorg. Chem.* **1994**, *33*, 5528-5534.

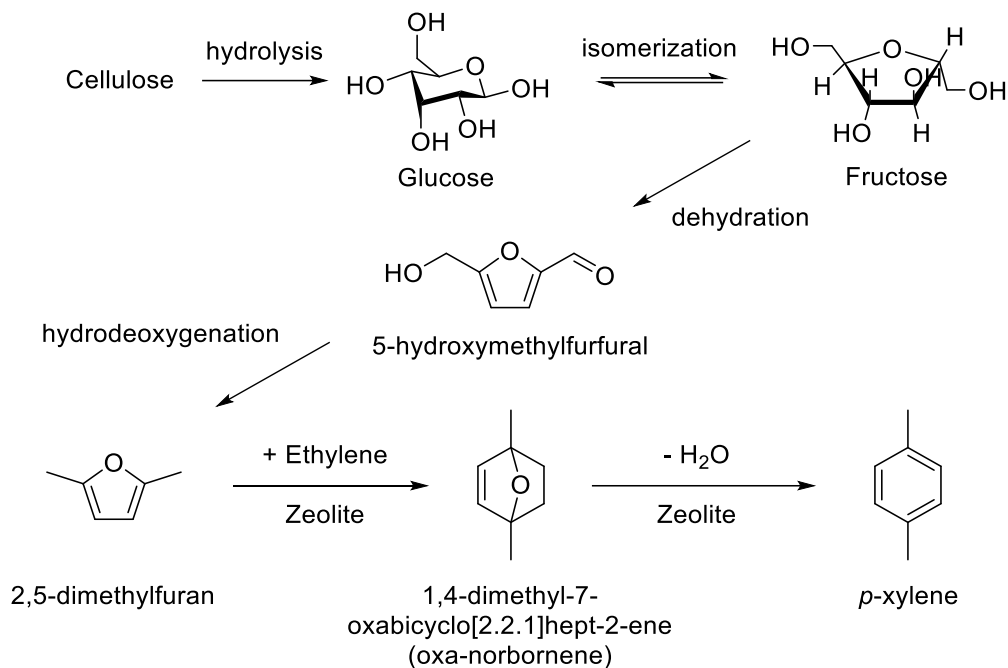
-
14. A. W. Addison, T. N. Rao, J. Reedijk, J. van Rijn, G. C. Verschoor, *J. Chem. Soc., Dalton Trans.* **1984**, 1349-1356.
 15. R. A. Heintz, R. L. Ostrander, A. L. Rheingold, K. H. Theopold, *J. Am. Chem. Soc.* **1994**, *116*, 11387-11396.
 16. K. A. Kreisel, G. P. A. Yap, K. H. Theopold, *Eur. J. Inorg. Chem.* **2012**, *2012*, 520-529.
 17. X.-J. Yang, J. Yu, Y. Liu, Y. Xie, H. F. Schaefer, Y. Liang, B. Wu, *Chem. Commun.* **2007**, 2363-2365.
 18. B. Cordero, V. Gomez, A. E. Platero-Prats, M. Reyes, J. Echeverria, E. Cremades, F. Barragan, S. Alvarez, *Dalton Trans* **2008**, 2832-2838.
 19. J. B. Lambert, G. T. Wang, R. B. Finzel, D. H. Teramura, *J. Am. Chem. Soc.* **1987**, *109*, 7838-7845.
 20. K. A. Nguyen, M. S. Gordon, G. T. Wang, J. B. Lambert, *Organomet.* **1991**, *10*, 2798-2803.
 21. S. G. Wierschke, J. Chandrasekhar, W. L. Jorgensen, *J. Am. Chem. Soc.* **1985**, *107*, 1496-1500.
 22. G. M. Sheldrick, *Acta Crystallogr. A* **2008**, *64*, 112-122.
 23. A. L. Spek, *J. Appl. Crystallogr.* **2003**, *36*, 7-13.

Chapter 4

SYNTHESIS, ISOLATION AND CHARACTERIZATION OF DIMETHYL-OXA-NORBORNENE AND CATALYSTS SEARCH FOR AROMATIZATION AND DIELAS-ALDER REACTIONS

4.1 Introduction

The worldwide consumption of polyethylene terephthalate (PET) has been increasing steadily and rapidly, while *p*-xylene (pX), as the precursor of PET, is still mainly produced from fossil fuels.¹ The annual demand of pX has reached 36 million tons in 2014 and is estimated to exceed 62 million tons by 2020.² Conventionally, xylenes are produced from petroleum refining or naphtha/gas oil cracking.^{1,3} High purity pX for PET synthesis can be obtained from the xylene rich mixture by either crystallization or adsorptive separation. This process is not only consuming fossil fuel but is also energetically costly. Due to the urgent need for sustainable production of *p*-xylene, conversion of biomass-derived 2,5-dimethylfuran and ethylene into high purity *p*-xylene has attracted much attention as one of the most promising methods (Scheme 4.1).⁴ The 2,5-dimethylfuran can be produced from lignocellulose by several steps: 1) hydrolysis of lignocellulose to glucose, 2) catalytic isomerization and dehydration of glucose to 5-hydroxymethylfurfural (HMF) and 3) catalytic hydrodeoxygenation of HMF.^{5,6} Then the biomass-derived dimethylfuran can be upgraded to pX via Diels-Alder reaction with ethylene and dehydration/aromatization.



Scheme 4.1 Process steps for dimethylfuran production from cellulose and synthesis of PX from dimethylfuran and ethylene with zeolite

Many catalysts have been developed and tested in order to promote the rate and selectivity of converting dimethylfuran and ethylene into pX.^{7-8,9,10} The CCEI has reported the use of beta-zeolite catalyst to convert 2,5-dimethylfuran and ethylene into *p*-xylene with impressive yield and selectivity. Yet, three challenges limited the application of this approach: no noticeable catalysis for cycloaddition of 2,5-dimethylfuran and ethylene;¹¹ high energy and material demands (typical condition: 500 psi ethylene pressure and 300 °C or higher reaction temperature); and decomposition of 2,5-dimethylfuran with water (as a byproduct from dehydration of 1,4-oxa-norbornene) into 2,5-diketohexa-3-ene at high temperature. Lowering the activation energy between 2,5-dimethylfuran/ethylene and 1,4-dimethyl-oxa-norbornene via catalyst promoted Diels-Alder reaction could decrease the temperature

and ethylene pressure demands and boost the reaction rate. Under milder condition, the hydrolysis of 2,5-dimethylfuran might also be less of a problem. Thus, finding a method of promoting Diels-Alder reaction between 2,5-dimethylfuran and ethylene would be a key toward industrialization of this process. According to computational studies, the high activation energy ($\Delta G^\ddagger_{573K} = +33$ kcal/mol) and thermodynamically up-hill ($\Delta G^0_{573K} = +2$ kcal/mol) from 2,5-dimethylfuran/ethylene to 1,4-dimethyl-oxa-norbornene challenged the test of catalysts for the Diels-Alder reaction (Figure 4.1).^{12,13} No literature has reported the experimental study of Diels-Alder reaction of dimethylfuran and ethylene, and all attempts of synthesizing the 1,4-dimethyl-oxa-norbornene directly from dimethylfuran and ethylene had failed. Thus, the synthesis of dimethyl-oxa-norbornene would be the key to enable a search for a catalyst for the retro-Diels-Alder reaction. By the principle of microscopic reversibility, such a catalyst would also facilitate the forward-Diels-Alder reaction. Even though 1,4-dimethyl-oxa-norbornene is widely accepted as the intermediate of the reaction, there is no detailed experimental study of 1,4-dimethyl-oxa-norbornene. To our surprise, while there are 949 isomers of $C_8H_{12}O$ with experimental properties found in the SciFinder database, 1,4-dimethyl-oxa-norbornene, such a simple compound, has never been synthesized or characterized before. Therefore, we decided to synthesize 1,4-dimethyl-oxa-norbornene and explore its kinetic data in detail.

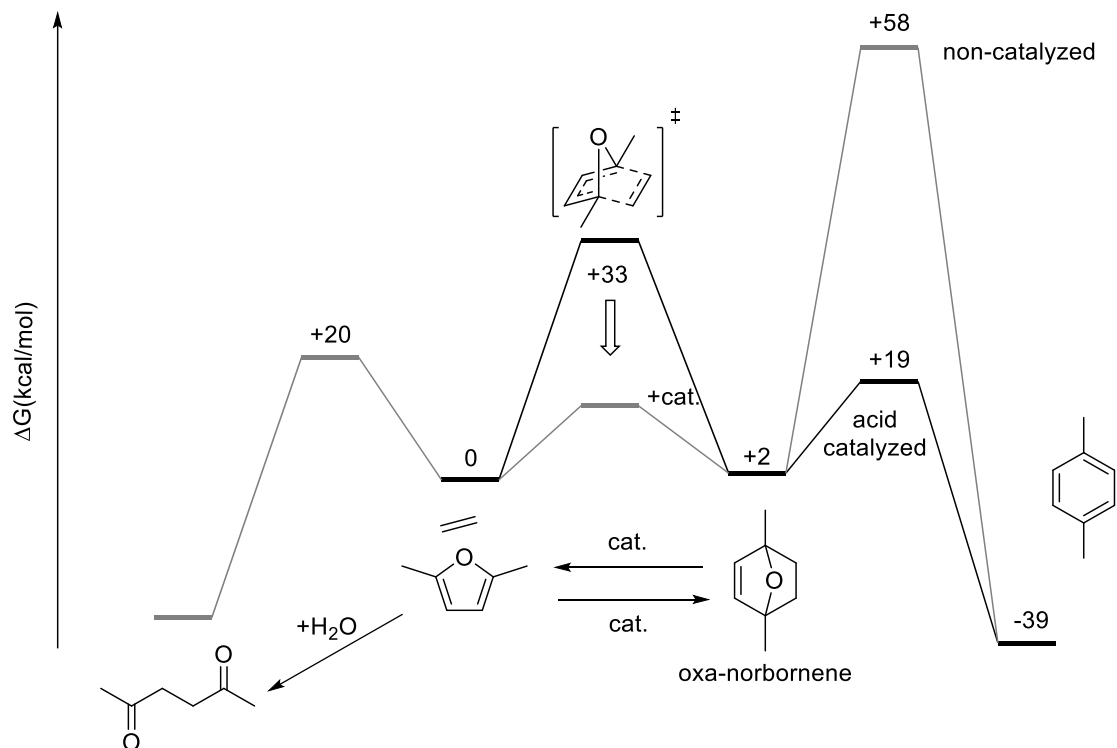


Figure 4.1 Computed free energy barriers of dimethylfuran converted to p-xylene with ethylene and to 2,5-hexanedione with water at 300 °C in H-BEA framework. All computed data are carried out calculations at the M062X/6-311+G(d,p) theory level.

4.2 Results and Discussion

There is no reliable report for the synthesis of 1,4-dimethyl-oxa-norbornene or its close analogues (only alkyl groups on 1,4-position)^{14,15,16}, and the attempts to synthesize 1,4-dimethyl-oxa-norbornene from 2,5-dimethylfuran and ethylene by heat (up to 300 °C) or/and pressure (up to 500 psi of ethylene pressure at room temperature) produced no Diels-Alder adduct.^{17,18,19} In a typical Diels-Alder reaction, the electron rich diene has a high HOMO to interact with the low LUMO of the electron deficient dienophile. In an inverse scenario, the low LUMO of the electron

poor diene and the high HOMO of the electron rich dienophile also engage in a strong interaction and facilitate the reaction (Figure 3.6).

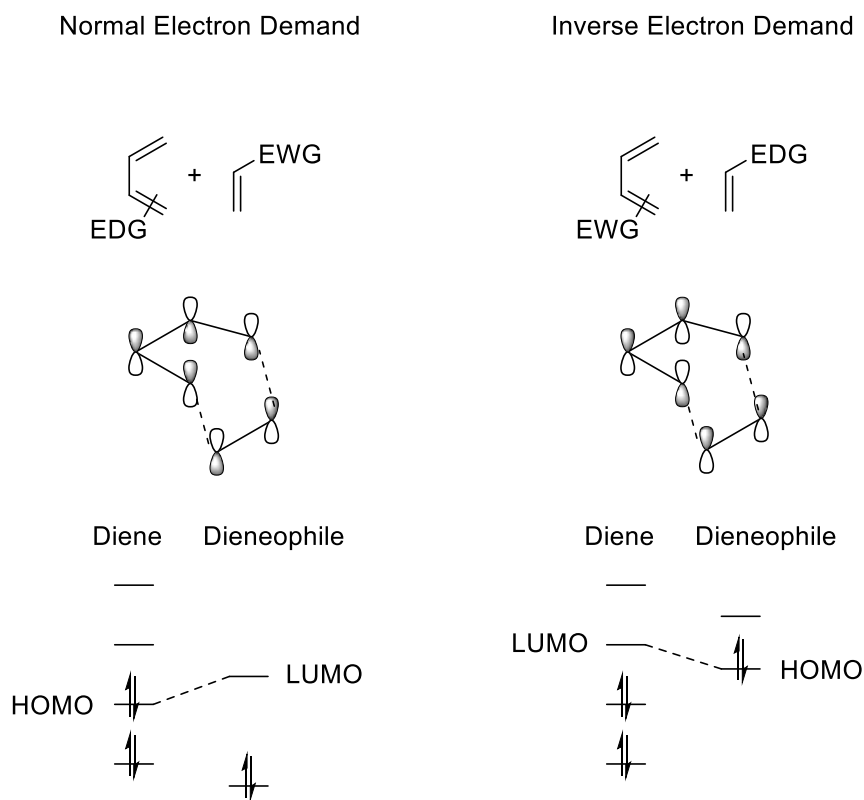
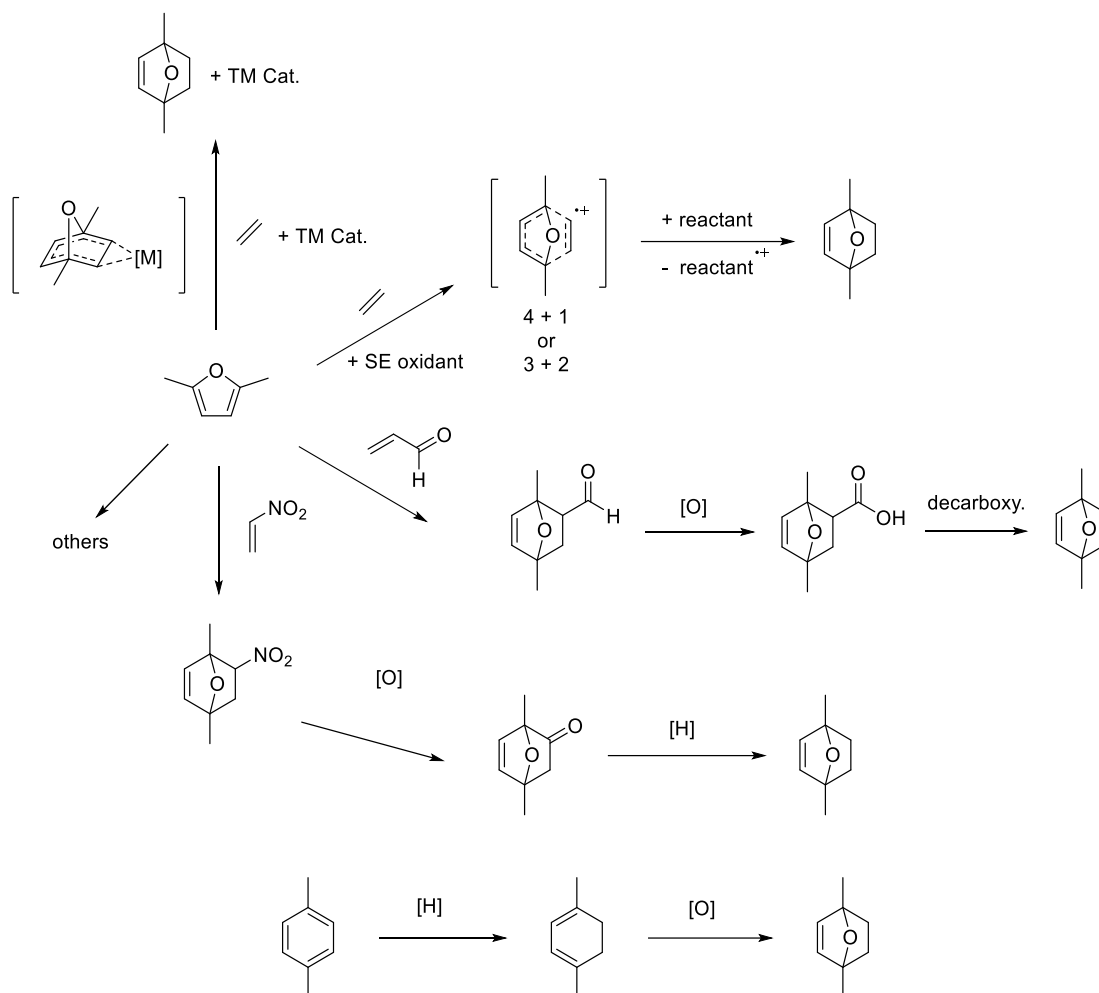


Figure 4.2 Electron demand for Diels-Alder reactions.

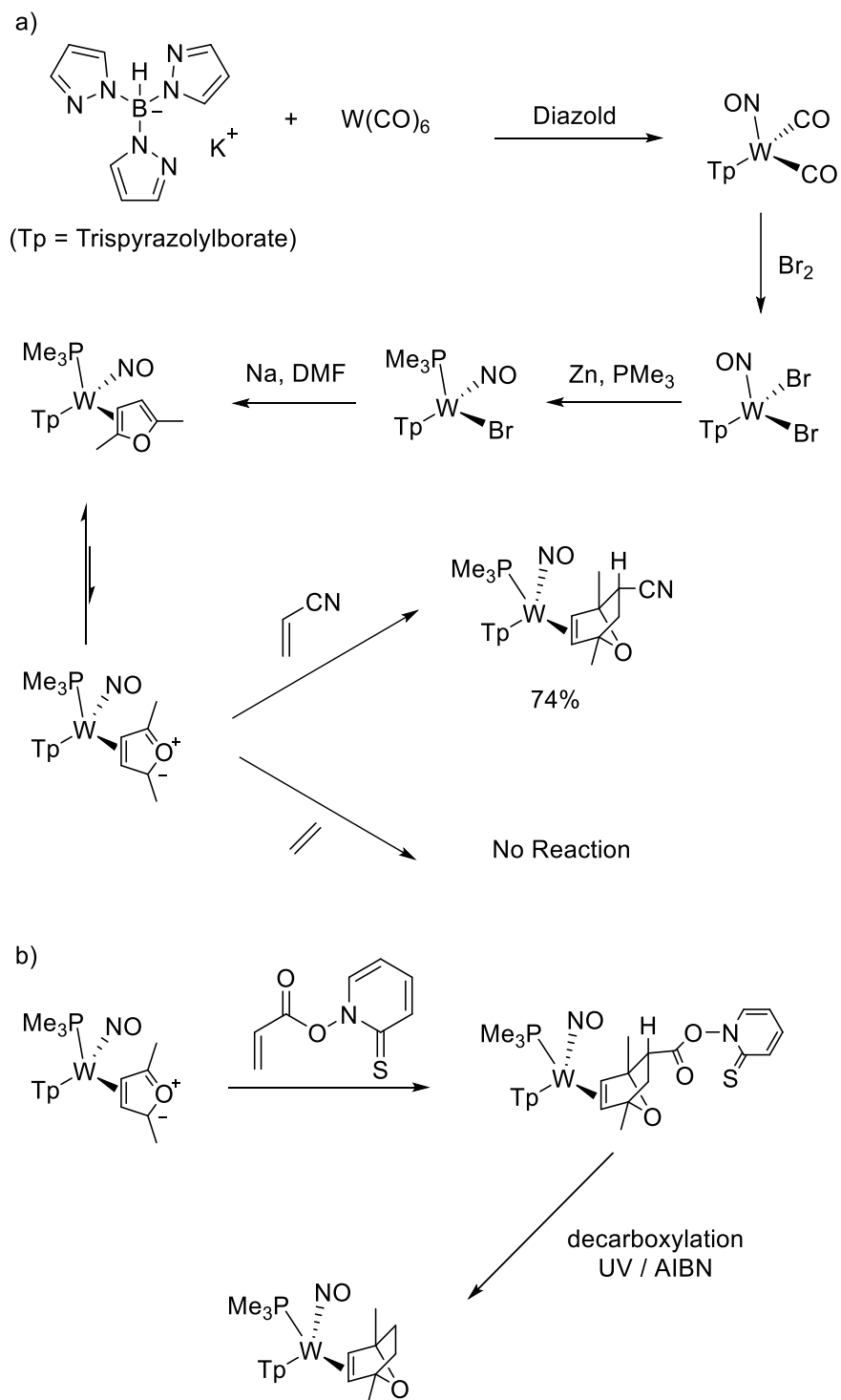
In the case of dimethylfuran and ethylene, the lack of strong electron donating or withdrawing functional groups on both components makes the cycloaddition very challenging. Since simply forcing the dimethylfuran and ethylene together did not provide the desired cycloaddition product, a new synthetic strategy was required toward this simple, yet "unknown" compound.



Scheme 4.2 Initial attempts of synthesizing dimethyl-oxa-norbornene

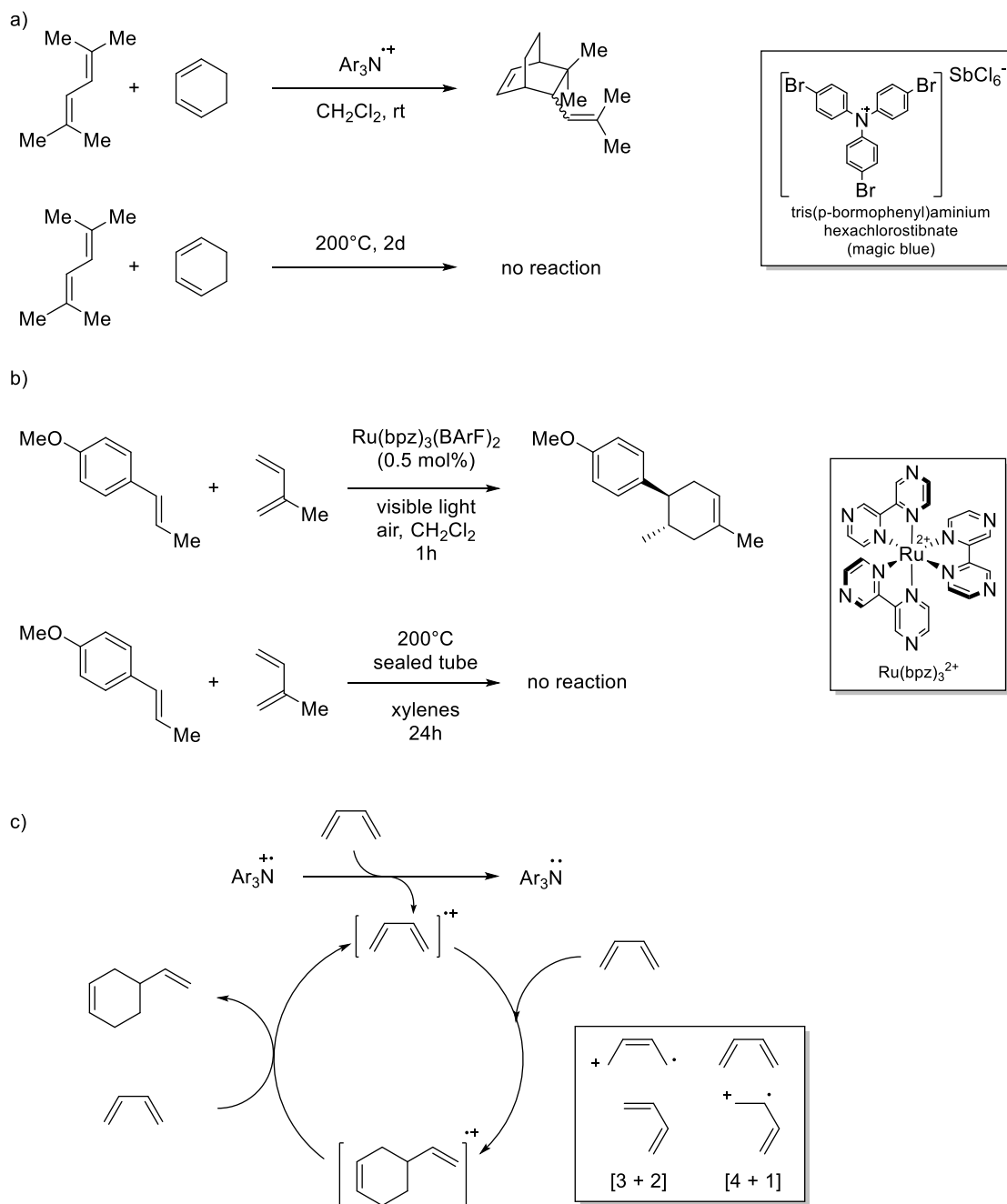
Our initial attempts included: 1) transition metal complexes catalyzed Diels-Alder reaction, 2) single electron oxidant promoted $[4+1]$ or $[3+2]$ cycloaddition, 3) Diels-Alder addition with nitro-ethylene followed by Nef reaction and reduction,²⁰ 4) epoxidation of 1,4-dimethyl-hexa-1,3-diene, and 5) decarboxylation of dimethyl-oxa-norbornene carboxylic acid precursor (Scheme 4.2).

In 2006, Harman *et al* demonstrated that $\text{TpW}(\text{PMe}_3)(\text{NO})(\text{furan})$ complex could promote the Diels-Alder reaction with various dienophile via [3+2] cycloaddition.²¹ The π -basic tungsten fragment could transfer the coordinated furan into a carbonyl ylide form through shifting of coordination site and enable the 1,3-dipolar cycloaddition with acrylonitrile (Scheme **4.3 a**). Such reaction without W complex could only obtain moderate yield (65%) under ultra-high pressure (1.5 GPa).¹⁷ $\text{TpW}(\text{PMe}_3)(\text{NO})(2,5\text{-dimethylfuran})$ was prepared by following the literature procedure and pressurized with ethylene gas to 80 psi in a Fisher tube at room temperature in CH_2Cl_2 , but no reaction was observed by $^1\text{H-NMR}$ spectroscopy (Scheme **4.3 a**). Considering that ethylene is not a good dipolarophile, an acrylic Barton ester was introduced for the [3+2] dipolar cycloaddition. We were hoping to capture the W coordinated 2,5-dimethyl-oxa-norbornene via decarboxylation of its Barton ester precursor (Scheme **4.3 b**). Unfortunately, the decarboxylation led to a complicated decomposition mixture and no desired product could be isolated. Similar ideas of utilizing ethylene coordinating complexes to promote the Diels-Alder reaction with 2,5-dimethylfuran also give no positive result.



Scheme 4.3 [3+2] Diels-Alder reaction promoted by TpW complex

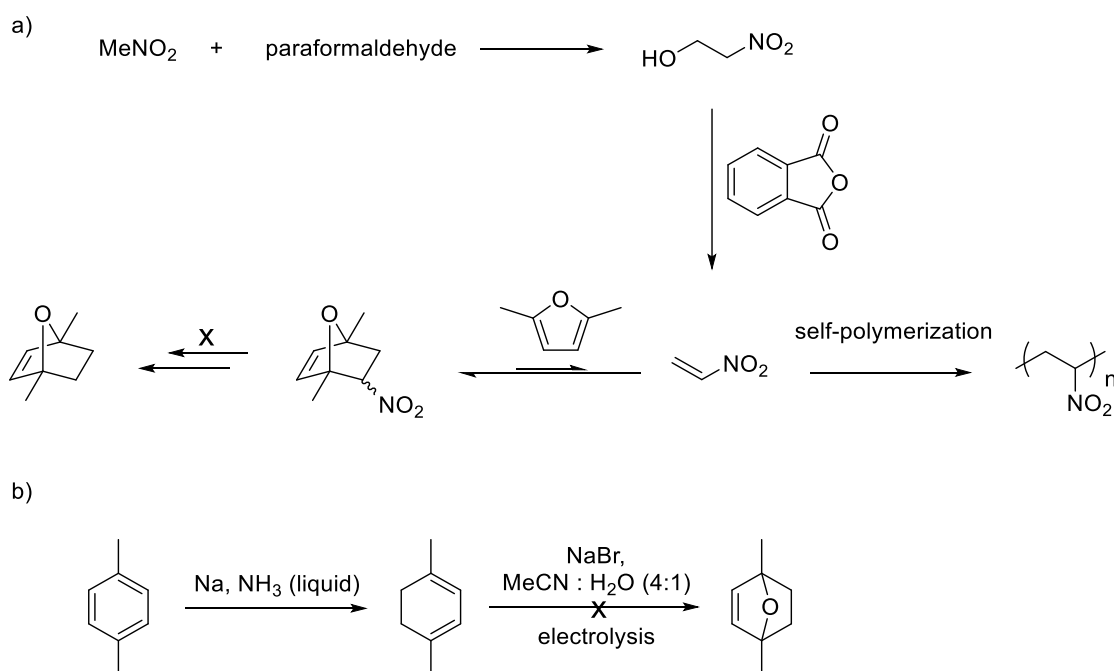
Single electron oxidation is another strategy of promoting electronically or sterically unfavored Diels-Alder reactions. In 1981 Bauld *et al.* reported that cation-radical salt tris(*p*-bromophenyl)aminium hexachlorostibnate (aka: magic blue) could promote cycloaddition of 1,3-cyclohexadiene and 2,5-dimethyl-2,4-hexadiene under mild reaction conditions (Scheme 4.4 a).²² Similar reactions could also be activated by Ru photocatalyst as reported by Tehshik Yoon *et al* in 2011 (Scheme 4.4 b).²³ In both cases, the catalyst initiated a single electron oxidation and generated a cation-radical of the diene (or dienophile), which would go through a [3+2] (or [4+1]) cycloaddition and proceed to oxidize another reactant thereafter to give a neutral Diels-Alder product (Scheme 4.4 c). Inspired by that, a test of Diels-Alder reaction between 2,5-dimethylfuran and ethylene catalyzed by magic blue was performed in CD₂Cl₂ in a sealed J-Young tube. One atmosphere of ethylene gas was introduced into the degassed CD₂Cl₂ solution of 2,5-dimethylfuran and magic blue (0.2 eq. based on 2,5-dimethylfuran). The color change of deep blue to brown indicated the consumption of aminium cation-radical. However, no cycloadduct was detected by ¹H-NMR or GCMS. In order to rule out the possible cause of poor ethylene solubility, a degassed CD₂Cl₂ solution of 2,5-dimethylfuran and magic blue (0.2 eq. based on 2,5-dimethylfuran) was pressurized with ethylene gas to 500 psi at room temperature in a Parr bomb. Only 2,5-hexadione, as the hydrolysis product of 2,5-dimethylfuran, was produced in the reaction. The water might come from moisture in the air due to the handling of the Parr bomb in fume hood.



Scheme 4.4 Examples of cation-radical catalyzed Diels-Alder reactions

Nitroethylene, as a strong dienophile, was prepared and reacted with 2,5-dimethylfuran. With the strong electron withdrawing ability of nitro group, the Diels-Alder reaction of 2,5-dimethylfuran and nitroethylene is rapid and efficient (Scheme 4.5 a). Unfortunately, the strong electron withdrawing nitro group also facilitated the retro-Diels-Alder reaction. The self-polymerization of nitroethylene even drove the equilibrium further toward the retro-Diels-Alder products. The instability of 1,4-dimethyl-2-nitro-oxa-norbornene prohibits the following reactions as planned. In most cases, only decomposition compounds were detected.

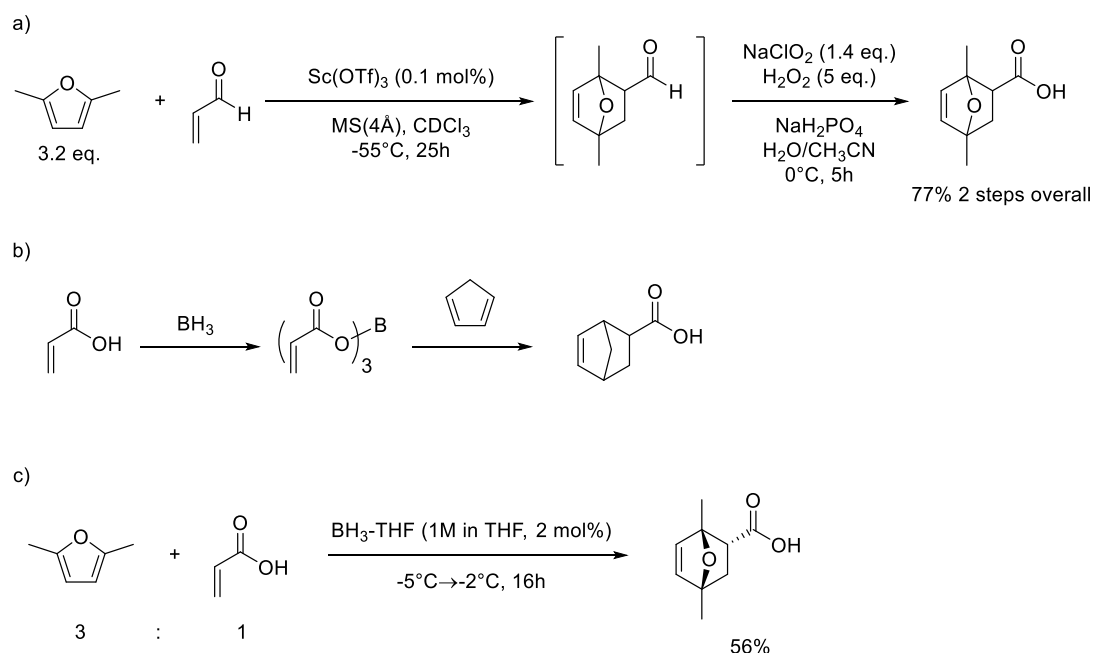
Epoxidation of 1,4-dimethylhexa-1,3-diene was also repeated with the same method reported by Maria Medeiros *et al* (Scheme 4.5 b). But no 1,4-epoxide compound was observed by $^1\text{H-NMR}$.



Scheme 4.5 Synthesis plans of 2,5-dimethyl-oxa-norbornene via nitroethylene and epoxidation

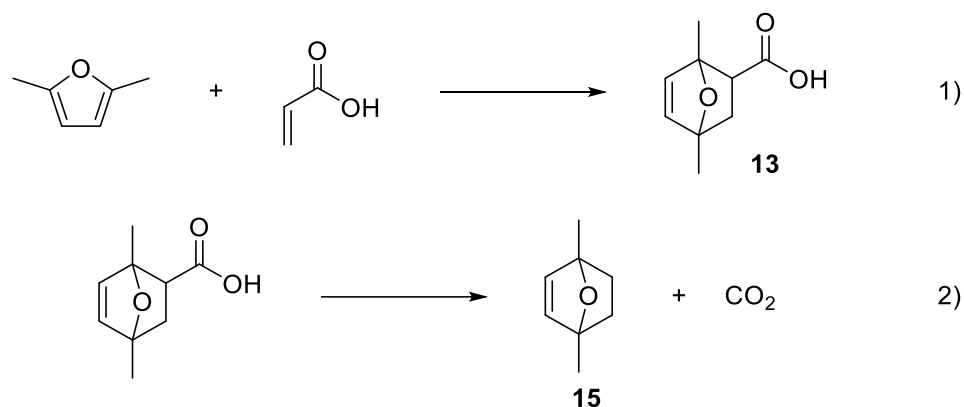
In 2011, Dean Toste *et al* reported a synthesis route of pX from 2,5-dimethylfuran involving a 2,5-dimethyl-oxa-norbornene carboxylic acid precursor (Scheme 4.6 a).²⁴ Presumably, the 2,5-dimethyl-oxa-norbornene could be synthesized by decarboxylation of its carboxylic acid precursor. The complicated synthesis route and harsh condition of Toste's method limited the investigation of decarboxylation.

Hisashi Yamamoto reported the catalytic effect of borane for the Diels-Alder reaction of cyclopentadiene and acrylic acid in 1988 (Scheme 4.6 b).²⁵ Luckily, the tris-acrylate borate as catalyst could also react with 2,5-dimethylfuran and gave the desired 2,5-dimethyl-oxa-norbornene carboxylic acid (Scheme 4.6 c). The discovery of borane catalyzed Diels-Alder reaction with acrylic acid greatly simplified the preparation of 2,5-dimethyl-oxa-norbornene carboxylic acid and accelerated the study of its decarboxylation toward 1,4-dimethyl-oxa-norbornene.



Scheme 4.6 Preparation of 1,4-dimethyl-oxa-norbornene-5-carboxylic acid

Thus, our new synthesis strategy contained two steps: 1) Diels-Alder reaction of 2,5-dimethylfuran and acrylic acid to give endo-1,4-dimethyl-7-oxabicyclo[2,2,1]hept-5-ene-2-carboxylic acid, **13**; and 2) reductive decarboxylation of **13** to form 1,4-dimethyl-7-oxabicyclo[2,2,1]hept-2-ene, **15**. (Scheme 4.7)



Scheme 4.7 Synthetic strategy from dimethylfuran to oxa-norbornene

Compound **13** can be easily obtained via borane catalyzed Diels-Alder reaction. By adding 2 mole % of borane-THF complex to a 3:1 (mole ratio) mixture of 2,5-dimethylfuran and acrylic acid under -5°C , we can get **13** in moderate yield (56%) and high diastereo-purity (>99% endo selectivity). The retro-Diels-Alder decomposition of **13** is relatively fast at room temperature and even faster at higher temperature. This raised a severe practical problem: the conventional decarboxylation techniques, like the Barton decarboxylation, could not be applied to **13** due to the requirement for heating.^{26,27,28} In order to address the issue, we investigate the kinetics of the thermal retro-Diels-Alder reaction of **13**. The retro-Diels-Alder reactions were

carried out by heating a C_6D_6 solution (0.6 ml) of **13** with 2.6 μ L of $CHCl_3$ as internal standard in a sealed J-Young tube to prevent solvent evaporation.

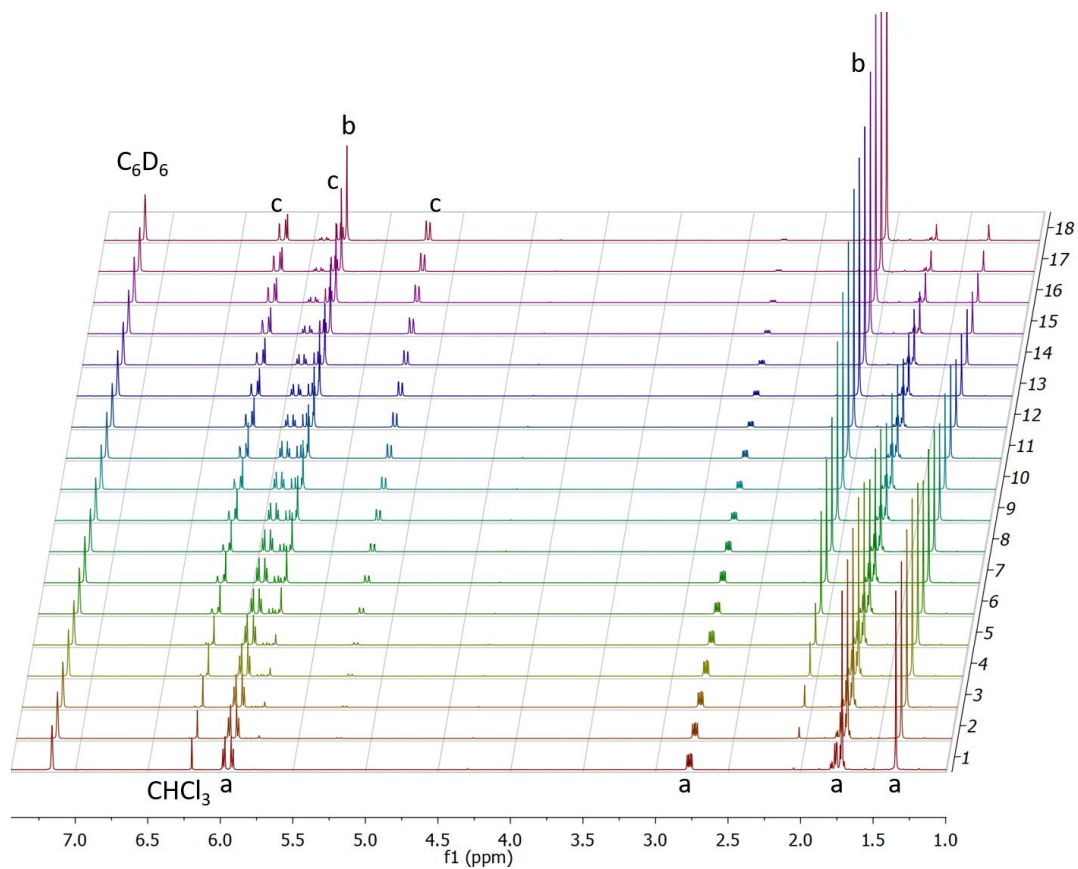


Figure 4.3 First order decay of **13** monitored by 1H -NMR at 19 °C over 172 h. The time between two spectra is not fixed. (a) denotes the chemical shifts of **13**; (b) denotes the chemical shifts of 2,5-dimethylfuran; (c) denotes the chemical shifts of acrylic acid.

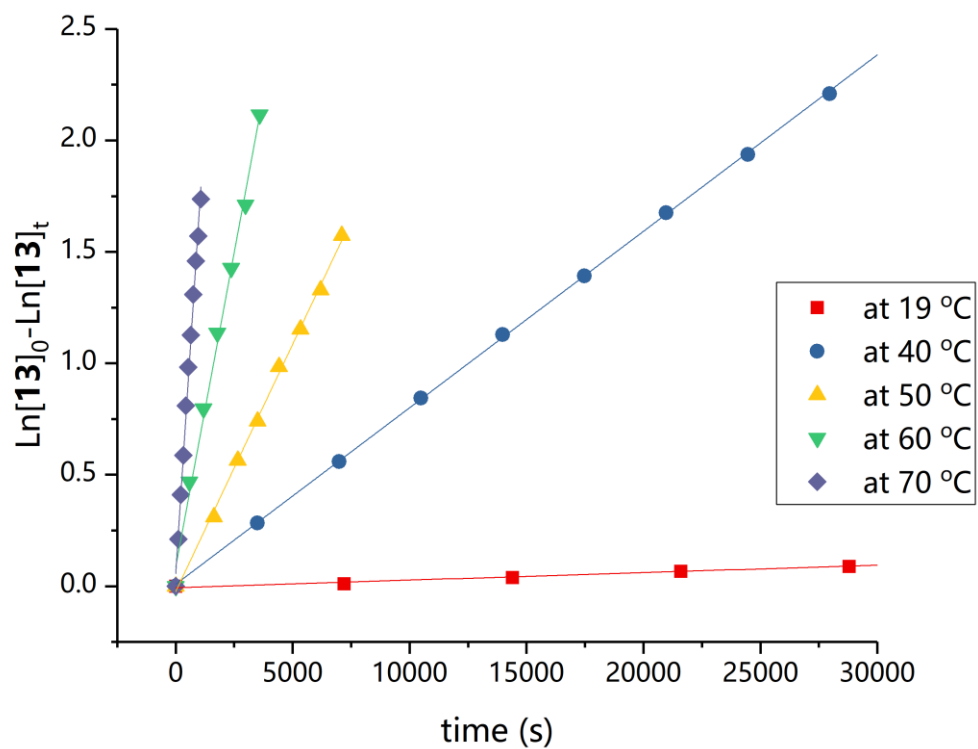


Figure 4.4 The rate measurements of thermal retro-Diels-Alder reaction of 13 at different temperature

Table 4.1 Rate constants of thermal retro-Diels-Alder reaction of 13

Equation	$\text{Ln}[13]_0 - \text{Ln}[13]_t = k t$				
Temp. (C°)	19	40	50	60	70
k ($\times 10^{-5} \text{s}^{-1}$)	0.355 ± 0.002	7.92 ± 0.04	22.19 ± 0.38	56.45 ± 1.88	161.68 ± 3.88
R^2	0.999	0.999	0.998	0.993	0.994

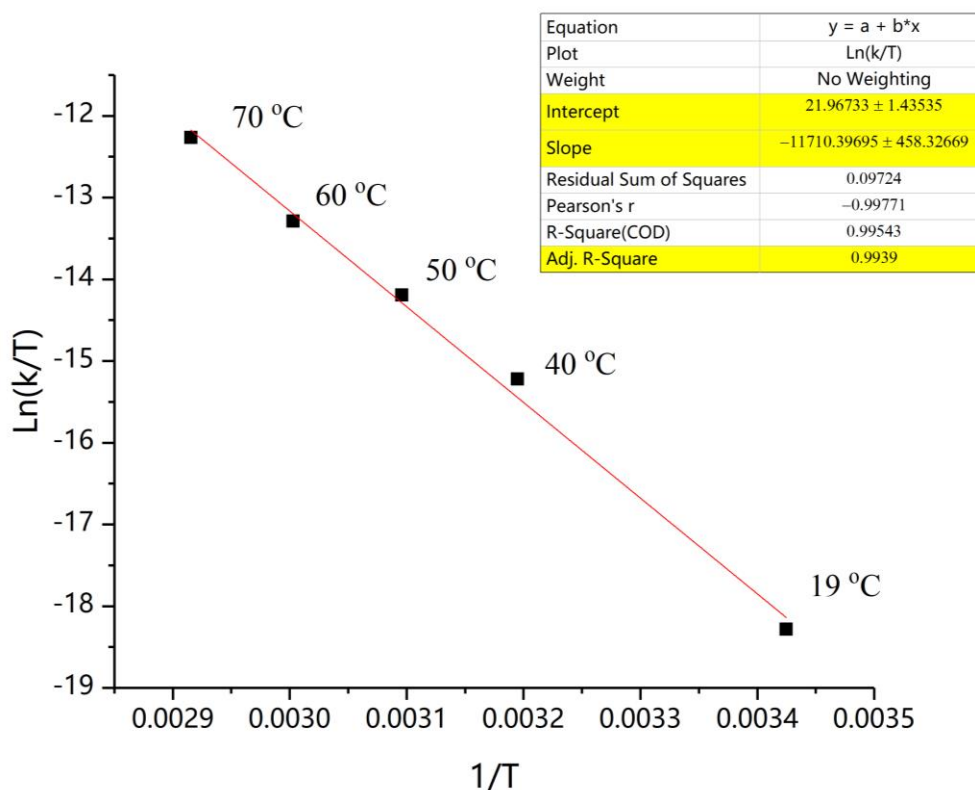


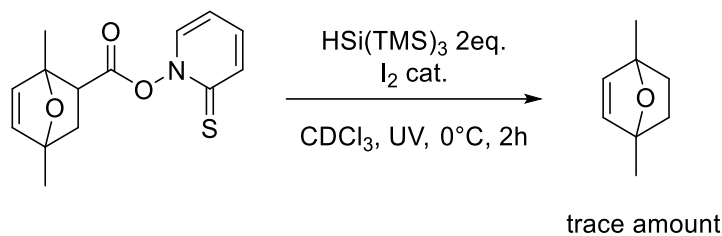
Figure 4.5 Linear fitting for Eyring equation of the first order decay of **13**

Table 4.2 Rate constants and activation parameters of thermal retro-Diels-Alder reaction of **13**

Temp. [°C]	k_{RT} [$\times 10^{-5} s^{-1}$]	$t_{1/2}$	ΔH^\ddagger [kcal mol ⁻¹]	ΔS^\ddagger [cal mol ⁻¹ K ⁻¹]	ΔG^\ddagger [kcal mol ⁻¹]
19	0.355 ± 0.002	56.6 h			24.2 ± 2.0
40	7.92 ± 0.04	2.4 h			24.3 ± 2.0
50	22.19 ± 0.38	52.1 min	23.2 ± 0.9	-3.6 ± 2.9	24.4 ± 2.0
60	56.45 ± 1.88	20.5 min			24.4 ± 2.0
70	161.68 ± 3.88	7.1 min			24.4 ± 2.0

The first-order decay of **13** in C₆D₆ monitored by ¹H-NMR spectroscopy at different temperatures is presented in Figure 4.4, and the rate constants (k), half-lives ($t_{1/2}$), and activation parameters (ΔG^\ddagger , ΔH^\ddagger , ΔS^\ddagger) at various temperatures were

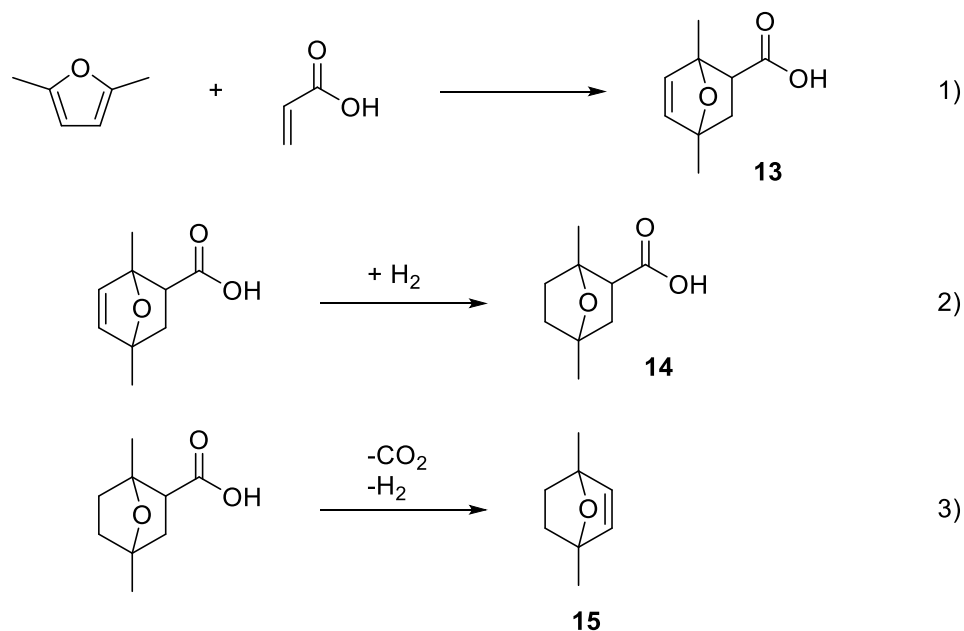
determined (Figure 4.5 and Table 4.2). Based on the ΔH^\ddagger and ΔS^\ddagger obtained from the kinetic investigation, a suitable temperature for decarboxylation of **13** should be lower than 15°C. Thus, several unconventional methods were tested on compound **13**.^{29,30,31} But only trace amounts of 1,4-dimethyl-oxa-norbornene were detected by ¹H-NMR from an optimized Barton decarboxylation: low-temperature decarboxylation of Barton-ester of **13** initiated by UV-light (256 nm) (Scheme 4.8). The corresponding ¹H-NMR chemical shifts were very close to those of authentic 1,4-dimethyl-oxa-norbornene, which was synthesized later.



Scheme 4.8 Barton decarboxylation of **13** initiated by UV-light

The complicated mixture of crude products involving unreacted chemicals and many by-products raised significant questions regarding the isolation of the desired product, **15**. Due to the limited choices of decarboxylation techniques and the difficulty of purification, we considered to solve the problem of the retro-Diels-Alder decomposition via hydrogenation of **13** to a much more stable 1,4-dimethyl-oxa-norbornane-2-carboxylic acid, **14**. Therefore, we proposed an alternative strategy: 1) Diels-Alder reaction of 2,5-dimethylfuran and acrylic acid to construct endo-1,4-dimethyl-7-oxabicyclo[2,2,1]hept-5-ene-2-carboxylic acid, **13**; 2) hydrogenation of **13** to give endo-1,4-dimethyl-7-oxabicyclo[2,2,1]heptane-2-carboxylic acid, **14**; 3)

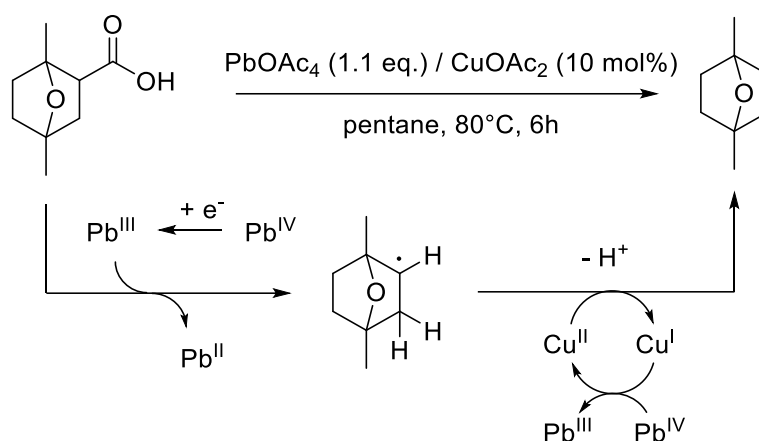
oxidative decarboxylation of **14** to form 1,4-dimethyl-7-oxabicyclo[2,2,1]hept-2-ene, **15** (Scheme 4.9).



Scheme 4.9 Alternative synthetic strategy from dimethylfuran to oxanorbornene

The hydrogenation of **13** was simply conducted by bubbling H₂ gas into the slurry of **13** and 2 mol% of palladium on activated carbon in methanol for 30 minutes. After filtration and removing solvent via vacuum, the white solid of **14** was obtained in high purity and yield (99%). Without double bond in the bicyclic ring, compound **14** is very stable and could not undergo retro-Diels-Alder dissociation at all. In order to transform **14** into 1,4-dimethyl-oxa-norbornene, an oxidative decarboxylation is required to re-form the double bond. There are only a few reported methods that can remove the carboxylic acid and give an alkene as final product.^{32,33,34,35}

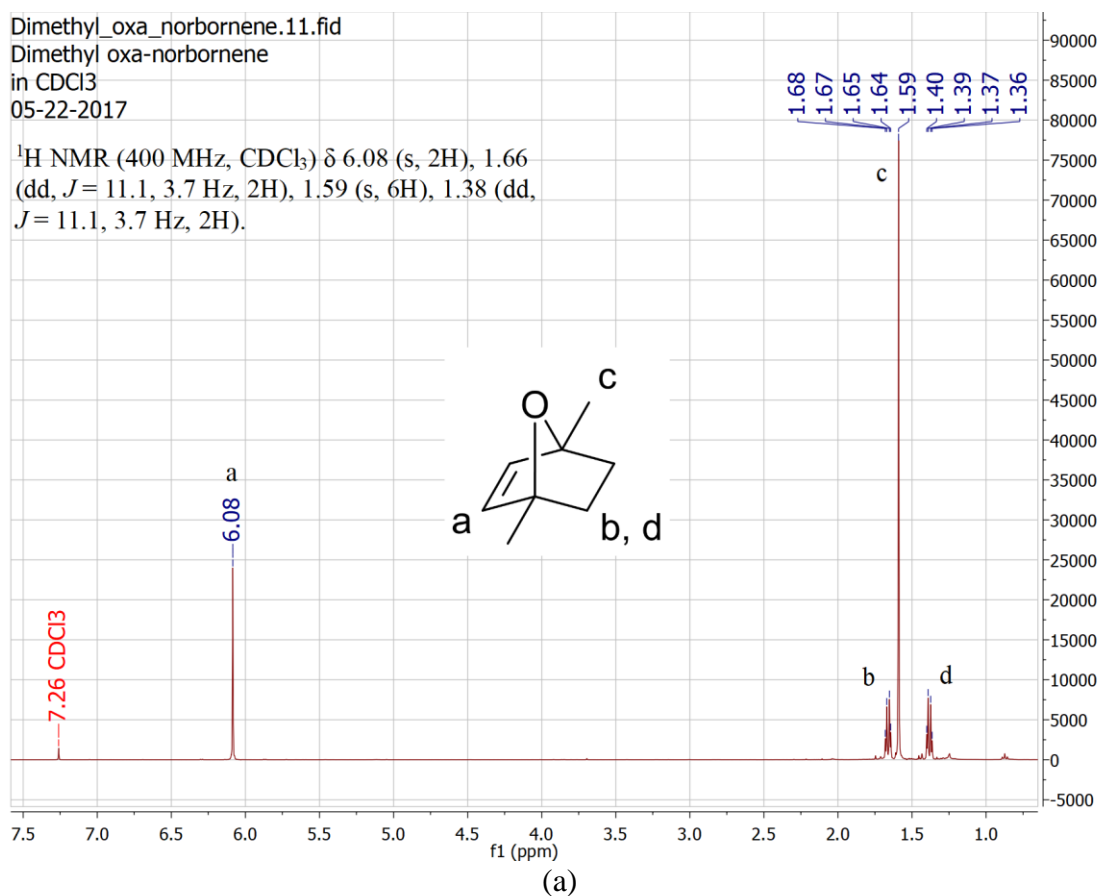
Decarboxylative halogenation followed by hydro halide elimination is one of the options. But the synthesis of dimethyl-oxa-norbornyl halide encountered the problems of low selectivity and purification difficulty. Fortunately, the oxidative decarboxylation reported by J. Kochi using Lead(IV) acetate/Copper(II) acetate combination would successfully convert **14** into **15** under mild condition in high yield (Scheme 4.10).³⁶



Scheme 4.10 Oxidative decarboxylation of 14

By heating a pentane solution of **14** with 1.1 eq. of Pb(OAc)_4 and 10 mol% of Cu(OAc)_2 to 80°C in a sealed vessel for 6 h, **15** was produced as a colorless liquid with strong odor. The resulting blue slurry was degassed and vacuum transferred into an ampule. The colorless mixture of 1,4-dimethyl-7-oxabicyclo[2,2,1]hept-2-ene, acrylic acid as by-product and pentane in the ampule was washed with 10 ml saturated NaHCO_3 (aq.) 3 times and 10 ml of DI water. The organic phase was dried over anhydrous MgSO_3 and filtered. Then the colorless mixture of 1,4-dimethyl-oxa-

norbornene (1,4-dimethyl-7-oxabicyclo[2,2,1]hept-2-ene) and pentane was gently distilled at 45°C to remove most of the pentane solvent. The residue was collected as crude product which still contains about 50 mol% of pentane. Analytically pure samples can be prepared by cooling down the mixture to -100°C and removing all the remaining pentane under high vacuum. Thus, for the first time, 1,4-dimethyl-oxa-norbornene, the intermediate of 2,5-dimethylfuran/ethylene to *p*-xylene synthesis was synthesized and isolated. Figure 4.5 shows its ¹H-NMR, ¹³C-NMR and heteronuclear single quantum correlation experiment (HSQC) spectra.



Dimethyl_oxa_norbornene.12.fid

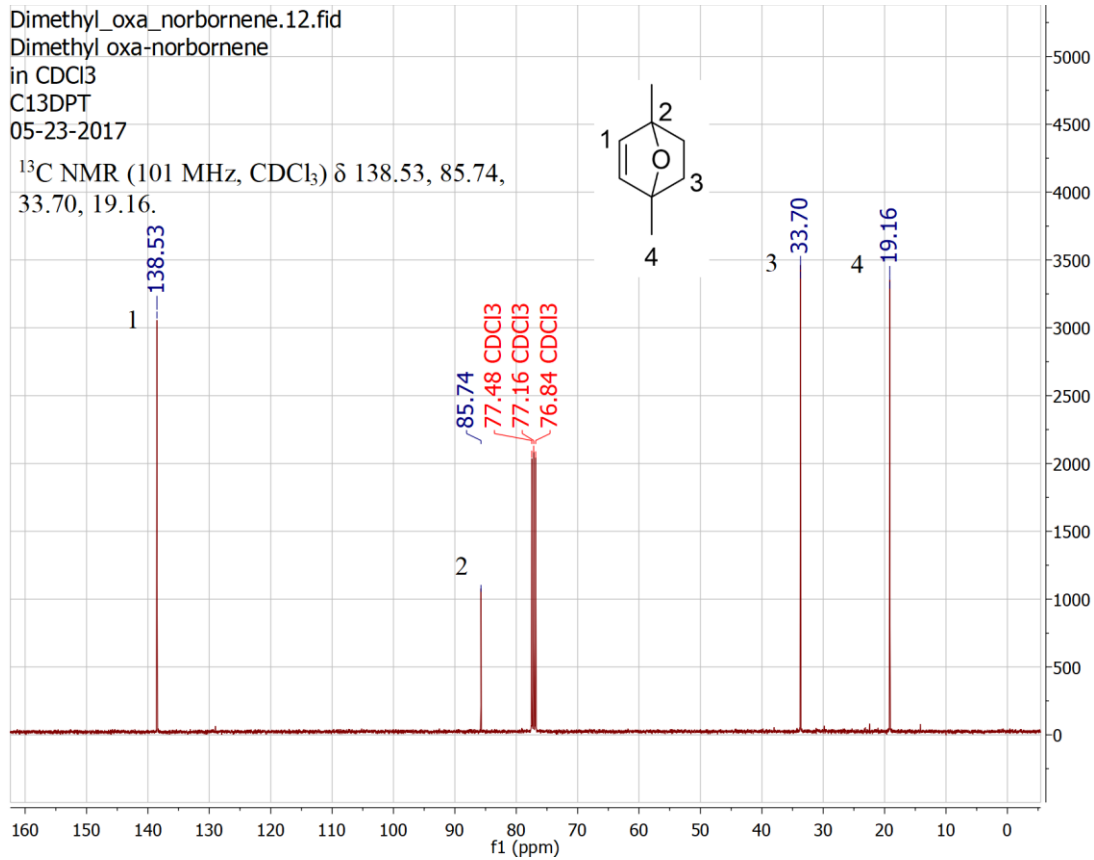
Dimethyl oxa-norbornene

in CDCl₃

C13DPT

05-23-2017

¹³C NMR (101 MHz, CDCl₃) δ 138.53, 85.74,
33.70, 19.16.



(b)

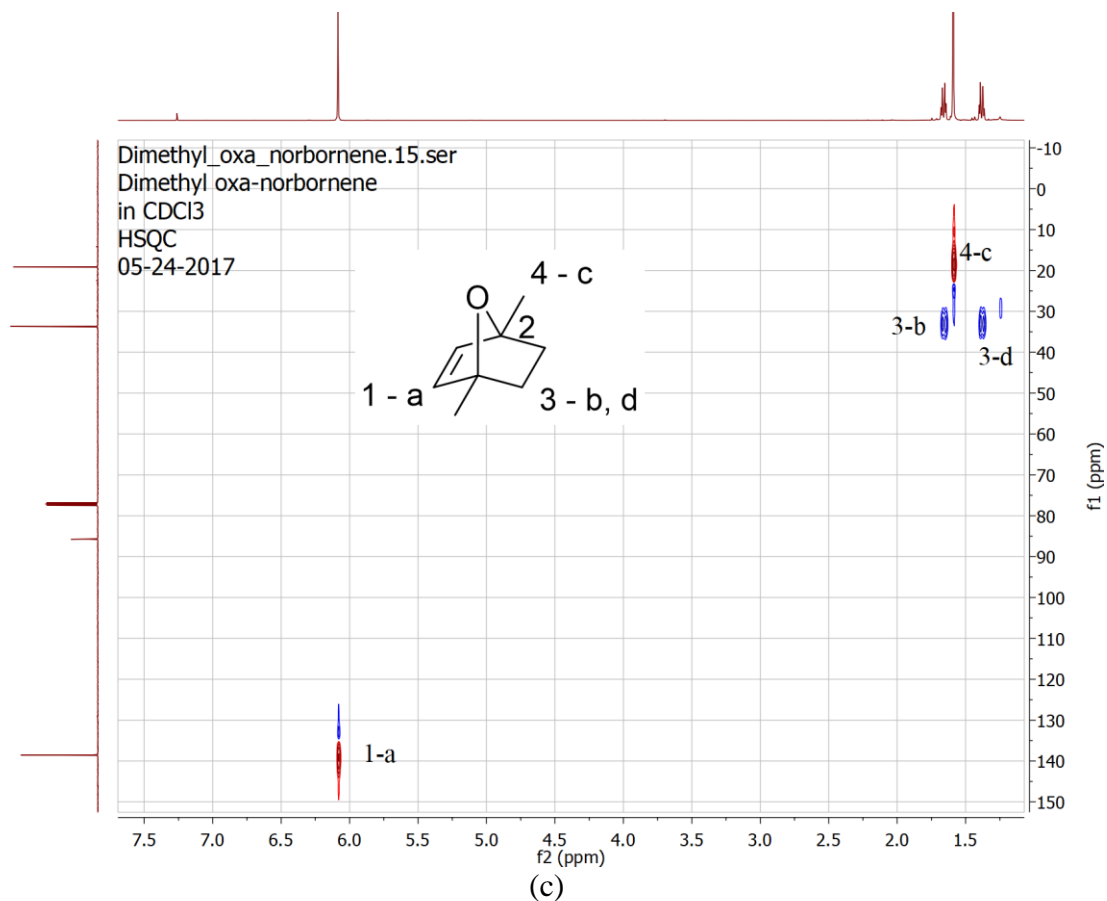
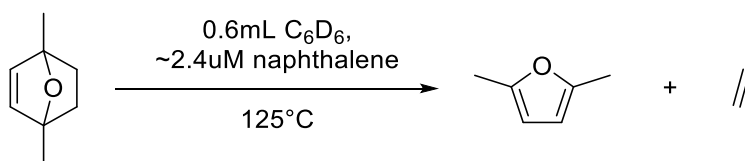


Figure 4.6 NMR spectra of **15**: (a) ^1H -NMR spectrum of **15** in CDCl_3 ; (b) ^{13}C -NMR spectrum of **15**; (c) HSQC spectrum of **15**.

Figure 4.6 shows the NMR spectra of dimethyl-oxa-norbornene in CDCl_3 . Due to its symmetry, **15** shows two singlet peaks of alkene protons at 6.08 ppm and of methyl groups at 1.59 ppm, two pairs of methylene protons give two doublets of doublets signal around 1.66 and 1.38 ppm (Figure 4.6 a). In the ^{13}C -NMR spectrum (Figure 4.6 b), only 4 peaks of 138.53, 85.74, 33.70 and 19.16 ppm show up. With the help of HSQC (heteronuclear single quantum correlation experiment) (Figure 4.6 c), those 4 peaks were signed as alkene carbon, tertiary carbon, methylene carbon and

methyl carbon. High-resolution MS (Thermo Q-Exactive Orbitrap) give a peak of 125.09593 Da for $C_8H_{13}O^+$ ($m+1$, Calculated: 125.09609 Da).

With isolated **15** in hand, we were then able to study the kinetics of its retro-Diels-Alder reaction at various temperatures. The aromatization reactions were also tested with different catalysts. The retro-Diels-Alder reaction was conducted by heating a C_6D_6 (0.6 ml) solution of **15** (~0.015 M) in a sealed and degassed J-Young tube with some naphthalene (2.5 mM) as internal standard. **15** is incredibly thermally stable and would not undergo retro-Diels-Alder decomposition until heated to 125°C or higher temperature. The first order decay of **15** in C_6D_6 was observed by 1H -NMR at 125°C, 130°C, 140°C, 145°C and 150°C (Figure 4.7 and 4.8). Its rate constants (k), half-lives ($t_{1/2}$) and activation parameters (ΔG^\ddagger , ΔH^\ddagger , ΔS^\ddagger) are shown in Table 4.4 (linear fitting for Eyring equation in Figure 4.9). The Gibbs free energy of activation at 300°C determined based on our experimental activation parameters is close to the reported DFT calculation (37.8 ± 4.1 kcal/mol vs 33 kcal/mol at 300 °C).³⁷ The large energy barrier between 2,5-dimethylfuran/ethylene and 1,4-dimethyl-oxa-norbornene is confirmed and a catalyst for the Diels-Alder reaction would be the key to make the conversion of 2,5-dimethylfuran/ethylene into pX competitive with fossil-fuel-based method.



Scheme 4.11 retro-Diels-Alder of dimethyl-oxa-norbornene

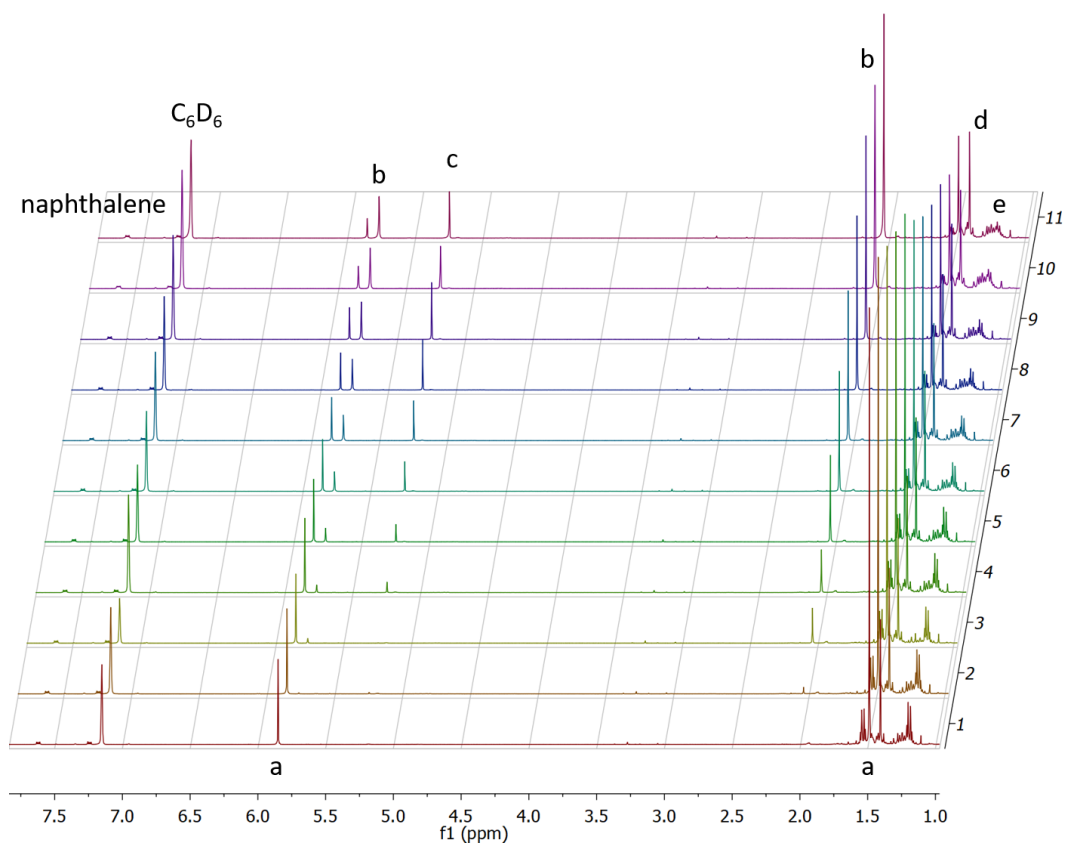


Figure 4.7 First order decay of 15 monitored by ^1H -NMR at 125 °C over 192 h. (a) denotes the chemical shifts of 15; (b) denotes the chemical shifts of 2,5-dimethylfuran; (c) denotes the chemical shifts of ethylene; (d) denotes the chemical shifts of 1,4-dimethyl-oxa-norbornane; (e) denotes the chemical shifts of pentanes

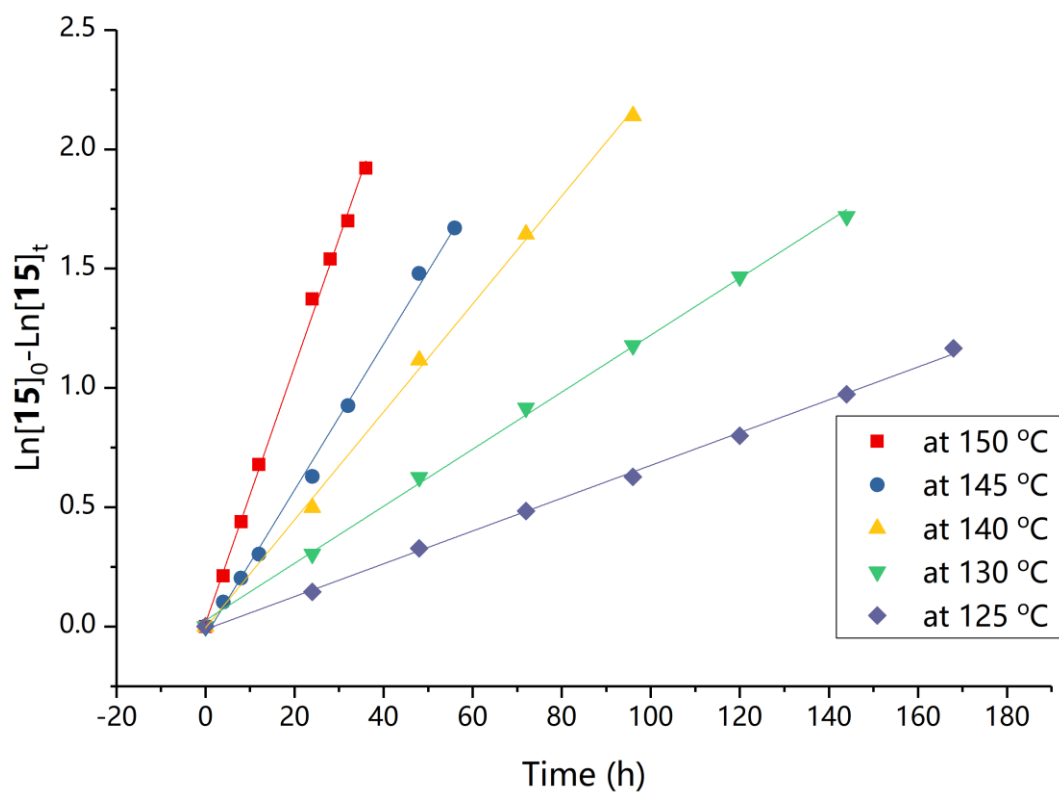


Figure 4.8 The rate measurements of thermal retro-Diels-Alder reaction of **15** at different temperature

Table 4.3 Rate constants of thermal retro-Diels-Alder reaction of **15**

Equation	$\text{Ln}[15]_0 - \text{Ln}[15]_t = k t$				
Temp. (C°)	125	130	140	145	150
k ($\times 10^{-6} \text{s}^{-1}$)	1.91 ± 0.03	3.32 ± 0.05	6.28 ± 0.13	8.49 ± 0.20	14.94 ± 0.28
R²	0.999	0.998	0.998	0.996	0.997

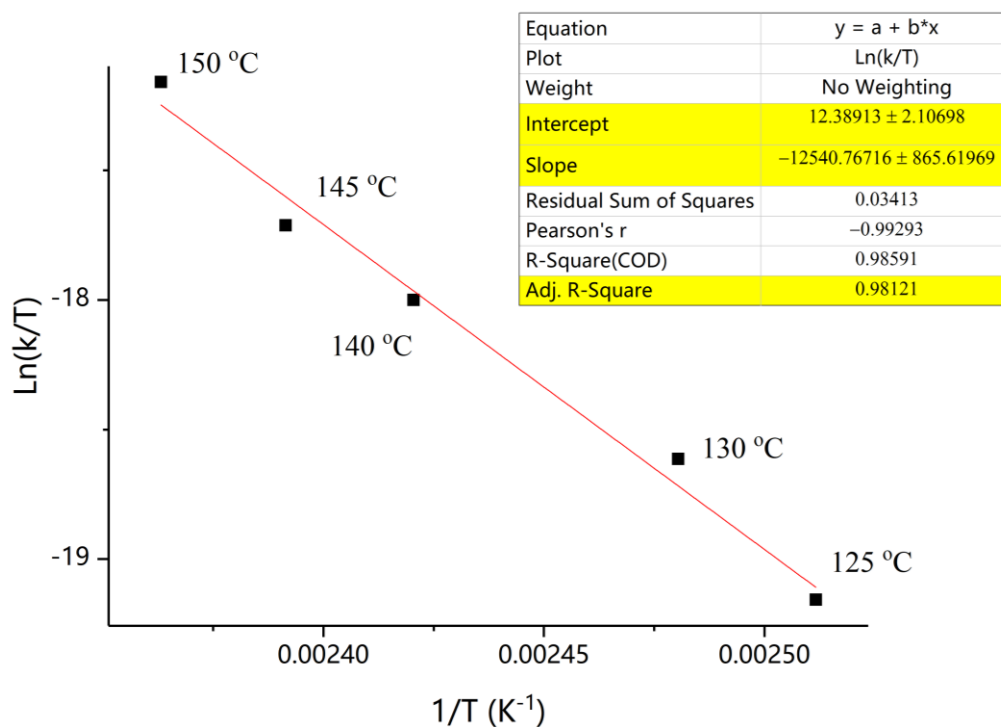


Figure 4.9 Linear fitting for Eyring equation of the first order decay of 15

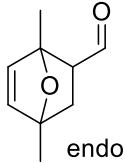
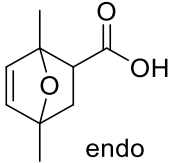
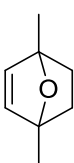
Table 4.4 Rate constants and activation parameters of thermal retro-Diels-Alder reaction of 15

Temp. [°C]	k_{RT} [$\times 10^{-6} s^{-1}$]	$t_{1/2}$	ΔH^\ddagger [kcal mol ⁻¹]	ΔS^\ddagger [cal mol ⁻¹ K ⁻¹]	ΔG^\ddagger [kcal mol ⁻¹]
125	1.91 ± 0.03	100.9 h			33.9 ± 3.4
130	3.32 ± 0.05	58.0 h			34.0 ± 3.4
140	6.28 ± 0.13	30.7 min	24.9 ± 1.7	-22.6 ± 4.2	34.2 ± 3.4
145	8.49 ± 0.20	22.7 min			34.4 ± 3.4
150	14.94 ± 0.28	12.9 min			34.5 ± 3.5

A comparison of retro-Diels-Alder kinetic data of three 1,4-dimethyloxanorbornene derivatives is shown in Table 4.5. The absence of strong electron donating or withdrawing functional group on dimethyl-oxa-norbornene lead to unbelievable stability. The half life of ketone, carboxylic acid and oxa-norbornene at room

temperature are 9.99 h, 21.7 h and over 500 years! The surprisingly high stability raises the question: what kind of catalyst is able to activate it and toward which direction (retro-Diels-Alder or aromatization)?

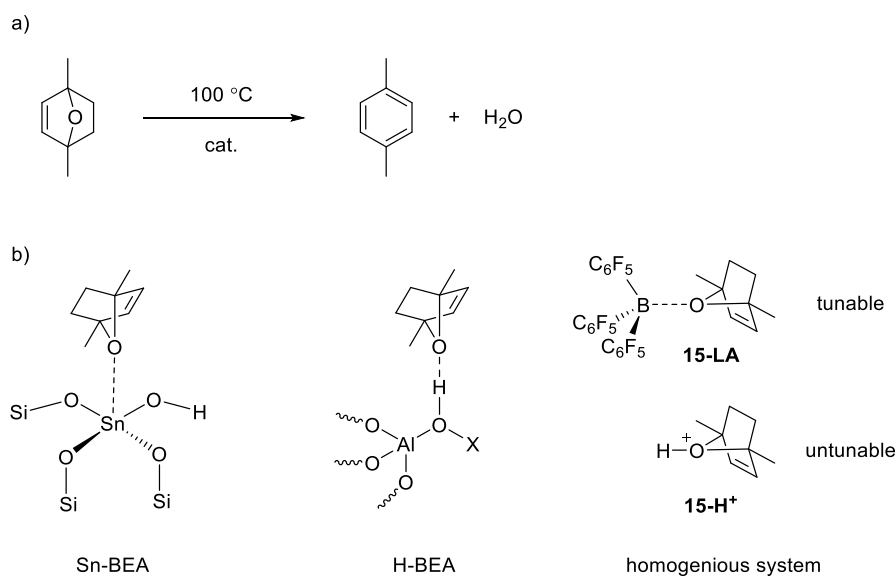
Table 4.5 Stability of three 1,4-dimethyloxa-norbornene derivatives

			
Solvent	d ₈ -Toluene*	d ₆ -Benzene	d ₆ -Benzene
k_{298K} (s⁻¹)	1.93×10 ⁻⁵ *	8.88×10 ⁻⁶	4.17×10 ⁻¹¹
ΔH[‡] (kcal/mol)	N/A	23.2 ± 0.9	24.9 ± 1.7
ΔS[‡] (cal/mol K)	N/A	-3.6 ± 2.9	-22.6 ± 4.2
ΔG[‡]_{298K} (kcal/mol)	23.87*	24.2	31.6
t_{1/2} (298K)	9.99 h*	21.7 h	4.6×10 ⁶ h

* data from reference²⁴

The aromatization by dehydration of **15** with different catalysts was also investigated by ¹H-NMR. In particular, we studied the rate constants of dehydrations of **15** with catalytic amount of tris(pentafluorophenyl)borane and trifluoroacetic acid (TFA). As the concentration of acid is constant, the observed rate, k_{obs}, equals to k[acid] and should result in a first order reaction. Thus, the reactions were monitored by ¹H-NMR of a C₆D₆ solution of **15** (~0.027 M) with acid (0.008 M) and naphthalene (2.5 mM) as internal standard. Because the Lewis acid (LA) is much more efficient than the Brønsted acid, we had to monitor the reactions at 50°C for B(C₆F₅)₃ and at

100°C for TFA. Even through there is a 50°C difference, the reaction catalyzed by borane ($k_{\text{obs}} = 9.6 \times 10^{-4} \text{ s}^{-1}$) is still about 250 times faster than that catalyzed by TFA ($k_{\text{obs}} = 3.9 \times 10^{-6} \text{ s}^{-1}$) with the same concentration of catalyst (Figure 4.11). A similar result was observed with Scandium(III) triflate, which can fully convert **15** into pX at room temperature within half an hour. Our experimental result suggest that Lewis acid is a much better catalyst for dehydration, but this goes against the result of reactions catalyzed by H-BTA and Zn-BTA.^{11,38} The differences might due to the combination of poorer accessibility of Lewis acid toward the bridging oxygen and the weaker acidity than Brønsted acid in the zeolite-catalyzed system (Scheme 4.12 b).



Scheme 4.12 Dehydration of dimethyl-oxa-norbornene and accessibility toward different catalyst.

For the dehydration of **15**, the first C-O bond cleavage was considered as the rate determining step.^{11,13,38} Thus, the reaction rate depended on the reactivity of acid

coordinated intermediate **15-LA** (Lewis acid coordinated oxa-norbornene) or **15-H⁺** (oxonium intermediate). For Lewis acid coordinated **15-LA**, the reactivity can be tuned by the acidity of Lewis acid. The more acidic (or more electron deficient) Lewis acid would result in stronger LA-O bond and weaker C-O bond and therefore promote the rate constant of Lewis-acid-catalyzed dehydration. On the contrary, the activity of oxonium intermediate **15-H⁺** could not be changed as the acidity of proton is fixed. The reaction rate would depend on the H⁺ concentration (or pH) of the reaction mixture. In conclusion, for dehydration of **15**, at least in homogeneous system, the strong Lewis acid is a much better catalyst than Brønsted-acid.

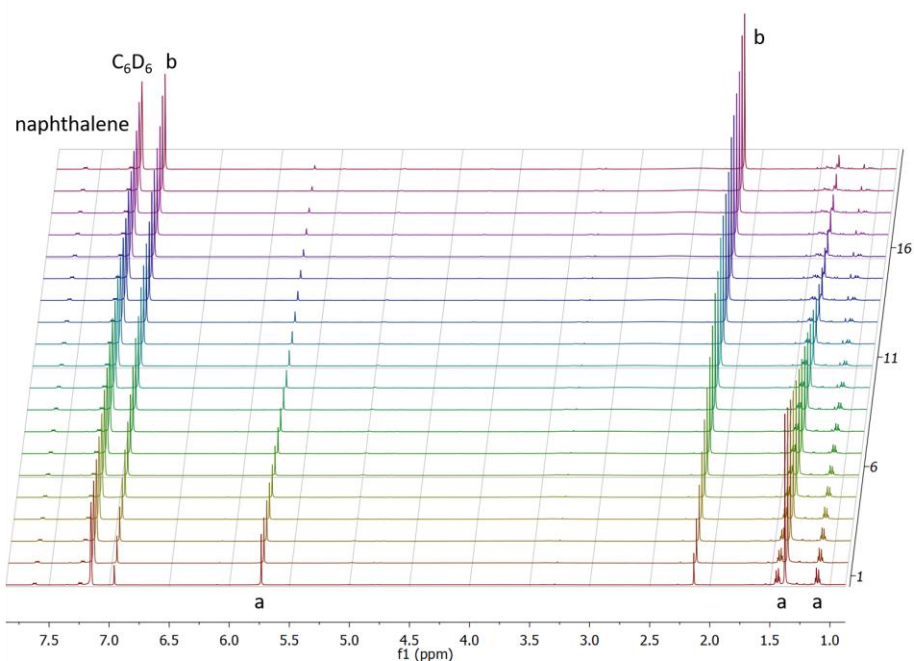


Figure 4.10 First order dehydration of **15** (0.024 M) with $\text{B}(\text{C}_6\text{F}_5)_3$ (0.008 M) acid catalyst monitored by ^1H -NMR at 45 °C over 40 min. (a) denotes the chemical shifts of **15**; (b) denotes the chemical shifts of **pX**.

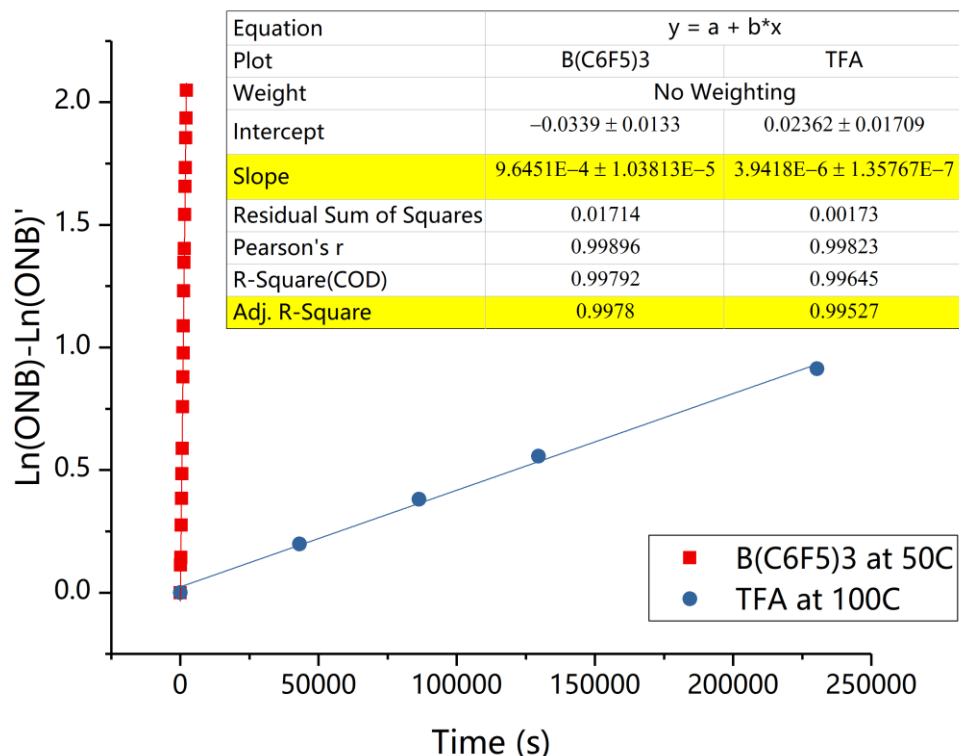


Figure 4.11 First order dehydration of **15 catalyzed by TFA and B(C₆F₅)₃.**

Moreover, a series of potential catalysts were tested for retro-Diels-Alder reaction. The selection of potential catalysts is based on several of our previous hypothesis: 1) retro-Diels-Alder reaction promoted by Lewis acid coordination; 2) Transition metal coordination to enable retro-Diels-Alder; 3) [3+2] or [4+1] Style retro-Diels-Alder via single electron oxidation. The first hypothesis of changing electronic structure of dimethyl-oxa-norbornene with Lewis acid was found unreliable soon after the aromatization activity test of **15**. A catalytic amount (~ 10 mol%.) of Cu(OTf)₂, AgOTf and Sc(OTf)₃ were added into a C₆D₆ solution of **15** with naphthalene as internal standard, and the reaction was monitored by ¹H-NMR at

100°C in a sealed J-Young tube. As we learned from the thermal stability test, no uncatalyzed retro-Diels-Alder or dehydration reaction occurs at 100°C. The metal triflates can transform dimethyl-oxa-norbornene into p-xylene rapidly and completely at 100°C and Sc(OTf)₃, as the strongest Lewis acid, can effect the dehydration at room temperature within 30 min. Presumably, the strong interaction between Lewis acidic metal and oxygen greatly accelerates dehydration/aromatization reaction and leaves no opportunity to examine the retro-Diels-Alder reaction.

As shown in Scheme 4.3, the π -basic tungsten metal fragment of TpW(NO)(PMe₃) can promote the [3+2] addition of 2,5-dimethylfuran with various alkenes by disrupting the aromatic stabilization of the heterocycle. And complexes like W(CO)₆ and Mo(CO)₆ are well known of their affinity to norbornene double bond.³⁹ Inspired by that, a series of transition metal complexes were tested for retro-Diels-Alder of **15**. In the tests of Pd/C, Rh₄(CO)₁₂, AgNO₂ and Pt(PPh₃)₄, weakening the metal-oxygen interaction indeed stopped the aromatization toward p-xylene, but no further reaction was observed either. With PdCl₂ and RhCl(PPh₃)₃, only small portion of dimethyl-oxa-norbornene was converted into pX and no retro-Diels-Alder product was observed. W(CO)₆ and Mo(CO)₆ did show strongest interaction with **15**, but the reaction went toward aromatization.

Single electron oxidation is an useful strategy of promoting electronically or sterically unfavorable Diels-Alder reactions as shown in Scheme 4.4. Despite the failure of promoting the Diels-Alder reaction of dimethylfuran and ethylene by magic blue, the possibility of inducing the retro-Diels-Alder reaction of **15** by single electron oxidant still existed. In order to simplify ¹H-NMR monitoring, magic blue was selected because it only has aryl proton signals. A THF-d₈ solution of **15** was charged

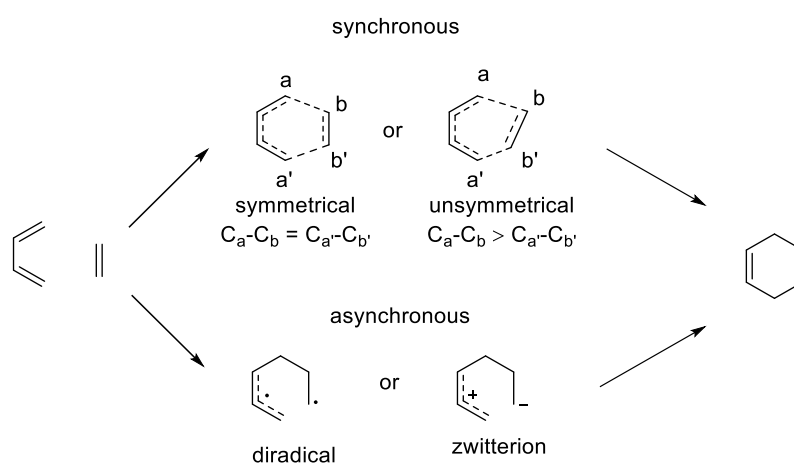
with a catalytic amount of magic blue and monitored by $^1\text{H-NMR}$. The rapid color change from deep blue to brown indicated that the aminium cation-radical was consumed and something was oxidized. Control experiment without **15** showed no color change after 1h. Unfortunately, no evidence of retro-Diels-Alder reaction was observed at the end of the reaction and all dimethyl-oxa-norbornene was converted into pX.

Table 4.6 Summary of retro-Diels-Alder tests with dimethyl-oxa-norbornene

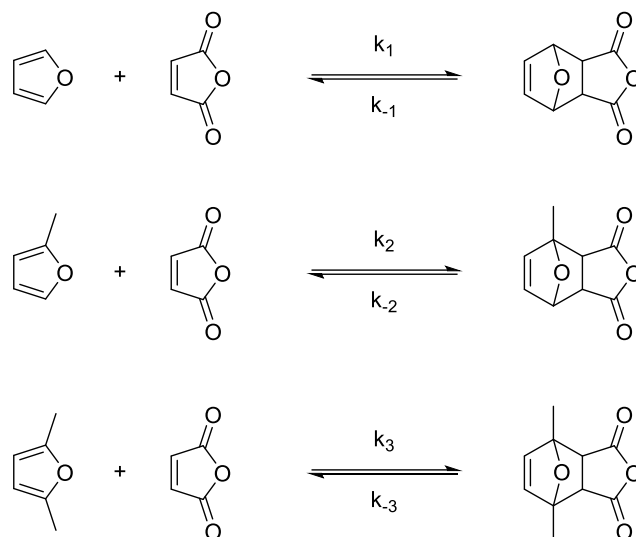
Entry	Catalyst	Solvent	Temp. ($^{\circ}\text{C}$)	Product (%)
1	Ag(OTf)	C_6D_6	100	pX (100%)
2	Cu(OTf) $_2$	C_6D_6	100	pX (100%)
3	Sc(OTf) $_3$	C_6D_6	25	pX (100%)
4	AgNO $_2$	C_6D_6	100	no reaction
5	Pd/C	C_6D_6	100	no reaction
6	Rh $_4$ (CO) $_{12}$	C_6D_6	100	no reaction
7	Pt(PPh $_3$) $_4$	C_6D_6	100	no reaction
8	PdCl $_2$	C_6D_6	100	pX (<5%)
9	RhCl(PPh $_3$) $_3$	C_6D_6	100	pX (50%)
10	W(CO) $_6$	C_6D_6	100	pX (100%)
11	Mo(CO) $_6$	C_6D_6	100	pX (100%)
12	magic blue	THF-d $_8$	25	pX (100%)

In the test of retro-Diels-Alder reaction, we observed only promotions for aromatization reactions in most cases and no retro-Diels-Alder product was detected in any reaction (Table 4.6). It is very challenging to enable the retro-Diels-Alder reaction without triggering the aromatization. The 1,4-dimethyl-oxa-norbornene has only two activation sites: the bridging oxygen and the C=C double bond. Any interaction with bridging oxygen would promote the rapid dehydration toward pX. We are still searching for an efficient catalyst for Diels-Alder/retro Diels-alder reaction in our lab.

In the literature, there are only a couple of papers reporting activation parameters of retro-Diels-Alder reactions of simply cycloadducts.^{40-41,42,43,44} The selected experimental results are shown in Table 4.7.^{45,46,47,48} Those papers were mainly focusing on the theoretical debate whether Diels-Alder reactions go via a synchronous one-step mechanism (cyclic aromatic transition state) or a two-step or two-stage mechanism (biradical or zwitterion intermediate), as shown in Scheme 4.13. Dewar *et al.* claimed that their kinetic studies of Diels-Alder and retro-Diels-Alder reactions of furans and maleic anhydride shown very unsymmetrical transition states (TS) where one of the new C-C bonds is almost completely formed when the other is beginning to form (Scheme 4.14).⁴⁶ The analysis in their paper provided us a new insight to the search of catalyst for Diels-Alder reactions.



Scheme 4.13 Possible mechanisms of Diels-Alder reaction



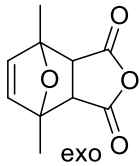
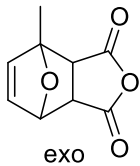
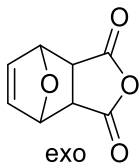
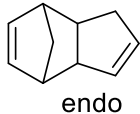
$k_2 = 1/2(k_1+k_3)$ if the TS is unsymmetrical

$k_2 = (k_1 \times k_3)^{1/2}$ if the TS is symmetrical

Scheme 4.14 Kinetic studies of Diels-Alder and retro-Diels-Alder reactions of furans and maleic anhydride by Dewar *et al.*

Table 4.7 Activation parameters of the retro-Diels-Alder reactions

Entry	Starting material	Conditions	ΔH^\ddagger [kcal mol ⁻¹]	ΔS^\ddagger [eu]	$\Delta G^\ddagger_{298K^*}$ [kcal mol ⁻¹]	Ref.
1		70-80 °C cyclohexane	25.6	-5.3	27.2	45
2		125-150 °C C ₆ D ₆	24.9 ± 1.7	-22.6 ± 4.2	31.6	this work
3		19-70 °C C ₆ D ₆	23.2 ± 0.9	-3.6 ± 2.9	24.3	this work

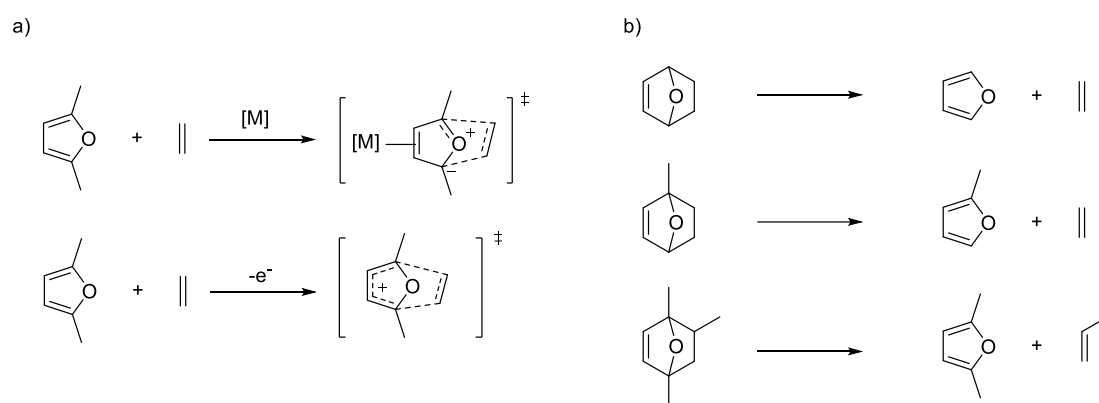
4		33.2-58.8 °C acetonitrile, UV-Vis, 211 nm	20.3	-2.17	20.9	46
5		33.2-58.8 °C acetonitrile, UV-Vis, 211 nm	20.8	-8.59	23.4	46
6		33.2-58.8 °C acetonitrile, UV-Vis, 211 nm	25.0	0.17	24.9	46
7		304-398 °C Flow reactor, 1 atm.	38.4 ± 1.0*	-2.84 ± 1.7*	39.2	47
8		200.5-351.9 °C Gas phase	33.0 ± 0.5	-1.9 ± 1.0	33.6	48

* calculated result based on data from references

As shown in Table 4.7 entry 1-6, most of the furan cycloadducts have very similar enthalpies of activation ($\Delta H^\ddagger = \sim 25 \text{ kcal mol}^{-1}$) and most of the entropies of activation are negative but small. The unexpectedly large and negative value of ΔS^\ddagger of retro-Diels-Alder reaction of **15** might result from the narrow temperature window of the kinetic measurements. The entropy of activation calculated from Eyring plot is very sensitive to the slope which would be more accurate with wider temperature window. Unfortunately, the retro-Diels-Alder reaction of **15** would be too fast to be measured at temperature higher than 150°C and too slow at temperature lower than 125°C by current method ($^1\text{H-NMR}$ in a sealed J-Young tube).

In previous discussion, the successes of promoting unfavorable Diels-Alder reaction reported by Harmen *et al.* and Bauld *et al.* have demonstrated that altering the electronic structures of either dienes or dienophiles was useful. Both of their reactions

should go through very unsymmetrical transition states due to the [3+2] mechanisms. Therefore, the future search of catalyst for the Diels-Alder reaction of dimethylfuran and ethylene should focus on breaking the symmetry of TS by either single-electron-oxidation or transition-metal-coordination to the diene or dienophile (Scheme 4.15a). Besides, the kinetic studies of oxa-norbornene, 1-methyl-oxa-norbornene or/and 1,2,4-trimethyl-oxa-norbornene could provide more informative details (Scheme 4.15b).



Scheme 4.15 Proposed future works

In conclusion, 1,4-dimethyl-oxa-norbornene was synthesized, isolated and characterized for the first time. A series of kinetic measurements of retro-Diels-Alder reaction of 2,5-dimethyl-oxa-norbornene and its derivatives were performed by ^1H -NMR experiments. The kinetic parameters of those retro-Diels-Alder reactions were calculated and compared with reported DFT calculation. A dozen of selected catalysts were test for retro-Diels-Alder reaction of dimethyl-oxa-norbornene. Although no promising catalyst was observed in retro-Diels-Alder test, the successful synthesis and

isolation of 2,5-dimethyl-oxa-norbornene provide us a key to further study of its reactivity and search for an efficient Diels-Alder reaction catalyst.

4.3 Experimental

4.3.1 General Considerations

The synthesis of **13** and **15** were carried out with standard Schlenk, high vacuum line. Pentane, diethyl ether, tetrahydrofuran, and toluene were dried by passing the solvent through activated aluminum columns followed by a nitrogen purge to remove dissolved oxygen. All other reagents were purchased from Aldrich or Acros and dried using standard procedures when necessary.

NMR spectra were recorded on a Bruker DRX-400 spectrometer and were referenced to the residual protons of the solvent (THF-d₈, 1.73 and 3.58 ppm; CD₂Cl₂, 5.32 ppm; CDCl₃, 7.27 ppm; C₆D₆, 7.15 ppm). FTIR spectra were taken on a Magna-IR E. S. P. 560 spectrometer. Mass spectral data were collected at the University of Delaware Mass Spectrometry Facility in electron ionization mode (+15eV).

4.3.2 Preparation of 1,4-dimethyl-7-oxa-bicyclo[2,1]hept-2-ene-5-endo-carboxyl-acid (**13**)

To an oven dried round-bottom flask under nitrogen atmosphere was added 2,5-dimethylfuran and acrylic acid. The mixture was cooled to -5 °C. Then, BH₃-THF complex was added under nitrogen atmosphere drop wise. The resulting mixture was stirred 16 hours at 0~-5 °C. A white solid slowly formed after a few hours. After 16 hours, the white solid was filtered, washed with a small amount of cold hexanes, dried in vacuum and collected as pure product. White solid; ¹H-NMR (CDCl₃):. 6.26 (d, J = 5.6 Hz, 1H, -CH=CH-), 6.13 (d, J = 5.6 Hz, 1H, -CH=CH-), 2.96 (dd, J = 9.1, 3.8 Hz,

1H, -CH<), 2.00 (dd, J = 11.6, 9.1 Hz, 1H, -CH₂-), 1.82 (dd, J = 11.6, 3.9 Hz, 1H, -CH₂-), 1.75 (s, 3H, Me), 1.60 (s, 3H, Me) ppm. The ¹H-NMR is identical to literature reported.²³

4.3.3 Preparation of 1,4-dimethyl-7-oxa-bicyclo[2,1]heptane-5-endo-carboxyl-acid (14)

13 and activated Pd/C was dissolved in an oven dried round-bottom flask with 25 ml of methanol. The resulting slurry was stirred and hydrogen gas bubbled though for 30 min. After filtration, the filtrate was dried under vacuum to give white solid as pure product. White solid; ¹H NMR (CDCl₃): 2.89 (ddd, J = 11.5, 4.8, 2.2 Hz, 1H, -CH<), 2.14 (dd, J = 12.2, 4.8 Hz, 1H, -CH₂-), 1.94-1.76 (m, 3H), 1.68-1.52 (m, 2H, -CH₂-) 1.62 (s, 3H, Me), 1.46 (s, 3H, Me) ppm. ¹³C NMR (CDCl₃): 177.63, 85.82, 84.66, 54.00, 40.87, 37.41, 34.13, 21.27, 21.13 ppm. HRMS calcd 171.10157 Da for C₉H₁₅O₃ (m+1), found 171.10136 Da.

4.3.4 Preparation of 1,4-dimethyl-7-oxa-bicyclo[2,1]hept-2-ene (15)

To an oven dried thick wall tube was added 170 mg endo-1,4-dimethyl-7-oxabicyclo[2,2,1]heptane-2-carboxylic acid (1 mmol), 531 mg lead(IV)tetraacetate (1.2 mmol), 18 mg copper(II)acetate (0.1 mmol) and 10 ml of anhydrous pentane under nitrogen atmosphere. After sealing the tube with Teflon screw cap, the slurry was stirred and heated to 80°C for 6h. Thereafter, the mixture was cooled down to 0°C, and was slowly opened to release the pressure. The resulting blue slurry was poured into an oven dried round-bottom flash which was then equipped with a needle valve. After three freeze-pump-thaw cycles, the volatile components of the degassed mixture were then vacuum-transferred into an ampule. The colorless mixture of 1,4-dimethyl-7-oxabicyclo[2,2,1]hept-2-ene, acrylic acid and pentane in the ampule was

washed 3 times with 10 ml saturated NaHCO₃ and 10 ml of DI water. The organic phase was dried over anhydrous MgSO₃ and filtered. Now the colorless mixture of 1,4-dimethyl-7-oxabicyclo[2,2,1]hept-2-ene and pentane was gently distilled at 45°C to remove most of the pentane solvent. The residue was collected as crude product which still contained about 50% of pentane. Pure sample were prepared by cooling down the mixture to -100°C and removing all pentane solution by high vacuum. Colorless oil; ¹H NMR (CDCl₃):. 6.08 (s, 2H, -CH=CH-), 1.66 (dd, 2H, -CH₂-), 1.59 (s, 6H, Me), 1.39 (dd, 2H, -CH₂-) ppm. ¹³C NMR (CDCl₃): 138.60, 85.81, 33.77, 19.23 ppm. IR (KBr): 3065 (w), 2972 (s), 2937 (s), 2859 (m), 1762 (w), 1727 (w), 1450 (m), 1376 (m), 1334 (m), 1264 (w), 1229 (w), 1193 (m), 1127 (m), 1081 (w), 1034 (w), 898 (m), 867 (m), 839 (w), 707 (m). HRMS calcd 125.09609 Da for C₈H₁₃O (m+1), found 125.09593 Da.

4.3.5 Typical Aromatization Procedure for reactions

A C₆D₆ solution (0.6 ml) of **15** (~ 0.025 M) with naphthalene (2.5 mM) as internal standard was charged into a J-Young tube. The catalyst (0.008 M) was added into the tube right before starting the ¹H-NMR monitor. The sealed tube was kept at 100 °C, and was measured by ¹H-NMR every 12h. The borane catalyzed dehydration was heated by NMR probe to 50 °C while acquiring data and a new set of data was collected every 100s (40 sets in total). The concentration of **15** and *p*-xylene were determined by integration of naphthalene chemical shifts at 7.63 ppm, double bond chemical shift of **15** at 5.85 ppm and aromatic chemical shifts of *p*-xylene at 6.96 ppm.

4.3.6 Typical retro-Diels-Alder procedure for reactions

For **13**, a C₆D₆ solution (0.6 ml) of **13** (~ 0.025 M) with chloroform (10 μL) as internal standard was charged into a J-Young tube. The sealed tube was heated in the NMR probe to corresponding temperature while acquiring data. The low temperature measurements were kept at corresponding temperature by water bath and the data was collected every 2h. The concentration of **13**, 2,5-dimethylfuran and acrylic acid were determined by integration of chloroform chemical shifts at 6.19 ppm, -CH₂- chemical shift of **13** at 2.76 ppm and double bond chemical shifts of acrylic acid at 5.21 ppm.

For **15**, a C₆D₆ solution (0.6 ml) of **15** (~ 0.025 M) with naphthalene (2.5 mM) as internal standard was charged into a J-Young tube. The catalyst (0.008 M) was added into the tube right before starting the ¹H-NMR monitor. The sealed tube was kept at corresponding temperature by oil bath, and was measured by ¹H-NMR every 12h. The concentration of **15** and 2,5-dimethylfuran were determined by integration of naphthalene chemical shifts at 7.63 ppm, double bond chemical shift of **15** at 5.85 ppm and double bond chemical shifts of dimethylfuran at 5.75 ppm.

REFERENCES

1. M. J. Bidy, C. Scarlata, C. Kinchin, *Chemicals from Biomass: A Market Assessment of Bioproducts with Near-Term Potential*, NREL/TP-5100-65509, **2016**
2. *Paraxylene Market Analysis By Application (Dimethyl Terephthalate (DMT), Purified Terephthalic Acid (PTA)) And Segment Forecasts To 2022*, Grand View Research, **2016**
3. H. O'Neil, P. Wantanachaisaeng, *Capturing Opportunities for para-Xylene Production: A Report from the Aromatics (Thailand) Public Co., Ltd. And UOP LLC*, **2007**.
4. (a) J. Y. Yu, S. Y. Zhu, P. J. Dauenhauer, H. J. Cho, W. Fan, R. J. Gorte, *Catal Sci Technol* **2016**, *6*, 5729-5736; (b) J. J. Pacheco, J. A. Labinger, A. L. Sessions, M. E. Davis, *ACS Catal.* **2015**, *5*, 5904-5913; (c) X. Feng, C. Shen, C. Tian, T. Tan, *Ind. Eng. Chem. Res.* **2017**, *56*, 5852-5859; (d) J. C. Kim, T. W. Kim, Y. Kim, R. Ryoo, S. Y. Jeong, C. U. Kim, *Appl. Catal., B* **2017**, *206*, 490-500; (e) Y. P. Wijaya, H. P. Winoto, Y. K. Park, D. J. Suh, H. Lee, J. M. Ha, J. Jae, *Catal. Today* **2017**, *293*, 167-175.
5. J. B. Binder, R. T. Raines, *J. Am. Chem. Soc.* **2009**, *131*, 1979-1985.
6. T. Thananathanachon, T. B. Rauchfuss, *Angew. Chem. Int. Ed. Engl.* **2010**, *49*, 6616-6618.
7. I. F. Teixeira, B. T. Lo, P. Kostetsky, M. Stamatakis, L. Ye, C. C. Tang, G. Mpourmpakis, S. C. Tsang, *Angew. Chem. Int. Ed. Engl.* **2016**, *55*, 13061-13066.
8. E. Mahmoud, J. Yu, R. J. Gorte, R. F. Lobo, *ACS Catal.* **2015**, *5*, 6946-6955.
9. C. C. Chang, S. K. Green, C. L. Williams, P. J. Dauenhauer, W. Fan, *Green Chem.* **2014**, *16*, 585-588.
10. S. Song, G. J. Wu, W. L. Dai, N. J. Guan, L. D. Li, *J. Mol. Catal. A: Chem.* **2016**, *420*, 134-141.

-
11. R. E. Patet, W. Fan, D. G. Vlachos, S. Caratzoulas, *Chemcatchem* **2017**, *9*, 2523-2535.
 12. C. L. Williams, C. C. Chang, P. Do, N. Nikbin, S. Caratzoulas, D. G. Vlachos, R. F. Lobo, W. Fan, P. J. Dauenhauer, *ACS Catal.* **2012**, *2*, 935-939.
 13. Y.-P. Li, M. Head-Gordon, A. T. Bell, *J. Phys. Chem. C* **2014**, *118*, 22090-22095.
 14. G. O. Schenck, K. Gollnick, G. Buchwald, S. Schroeter, G. Ohloff, *Liebigs Ann.* **1964**, *674*, 93-117.
 15. S. Mirsadeghi, B. Rickborn, *J. Org. Chem.* **1985**, *50*, 4340-4345.
 16. M. Ines, A. J. Mendonca, A. P. Esteves, D. I. Mendonca, M. J. Medeiros, *C R Chim* **2009**, *12*, 841-849.
 17. W. G. Dauben, H. O. Krabbenhoft, *J. Am. Chem. Soc.* **1976**, *98*, 1992-1993.
 18. W. G. Dauben, Kozikows.Ap, *J. Am. Chem. Soc.* **1974**, *96*, 3664-3666.
 19. in *Category 5, Compounds with One Saturated Carbon Heteroatom Bond, Vol. 37*, 1st Edition ed. (Ed.: C. J. Forsyth), Georg Thieme Verlag, Stuttgart, **2008**.
 20. (a) R. Ballini, M. Petrini, *Tetrahedron* **2004**, *60*, 1017-1047.; (b) S. M. Kelly, B. H. Lipshutz, *Org. Lett.* **2014**, *16*, 98-101.; (c) W. Adam, M. Makosza, C. R. Saha-Möller, C.-G. Zhao, *Synlett* **1998**, *1998*, 1335-1336.
 21. K. C. Bassett, F. You, P. M. Graham, W. H. Myers, M. Sabat, W. D. Harman, *Organomet.* **2006**, *25*, 435-439.
 22. D. J. Bellville, D. D. Wirth, N. L. Bauld, *J. Am. Chem. Soc.* **1981**, *103*, 718-720.
 23. S. Lin, M. A. Ischay, C. G. Fry, T. P. Yoon, *J. Am. Chem. Soc.* **2011**, *133*, 19350-19353.
 24. M. Shiramizu, F. D. Toste, *Chem. Eur. J.* **2011**, *17*, 12452-12457.

-
25. K. Furuta, Y. Miwa, K. Iwanaga, H. Yamamoto, *J. Am. Chem. Soc.* **1988**, *110*, 6254-6255.
 26. M. F. Saraiva, M. R. C. Couri, M. Le Hyaric, M. V. de Almeida, *Tetrahedron* **2009**, *65*, 3563-3572.
 27. L. J. Goossen, C. Linder, N. Rodriguez, P. P. Lange, A. Fromm, *Chem. Commun. (Camb.)* **2009**, 7173-7175.
 28. D. H. R. Barton, D. Crich, W. B. Motherwell, *J. Chem. Soc., Chem. Commun.* **1983**, 939-941.
 29. J. D. Griffin, M. A. Zeller, D. A. Nicewicz, *J. Am. Chem. Soc.* **2015**, *137*, 11340-11348.
 30. Z. Wang, L. Zhu, F. Yin, Z. Su, Z. Li, C. Li, *J. Am. Chem. Soc.* **2012**, *134*, 4258-4263.
 31. F. Yin, Z. Wang, Z. Li, C. Li, *J. Am. Chem. Soc.* **2012**, *134*, 10401-10404.
 32. J. D. Bacha, J. K. Kochi, *J. Org. Chem.* **1968**, *33*, 83-93.
 33. S. Coseri, K. U. Ingold, *Org. Lett.* **2004**, *6*, 1641-1643.
 34. J. A. Bravo, J. L. Vila, *Rev. Boliv. Quím.* **2015**, *32*, 45-52.
 35. G. A. Kraus, S. Riley, *Synthesis* **2012**, *44*, 3003-3005.
 36. J. D. Bacha, J. K. Kochi, *J. Org. Chem.* **1968**, *33*, 83-93.
 37. C. L. Williams, C. C. Chang, P. Do, N. Nikbin, S. Caratzoulas, D. G. Vlachos, R. F. Lobo, W. Fan, P. J. Dauenhauer, *ACS Catal.* **2012**, *2*, 935-939.
 38. R. E. Patet, M. Koehle, R. F. Lobo, S. Caratzoulas, D. G. Vlachos, *J. Phys. Chem. C* **2017**, *121*, 13666-13679.
 39. M. Gorski, A. Kochel, T. Szymanska-Buzar, *Organomet.* **2004**, *23*, 3037-3046.
 40. J. W. Wijnen, J. B. F. N. Engberts, *J. Org. Chem.* **1997**, *62*, 2039-2044.

-
41. B. R. Beno, S. Wilsey, K. N. Houk, *J. Am. Chem. Soc.* **1999**, *121*, 4816-4826.
 42. R. Walsh, J. M. Wells, *J. Chem. Soc., Perkin Trans. 2* **1976**, 52-55.
 43. J. T. Manka, A. G. Douglass, P. Kaszynski, A. C. Friedli, *J. Org. Chem.* **2000**, *65*, 5202-5206.
 44. V. D. Kiselev, *Int. J. Chem. Kinet.* **2010**, *42*, 117-125.
 45. G. Jenner, M. Papadopoulos, J. Rimmelin, *J. Org. Chem.* **1983**, *48*, 748-749.
 46. M. J. S. Dewar, A. B. Pierini, *J. Am. Chem. Soc.* **1984**, *106*, 203-208.
 47. W. C. Herndon, W. B. Cooper, M. J. Chambers, *J. Phys. Chem.* **1964**, *68*, 2016-2018.
 48. W. C. Herndon, C. R. Grayson, J. M. Manion, *J. Org. Chem.* **1967**, *32*, 526-529.

Appendix
ABBREVIATION

Cp = cyclopentadienyl

Cp* = pentamethylcyclopentadienyl

Et₂O = diethyl ether

Nacnac = 2, 4-Pentane-N,N'-bis(aryl or alkyl) ketiminato

^HL^{iPr} = N,N'-bis(2,6-diisopropylphenyl)-1,4-diazadiene

L-CO₂ = ArN=CH-CH(COOH)-NHAr (Ar = 2,6-diisopropylphenyl)

Me, H₂L^{iPr} = ArN=C(Me)-CH₂-NHAr (Ar = 2,6-diisopropylphenyl)

Ph = phenyl

ⁱPr = isopropyl

^tBu = tert-butyl

TMS = trimethylsilyl

THF = tetrahydrofuran

Tp = tris(pyrazolyl)borate

Magic blue = tris(4-bromophenyl)ammoniumyl hexachloroantimonate

HMF = 5-hydroxymethylfurfural

pX = *para*-xylene

LA = Lewis acid

TS = transition state

DA = Deils-Alder